Imperial College London

TOWARDS THE DEVELOPMENT OF A NOVEL PROTEOMIC TOOL TO MAP TRIMETHYLLYSINE MARKS ON HISTONES VIA A HOFMANN-TYPE CHEMICAL MODIFICATION

A Thesis Submitted by:

Melis Eda Ekinci

In partial fulfilment of the requirements for the degree of:

Doctor of Philosophy

October 2019

Supervisors: Professor Matthew J. Fuchter & Doctor Peter DiMaggio

Department of Chemistry

Imperial College London

Declaration of Originality

I, Melis Eda Ekinci, hereby confirm that the work presented within this thesis is entirely my own, conducted under the supervision of Prof Matthew J. Fuchter and Dr Peter DiMaggio, at the Department of Chemistry, Imperial College London, unless otherwise stated. All work performed by others has been acknowledged within the text and referenced where appropriate.

Melis Eda Ekinci

London, 18th October 2019

ABSTRACT

One of the key epigenetic processes for transcriptional control is dynamic post-translational modification (PTM) of histone proteins. Dysregulation of these epigenetic mechanisms have been linked to the aetiology of human diseases such as cancer and neurological disorders. To decipher the epigenetic pathways leading to the development of disease and to gain insight into the function of post-translational modifications of histones, a great interest was taken on the genome-wide mapping of epigenetic marks. The most commonly used method to profile PTMs on histones is the ChIP-seq technique (chromatin immunoprecipitation followed by DNA sequencing), which is based on the use of antibodies to target and enrich specific epigenetic marks. However, the dependence of ChIP-seq on antibodies constitutes a significant limitation due to possible cross-reactivity and poor specificity of those antibodies towards the targeted epigenetic marks. In addition, the ChIP-seq technique only allows the mapping of *single* epigenetic marks to genomic loci. Here we present a novel antibody-free chemical biological tool 'CLICK-seq' to map *combinatorial* histone lysine trimethylation marks on intact mono-nucleosomes. It is based on the selective modification of trimethyllysine residues on histone proteins to obtain an alkene functionality on these substrates, which enables the introduction of affinity tags via a thiol-ene click chemistry for selective enrichment. This work demonstrates diverse chemical approaches taken towards the elimination of trimethylamine in quaternary ammonium substrates to achieve the formation of an alkene under mild and 'protein-compatible' conditions. With the development of a novel reaction - Pd-catalysed Hofmann-type elimination – the removal of trimethylamine was achieved at low temperature on model small molecules (albeit in a low yield).

In the second project, a novel design for acid-cleavable cross-linkers was developed to simultaneously achieve the cross-linking of histone protein complexes and the subsequent chemical labelling of histone lysine residues upon acid-catalysed cleavage. This work portrays our efforts towards the synthesis of a small library of acid-cleavable cross-linkers.

ACKNOWLEDGEMENTS

First, I would like to thank my supervisors, Prof Matthew Fuchter and Dr Peter DiMaggio for their support and guidance throughout this project. In addition, a thank you to Prof Phil Parsons for many insightful chats in the lab or at the coffee table. I would also like to thank Sandeep for always helping with any questions I had throughout my first year of PhD. Special thanks must go to Ainoa, who always supported me in and outside the lab and who put me in the right path to complete this PhD. For that, I will always be grateful. I would also like to thank Harry for introducing me to the world of proteomics and taking care of the countless technical difficulties we encountered.

A big thank you to all the past and present members of the Fuchter, Barrett and DiMaggio groups for keeping me going throughout my PhD with karaoke sessions in the lab, philosophical discussions, numerous brainstorming sessions or crazy office parties. Thank you for being part of my journey here at Imperial College London. I will always treasure those moments. I am very grateful that I have met Katie, Luiza, Hannah and Alex during my PhD, who have now become part of my extended family. In particular, I am very lucky to have found a great friend and soulmate in Katie, who has supported me through thick and thin all those years. I would also like to thank Linda for all those late-night discussions about the present and the future and James for supporting me through many moments of despair. Being part of the Institute of Chemical Biology also allowed me to meet many amazing scientists, especially in my CDT cohort, who have introduced me to the British way of life. I am also thankful for the analytical staff at Imperial College, especially Pete Haylock, who I consider a friend after having survived attending a match at Stamford Bridge.

I also would like to thank Franziska, one of my dearest friends, who has supported me all the way from Germany with countless voice messages during the last year of my PhD.

Finally, I would like to thank my parents, Metin and Gülizar Ekinci, and my brother, Orkan Ekinci, without whom I would have not been able to pursue a PhD at Imperial College London. They have continuously supported me in any way possible and always believed in me.

It has been a long journey, but I am very grateful that I have had the opportunity to share it with so many wonderful people and that I made great memories, which I will carry with me for the rest of my life.

.

To always follow your dreams.

TABLE OF CONTENTS

DECLARATION OF ORIGINALITY **3**

COPYRIGHT DECLARATION **3**

ABSTRACT **5**

ACKNOWLEDGEMENTS **7**

ABBREVIATIONS **15**

1 GENERAL INTRODUCTION **19**

1.1 A BRIEF INTRODUCTION TO EPIGENETICS 19

1.2 HISTONE LYSINE METHYLATION 22

1.3 PROFILING OF PROTEIN LYSINE METHYLATION 27

1.3.1 The role of chromatin immunoprecipitation in the profiling of protein lysine methylation 27

1.3.2 Integration of mass spectroscopy into the investigation of the methylome 29

1.3.2.1 The use of antibodies and methyllysine 'reader' domains to enrich lysine methylation marks 30

1.3.2.2 In vivo isotopic chemical labelling of histone residues 32

1.3.2.3 Chemical labelling of lysine residues via chemical derivatisation assays 34

1.3.2.4 Chemical labelling of histone residues using activity-based probes 37

1.3.2.5 Bioorthogonal profiling protein methylation technology for the analysis of lysine methylomes 38

1.4 PROJECT OVERVIEW 45

2 RESULTS AND DISCUSSION I – SITE-SPECIFIC CHEMICAL MODIFICATION OF HISTONE PROTEINS **47**

2.1 HOFMANN ELIMINATION OF QUATERNARY AMMONIUM COMPOUNDS 47

2.1.1 Background: Introducing the Hofmann elimination reaction 47

2.1.2 Hofmann elimination screening using trimethyllysine 51

2.1.2.1 Synthesis of trimethyllysine analogues 51

2.1.2.2 Hofmann elimination screening using trimethyllysine as the starting material 57

2.1.3 Hofmann elimination of quaternary ammonium groups in organic small molecules 64

2.1.4 Micelle-catalysed Hofmann elimination of quaternary ammonium groups in small molecules 70

2.2 PD-CATALYSED HOFMANN-TYPE ELIMINATION OF QUATERNARY AMMONIUM GROUPS IN ORGANIC SMALL MOLECULES 78

2.2.1 Background: The Heck reaction as the foundation for the Pd-catalysed Hofmann-type elimination 81

2.2.2 Pd-catalysed Hofmann-type elimination 84

2.2.3 Initial investigation of the Pd-catalysed Hofmann-type elimination 86
2.2.4 Investigation of the solvent effects on the Pd-catalysed Hofmann-type elimination 90
2.2.5 Analysis of the Reductive Elimination step in the catalytic cycle 93
2.2.6 Oxygen as the destroyer of the active catalyst? 98
2.2.7 The investigation of the metal-to-ligand ratio and the catalyst loading 101
2.2.8 Pd-catalysed Hofmann-type elimination with stoichiometric amount of catalyst 105
2.2.9 Is the formation of the alkene based on the oxidative addition of the Pd-catalyst? 108
2.2.10 Possible side reactions of the formed alkene 111
2.2.11 Investigation of the electrophile – the effect of the counterion 114
2.2.12 Examination of the Pd-catalysed Hofmann-type elimination in deuterated acetonitrile 117
2.2.13 Ligandless Pd-catalysed Hofmann-type elimination – oxidative addition by stabilised Pd^0 nanoparticles 119
2.2.14 $Pd_2(dba)_3$ – an alternative palladium source 122
2.2.15 Investigation of Suzuki cross-coupling of alkyl trimethylammonium substrates 125
2.2.16 NHC complexes for the Pd-catalysed Hofmann-type elimination – an attempt to improve oxidative addition 128
2.3 Pd-catalysed Hofmann-type elimination screening on model synthetic peptide 144
2.3.1 Background: Palladium chemistry in protein modifications 144
2.3.2 The design of the synthetic peptide used for the Pd-catalysed Hofmann-type elimination 147
2.3.3 Attempted Pd-catalysed Hofmann-type elimination on the model peptide using amine-based ligands 152
2.3.4 Attempted Pd-catalysed Hofmann-type elimination on the model peptide using phosphine ligands 157
2.3.5 Attempted Pd-catalysed cleavage of the $C(sp^3)$ – $N(Me_3)$ bond in the model peptide using NHC ligands 161
2.4 Conclusion and Future Work 176

3 RESULTS AND DISCUSSION II – ACID-CLEAVABLE CROSS-LINKER FOR BOTTOM-UP MS ANALYSIS OF HISTONE INTERACTIONS 180

3.1 Background: Cross-linking mass spectroscopy 180
3.2 The development of an acid-cleavable cross-linker for XL-MS analysis of histone proteins 184
3.3 Synthetic efforts towards generation of the acid-cleavable cross-linker 186
3.3.1 Towards the synthesis of the diaryldialkoxysilyl cross-linker 186
3.3.2 New design of the acid-cleavable cross-linker 189
3.3.3 Synthesis of the bis-lactone precursors 192
3.3.3.1 Baeyer-Villiger approach for the synthesis of the pyrano[3,2-b]pyran lactone 192
3.3.3.2 Synthesis of the pyrano[3,2-*b*]pyran lactone via iodine-catalysed lactonisation 194
3.3.3.3 Synthesis of the furo[3,2-*b*]furan lactone via iodine-catalysed lactonisation 198

3.3.4 Acetalisation of the furo[3,2-*b*]furan lactone 199
3.3.5 The carbonate cross-linker – a backup design 202
3.4 Conclusion and Future Work 204
4 FINAL REMARKS 205
5 EXPERIMENTAL 206
5.1 General methods 206
5.2 Experimental for R&D I 208
5.2.1 General Procedures 208
5.2.2 Synthesis of trimethyllysine 210
5.2.3 First generation Hofmann elimination screening 217
5.2.4 Second generation Hofmann elimination screening 219
5.2.5 Micelle-catalyzed elimination of phenylbutyl trimethylamine 222
5.2.6 Pd-catalyzed Hofmann-type elimination on model small molecules 224
5.2.6.1 Synthetic procedures 224
5.2.6.2 Screening of the Pd-catalysed Hofmann-type elimination 230
5.2.7 Investigation of Pd-catalysed Hofmann-type elimination on model peptide 248
5.2.7.1 Pd-catalysed Hofmann-type elimination using amine ligands 248
5.2.7.2 Pd-catalysed Hofmann-type elimination using phosphine ligands (Subchapter 2.3.4) 250
5.2.7.3 Pd-catalysed Hofmann-type elimination using NHC ligands (Subchapter 2.3.5) 251
5.3 Experimental for R&D II 255
5.3.1 Synthetic efforts towards the diaryldialkoxysilyl cross-linker 255
5.3.2 Synthetic efforts towards the pyrano[2,3-*b*]pyran cross-linker 257
5.3.3 Synthetic efforts towards the furo[2,3-*b*]furan cross-linker 263
5.3.4 Synthetic efforts towards the carbonate cross-linker 266
6 REFERENCES 268

ABBREVIATIONS

Ab-SAM	4-Azidobut-2-enyl SAM
ADHP	Disodium salt of *N,N*-dimethyl-2-amino-4,6-dihydroxypyrimidine
AmBic	Ammonium bicarbonate buffer
ATP	Adenosine-5'-triphosphate
Bn	Benzyl group
Boc	*Tert*-butyloxycarbonyl protecting group
BPPM	Biorthogonal profiling protein methylation
BrettPhos	Dicyclohexyl-[3,6-dimethoxy-2-[2,4,6-tri(propan-2-yl)phenyl]phenyl] phosphane
BTMG	2-*Tert*-butyl-1,1,3,3-tetramethylguanidine
Cbz	Carboxybenzyl protecting group
CDI	1,1′-Carbonyldiimidazole
ChIP	Chromatin immunoprecipitation
ChIP-chip	Chromatin immunoprecipitation – DNA microarrays
ChIP-seq	Chromatin immunoprecipitation – next-generation sequencing
CID	Collision-induced dissociation
CliEN-seq	Clickable chromatin enrichment with parallel DNA sequencing
18-crown-6	1,4,7,10,13,16-Hexaoxacyclooctadecane
CTAB	Cetyltrimethylammonium bromide
CuAAC	Cu(I)-catalyzed azide–alkyne cycloaddition
DBN	1,5-Diazabicyclo[4.3.0]non-5-ene
DBU	1,8-Diazabicyclo(5.4.0)undec-7-ene
DIBAL	Diisobutylaluminium hydride
DLS	Dynamic light scattering
DTT	1,4-Dithiothreitol
EnYn-SAM	(*E*)-pent-2-en-4-ynyl-SAM
FDR	False discovery rate
Fmoc	Fluorenylmethyloxycarbonyl protecting group
GC-MS	Gas chromatography – mass spectroscopy
G9a	Euchromatic histone-lysine *N*-methyltransferase 2 (also EHMT2)
GLP1	Euchromatic histone-lysine *N*-methyltransferase 1 (also EHMT1)
H1, H2A, H2B, H3 or H4	Histone 1, 2A, 2B, 3 or 4 proteins
HEK 293T	Human embryonic kidney cells transformed with SV40 large T antigen

HeLa	Immortal human cell line
Hey-SAM	(*E*)-hex-2-en-5-ynyl-SAM
HP1	Heterochromatin protein 1
IMes • HCl	1,3-Bis(2,4,6-trimethylphenyl)imidazolinium chloride
IPr • HCl	1,3-Bis(2,6-diisopropylphenyl)imidazolinium chloride
JHDM1D	JmjC-domain-containing histone demethylation protein 1D
JmjC-domain	Jumonji-domain
K	Lysine
K(me), K(me_2), K(me_3)	Mono-, Di-, Trimethyllysine
KDM	Lysine demethylase
KHMDS	Potassium bis(trimethylsilyl)amide
KTM	Lysine methyltransferase
(HP-) LC	(High performance-) Liquid chromatography
LDA	Lithium diisopropylamide
LSD1	Lysine-specific histone demethylase 1A
Lys	Lysine
MAT	Methionine adenosyltransferase
MBT	Malignant brain tumor domain protein
MPA	3-Mercaptopropionic acid
MS(/MS)	(Tandem) Mass spectroscopy
NHC	*N*-Heterocyclic carbene
NHS	*N*-Hydroxysuccinimide
Ni[cod]$_2$	Bis(1,5-cyclooctadiene)nickel(0)
NMR	Nuclear magnetic resonance spectroscopy
P (or Prod.)	Product
PCR	Polymerase chain reaction
Pd	Palladium
$Pd_2(dba)_3$	Tris(dibenzylideneacetone)dipalladium(0)
$Pd(OAc)_2$	Palladium(II) acetate
Pd-PEPPSI-IPr	[1,3-Bis(2,6-Diisopropylphenyl)imidazol-2-ylidene](3-chloropyridyl) palladium(II) dichloride
PHD	Plant homeodomain
PHF8	Plant homeodomain finger protein 8
PMT	Protein methyltransferase
Pob-SAM	4-Propargyloxy-but-2-enyl-SAM
PPI	Protein-protein interaction

PTM	Post-translational modification
ProSeAM	*Se*-adenosyl-selenomethionine
PS	Proton sponge
SAM	*S*-adenosyl methionine
SCX	Strong cation exchange chromatography
SET domain	Protein domain found in Suppressor of variegation [Su(var)3-9], Enhancer of zeste and Trithorax
SILAC	Stable Isotope Labelling by Amino acids
SM	Starting material
T	Temperature
t	Reaction time
TBAB	Tetrabutylammonium bromide
TBD	1,5,7-Triazabicyclo[4.4.0]dec-5-ene
TCEP	Tris(2-carboxylethyl)phosphine
TFA	Trifluoroacetic acid
TIC	Total ion chromatogram
TLC	Thin-layer chromatography
TM	Transition-metal
TMSOTf	Trimethylsilyl trifluoromethanesulfonate
XL-MS	Cross-linking mass spectroscopy

1 GENERAL INTRODUCTION

1.1 A brief introduction to epigenetics

In 1942, Conrad H. Waddington introduced the term 'epigenetics' and defined it as "the branch of biology which studies the causal interactions between genes and their products, which bring the phenotype into being".[1] Since then, modern biologists have further refined the term 'epigenetics' ('above genetics') describing all changes in gene expression, heritable through mitosis and meiosis, which do not occur due to modifications of the genetic sequence (known as 'epigenetic inheritance').[2]

Inspired from Waddington's interpretation of epigenetics, an extensive pioneering work has been carried out to understand the manifestation of a phenotype as a result of the interplay between the genotype, the environment and the newly introduced epigenotype.[3,4] For example, Muller[5] and by McClintock[6] laid the foundation on the concept of 'epigenetic inheritance' with their research on the position-effect variegation, which was further consolidated by the introduction of the concept of X-chromosome inactivation[7] and imprinting[8,9]. The importance of epigenetics in developmental biology is well substantiated with the discovery that unlike genetic information the epigenetic state of an organism goes through changes during one's lifetime.[10,11] Daley *et al.* demonstrated that human somatic cells can be reprogrammed to pluripotency by controlling the expression of various transcription factors.[12] In addition, many studies have inferred that the cell differentiation of embryonic stem cells is associated with epigenetic changes and the consequences in chromatin accessibility at key developmental genes.[13,14] Epigenetic processes have also been associated with cell plasticity being linked to cellular reprogramming and response to the environment.[15] In addition, they have an important role in the development of human diseases being implicated in cancer, metabolic diseases and neuropsychiatric disorders.[16] The dynamic nature of epigenetics inspired a great interest in epigenetic therapy, in which researchers are investigating novel and efficient methods to reverse epigenetic processes, which led to the development of disease-associated epigenetic states.[17–19]

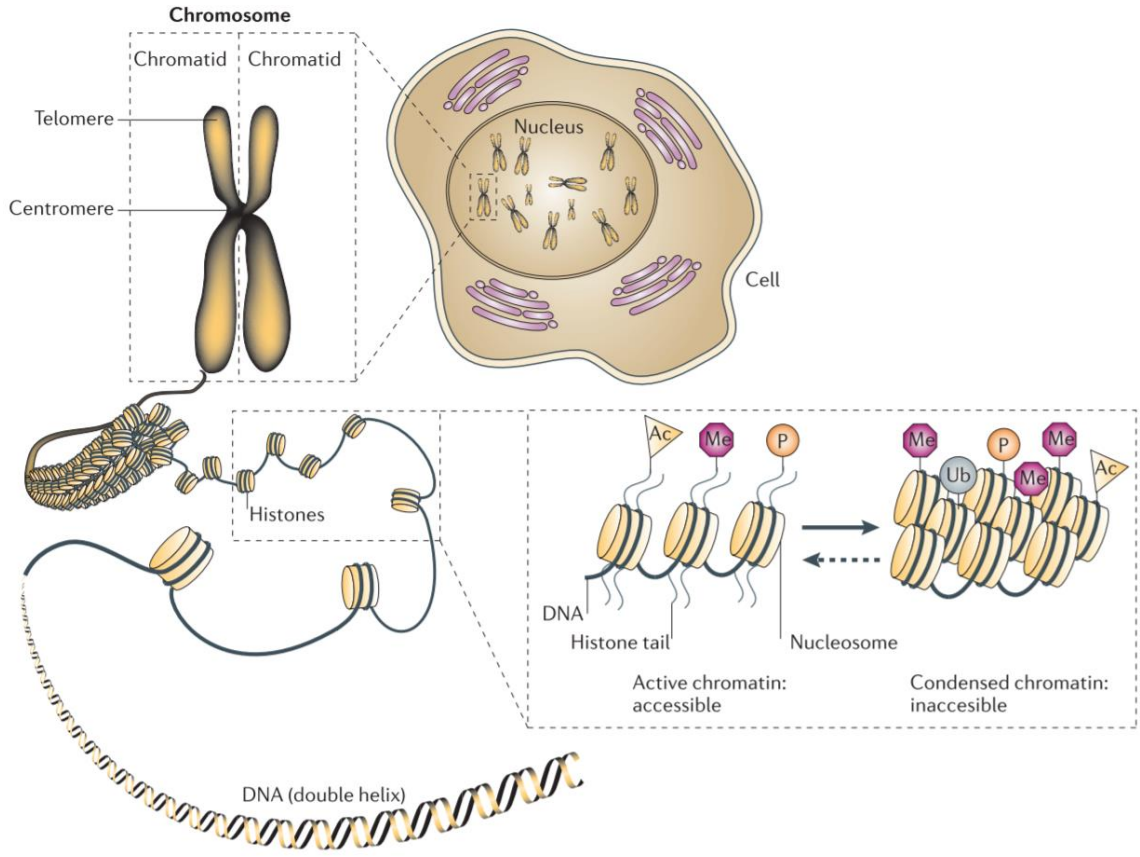

Figure 1.1.1 The genetic information is stored in the chromosome in eukaryotic cells, in which the DNA helix is wrapped around an octamer of histone proteins. (Image reproduced with permission from the rights owner, Springer Nature.[20])

Genetic information encoded in the double-stranded DNA is packaged in the form of chromatin in eukaryotic cells (see Figure 1.1.1). Chromatin is a nucleoprotein complex consisting of DNA, histone proteins and non-histone proteins. The base unit of chromatin is the nucleosome, which is composed of an octamer of four core histone proteins – H2A, H2B, H3 and H4. Approximately 147 base-pairs of DNA is then wrapped around the histone octamer. Each unit of nucleosome is connected to the adjacent nucleosome by a segment of linker DNA (~ 20 bp). The higher-order structure of a poly-nucleosome fibre is additionally stabilised by coordination of a linker histone protein (H1 or H5) to each nucleosome and to the linker DNA. The construct of a nucleosome unit with the linker histone and the linker DNA is known as the chromatosome.[21] The packaging of chromatin in the nucleus results in the structure of a chromosome.

The topology of the nucleosome consists of a disk shape, from which the *N*-terminal tails of the histone proteins protrude. Consisting of 15 to 36 amino acids, these histone tails are prone to post-translational modifications (PTMs) such as methylation, acetylation or phosphorylation to name a few.[22] The histone proteins have been shown to get modified at over 60 different residues. The modification of chromatin structure has an impact on the regulation of gene expression, since such changes can modulate the accessibility and the consecutive recruitment of regulatory proteins to the underlying DNA sequence. Depending on the degree of chromatin modification, there are two main states of the chromatin structure, which define transcriptional activation or transcriptional repression. Condensed chromatin (heterochromatin), in which the nucleosomes are packed tightly together, results in the repression of gene transcription. In contrast, the more accessible and loosely packed euchromatin is associated with the activation of gene transcription. Post-translational modifications of histone proteins together with DNA methylation[23,24] and post-translational gene alteration by non-coding microRNAs (miRNAs)[25,26] are the key epigenetic mechanisms for transcriptional control.

1.2 Histone Lysine Methylation

Among the array of post-translational modifications of histones, histone lysine methylation plays a central role in the regulation of gene expression, cell cycle and chromatin remodelling. The complexity of histone lysine methylation lies within the influence of the specific position of the methylation sites on histone proteins (see Figure 1.2.2) as well as the level of methylation (mono-, di- and trimethyllysine as shown in Figure 1.2.1) on transcriptional control. In contrast to acetylation, which activates transcription, histone lysine methylation can signal both transcriptional activation and repression. The methylation of lysine residues is tightly regulated by lysine methyltransferases (KTMs), which transfer a methyl group ('Me') from the *S*-adenosyl methionine (SAM) co-factor to the target lysine amine (see Figure 1.2.1), and lysine demethylases (KDMs), which remove the methyl groups, making lysine methylation a dynamic reversible epigenetic mark.

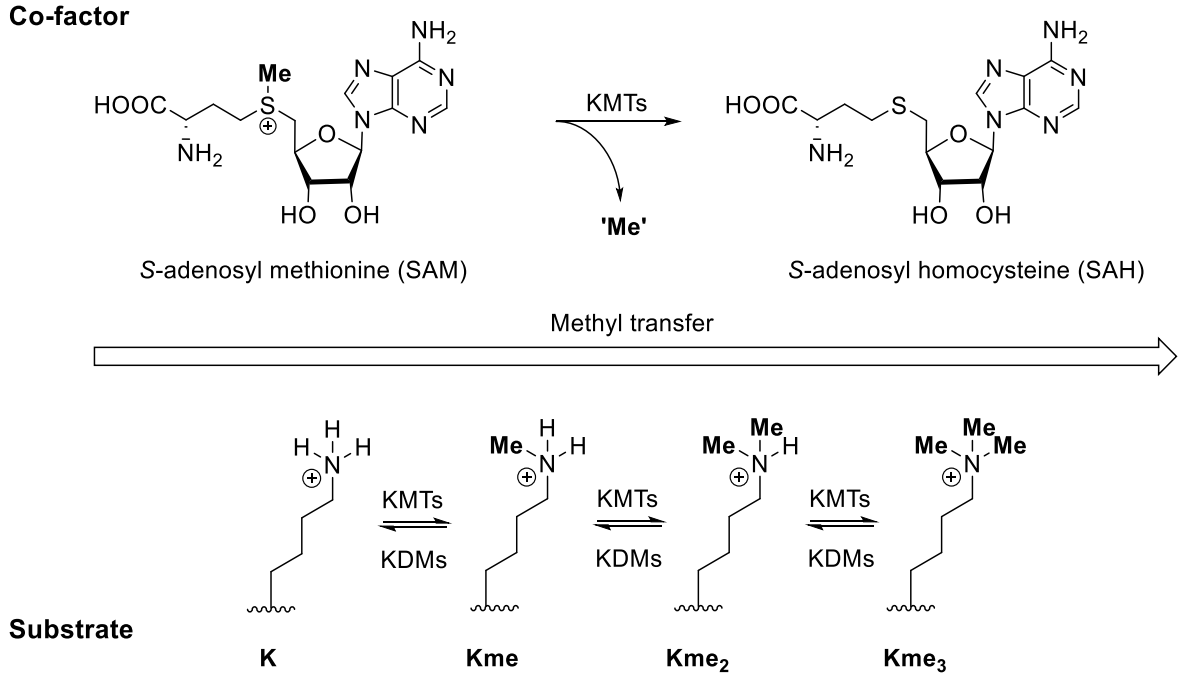

Figure 1.2.1 Histone lysine methylation is regulated by lysine methyltransferases (KTMs) and lysine demethylases (KDMs). KMTs transfer a methyl group ('Me') from the *S*-adenosyl methionine (SAM) co-factor to the target lysine substrate generating mono-, di- and trimethyllysine and *S*-adenosyl homocysteine (SAH) as the by-product of methylation.

The most extensively studied lysine methylation sites and the enzymes in charge of their modification are shown in Figure 1.2.2. The methylation sites H3K4, H3K36 and H3K79 are primarily associated with transcriptional activation, whereas H3K9, H3K27 and H4K20 are connected to transcriptional repression.[22] However, it is noteworthy that these observations should be solely acknowledged as a general trend of activity, since the effects of lysine methylation have been proven to be context-dependent. For example, di- and trimethylated H3K4 marks are generally linked to transcriptional activation[27,28], however, a few studies have shown that H3K4 methylation sites can also be associated with transcriptional repression as a result of interactions with different protein complexes[14,29]. Similarly, depending on the degree of methylation, both H3K9 and H4K20 can regulate transcriptional output in different ways. For example, it has been reported that trimethylated H3K9 and H4K20 are specifically enriched at pericentric heterochromatin, whereas mono- and dimethylated H3K9 and H4K20 have been found within euchromatin.[30–32]

An additional intricacy in characterising histone lysine methylation sites and understanding their direct biological impact exists due to crosstalk between these sites with other histone modification as well as DNA methylation.[33,34] An example is given by Sun *et al.*, who demonstrated the importance of H2B ubiquitylation for the recruitment of lysine methyltransferases to methylate H3K4 and H3K79.[35] Many reviews have summarised the observed activity of common histone lysine methylation sites and their biological significance, which provide the reader with further detail.[36–39]

As illustrated in Figure 1.2.2, a vast number of histone lysine methyltransferases ('writers') and demethylases ('erasers') have been identified in the regulation of histone lysine methylation. The catalytic activity of all KMTs except the DOT1 family[40], is based on the presence of the so-called SET domain. KMTs are able to methylate both histone and non-histone proteins.[41] Following the discovery of the first histone lysine demethylases LSD1 in 2004, many other such enzymes have been identified, which can be mainly categorised in two families: the amine oxidases such as LSD1[42] and the JmJC-domain-containing, iron-dependent dioxygenases[43]. While many alternative elements can recruit the lysine modifying KMTs and KDMs such as specific DNA sequences[44,45], non-coding RNAs[46,47] or DNA methylation[48], the co-existence of distinct lysine methylation sites can also direct the activities of these enzymes. For example, PHF8 and JHDM1D are two related human KDMs, which consist of a PHD domain that binds H3K4me3 and a JmJC domain that demethylates either H3K9me2 or H3K27me2. In the presence of H3K4me3, PHF8 demethylates H3K9me2. On the contrary, the

presence of H3K4me3 diminishes the H3K9me2 demethylase activity of JHDM1D directing it towards the demethylation of H3K27me2.[49]

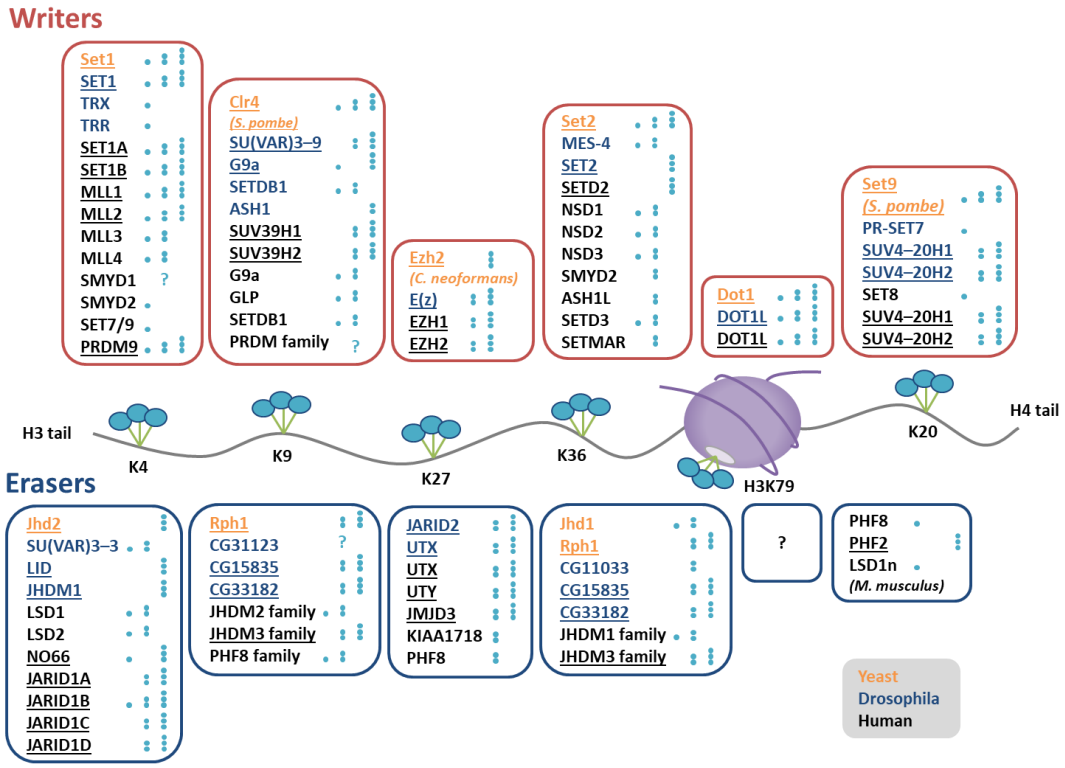

Figure 1.2.2 The principle methylation sites on histone H3 and H4, which can be modified by various histone lysine methyltransferases (writers) or histone lysine demethylases (erasers). The circles next to the enzymes specifies its activity regarding the level of methylation (mono-, di- or tri-). The enzymes underlined are associated with trimethyllysine marks. (Image adapted from Kim *et al.*[39])

Since lysine methylation does not alter the overall charge of the substrate, its immediate effect on the structural remodelling of chromatin is likely minimal. The major function of lysine methylation is instead to act as a docking site for effector proteins, which contain methyl-binding domains triggering downstream effects upon binding.[50,51] The methyllysine reader domains of these effector proteins consist of two to four aromatic residues forming a cage-like structure. As a result of cation–π and van der Waals interactions, the methyllysine substrate inserts into the aromatic cage of the reader domain. Depending on the composition and the size of this cage, distinct methyl reader domains have preferences towards mono-, di- or trimethyllysine sites, which are summarised in Table 1.2.1.[52–54] In addition to the caging effect,

surrounding histone residues and their PTM status can also influence the binding of effector proteins to the methyllysine marks. An example is given by Allis *et al.*, who described that the phosphorylation of serine 10 on H3 impeded the binding of the chromodomain containing HP1 effector protein to the trimethylated H3K9 mark.[55]

Table 1.2.1 List of known methyllysine reader domains and their target methylation site. (Table adapted from Kutateladze *et al.*[53])

Methyllysine reader domains	Methyllysine target
ADD	H3K9me3
Ankyrin	H3K9me2/1
BAH	H4K20me2, H3K9me2
Chromo barrel	H3K36me3/2, H4K20me1
Chromodomain (CD)	H3K9me3/2, H3K27me3/2
Double chromodomain (DCD)	H3K4me3/2/1
HEAT	H4K20me1
MBT	H3Kme1/2, H4Kme1/2
PHD	H3K4me3/2, H3K9me3
PWWP	H3K36me3, H4K20me1/3, H3K79me3
SAWADEE	H3K9me1/2/3
Tandem Tudor domain (TTD)	H3K4me3, H3K9me3, H4K20me2
Tudor	H3K36me3
WD40	H3K27me3, H3K9me3
zf-CW	H3K4me3

The maintenance of histone lysine methylation processes and their biological functions in the cell nuclei is based on a complex network of regulatory players. The precise location of the a single methylation site as well as the degree of methylation are not the only elements contributing to the biological significance of histone lysine methylation, but the co-existence of methylation sites with various methylation levels, the presence of other PTMs, the interplay of KMTs and KDMs, the recruitment process of effector proteins and the interactions with non-histone proteins all factor into the management of cell fate and genomic stability. Hence, dysregulation of these methylation processes can contribute to the generation of many human diseases such as cancer and neurodegenerative and neurological disorders to name a few.[16,56–58] As modulators of lysine methylation, the overexpression, deletion, dysregulation and

mutation of many KMTs and KDMs have been directly associated with the generation of these diseases.[59,60] Even though many KMTs and KDMs have been individually identified as the cause for certain diseases, little is known if any phenotypic changes are based on histone methylation events caused by a cooperation of lysine-modifying enzymes. In addition, while the consequences that alteration of histone lysine methylation has on transcription is widely studied, it is still unclear if the dysregulation of histone lysine methylation has any ramifications on the architecture of chromatin. Beyond transcriptional regulation, the discovery of lysine methylation of non-histone proteins provides a requirement to enhance our understanding of the functional impact of such non-histone methylation.[41,61] Hence, an important focus in the future research of histone lysine methylation will be the development of novel technologies to precisely map the protein methylation and the epigenome. Furthermore, since histone lysine methylation is a dynamic epigenetic mark, it is particularly of interest to investigate lysine methylation levels *in vivo*, which is still a major challenge to date. An overview of existing methods for the profiling of histone lysine methylation will be presented next.

1.3 Profiling of Protein Lysine Methylation

Given the pivotal role of histone lysine methylation for gene regulation in eukaryotic cells, many biological and chemical tools have emerged to profile global methylation levels for diverse histone and non-histone targets. However, it is noteworthy that since lysine methylation only induces a small change in size while maintaining the charge (+1) of the lysine side chains, the mapping of the global methylation profiles (also known as methylomes) becomes challenging and is not straightforward using conventional methods.[62] Therefore, the development of novel techniques to specifically profile methyllysine marks on proteins is continually gaining importance. An overview of the recent biological and chemical approaches to study histone lysine methylation is given below.

1.3.1 The role of chromatin immunoprecipitation in the profiling of protein lysine methylation

One of the most common methods to analyse histone modifications including methylation is chromatin immunoprecipitation (ChIP). The ChIP technique has been widely applied for the localisation of PTMs on histone proteins.[63] The main principle of ChIP is based on the immunoprecipitation step, in which specific antibodies are employed to target the PTM of interest and thus selectively enrich the chromatin fragment containing that PTM.[64] Traditionally, the ChIP experiment was coupled with either PCR amplification or hybridization to investigate the obtained protein-DNA adducts limiting this technique to monitor histone modifications at specific genomic loci.[65] However, with the incorporation of novel technologies such as DNA microarrays (ChIP-chip)[66] and next-generation sequencing (ChIP-seq)[67,68], the mapping of histone modifications was enabled throughout the genome.[69] Two of the biggest applications of the ChIP-seq assay to analyse histone modifications was made by the ENCODE Project Consortium[70,71] and the NIH Roadmap Epigenomics Mapping Consortium[72]. The ChIP assay is displayed in Figure 1.3.1. Upon cross-linking DNA and proteins, the isolated chromatin is fragmented either by sonication or by micrococcal nuclease (MNase) digestion. The chromatin fragments containing the PTM of interest is next collected using specific antibodies in the immunoprecipitation step. After reversing the cross-linking, the released DNA is investigated using various methods (qPCR, microarray, DNA sequencing etc.).

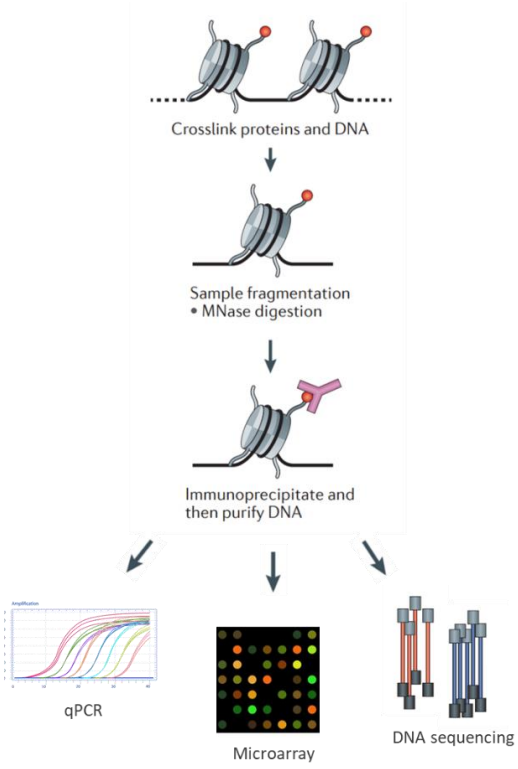

Figure 1.3.1 The procedure of chromatin immunoprecipitation (ChIP) to enrich histone modification, which can then be analysed via various methods. (Top image reproduced with permission from the rights owner, Springer Nature Image.[68])

Even though ChIP has become one of the most established tools to recognize histone modifications, it displays several limitations. In case of histone lysine methylation, the use of antibodies has shown a major drawback due to their poor selectivity towards distinct methylation levels of histone marks (*e.g.* H3K4me3 vs H3K4me2).[73] Consequently, cross-reactivity between distinct epigenetic marks can occur when using antibodies. While assessing the quality of more than 200 antibodies for histone modifications, Lieb *et al.* discovered that specificity issues were found with at least 25% of the commercially available antibodies and more than 20% of these failed in ChIP experiments.[74] In addition, the recognition of a targeted antigen by an antibody can be often affected when a combination of modifications are present on the same histone tail.[75] The need for large sample sizes (~ 1 million cells for the investigation of histone modifications) and the limited resolution are two further restrictions of the ChIP techniques.[76] Alternative immunoassays such as Western blotting[77] and immunofluorescence[78] have been used for the analysis and quantification of histone modifications, however, their dependence on antibodies to enrich the targeted epigenetic marks exhibits the same disadvantages as seen in the common ChIP techniques.

1.3.2 Integration of mass spectroscopy into the investigation of the methylome

The integration of mass spectroscopy (MS) as an analytical tool for the investigation of histone modifications has provided the possibility of simultaneously studying combinatorial epigenetic marks in contrast to the beforementioned antibody-based approaches, which are limited in interrogating individual modification sites. The high sensitivity and accuracy of mass spectroscopy made it successful in discovering many new histone PTMs in a high-throughput fashion.[79–81] Distinct MS methods have been applied in the analysis of histone methylation (see Figure 1.3.2).

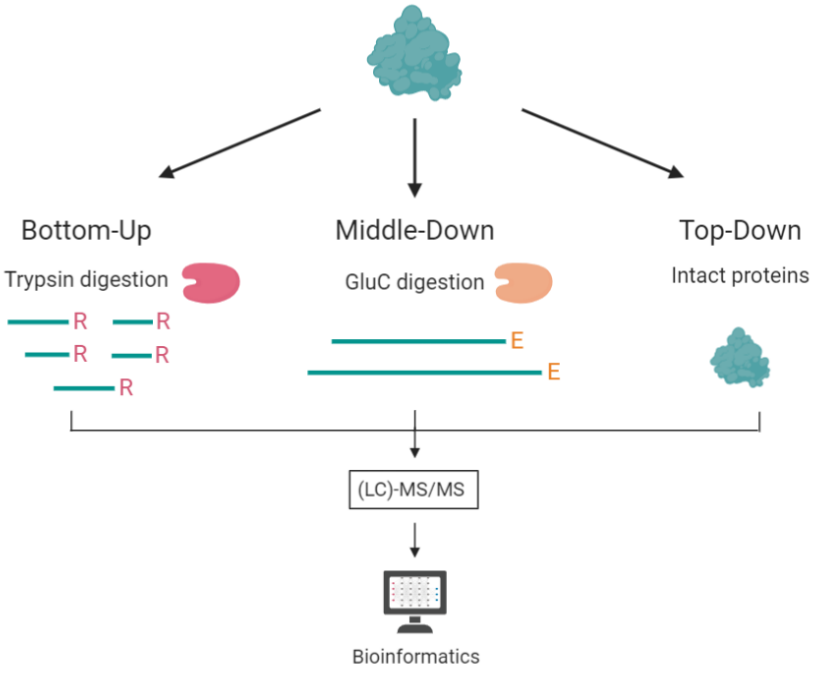

Figure 1.3.2 Bottom-up, middle-down and top-down strategies to study histone proteins via mass spectroscopy. The tryptic peptides obtain in the bottom-up approach can be separated via HPLC prior to their MS/MS analysis.

The top-down approach directly analyses intact histone proteins facilitating a complete view of their PTM network including the methylation levels.[82,83] Additionally, the stoichiometry of all the PTMs can be determined with this approach by incorporating MS profiling and protein fragmentation. However, the top-down MS analysis is restricted to proteins, which have undergone excessive separation and purification processes. Due to the complexity of the full-

length histone proteins and the difficulty in obtaining pure single protein samples, the resolution of the top-down method is limited. The inadequate fragmentation of the entire histone proteins during MS examination results in the unambiguous assignment of PTMs and portrays a barrier for the achievement of full sequence coverage.[84] An improvement in resolution was procured with the use of the middle-down MS approach, in which the histone proteins are digested enzymatically to obtain long histone peptides (> 5 kDa).[85] Since proteases such as Glu-C or Asn-N are able to cleave at less frequently occurring amino acid residues, the middle-down method is able to produce histone tails with combinatorial modifications present. In comparison to the top-down and middle-down approaches, the bottom-up MS method is the most commonly used tool for the analysis of histone modifications due to its high sensitivity. In the bottom-up approach, the PTM-containing histone proteins are enzymatically digested to give peptides, which are subsequently separated by HPLC prior to MS analysis. Due to the decrease in size, the separation of the peptides via HPLC can be performed with much higher resolution resulting in the up to 100-fold enrichment of the peptide sample.[86] In addition, the higher efficiency of the fragmentation of the peptides during MS/MS analysis enables a more precise investigation of the peptide sequence, which is crucial in the identification of isobaric peptides. The high sensitivity of the bottom-up approach only requires small sample sizes, which can be analysed more rapidly using MS/MS than the top-down or middle-down approaches. One major drawback of the bottom-up method is, however, the loss of connectivity due to the proteolysis step resulting in a deprivation of information regarding combinatorial PTMs.

1.3.2.1 The use of antibodies and methyllysine 'reader' domains to enrich lysine methylation marks

Like the beforementioned ChIP techniques, the use of antibodies to specifically recognize and enrich methylated lysine have been also employed in the discovery of histone lysine modification sites by means of MS analysis. To overcome the challenges based on the low quality of an individual antibody for single enrichment as experienced by Mann *et al.*[87], the incorporation of a pool of broadly specific anti-methyllysine antibodies enabled an improved enrichment of the target peptides containing the methylated lysine marks. A set of antibodies against all possible methylation levels of lysine was used by Bonaldi *et al.*, which led to the identification of 74 lysine modification sites.[88] With the use of three antibodies recognizing the

three degrees of lysine methylation, Garcia *et al.* successfully discovered 552 lysine modification sites on 413 human proteins.[89] Nevertheless, the use of antibodies for the enrichment of histone lysine methylation exhibits many obstacles, which were discussed above for the ChIP techniques. An alternative to antibodies is the employment of methyllysine 'reader' domains to recognise and enrich proteins modified by lysine methylation. As described in Subchapter 1.2, effector proteins bind to methyllysine marks through their methyl-binding domains, which specifically recognise the methylated lysine residues and hence can be used in a similar way as anti-methyllysine antibodies. Malignant brain tumor domain proteins (MBTs) have been studied in their specificity to bind methylated histone lysine residues confirming that all MBTs bind mono- and/or dimethyllysine marks on histone proteins through a conserved aromatic cage binding pocket.[90] Gozani *et al.* took advantage of their methyllysine sensitivity and engineered an affinity reagent from the three MBT domain repeats (3xMBT) of L3MBTL1 to recognize and enrich mono- and dimethyllysine modifications (see Figure 1.3.3 **A**, for structural details).[91] With 3xMBT as an enrichment reagent, Gozani and co-workers identified several hundred proteins from HEK 293T cells, of which, however, methylated lysine was directly discovered on only 26 proteins.[92,93] Nevertheless, the incapability to distinguish between methylation sites on individual lysine residues and between the different degrees of methylation (mono- and di-) portrays a great limitation of the protocol developed by Gozani and his group.[92] Additionally, the 3xMBT domain does not recognize trimethyllysine marks.

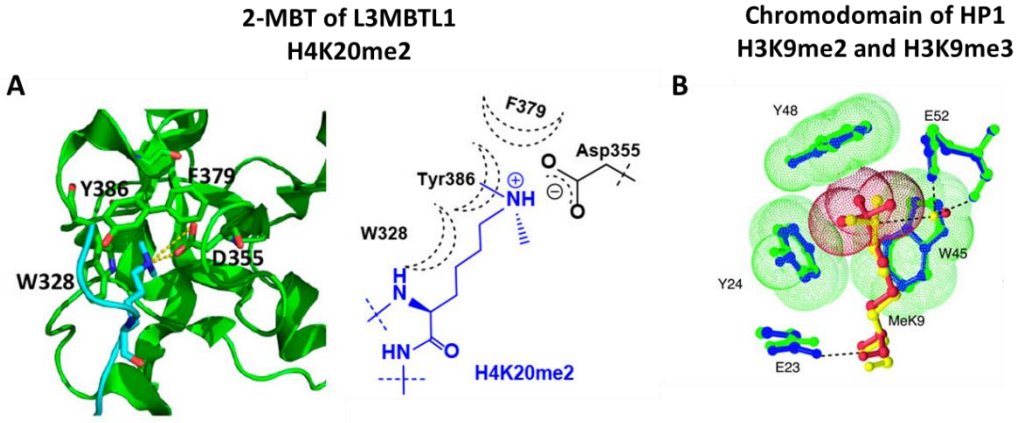

Figure 1.3.3 Structure of the methyllysine reader domain of L3MBTL1 (A) and HP1 (B) bound with the lysine substrate. ((A) Reprinted (adapted) with permission from M. Luo. Chemical and Biochemical Perspectives of Protein Lysine Methylation. *Chem. Rev.,* 2018, 118, 6656–6705. Copyright (2018) American Chemical Society [62]; (B) Image reproduced with permission of the rights holder, The American Association for the Advancement of Science.[94])

With the structural characterisation of the chromodomain of the heterochromatin-associated protein 1 (HP1), which is a known methyllysine reader domain to recognize dimethyl- and trimethyl marks on H3K9 (see Figure 1.3.3 **B**)[94], Li *et al.* developed an additional enrichment reagent for proteomic pull-down experiments by covalently linking the chromodomain of recombinant HP1*β* to carboxyl magnetic beads.[95] Li and co-workers identified 109 proteins in HEK 293T cells *in vitro* using this chromodomain-based affinity reagent, of which 29 were methylated on 40 lysine residues. Since no control experiment using an inactive version of the enrichment reagent was performed, it was questioned if all the detected proteins were based on the interaction of presumably existing di- or trimethyllysine marks with the chromodomain.[62,95]

1.3.2.2 *In vivo* isotopic chemical labelling of histone residues

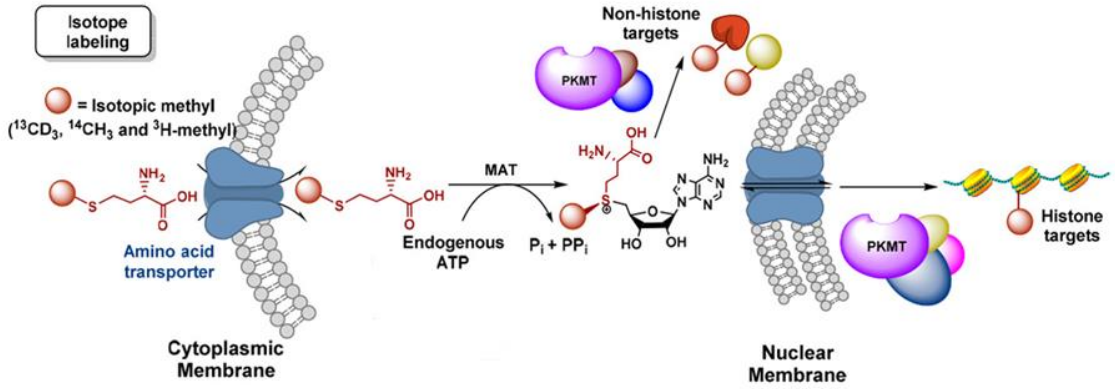

Figure 1.3.4 Isotope labelling of histone proteins *in vivo*. (Reprinted (adapted) with permission from M. Luo. Chemical and Biochemical Perspectives of Protein Lysine Methylation. *Chem. Rev.,* 2018, 118, 6656–6705. Copyright (2018) American Chemical Society.[62])

As previously described, the methylation of the lysine residues on histone tails is installed by histone methyltransferases, which transfer the sulfonium methyl group of the SAM co-factor to the lysine substrate. With the aim of improving the global profiling of histone lysine methylation, chemical labelling has been introduced using isotopic isosteres of the SAM co-factor.[96] Accordingly, heavy methyl groups such as CD_3, $^{13}CD_3$, CT_3 and $^{14}CH_3$ have been added to the sulfonium side chain of SAM with the objective of transferring these heavy chemical labels to the lysine residues on histone tails by means of histone methyltransferases.

Due to the poor membrane permeability of SAM, the application of heavy-methylated SAM co-factors for labelling of histone tails is restricted to *in vitro* experiments. A solution around this problem was found by taking advantage of the biosynthetic pathway for the formation of the SAM co-factor *in vivo* (see Figure 1.3.4). Methionine adenosyltransferases (MATs) are enzymes, which bio-synthesise SAM from endogenous ATP and methionine.[97] By introducing the isotopic label on the methionine precursor, these modified amino acid precursors can then be absorbed into living cells and processed by MATs to synthesise heavy-labelled SAM, which then targets the labelling of histone lysine residues.

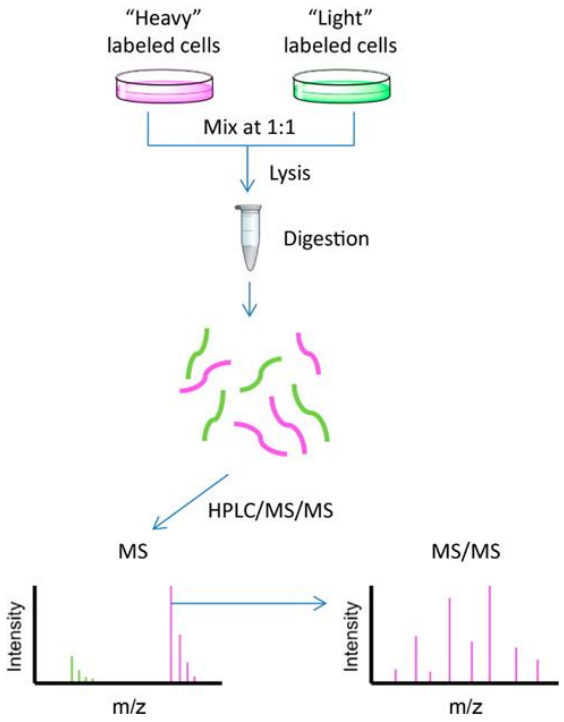

Figure 1.3.5 The procedure of the SILAC assay. (Reprinted (adapted) with permission from H. Huang, *et al.* Quantitative Proteomic Analysis of Histone Modifications. *Chem. Rev.*, 2015, 115, 2376–2418. Copyright (2015) American Chemical Society.[86])

A modified version of the Stable Isotope Labelling by Amino acids (SILAC) assay has been developed incorporating the metabolic labelling method for a quantitative proteomic analysis of histone methylation.[87] As illustrated in Figure 1.3.5, two cell populations are incubated with methionine ('light'-labelled) and isotopically labelled methionine ('heavy'-labelled), respectively, leading to the correspondingly 'light'- and 'heavy'-labelled histone lysine residues via the metabolic pathway summarised in Figure 1.3.4. The resulting samples are

combined, processed and analysed via MS/MS. The targeted histone residues can be characterised unambiguously by identifying the pair of light- and heavy-labelled products. In addition, the evaluation of the isotopic ratios of the obtained histone residues provides a quantitative analysis of the samples using MS.

Ever since Ong and Mann revolutionized the quantitative discovery of methylation sites with the SILAC method[98] and displayed its success through the identification of 59 methylation sites in HeLa cells[87], many examples followed applying the SILAC assay for the analysis of histone PTMs including methylation.[99–101] By means of the SILAC method, Van Oostrum *et al.* demonstrated the dependency of histone methylation on the cell cycle.[102] Van Oostrum and co-workers discovered that the methylation of the lysine residues K27 and K36 on histone H3 were decreased during the G2/M phase, whereas the methylation of K20 on histone H4 was increased highlighting the presence of dynamic changes of PTMs during mitosis. Mizzen *et al.* combined the SILAC method with the top-down MS approach to analyse the methylation of K20 on histone H4 revealing that the K20 residue on newly synthesised H4 histone proteins are progressively methylated during the G2, M and G1 phases of the cell cycle.[103] The metabolic labelling approach using heavy-labelled methionine was incorporated by Fodor *et al.* for the investigation of the relation of the Jmjd2b hydroxylase with distinct lysine methylation levels.[104] Zee *et al.* investigated the site-specific histone lysine methylation dynamic by combining the SILAC-based heavy-methyl labelling method with HPLC-MS/MS examination.[100] Studying the kinetics of residue-specific histone methylation, they have shown that the mono-, di- and tri-methylation of residues have progressively slower rates. In addition, the methylation associated with active genes possesses faster rates than those related to repressive genes.

1.3.2.3 Chemical labelling of lysine residues via chemical derivatisation assays

Chemical derivatisation is an alternative method to chemically label lysine residues on histones without the aid of enzymes. The high abundance of basic residues like lysine and arginine displays a challenge for the widely used bottom-up MS technique. The proteolytic digestion of the histone samples by trypsin leads to the generation of numerous highly charged small peptides, which are difficult to retain on the reverse-phased columns of HPLC instruments. Trypsin is known to cleave the amide bond at the carboxylic side of unmodified lysine and

arginine residues, however, residual cleavage after monomethylated lysine residues has also been observed. In addition, the presence of lysine PTMs such as acetylation and higher order methylation prevents proteolysis by trypsin, which means that depending on the state of histone modification trypsin digest can lead to the generation of peptide sequences with varying lengths.[62] Even though an alternative protease such as ArgC, which only cleaves at arginine residues without the influence of lysine methylation might overcome these challenges, however, additional obstacles might arise for the MS analysis of the resulting peptides due to the lower efficiency and specificity of ArgC. Chemical derivatisation was introduced to circumvent these problems, in which lysine residues on histones were chemically modified prior to trypsin digestion (see example in Figure 1.3.6).[105]

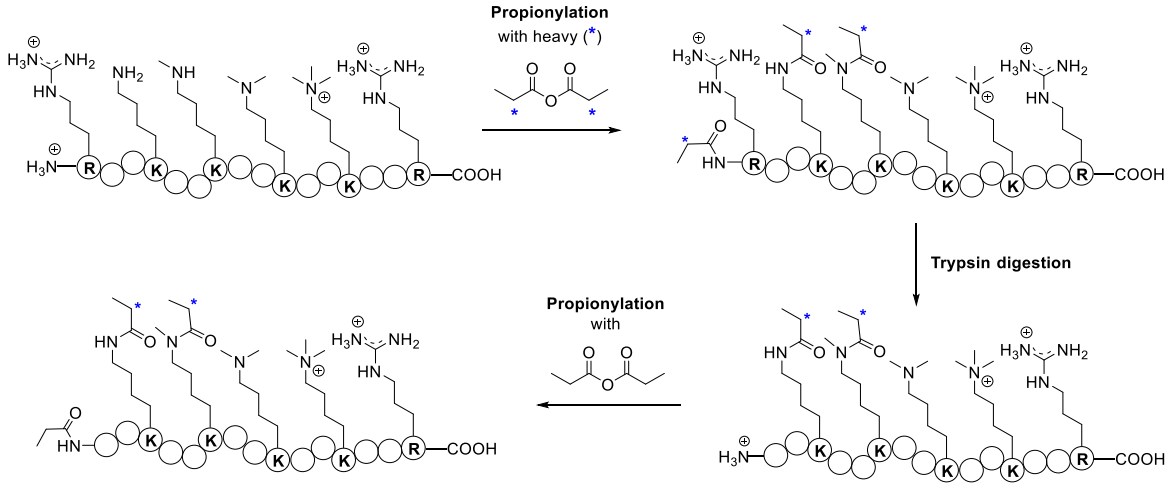

Figure 1.3.6 An example of chemical labelling of lysine residues with heavy (*) and light propionic anhydride. The relative MS ratios of light and heavy isotope masses are used for MS quantification.

Commonly used derivatisation reagents are propionic anhydride (propionylation as displayed in Figure 1.3.6)[105–107] or acetic anhydride[108,109], which transfer an acyl group to the unmodified and monomethylated lysine residues on histones. Reductive amination has also been performed using formaldehyde and sodium borohydride to chemically label lysine residues.[110] By introducing chemical derivatisation into the workflow of the bottom-up MS method, the tryptic proteolysis is conducted in a more homogeneous protein sample by preventing cleavage at all lysine sites with or without prior PTMs. Peptides with initially similar masses can also be

differentiated with the treatment of derivatising reagents. The blocking of the basic lysine residues additionally reduces the charges of the resulting peptides, while improving their chromatographic retention and their ionization efficiency. Regula *et al.* combined the chemical derivatisation method with isotopic labelling by using deuterated acetic anhydride to quantitatively analyse PTMs of histone proteins isolated from developing Drosophila embryos.[111] A similar approach was taken by Tackett *et al.*, who employed deuterated formaldehyde in the reductive amination of lysine residues to label the lysine amines with heavy methyl groups. This approach did not only enable a clear differentiation of the derivatising methyl labels from the prior states of lysine methylation, but it facilitated a quantitative analysis of the activity of the lysine demethylases LSD1.[110] Garcia *et al.* developed an additional isotope derivatisation procedure for the characterisation of histone modifications of proteins extracted from HeLa and yeast cells using deuterated propionic anhydride (such as the example given in Figure 1.3.6).[107] They expanded the effectiveness of this methodology by using it in combination with enzymatic knockdown experiments for the analysis of histone crosstalk events.[112] As expected, the knockdown of the lysine methyltransferases G9a and GLP1 resulted in the decrease of mono- and dimethylated H3K9 marks, however, Garcia and his team revealed that the depletion of these enzymes also effected H3K14 and H3K79 methylation, which are not direct methylation sites for G9a and GLP1 suggesting a histone PTM cross-talk amongst these sites on H3.

A drawback of the most common chemical derivatisation reagents such as propionic anhydride is the significant decrease in the ion abundance of the treated peptides, which is likely based on the occurrence of side reactions during the procedure. Due to the high abundance of nucleophilic sites in histone proteins such as serines or tyrosines, the chemical derivatisation procedure using anhydride reagents can lead to uncontrolled *O*-acylation reactions challenging the accurate profiling of histone PTMs. Yi *et al.* made a first step in tackling this obstacle with the synthesis of the *N*-hydroxysuccinimdyl propionate (NHS-propionate) reagent to use for the chemical derivatisation of lysine residues, which showed great initial success in preventing side reactions, especially with the development of a competitive inhibiting strategy.[113] Nevertheless, further optimisation of other chemical derivatisation protocols is needed to improve the efficiency and specificity of this procedure and simplify to the MS analysis of histone proteins and their PTMs.

1.3.2.4 Chemical labelling of histone residues using activity-based probes

Weinhold and co-workers transformed the SAM co-factor into an activity-based probe by replacing the methyl group on the sulfonium side chain by a clickable pent-2-en-4-ynyl moiety.[114] The modified SAM analogue (EnYn-SAM) was then utilized to transfer the clickable alkyne moiety to the target lysine residues with the aid of native histone methyltransferases (see Figure 1.3.7). Weinhold *et al.* validated the activity of the EnYn-SAM substrate by showing that they can be used by distinct enzymes (Dim-5, MILL1, MILL4) for target labelling.

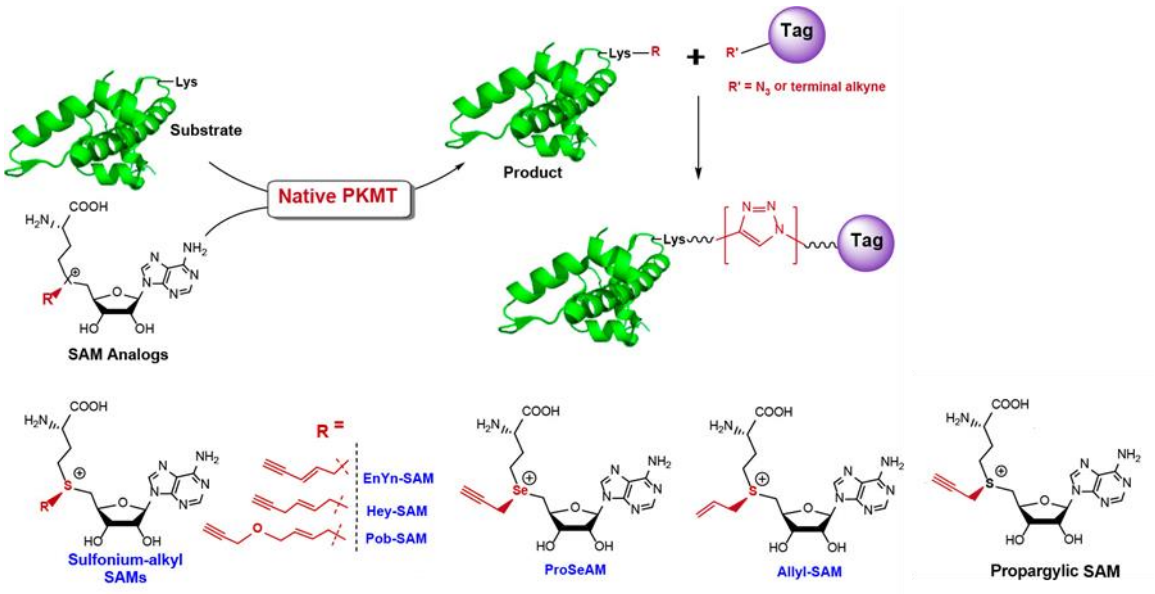

Figure 1.3.7 The library of activity based probes used for the alkylation of histone proteins. (Reprinted (adapted) with permission from M. Luo. Chemical and Biochemical Perspectives of Protein Lysine Methylation. *Chem. Rev.,* 2018, 118, 6656–6705. Copyright (2018) American Chemical Society[62])

Expanding the library of clickable SAM analogues, Luo *et al.* synthesised four additional SAM analogues including allyl-SAM with an alkene handle, Hey-SAM, Pob-SAM and propargyl-SAM (illustrated in Figure 1.3.7) and screened them against eight human PMTs (PRMT1, PRMT3, CARM1, SUV39H2, SET7/9, SET8, G9a and GLP1).[115] The allyl-SAM analogue was proven to be active towards native SUV39H2, G9a and GLP1, however, no activity was found for the bulkier SAM substrates (Hey-SAM, EnYn-SAM and Pob-SAM) against the tested enzymes. Surprisingly, propargyl-SAM did not depict any activity either, although it is

similar in size and structure to the allyl-SAM analogue. The observed inactivity of the propargyl-SAM analogue was found to be a question of stability, since at physiological pH it displayed a half-life shorter than 1 min.[116] The groups of Weinhold[117] and Luo[116], respectively, overcame the stability issues of the propargyl-SAM analogue by replacing sulfonium with selenium resulting in the formation of propargylic *Se*-adenosyl-selenomethionine (ProSeAM). By changing to selenium, the propargylic ProSeAM displayed activity towards native SUV39H2, G9a and GLP1, which was consistent with allyl-SAM.

The examples given above have demonstrated the feasibility of converting the SAM co-factor into an activity-based probe to evaluate the activity of PMTs and to label target lysine residues with clickable alkyl moieties. However, the activity of the synthesised SAM analogues towards native PMTs are generally low or non-existent. A major challenge is the bulk of the alkyl moieties of the modified SAM co-factors, which cannot be accommodated by native PMTs due to the size of their SAM-binding pocket. Additionally, uncontrolled labelling of distinct residues can occur in living cells, since a vast number of different PMTs are present and thus they are able to consume the modified SAM analogues for the labelling of their residues leading to an overall low labelling of the target substrate. To overcome these challenges, an alternative technology was applied for the analysis of the lysine methylome, which is biorthogonal profiling protein methylation (BPPM).

1.3.2.5 Bioorthogonal profiling protein methylation technology for the analysis of lysine methylomes

In the BPPM method, the SAM-binding pocket of native PMTs is engineered to process bulkier SAM-analogues eliminating the challenges experienced due to steric hindrance. A general scheme explaining the BPPM approach is shown in Figure 1.3.8. By mutating the PMT of interest to specifically accommodate the designed bulkier SAM analogue, the BPPM approach allows the identification of the labelled target substrates via either visualisation with clickable fluorescent dyes or enrichment using clickable biotin probes followed by MS proteomic analysis.

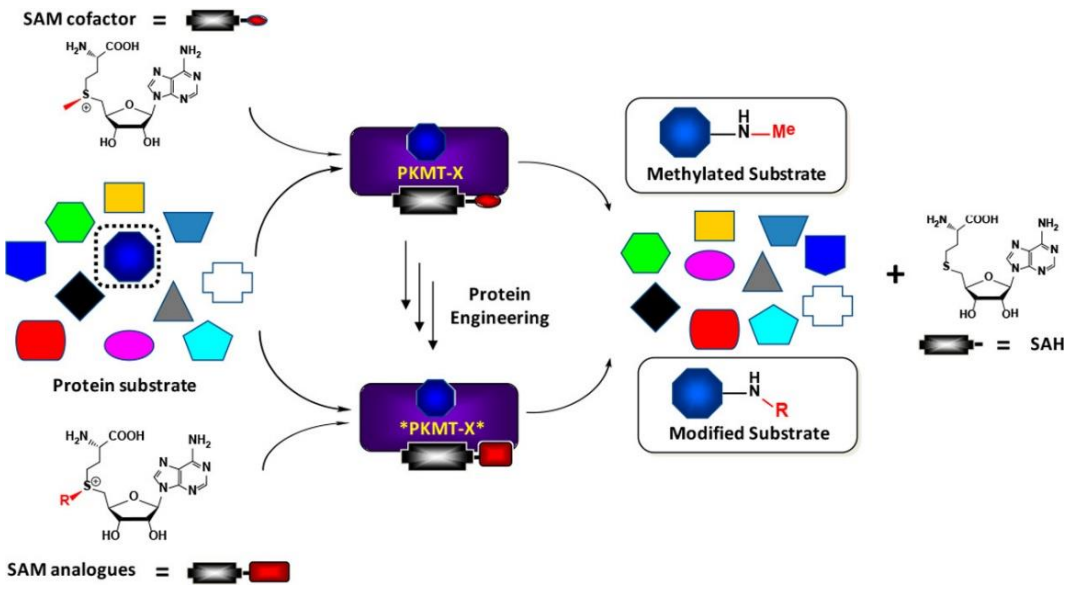

Figure 1.3.8 General scheme of the bioorthogonal profiling protein methylation (BPPM) technology. (Reprinted (adapted) with permission from M. Luo. Chemical and Biochemical Perspectives of Protein Lysine Methylation. *Chem. Rev.,* 2018, 118, 6656–6705. Copyright (2018) American Chemical Society.[62])

An early example for the successful application of the BPPM method (also known as the 'bump and hole' approach) to label target lysine residues was demonstrated by Luo *et al.*.[118] After screening the activity of a library of clickable SAM analogues towards a range of mutant G9a enzymes, Luo and colleagues discovered that both EnYn-SAM and Hey-SAM (structures are given in Figure 1.3.7) were active towards the Y1154A mutant of G9a. When these modified SAM analogues were used in combination with native G9a, no labelling of the target substrate occurred confirming their loss of activity. In order to determine the influence of unmodified SAM and native G9a to the activity of Hey-SAM-mutant G9a pair, Luo and co-workers performed a competition assay incubating a 1 : 1 mixture of native G9a and mutant G9a (Y1154A) with the physiological concentration of SAM and Hey-SAM (50 μM). As a result, a 1 : 1 product ratio of dimethylated and (E)-hex-2-en-5-ynylated peptides digested from H3 proteins was obtained confirming that Hey-SAM was able to efficiently label the target substrate even in the presence of native G9a and unmodified SAM.

Following on this study, Luo and his group synthesised an alternative modified SAM analogue, Ab-SAM (4-azidobut-2-enyl SAM), which replaced the clickable alkyne functional group by an azide group (see Figure 1.3.9).[119] Selective mutation of various sites of the EuHMT1/2 (GLP1 and G9a) was performed and these mutant enzymes were screened against

the Ab-SAM analogue to determine labelling of H3. As seen in Figure 1.3.9 **A,** (a), only the EuHMT1 (GLP1) protein containing the Y1211A mutation showed activity towards Ab-SAM, while having minimal activity against the unmodified SAM.

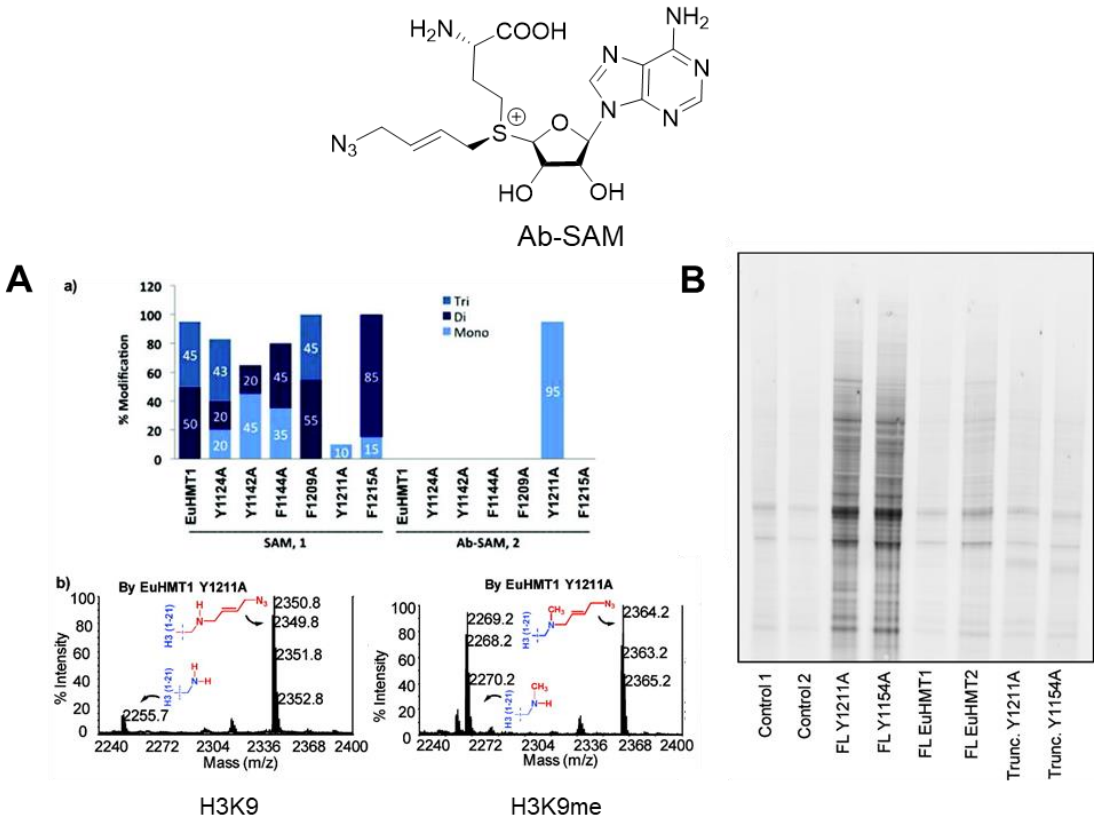

Figure 1.3.9 Labelling of histone targets with Ab-SAM using the BPPM technique. A: (a) Modification % of H3 peptide by engineered EuHMT1 with native SAM (left) or Ab-SAM (right) as co-factors; (b) MS spectra of 4-azido-2-butenylation of the H3K9 (left) and H3K9me (right) peptide by the Y1211A mutant. B: BPPM of native EuHMT1/2, their corresponding mutants and truncated EuHMT1/2 mutants (only catalytic domains) visualised with in-gel fluorescence. (Reprinted (adapted) with permission from K. Islam, *et al.* Bioorthogonal profiling of protein methylation using azido derivative of *S*-adenosyl-L-methionine. *J. Am. Chem. Soc.*, 2012, 134, 5909–5915. Copyright (2012) American Chemical Society.[119])

The interactions between Ab-SAM and the mutant GLP1 proteins were evaluated upon detecting the alkylated target substrate (see (b) in Figure 1.3.9 **A**). Native EuHMT1 specifically transfers the methyl group of the unmodified SAM to give the di- and trimethyl product.

Mutation of EuHMT1 has shown that the specificity for di- and trimethylation is shifted towards mono- and dimethylation as demonstrated in Figure 1.3.9 **A**. Evaluating the specificity of the Y1211A mutant in combination with Ab-SAM, only the mono-alkylated product was detected, which is a common limitation in the use of bulky SAM analogues. Analogously, the same observations were made with the investigation of Ab-SAM in combination with the EuHMT2 (G9a) protein, which is visualized with in-gel fluorescence as shown in Figure 1.3.9 **B**.

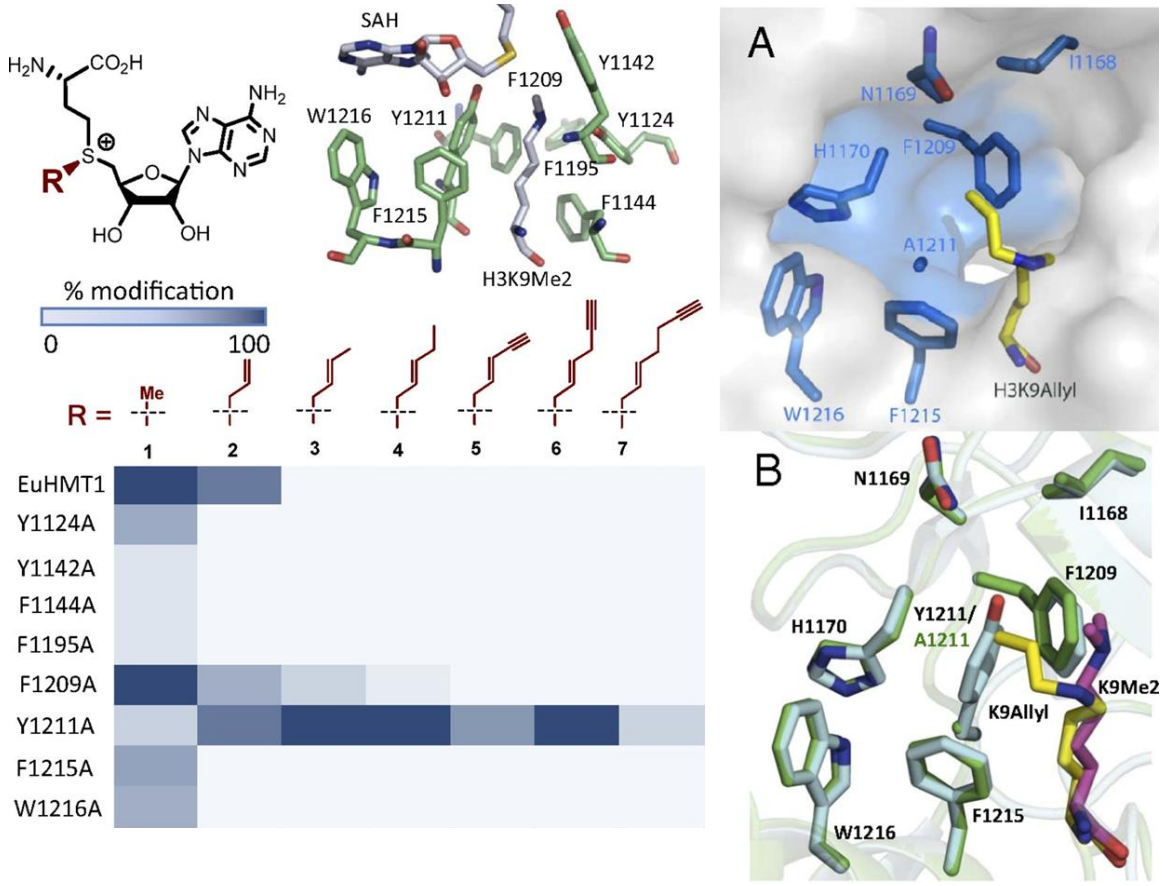

Figure 1.3.10 A library of SAM analogues investigated in combination with numerous EuHMT1 mutants (left) via the BPPM assay. Structural characterization of the Y1211A mutant of EuHMT1 in complex with SAH and the H3K9 peptide containing the allyl label (right). (Reprinted (adapted) with permission from K. Islam, *et al.* Defining efficient enzyme–cofactor pairs for bioorthogonal profiling of protein methylation. *Proc. Natl. Acad. Sci. U. S. A.,* 2013, 110, 16778-16783. Copyright (2013) National Academy of Sciences.[120])

The examples given above are proof-of-concept that the BPPM method can be utilised for the analysis of histone lysine methylation. In a later publication, Luo *et al.* generalised the application of the BPPM method to profile the methylomes of EuHMT1/2 identifying over 500 target substrates.[120] Luo and co-workers expanded the library of bulky SAM analogues to be investigated alongside a range of mutant EuHMT1/2 proteins as shown on the left of Figure 1.3.10. A closer structural examination of the SAM-binding pockets was performed in this study, which revealed that the previously confirmed specificity of both the Y1211A mutant of EuHMT1 and the Y1154A mutant of EuHMT2 towards the bulky SAM analogues was due to gained accessibility of pre-existing hydrophobic cavities (see Figure 1.3.10 **A** on the right side). The tyrosine residue at those positions in the native EuHMT1/2 proteins acts as a gatekeeper preventing the interaction of the bulky SAM analogues with the target substrate. In addition, Luo and his team have shown that the complex consisting of the Y1211A mutant and the allylated H3K9 substrate is superimposable with the complex consisting of the native EuHMT1 and the dimethylated H3K9 peptide (see Figure 1.3.10 **B** on the right side). The only differences in the interaction of these complexes were found in the area adjacent to the Y1211A mutation. The allylated H3K9 peptide displayed a slightly bended carbon side chain of Lys9 and the Y1211A mutation led to the loss of hydrogen bonding interactions with the Y1211 residue. Nevertheless, Luo *et al.* inferred that these observations confirm that the undertaken single point mutation expands the SAM-binding pocket without reducing the substrate specificity of these proteins.

A major advancement on the applicability of the BPPM technology was made by Luo and his group with the development of the CliEN-seq technology for the genome-wide profiling of chromatin methylation in living cells.[121] Figure 1.3.11 displays the procedure of CliEN-seq, which is based on three main step: (1) the biosynthesis of the clickable SAM analogue from the corresponding cell-permeable methionine analogue by an engineered MAT enzyme; (2) the *in situ* labelling of the target substrate by an engineered PMT enzyme; (3) the target enrichment by using an azide-biotin conjugate and the subsequent analysis of modified chromatin via sequencing. Luo and co-workers have shown that histone H3 and other chromatin targets were able to get labelled using the Hey-SAM analogue (see structure in Figure 1.3.7) in combination with G9a and GLP1 mutants *in vivo*.[121] The CliEN-seq technology not only allows an effective enrichment of the modified targets by means of an azide-alkyne click reaction, but it also enables the retracement of the identified targets to specific PMTs, since they do not accommodate other SAM analogues including native SAM. By using the CliEN-seq method in

living cells, it additionally provides the possibility to investigate dynamic methylation events, although it is expected that the alkylated target substrates are more stable against a possible removal by protein demethylases. In contrast to ChIP-seq, which is a widely used antibody-based method for genome-wide profiling of histone modifications (see Subchapter 1.3.1), the CliEN-seq technology is able to distinguish the lysine-modifying activities of closely related PMTs.

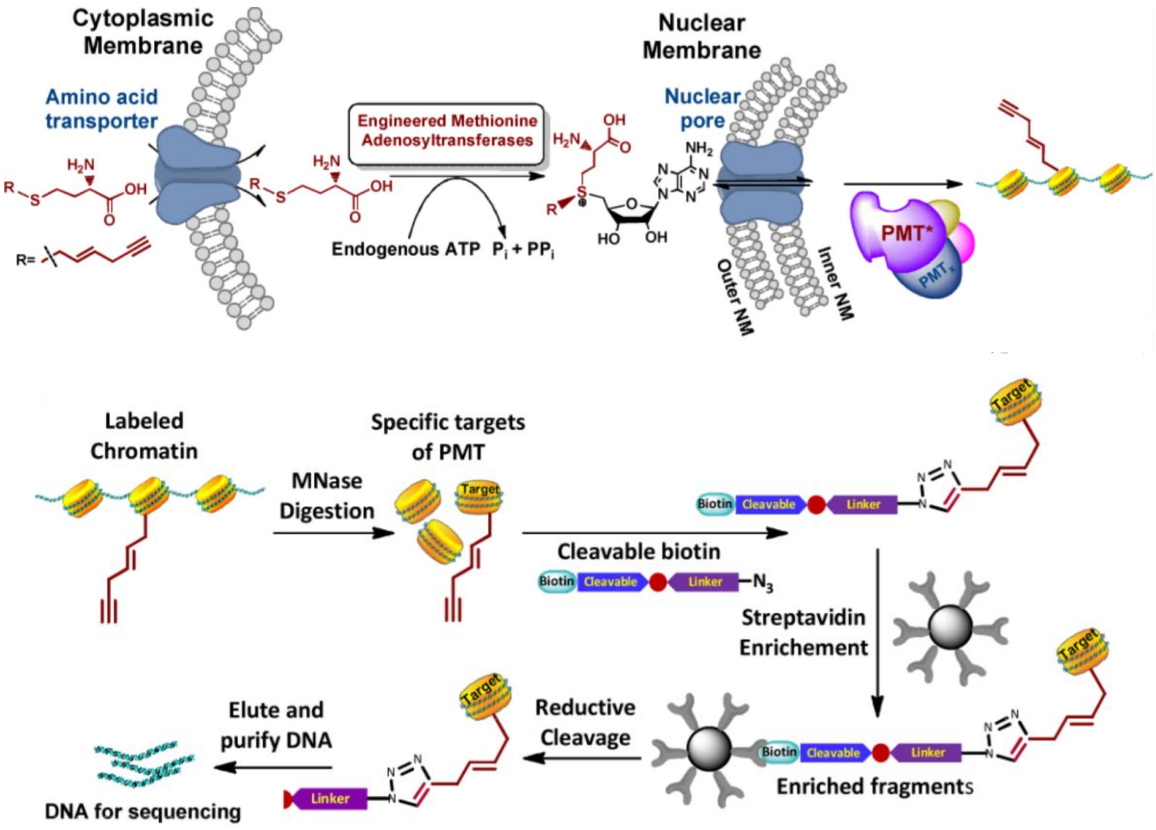

Figure 1.3.11 The procedure of CliEN-seq, a technology to probe chromatin methylation in living cells. (Reprinted (adapted) with permission from R. Wang, *et al.* Profiling Genome-wide Chromatin Methylation with Engineered Posttranslation Apparatus within Living Cells. *J. Am. Chem. Soc.*, 2013, 135, 1048–1056. Copyright (2013) American Chemical Society.[121])

Although the BPPM method allows the selective analysis of the activity of a certain PMT in a pool of many, it is limited by the prior knowledge of the structure of that particular PMT. In addition, it is unknown if the modification of the PMTs has any effects on their interactions with other proteins. The size of the alkyl-SAM analogue only allows the monitoring of the

engineered enzyme's activity responsible for mono-alkylation, since di- and tri-alkylation are impeded due to steric hindrance. The transfer of the bulky alkyl group onto the target lysine residue may disrupt the dynamic nature of the usual methylation events as it is uncertain if these alkylated marks can be reversed with common demethylases. Similarly, the recognition of these sites by effector proteins, which usually target methyllysine marks with their methyllysine reader domains may be hindered leading to significant changes in downstream cellular events. The crosstalk between lysine methylation sites and other PTMs and their importance in the generation of distinct PTMs and the recruitment of regulatory proteins have been displayed. Consequently, the alkylation of lysine residues may additionally interrupt the communication of the traditional PTMs leading to an overall change of the modification environment of the histone proteins.

1.4 Project Overview

With many open questions remaining in the understanding and localisation of histone lysine methylation sites on histone complexes, this project proposes the development of CLICK-seq, a novel chemical biological tool to map combinatorial histone lysine trimethylation (Kme_3) throughout the genome. CLICK-seq stands for the selective enrichment of target histone substrates by means of 'click' chemistry, which is followed by sequencing as the readout. As displayed above in the overview of the common techniques to profile the methylome, great challenges in specificity and efficiency have been experienced in the enrichment of histone lysine methylation due to the use of biological methods such as antibodies. The use of modified SAM analogues for the introduction of clickable handles on the target substrates have improved the issue of specificity in the enrichment of the histone sample by 'clicking' an affinity tag for pulldown experiments. However, the difficulty in incorporating the clickable handle and the disruption of native epigenetic processes of the nucleosomes *in vivo* (*e.g.* demethylation by KDMs or binding of effector proteins), which may lead to loss of information and hence to an inaccurate profiling of the methylome are major obstacles, which have not been overcome yet. In addition, these profiling techniques target single epigenetic marks and they do not address the importance of the co-existence of several PTMs on histone complexes.

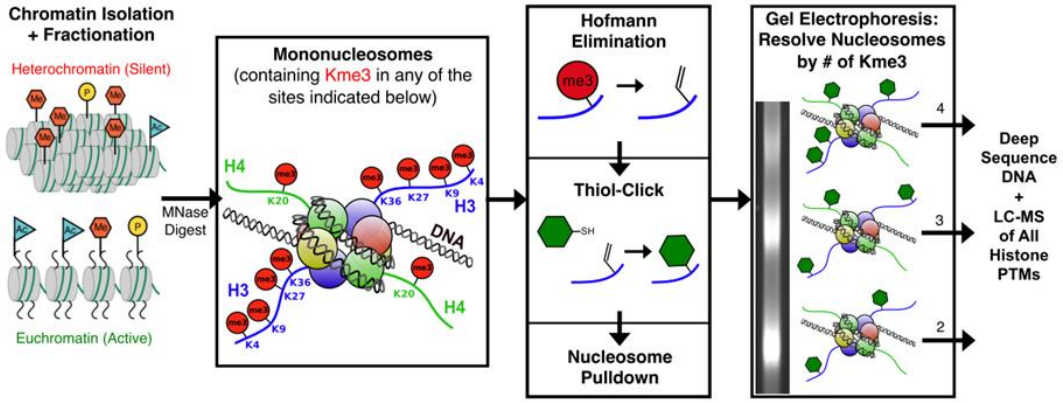

Figure 1.4.1 CLICK-seq: A novel chemical biological tool to map combinatorial histone lysine trimethylation on intact mono-nucleosomes.

CLICK-seq is designed to overcome these challenges firstly by directly modifying lysine methylation marks to form clickable alkene handles, which can be used for the introduction of affinity tags and thus for the enrichment of the histone substrates and secondly by providing a platform to analyse combinatorial PTMs on intact mono-nucleosomes rather than on individual

histone proteins. The procedure of the originally proposed CLICK-seq technique is illustrated in Figure 1.4.1. After the isolation and fractionation of chromatin from the cell nuclei, the trimethylated marks will undergo elimination to obtain the alkene residues on the mono-nucleosomes. The introduction of a chemical handle via a thiol-ene click reaction will allow the subsequent pulldown and separation of the modified mono-nucleosomes depending on their amount of lysine methylation marks. The purified mono-nucleosomes can then be analysed by mass spectroscopy and DNA sequencing to characterise combinatorial trimethyllysine marks and their co-existence with other PTMs.

The main aim of this project is to investigate chemical reactions to induce the elimination of trimethylamine and the subsequent generation of the terminal alkene in sensitive biological systems, which is the most important step of the CLICK-seq technique. Since the Hofmann elimination is a widely known reaction for the base-catalysed elimination of quaternary ammonium salts, it is chosen as a starting point. However, the classical Hofmann elimination is based on high temperatures (examples up to almost 300 °C) and strong bases, which is not feasible for its application on sensitive biomolecules. Consequently, the goal of this project is the screening of elimination conditions on model small molecules to determine protein-compatible conditions to induce the elimination of trimethylamine (temperature < 100 °C) and then to apply this reaction onto model peptides and ultimately proteins taking first steps towards the development of a MS protocol for the chemical modification of trimethyllysine residues. The research undertaken towards the discovery of mild reaction conditions for the desired site-specific chemical modification of histone proteins is discussed in Results and Discussion I.

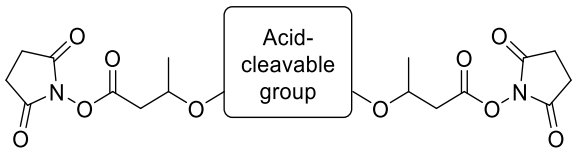

Figure 1.4.2 Acid-cleavable cross-linker for XL-MS experiments.

In addition, the aim of a secondary project is the design and synthesis of a small library of cross-linkers with various acid-labile linker groups (see structure in Figure 1.4.2) for cross-linking mass spectroscopy (XL-MS) experiments. These compounds will be used as both a cross-linker to covalently-tether protein complexes and a derivatising reagent for the chemical modification of lysine residues upon acid-catalysed cleavage. A brief introduction to the background of this side project as well as our synthetic effort towards the generation of an acid-cleavable cross-linker are displayed in Results and Discussion II.

2 RESULTS AND DISCUSSION I – SITE-SPECIFIC CHEMICAL MODIFICATION OF HISTONE PROTEINS

2.1 Hofmann elimination of quaternary ammonium compounds

2.1.1 Background: Introducing the Hofmann elimination reaction

Hofmann Elimination is a *β*-elimination involved in a heterolytic bond breaking leading to the formation of carbon-carbon double bonds, which was discovered by August Wilhelm von Hofmann in 1851.[122,123]. Hofmann analysed the thermolytic decay of tetraethylammonium iodide by firstly trapping the iodide counterion with silver(I) oxide and secondly heating the isolated ammonium hydroxide salt to identify the decomposition products of the molecule.[122] Upon reaching high temperatures, Hofmann identified that tetraethylammonium hydroxide decomposes into triethylamine, ethene and water (see Scheme 2.1.1), a chemical modification today known as Hofmann elimination. 30 years after his initial two publications on the Hofmann elimination, Hofmann published two additional papers on the thermal decomposition of other ammonium bases, which led to the widespread use of this reaction.[124,125]

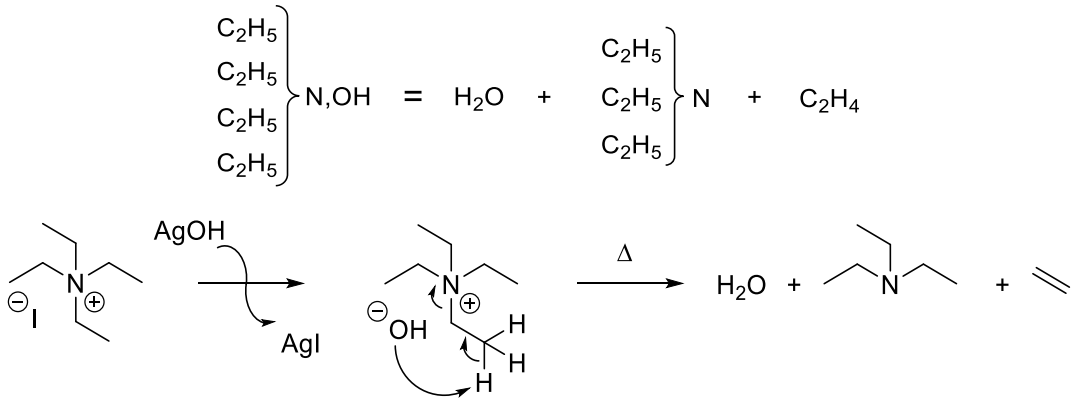

Scheme 2.1.1 The original Hofmann elimination scheme as illustrated by A.W. Hofmman (above) and the mechanism of the Hofmann elimination (below).

Today, the Hofmann elimination is generally known as the elimination of trialkylamine from tetrasubstituted ammonium substrates using a base and high temperatures to give alkenes as products.[126] As the name of the reaction suggests, the Hofmann elimination follows

predominantly the Hofmann rule meaning that the base B abstracts the *β*-hydrogen from the least substituted carbon forming the least substituted alkene as the product. In general, the following features have been discovered to favour the Hofmann rule: (1) poorer and/or positively charged leaving groups on the starting material, (2) stronger bases used for the proton removal,[127] and (3) the use of sterically-hindered bases and reactants[128]. Since the Hofmann elimination involves the removal of a poorer and bulkier leaving group and the acidity of the *β*-hydrogen to the leaving group is in general higher on primary carbons than secondary and tertiary carbons and it is particularly increased by the positively charged ammonium functionality in the molecule, it additionally confirms that the reaction obeys the Hofmann rule.[129] The Hofmann elimination follows the E2 mechanistic pathway undergoing an *anti*-elimination with the leaving groups being positioned antiperiplanar (see Scheme 2.1.2).[130]

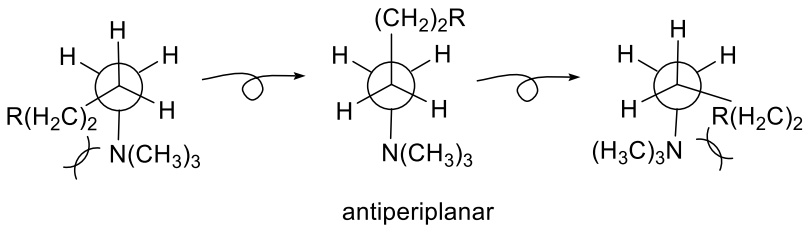

Scheme 2.1.2 Newman projections to demonstrate the preference of anti-elimination in the Hofmann reactions.

The mechanism of the Hofmann elimination was established by Hughes, Ingold and Patel in 1933.[131] The nature of the base and its behaviour in various solvents regarding ionization, aggregation and counterion identity influence not only the mechanism, through which the elimination occurs, but also the regiochemistry and the stereochemistry of the reaction.[132]

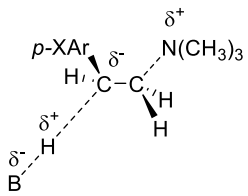

Figure 2.1.1 Distorted transition state reported by Fry *el al.*[133] to demonstrate the possibility of an E2 elimination with an E_{1cb} character for the Hofmann elimination.

Subsequent studies, however, have incorporated the theory of fluid transitions states and demonstrated that depending on the structure of the substrate the mechanism of the Hofmann elimination can be shifted towards a more carbanionic transition state leading to an E2 elimination with an $E1_{cb}$-like character.[133] While studying the mechanism of the Hofmann elimination of 2-phenylethyltrimethylammonium bromide, Fry *et al.* observed that by changing the para-substituents on the phenyl ring, the transition state of the elimination was distorted increasing its carbanionic character (see Figure 2.1.1).[133]

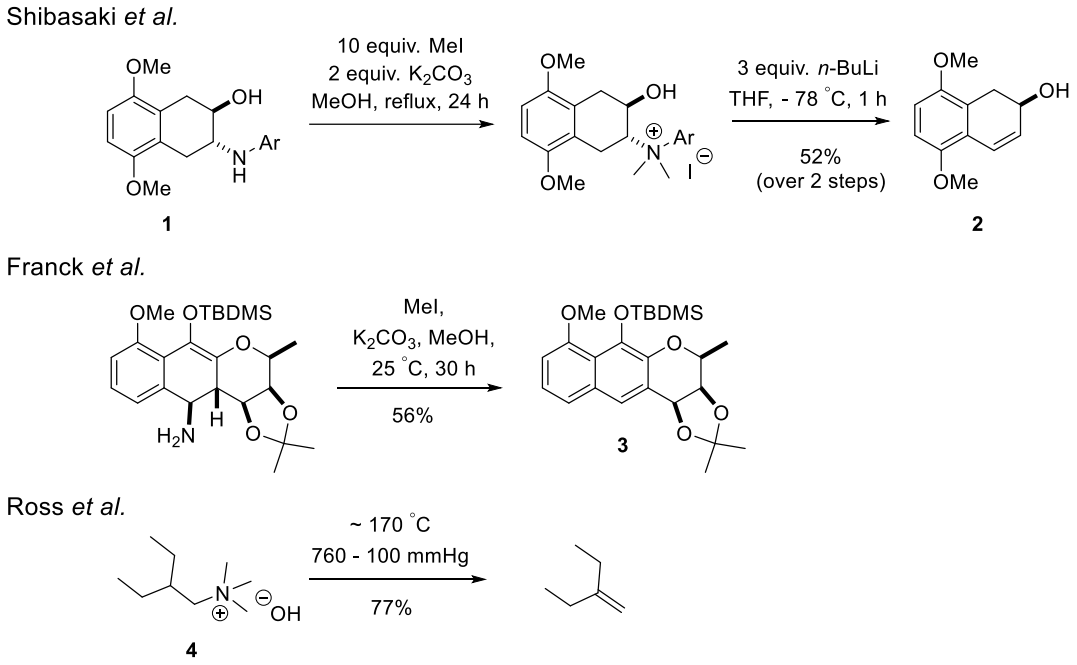

Scheme 2.1.3 Examples of the Hofmann elimination applied on various substrates.

A few examples on the application of the Hofmann elimination is given in Scheme 2.1.3. In the synthesis of 4-demethoxydaunomycin, an artificial derivative of the clinically relevant anthracycline antibiotics, Shibasaki *et al.* incorporated the Hofmann elimination to form the desired allylic alcohol **2** from the enriched trans-*β*-amino alcohol **1**.[134] By using a very strong base, *n*-BuLi, Shibasaki and his group achieved the desired elimination of the quaternary ammonium group without the removal of the alcohol and without a great decrease in ee (enantiomeric purity only went from 95% ee to 90% ee). Franck *et al.* applied the Hofmann elimination in the synthesis of the fungal metabolite (–)-cryptosporin.[135] Surprisingly, the trimethylation of the free amine in methanolic potassium carbonate solution led to the immediate elimination of the trimethylammonium salt at room temperature to give **3**, which

might have been due to the energetically favoured aromatisation of the central ring system. However, it is widely known that the Hofmann elimination of quaternary ammonium groups in non-activated, alkyl substrates is highly dependent on high temperatures. As shown in the example by Ross *et al.*, the elimination of trimethyl-2-ethylbutylammonium hydroxide [**4**] only started after reaching a temperature of about 170 ˚C at atmospheric pressure and it was further enhanced by reducing the pressure to 100 mmHg.[136]

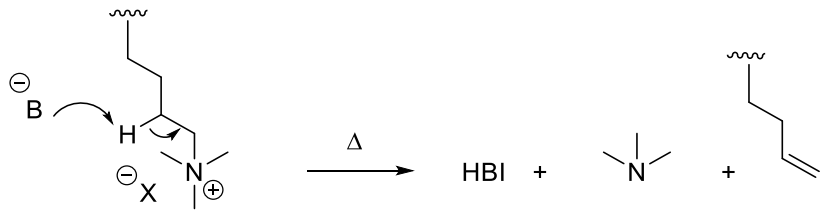

5 **6**

Scheme 2.1.4 The Hofmann elimination performed on trimethylammonium lysine residues of histone proteins.

The Hofmann elimination was chosen as the key transformation for the chemical modification of the target histone proteins in the proposed CLICK-seq assay due to its specificity towards the ammonium functionality in a pool of numerous functional groups. The application of the Hofmann elimination to achieve the desired formation of the alkene functionality on the lysine residues of histone proteins is illustrated in Scheme 2.1.4. The aim of the reaction is the base-mediated elimination of trimethylamine from butyltrimethylammonium substrates [**5**] to obtain the 4-butene moiety [**6**]. However, as shown in the given examples above and others in the literature[130,137,138], the classical Hofmann elimination reaction is based on high temperatures (examples up to almost 300 ˚C) and strong bases for the successful conversion of the quaternary ammonium salt to the corresponding alkene, which is not feasible for its application on sensitive biological systems. Consequently, a screening of Hofmann elimination conditions was necessary to discover the ideal experimental setting to apply this reaction onto peptides and proteins. Therefore, the screening of Hofmann elimination conditions on model small molecules was firstly conducted to determine protein-compatible conditions to achieve the desired transformation under mild conditions, which is discussed in this chapter.

2.1.2 Hofmann elimination screening using trimethyllysine

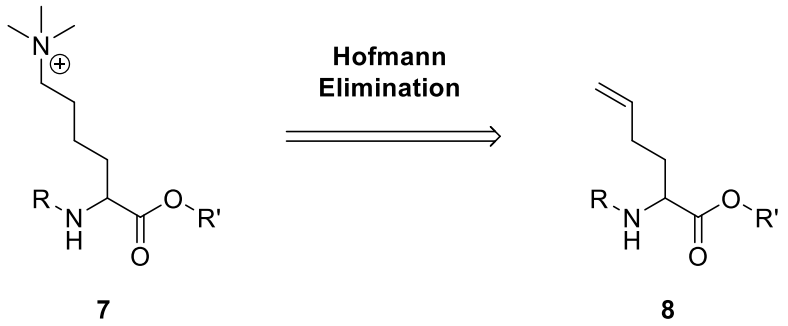

Scheme 2.1.5 Hofmann elimination of trimethyllysine.

Trimethyllysine **7** was chosen as the model system to conduct the Hofmann elimination screening in order to discover the ideal conditions for the elimination of trimethylamine and the generation of the olefin **8** (see Scheme 2.1.5**)**. The goal of the Hofmann elimination screening was the successful transformation of the trimethyl ammonium functionality to the terminal alkene using mild reaction conditions (temperature < 100 ˚C), which can be applied to peptides and proteins. The Hofmann elimination screening and its outcome is described in this chapter.

2.1.2.1 Synthesis of trimethyllysine analogues

A great deal of effort was made for the trimethylation of the Fmoc-protected lysine substrate with various protecting groups for the carboxylic acid moiety, but unfortunately the Fmoc-protected trimethyllysine could not be isolated. It was promptly confirmed that the use of an excess of methylation agent was not easily applicable to the methylation of lysine, since the stability of lysine, the incontrollable degree of methylation and thus the resulting difficulty in purification of the mono-, di- and trimethyllysine formed a major obstacle. Consequently, the use of acidic conditions and the more controllable methylation degree of the reaction made the Eschweiler-Clarke reaction relevant to use for the methylation of the Fmoc-protected lysine. The Eschweiler Clarke reaction is the reductive methylation of primary or secondary amines to the corresponding tertiary amines using formaldehyde and a reducing agent.[139,140] The mechanism of this reaction is shown in Scheme 2.1.6.

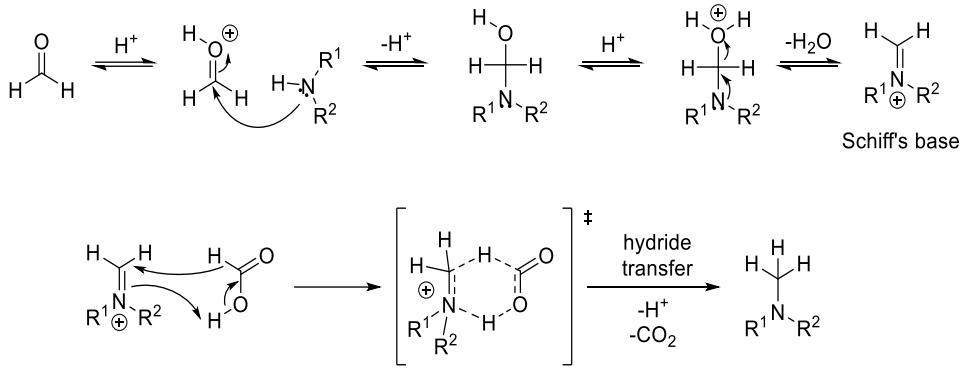

Scheme 2.1.6 The mechanism of the Eschweiler-Clarke reaction.

The synthesis of the Fmoc-protected trimethyllysine was attempted with the use of the Eschweiler-Clarke reaction as displayed in Scheme 2.1.7. Benzylation of Fmoc-Lys(Boc)-OH [**9**] using benzyl bromide and potassium carbonate in DMF (see Scheme 2.1.7) resulted in the generation of Fmoc-Lys(Boc)-OBn [**10**] in good yield (85%). Next, the benzylated lysine **10** was treated with TFA in DCM (1 : 1) at room temperature leading to the removal of the Boc protecting group and thus to the formation of Fmoc-Lys(NH_2)-OBn [**11**] in moderate yield (43%). The freshly synthesised amine **11** was exposed to Eschweiler-Clarke conditions using formaldehyde and formic acid under reflux to undergo dimethylation resulting in the formation of **12**. Sodium lauryl sulfate was added to the reaction to increase the overall solubility of the SM. LC-MS analysis revealed that the reaction resulted in a complex mixture of compounds highlighting the decay of the molecule.

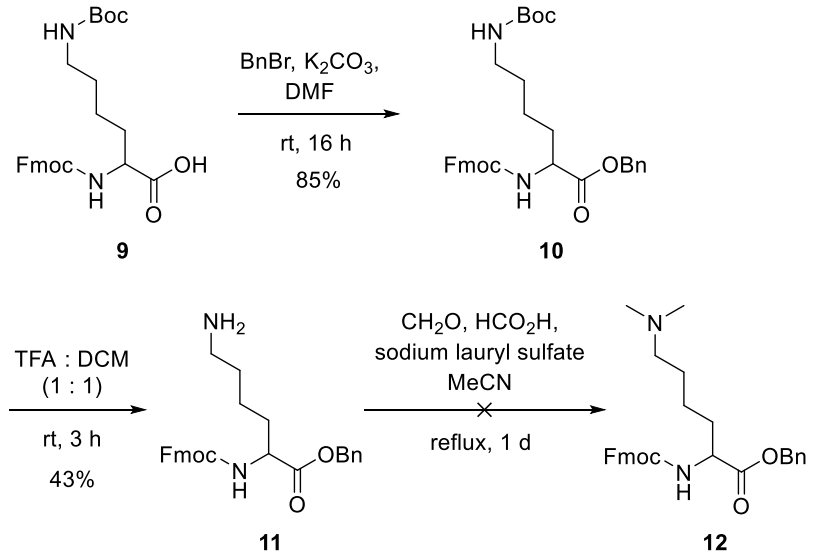

Scheme 2.1.7: Attempted synthetic route towards the synthesis of Fmoc-Lys(NMe_2)-OBn [12].

Upon closer investigation of the compounds detected in the MS chromatogram, the doubly-dimethylated Me_2N-Lys(NMe_2)-OBn [**13**] (m/z 293.35 ([M + H]$^+$, 100%) was identified accentuating the loss of the Fmoc group. At this moment, it became clear that the removal of the Fmoc group was caused by the ε-amine of the molecule.

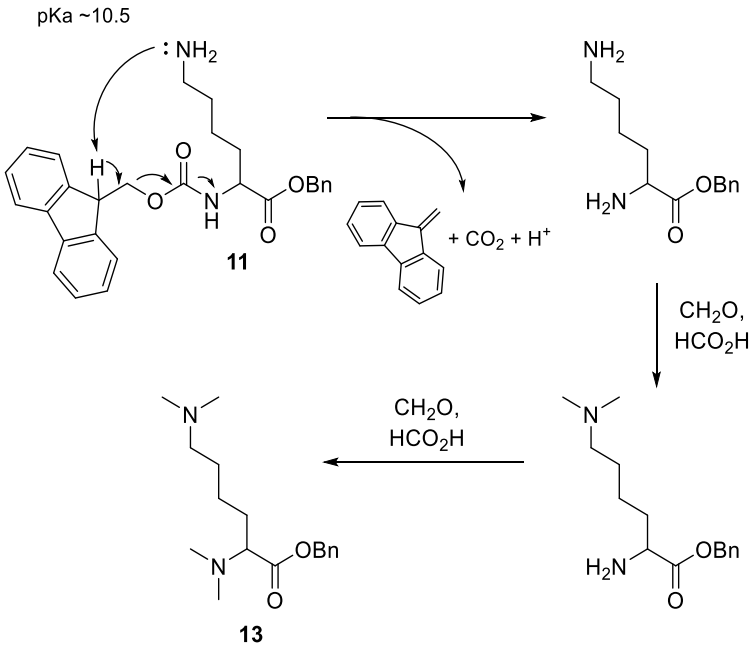

Scheme 2.1.8: Self-decomposition pathway of Fmoc-Lys-OBn [11] and the subsequent double Eschweiler-Clarke methylation.

With a pKa of ~10.5 (similar range as piperidine (pKa 11.123), which is usually used for Fmoc-deprotection)[141], the ε-amine of lysine is strong enough to extract the acidic proton on the Fmoc ring and thus to induce the removal of the Fmoc protecting group. The diamine can then undergo a double Eschweiler-Clark methylation and form the observed lysine substrate **13** as shown in Scheme 2.1.8.

Since the instability of the Fmoc-protected lysine **11** interfered with the methylation screening, the Fmoc protecting group was substituted for the more stable Cbz (*N*-carboxybenzyl) protecting group. Following the swap of the α - amino protecting group, the synthetic route in Scheme 2.1.7 was repeated with the commercially available Cbz-Lys(Boc)-OH [**14**]. As shown in Scheme 2.1.9, Cbz-Lys(Boc)-OH [**14**] was treated with potassium carbonate and benzyl bromide in DMF at room temperature to obtain the *O*-benzylated lysine

15 in good yield (69%). After Boc-protection with TFA, Cbz-Lys-OBn [**16**] was exposed to Eschweiler-Clarke conditions to give dimethyllysine **17** in 28% yield.

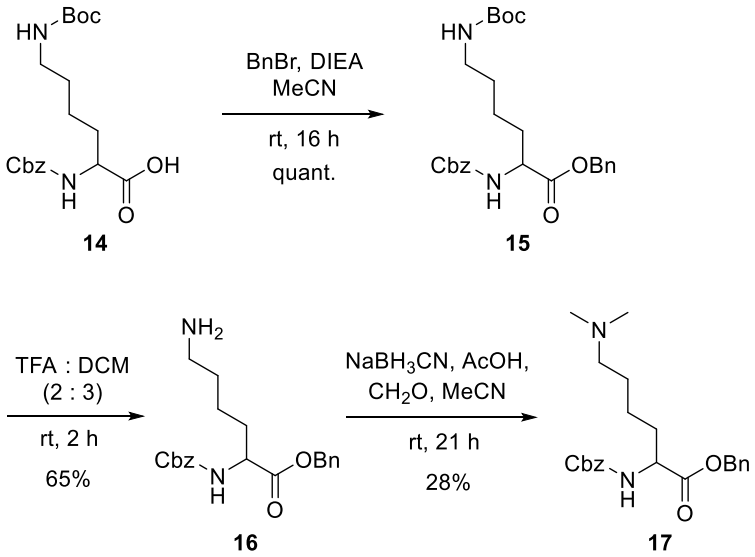

Scheme 2.1.9: Synthesis of Cbz-Lys(NMe$_2$)OBn [17].

With the aim of increasing the yield of the Eschweiler-Clarke reaction, the dimethylation of Cbz-Lys-OBn [**16**] was repeated, however, the previously used reaction condition (Entry a), was strategically modified (see Table 2.1.1). Based on the mechanism shown in Scheme 2.1.6, the nucleophilic attack of the amine to the precedently protonated formaldehyde leads to the formation of an imine, which is reduced by a reducing agent to methyl amine in the second step. Consequently, the order of addition of the reagents was adjusted accordingly. The formaldehyde was exposed to the acetic acid and the amine, before sodium cyanoborohydride was added to the reaction mixture (see Entry b). In addition, the amount of acetic acid was decreased to 2 equiv., since the rate of the conversion is pH-dependent and increases in acidic conditions with high pH.[142] However, these changes led to a decrease in yield (5%). A change in solvent to methanol (Entry c) did also result in a lower yield (10%) than the original conditions displayed in Entry a.

Table 2.1.1 Screening of Eschweiler-Clarke methylation conditions.

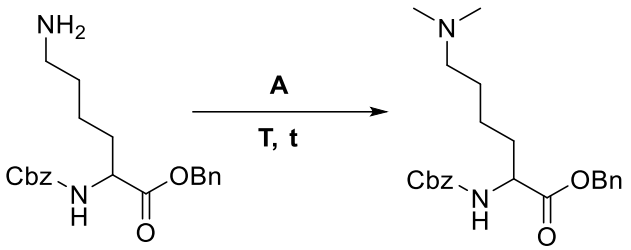

16 **17**

Entry	**A**	**T**	**t**	Reaction outcome
a	20 equiv. CH_2O, MeCN; then 2 equiv. $NaBH_3CN$; then 124.4 equiv. AcOH	rt	2 d	28%
b	10 equiv. CH_2O, MeCN; then 2 equiv. AcOH; then 2 equiv. $NaBH_3CN$	rt	1 d	5%
c	10 equiv. CH_2O, MeOH; then 2 equiv. AcOH; then 2 equiv. $NaBH_3CN$	rt	2 d	10%

Since the purification of the free amine **16** was challenging due to its polarity and it led to a loss in product, a small screening of Eschweiler-Clarke conditions starting from the ammonium trifluoroacetate salt **18** was also conducted. The further decrease in the amount of TFA in DCM (from the previously used 2 : 3 ratio to 1 : 4) resulted in the formation of the trifluoroacetate salt **18** in quantitative yield as shown in Scheme 2.1.10.

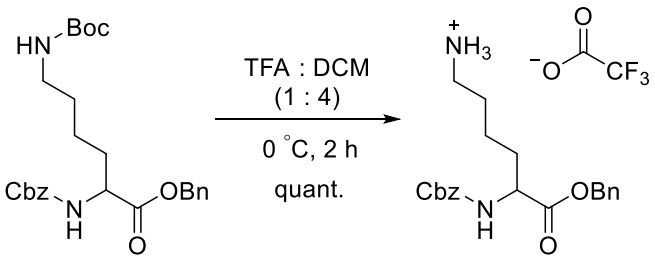

15 **18**

Scheme 2.1.10 Synthesis of the trifluoroacetate salt of Cbz-Lys-OBn.

As shown in Table 2.1.2, Entry a, the ammonium trifluoroacetate salt **18** was firstly treated with formaldehyde and sodium cyanoborohydride in the presence of acetic acid forming the dimethyllysine **17** in low yield (6%). Performing the reaction in absence of acetic acid also resulted in a conversion of the SM to the product in 6% yield (see Entry b). A procedure by Muir *et al.* was discovered in the literature, in which the trifluoroacetate salt of ornithine was dimethylated using Eschweiler-Clarke conditions (reported yield: 45%).[143] The published conditions were repeated on Cbz-Lys(NH_2)-OBn • TFA [**18**] leading to the generation of the desired dimethyllysine **17** in good yield (54%) as shown in Entry c.

Table 2.1.2 Eschweiler-Clarke dimethylation screening starting from Cbz-Lys(NH_2)-OBn • TFA [18].

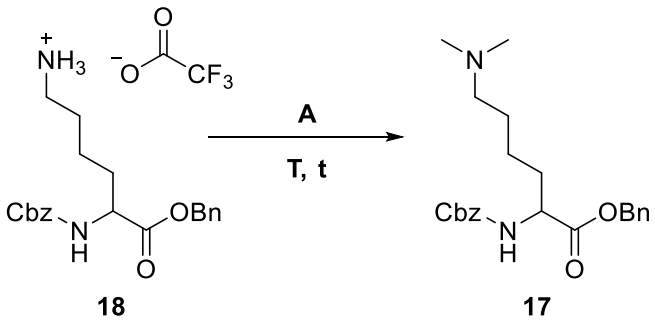

18 **17**

Entry	**A**	**T**	**t**	Reaction outcome
a	20 equiv. CH_2O, MeCN; then 5 equiv. $NaBH_3CN$; then 19.8 equiv. AcOH	rt	3 d	6%
b	20 equiv. CH_2O, MeCN; then 5 equiv. $NaBH_3CN$	rt	3 d	6%
c	3.6 equiv. CH_2O, MeOH; then 5 equiv. $NaBH_3CN$	0 °C - rt	1 d	54%

Upon optimisation of the synthetic route to produce sufficient amount of Cbz-Lys(NMe_2)-OBn [**17**], the final product was synthesised via monomethylation of dimethyllysine **17** with methyl iodide in THF leading to the formation of Cbz-Lys(NMe_3^+)-OBn • I^- [**19**] in quantitative yield (see Scheme 2.1.11). With the synthesised Cbz-Lys(NMe_3^+)-OBn • I^- [**19**] in hand, the Hofmann elimination screening was conducted next, which is discussed in the following chapter.

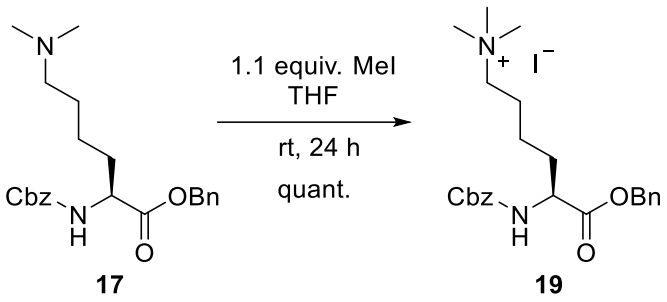

Scheme 2.1.11 Synthesis of the final product via the monomethylation of 17.

2.1.2.2 Hofmann elimination screening using trimethyllysine as the starting material

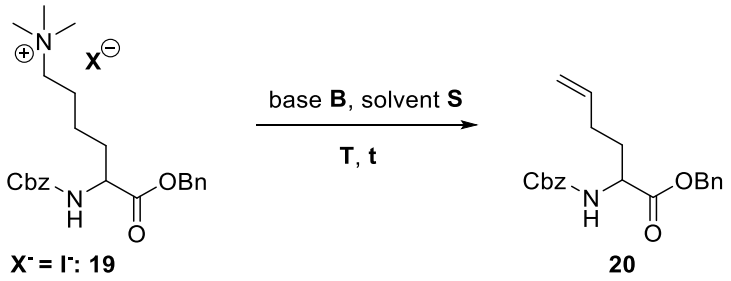

Scheme 2.1.12 Design of the Hofmann elimination screening of Cbz-Lys(NMe_3^+)-OBn • I^- [19].

Trimethyllysine [**19**] was used to start an initial screening of Hofmann elimination conditions to convert the quaternary ammonium functionality to an alkene [**20**]. As illustrated in Scheme 2.1.12, there are five possible factors that can be modified to achieve the successful elimination of trimethylamine: base **B**, solvent **S**, temperature **T**, reaction time **t** and counterion $\mathbf{X}^-$. The key aim of the Hofmann elimination screening is the development of mild and possibly water-friendly reaction conditions in order to adopt the most effective condition onto peptides and proteins with either no further or minimal alterations. With the knowledge gained from the synthesis and analysis of lysine derivatives, liquid chromatography - mass spectroscopy (LC-MS) was chosen as an adequate analytical method to instantly verify the success of the reaction and to elaborate most common side products. In case of initial hits validated by LC-MS analysis, it was then intended to further investigate and quantify those hits using supplemental analytical methods such as quantitative NMR spectroscopy.

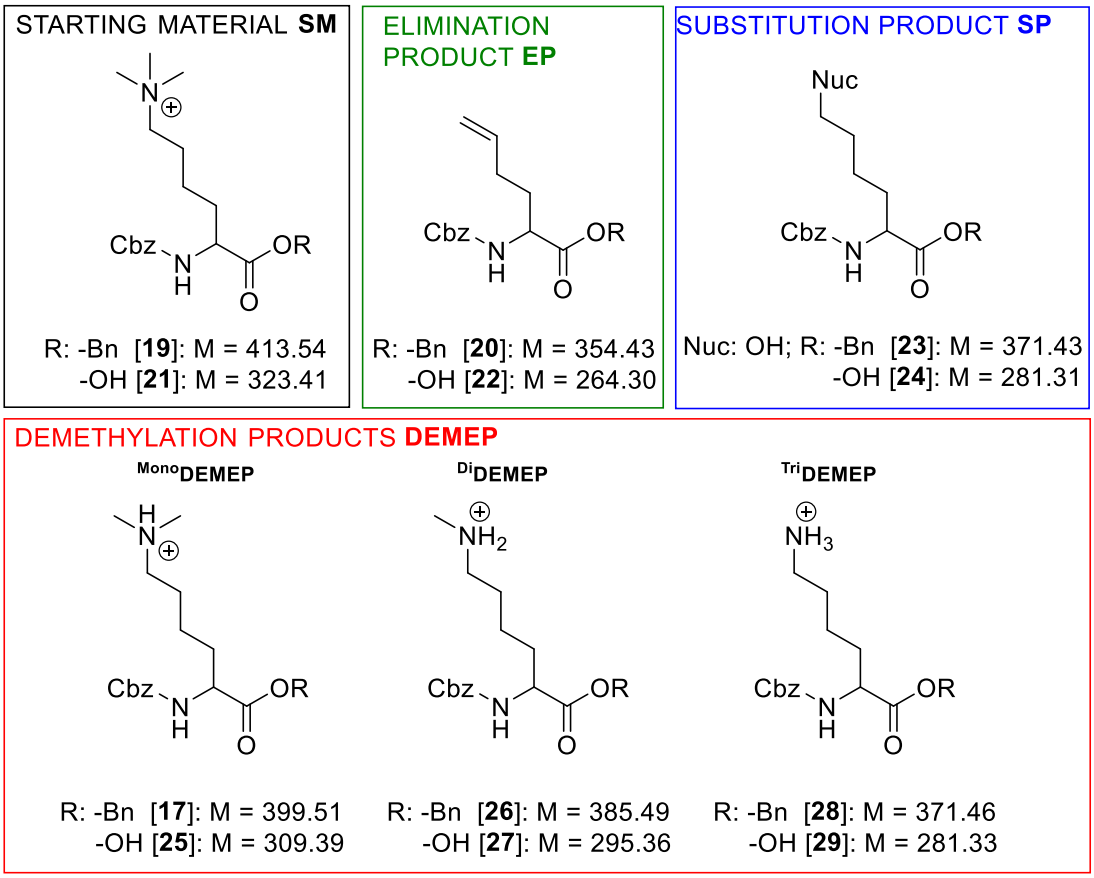

Figure 2.1.2 Summary of possible products generated during the Hofmann elimination screening and their corresponding molecular masses.

Figure 2.1.2 shows an overview of possible products, which can be generated from the Hofmann elimination screening. Although the main goal of the screening is the formation of the terminal alkene **20** (elimination product, EP, green) from trimethyllysine **19** (starting material, SM, black), possible side reactions can result in the formation of other products as illustrated in the blue and red boxes. Nucleophilic substitution can lead to the substitution product **23** (SP, blue) and demethylation can lead to the demethylation products **17**, **26** and **28** (DEMEP, red). In addition, the use of base can induce the hydrolysis of the benzyl ester resulting in the hydrolysed version of the products (P_{Hydro}), which were considered throughout the analysis of the elimination screening. Table 2.1.3 summarises the initial screening of Hofmann elimination conditions on Cbz-Lys(NMe_3^+)-OBn • I^- [**19**].

As a starting point for the elimination screening, the original Hofmann elimination condition using silver(I) oxide as the base was adopted (see Table 2.1.3, Entry a). Silver(I)

oxide in water forms hydroxide ions, which then act as the active base to deprotonate the *β*-hydrogen to the ammonium functionality leading to the formation of a terminal alkene. In addition to the release of the strong basic hydroxide ions, the use of silver(I) oxide simultaneously leads to the trapping of the iodide counterion by forming insoluble silver(I) iodide. The precipitation of silver(I) iodine forces the positively charged trimethyllysine to exchange its iodide counterion to the freshly formed hydroxide in solution. The silver(I) oxide used for the elimination reaction was synthesised freshly in quantitative yield reacting silver(I) nitrate with potassium hydroxide in water. Cbz-Lys(NMe_3^+)-OBn • I^- [**19**] was reacted with 5 equiv. of the freshly synthesised silver(I) oxide in MeOH : H_2O (2 : 1) at 100 °C (see Table 2.1.3, Entry a). After 2 days of heating, the reaction outcome was analysed via LC-MS confirming starting material **19** as the major product of the reaction. The MS spectrum detected a complex mixture of compounds, in which traces of Cbz-Lys(NMe_2)-OBn [**17**] were identified verifying demethylation as a side reaction to the Hofmann elimination of quaternary ammonium salts.

Table 2.1.3 Initial Hofmann elimination screening.

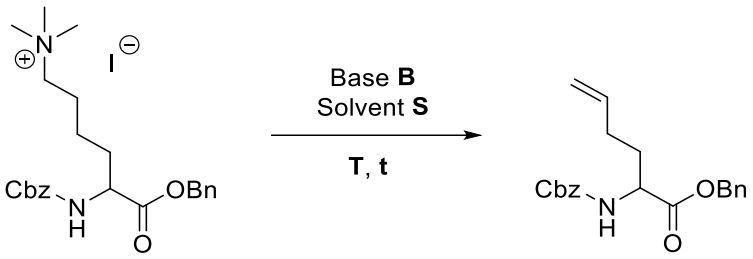

19 **20**

Entry	**B**	**S**	**T**	**t**	**Reaction outcome**
a	5 equiv. Ag_2O	MeOH : H_2O (2 : 1)	100 °C	2 d	Major P: SM, **19** Traces: ^{Mono}DEMEP, **17**
b	1.5 equiv. NaOH	MeOH : H_2O (2 : 1)	150 °C (MW)	18 h	Major P: SP_{Hydro}, **24** Minor P: ^{Mono}DEMEP, **17**
c	10 equiv. NaOH	DMF	145 °C	1 d	EP **22** present, but both substitution and demethylation are occurring.
d	10 equiv. K_2CO_3	DMF	145 °C	3 d	
e	10 equiv. piperidine	DMF	145 °C	2 d	
f	10 equiv. DIPA	DMF	145 °C	1 d	

Since SM [**19**] was predominantly detected as a result from the original Hofmann elimination conditions (Entry a), it was acknowledged that harsher conditions needed to be used in order to force the elimination of trimethylamine. Consequently, Cbz-Lys(NMe_3^+)-OBn • I^- [**19**] was treated with 1.5 equiv. of sodium hydroxide in MeOH : H_2O (2 : 1) at 150 °C under microwave radiation (MW) for 18 hours (listed in Table 2.1.3, Entry b). It was anticipated that the use of microwave chemistry in the Hofmann elimination reaction would not only allow the reaction to reach higher temperatures, but it would also allow it to run at higher internal pressure. LC-MS analysis of the reaction outcome showed that the SM was consumed completely. Two main products of the reaction were identified, which confirmed that the expected elimination reaction did not occur as no alkene product **20** was detected. One of the identified products is the result of the nucleophilic substitution reaction, which is widely known in the field to compete against the elimination reaction.[144] The hydroxide ions of the base act as a nucleophile to displace the trimethyl ammonium functionality and form an alcohol as the product. The detected peak additionally shows that the benzylated carboxylic acid of the SM was hydrolysed during the reaction. Hence, the detected ion in the MS chromatogram was recognized to be Cbz-Lys(OH)-OH [**24**] with m/z 282.39 ($[M+H]^+$, 100 %), which complies with the mass of the compound SP_{Hydro} given in Figure 2.1.2. The second product of the reaction characterised from the mass spectrum is the result of the demethylation reaction, a second reaction known in the literature to also compete against the elimination reaction when quaternary ammonium compounds are used.[145] The nucleophilic hydroxide ions attack one of the methyl groups on the ε-nitrogen to form a tertiary amine and methanol. The identified second product is accordingly Cbz-Lys(NMe_2)-OBn [**17**] with the detected m/z 421.25 ($[M+Na]^+$, 100%), 399.33 ($[M+H]^+$, 60%).

Since the reaction using microwave radiation (see Table 2.1.3, Entry b) did not result in the elimination of trimethylamine, but it favoured the competing nucleophilic substitution and demethylation reactions, milder conditions without microwave exposure were investigated next (see Table 2.1.3, entries c – f). Thereby, the amount of base was increased to 10 equiv. and the solvent was exchanged to DMF in order to continue using high reaction temperatures and to decelerate the removal of the benzyl protecting group by using a non-aqueous solvent. As displayed in Table 2.1.3, Cbz-Lys(NMe_3^+)-OBn • I^- [**19**] was reacted with 10 equiv. of a variation of inorganic and organic bases ranging from sodium hydroxide (Entry c), potassium carbonate (Entry d), piperidine (Entry e) and diisopropylamine (Entry f) in DMF at 145 °C. The selection of the investigated bases was based on their difference in chemical properties including varying pKa values, steric effects and solubility and solvation characteristics. To

demonstrate the complexity of the reaction outcomes, the measured total ion current (TIC) chromatograms of all four reactions are shown in Figure 2.1.3. As seen in the TIC chromatograms, all four reactions have similar reaction outcomes, of which the significant products are annotated in colour. The hydrolysed elimination product **22** (EP_{Hydro} in green) was detected in all four reactions confirming the formation of the desired terminal alkene and the reoccurring hydrolysis of the benzylated carboxylic acid. The m/z peaks seen at the retention time of about 10.20 min (coloured in green) represents the elimination product Cbz-Lys(alkene)-OH [**22**] with the detected m/z 264.29 ($[M+H]^+$, 100%). Nevertheless, the bulk of the mass balance of the reactions consists of the compounds produced by competing side reactions, the remaining SM and decomposition products. It can be inferred from these experiments, that the partial elimination of trimethyllysine **19** is observed at high temperature (145 ˚C), however, further optimisation is needed to increase the yield of elimination by preventing the formation of side products.

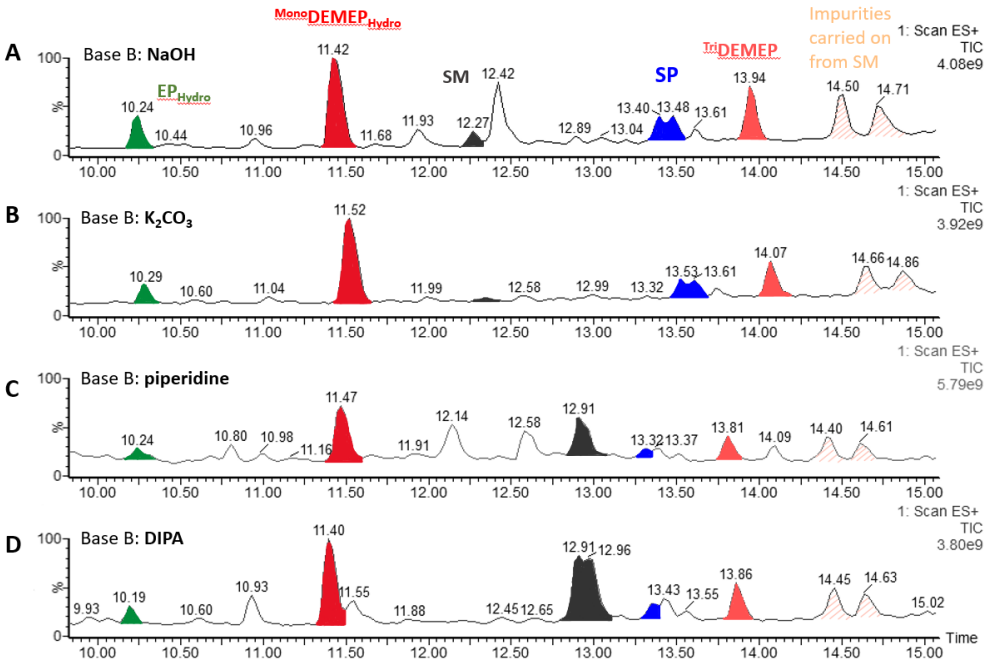

Figure 2.1.3 Total ion current (TIC) chromatograms of the results from the Hofmann elimination reactions in Entries c – f (Table 2.1.3).

Hofmann elimination screening using non-nucleophilic bases

The preliminary Hofmann elimination data summarised in Table 2.1.3 has shown some successful conversion of the quaternary ammonium lysine substrate **19** to the terminal alkene **22**, however, competing side reactions led to the greater consumption of the SM and thus to the limited generation of the desired elimination product. Since the substitution and the demethylation reactions are both based on the nucleophilic character of the bases used in the reactions so far, they were exchanged by sterically-hindered, non-nucleophilic bases. The aim of the change in base was to prevent the nucleophilic attack of the base to the SM and thus to increase the yield of elimination.

Table 2.1.4 Hofmann elimination screening using non-nucleophilic bases.

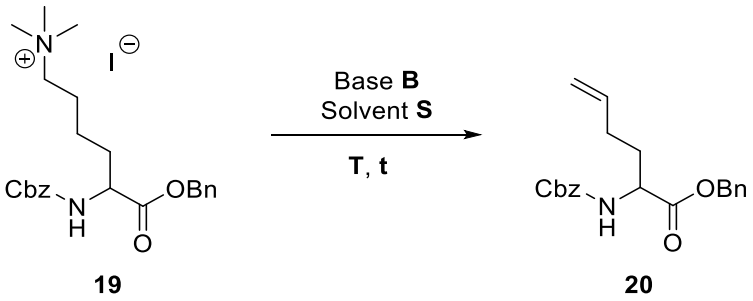

19 **20**

Entry	**B**	**S**	**T**	**t**	Reaction outcome
a	10 equiv. DBU	DMF	145 °C	2 d	Complex mixture, traces of EP
b	10 equiv. DBU	DMF	70 °C	2 d	Complex mixture, no EP detected
c	10 equiv. BTMG	DMF	70 °C	2 d	Complex mixture, no EP detected
d	10 equiv. proton sponge	DMF	70 °C	2 d	Complex mixture, no EP detected
e	10 equiv. KHMDS	DMF	70 °C	2 d	Complex mixture, no EP detected

A summary of the second screening of Hofmann elimination reactions using sterically-hindered bases is displayed in Table 2.1.4. First, Cbz-Lys(NMe_3^+)-OBn • I^- [**19**] was treated with 10 equiv. of 1,8-diazabicyclo(5.4.0)undec-7-ene (DBU) in DMF at 145 °C for 2 days (see Table 2.1.4, Entry a). The reaction led to a complex mixture, which was analysed via LC-MS. The investigation of the reaction outcome confirmed that the use of the sterically-hindered DBU inhibited the formation of the side products seen in the initial Hofmann elimination screening.

Marginal generation of the elimination product **20** was observed in the mass chromatogram, however, the harsh conditions of the Hofmann elimination mainly led to the decomposition of the SM. Consequently, the reaction was repeated under milder conditions by decreasing the temperature to 70 ˚C (see Entry b). Nevertheless, the reaction resulted in a complex mixture even at the decreased temperature. No elimination product was detected within the complex mixture, and the mass spectrum indicated the decomposition of the SM. Next, alternative non-nucleophilic bases were applied to the Hofmann elimination to force the generation of the terminal alkene without increasing the reaction temperature. As shown in Table 2.1.4, trimethyllysine **19** was exposed to 10 equiv. of 2-*tert*-butyl-1,1,3,3-tetramethylguanidine (BTMG, Entry c), proton sponge (Entry d) and potassium bis(trimethylsilyl)amide (KHMDS, Entry e), respectively, in DMF at 70 ˚C. Similar to the previous reaction with DBU, all three reactions resulted in a complex mixture. LC-MS analysis of these experiments confirmed that the elimination product **20** was not formed during the reaction. Residual SM was detected in the MS chromatograms; however, the low m/z peaks present in the mass spectra supported the decomposition of the lysine substrate.

The first generation Hofmann elimination screening gave a preliminary understanding on the feasibility of the elimination of trimethylamine on lysine substrates. The conclusions drawn from the initial Hofmann elimination screening using trimethyllysine **19** as the starting material are as follows: (i) the use of nucleophilic bases resulted in the nucleophilic substitution and/or demethylation of trimethyllysine, which are known competing side reactions to elimination; (ii) the use of sterically-hindered and thus non-nucleophilic bases prevented the side reactions; (iii) traces of the elimination product were identified as a result of high temperature reactions; (iv) trimethyllysine decomposes under harsh elimination conditions (high temperature and strong bases); (iv) the complexity of the SM and the complex mixtures gained from the reactions made the analysis of the reaction challenging.

2.1.3 Hofmann elimination of quaternary ammonium groups in organic small molecules

Incorporating the conclusions drawn in the previous subchapter, the aim for the next stage of the Hofmann elimination screening was to overcome the stability issues of the tested substrate and to quantify the formation of the desired product. The analytical LC-MS method was substituted for quantitative ^{1}H-NMR measurements using an internal standard to obtain the absolute concentration and yield of the reaction products. The use of trimethyllysine **19** as the starting material presented several obstacles in the first generation Hofmann elimination screening due to its polarity, structural instability and thus the generation of complex mixtures as the result of the base-mediated reactions. Consequently, it was decided to simplify the starting material by exchanging the amino acid functionality for a phenyl group, which eliminated the problems with its polarity and stability yet maintained the immediate structural environment around the trimethyl ammonium functionality. The second generation Hofmann elimination screening was conducted using trimethyl-(4-phenylbutyl)-ammonium iodide [**31**] as the starting material, which was synthesised in one step by trimethylating the commercially available 4-phenylbutyl amine [**30**] with methyl iodide in THF to give the desired product **31** in moderate yield (36%) as shown in Scheme 2.1.13. The change in starting material to substrate **31** additionally guaranteed an ease of access to a low-cost, readily synthesised, simple, pure and stable substrate to use in the second generation Hofmann elimination screening.

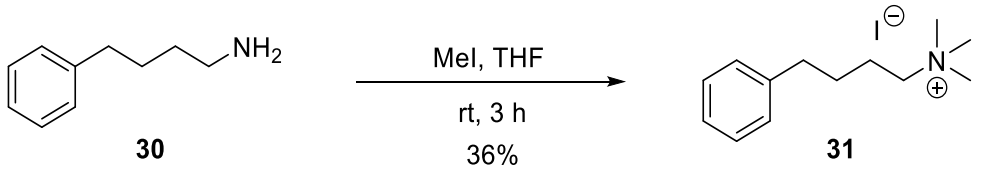

30 **31**

Scheme 2.1.13 Synthesis of trimethyl-(4-phenylbutyl)-ammonium iodide [31].

The main features of a suitable internal standard to use for the quantitative ^{1}H-NMR analysis are that its proton signals do not overlap with those of the starting material and possible products and that it is chemically inert and highly soluble in the used solvent. Thus, trimethyl benzene-1,3,5-tricarboxylate [**33**] was selected. Figure 2.1.4 shows the ^{1}H-NMR spectrum of

the starting material **31**, the desired alkene product **32** and the internal standard **33** combined. Their characteristic protons are annotated (*). As seen in the ^{1}H-NMR spectrum, the proton signals for the trimethyl benzene-1,3,5-tricarboxylate [**33**] (^{1}H NMR (400 MHz, CD_3CN) δ 8.74 (s, 3H), 3.86 (s, 9H).) do not overlap with any other signals. The conversion from the starting material to the desired product is distinguishable by the generation of the alkene proton peaks in the area of 4.5 – 5.5 ppm. Since the proton peaks of a terminal alkene **32** are distinctive in shape due to their proton coupling and their chemical shift is in a particular ppm window, the use of trimethyl-(4-phenylbutyl)-ammonium iodide [**31**] as the starting material and trimethyl benzene-1,3,5-tricarboxylate [**33**] as the internal standard represented an appropriate layout for the second generation Hofmann elimination screening.

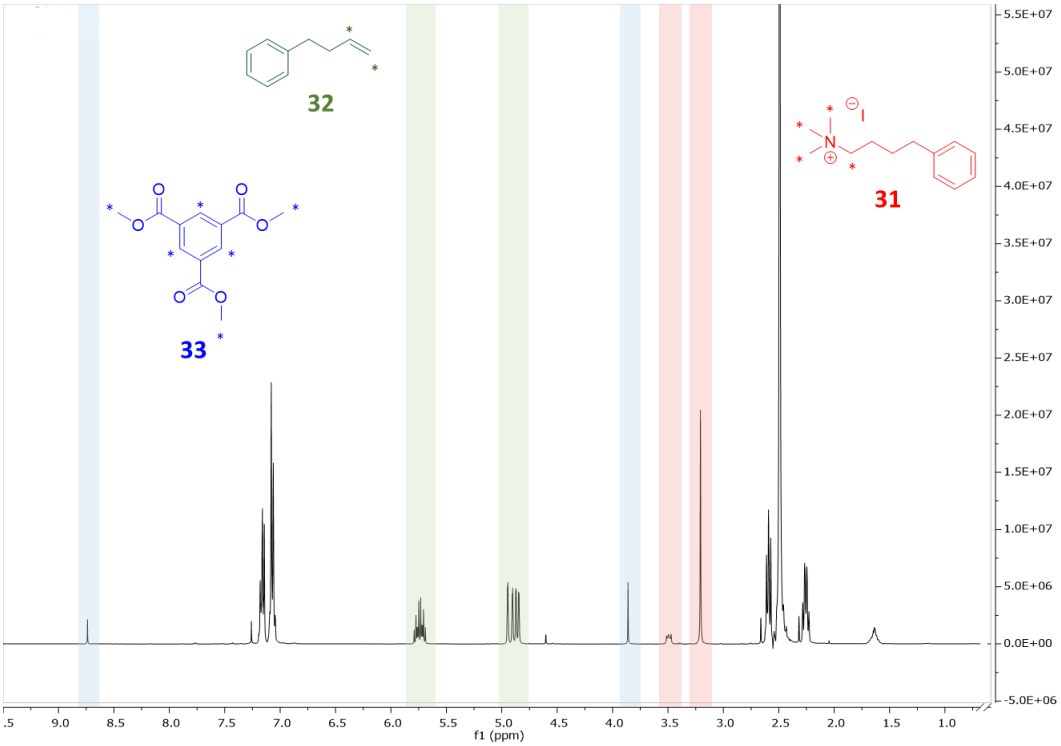

Figure 2.1.4 ^{1}H NMR spectrum of the starting material 31, the desired alkene product 32 and the internal standard 33 in $CDCl_3$ (400 MHz).

A range of sterically-hindered, non-nucleophilic bases were tested in three different solvent systems. A summary of the investigated reaction conditions for the Hofmann elimination of trimethyl-(4-phenylbutyl)-ammonium iodide [**31**] is displayed in Table 2.1.5. Trimethyl-(4-phenylbutyl)-ammonium iodide [**31**] was exposed to a variety of non-nucleophilic bases

including 1,8-diazabicyclo(5.4.0)undec-7-ene (DBU), 1,5-diazabicyclo[4.3.0]non-5-ene (DBN), 1,5,7-triazabicyclo[4.4.0]dec-5-ene (TBD), proton sponge (PS) and 2-*tert*-butyl-1,1,3,3-tetramethylguanidine (BTMG) in DMF, DMSO and MeCN, respectively, at 75 ˚C for 48 hours. The reactions were processed and analysed via quantitative ^{1}H-NMR spectroscopy. Unfortunately, the obtained ^{1}H-NMR spectra confirmed that no terminal alkene **32** was formed during these reactions. Only starting material **31** was apparent in the ^{1}H-NMR spectra.

Table 2.1.5 Second generation Hofmann elimination screening using sterically-hindered, non-nucleophilic bases.

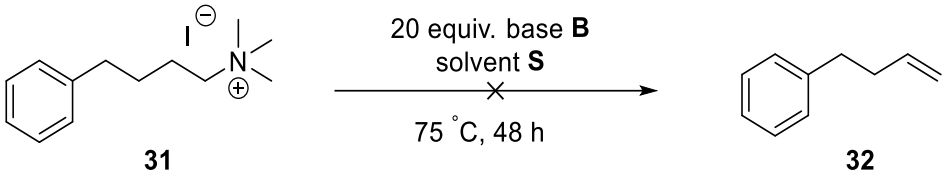

31 **32**

*No product, just SM

Solvent S	Base B: DBU	DBN	TBD	PS	BTMG
DMF	*	*	*	*	*
DMSO	*	*	*	*	*
MeCN	*	*	*	*	*

Due to the ultimate goal of applying the developed Hofmann elimination conditions to biological systems, the temperature was kept under 100 ˚C. However, these experiments verified that the success of elimination is dependent on high temperature. Therefore, a temperature study was conducted to investigate the conversion rate of the ammonium substrate **31** to the alkene **32** in relation to the temperature. As shown in Table 2.1.6, trimethyl-(4-phenylbutyl)-ammonium iodide [**31**] was treated with 20 equiv. of DBU in DMF at temperatures rising from 75 ˚C to 200 ˚C with an interval of 25 ˚C. There was no alkene product **32** detected in the ^{1}H-NMR spectra of the reactions in the Entries a – c. Upon reaching reaction temperatures of 150 ˚C (Entry d) and 200 ˚C (Entry e), only traces of the elimination product **32** appeared in the

^{1}H-NMR spectra. The temperature study confirmed that the Hofmann elimination of quaternary ammonium substrates requires high temperature to overcome the energy barrier for the elimination of trimethylamine. Even an increase in temperature to 200 °C only resulted in the minimal formation of the desired terminal alkene **32**.

Table 2.1.6 Effect of temperature on the Hofmann elimination of trimethyl-(4-phenylbutyl)-ammonium iodide [31]. *Neat. †The conversion was calculated using quantitative ^{1}H NMR with trimethyl benzene-1,3,5-tricarboxylate in DMSO (0.1 M) as internal standard.

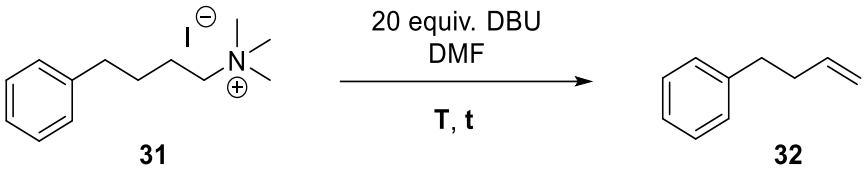

31 **32**

Entry	**Temperature T**	**Reaction time t**	Conversion to **Product**†
a	75 °C	3 d	-
b	100 °C	3 d	-
c	125 °C	3 d	-
d	150 °C	3 d	Traces (< 0.5%)
e*	200 °C	2 d	Traces (< 0.5%)

The library of bases investigated for the Hofmann elimination of the quaternary ammonium salt **31** was expanded with the aim of increasing the yield of the desired transformation. As displayed in Table 2.1.7, inorganic potassium salts were used as bases in the presence of crown ether (1,4,7,10,13,16-hexaoxacyclooctadecane) to trap the potassium cation and thus increase the efficiency of the deprotonation by the base. The use of potassium-*tert*-butoxide and crown ether for the Hofmann elimination of trimethyl-(4-phenylbutyl)-ammonium iodide [**31**] at 150 °C resulted in traces of the terminal alkene **32** (see Entry a). A change to both potassium fluoride (Entry b) and potassium phenolate (Entry c) in the presence of crown ether did not improve the conversion rate of the Hofmann elimination reaction. On the contrary, the reaction did not yield the desired elimination product **32**. Since the aim of the Hofmann elimination screening was the development of reaction conditions to be used in biological settings, an

attempt to achieve the elimination of the quaternary ammonium substrate in aqueous media was undertaken (see Entry d). Aqueous ammonium bicarbonate solution was chosen to be investigated for the Hofmann elimination instead of other basic solutions (*e.g.* ammonium hydroxide), because it was already in use as a common buffer for *in vitro* histone experiments, our target system. Trimethyl-(4-phenylbutyl)-ammonium iodide [**31**] was treated with aqueous ammonium bicarbonate solution (100 mM) at 125 ˚C for 3 days. Nevertheless, the reaction in Entry d did not give the desired alkene **32**, but only starting material **31** was observed in the ^{1}H-NMR spectrum.

Table 2.1.7 Expanding the library of bases investigated for the Hofmann elimination trimethyl-(4-phenylbutyl)-ammonium iodide [31]. †The conversion was calculated using quantitative ^{1}H NMR with trimethyl benzene-1,3,5-tricarboxylate in DMSO (0.1 M) as internal standard.

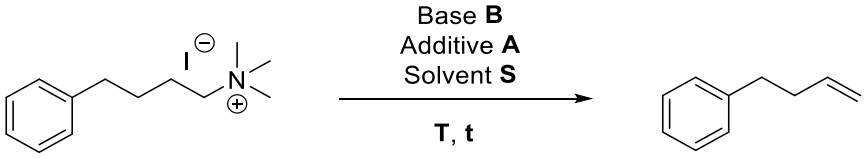

31 **32**

Entry	**B**	**A**	**S**	**Temperature T**	**Reaction time t**	Conversion to **Product**†
a	20 equiv. KO^{t}Bu	18-crown-6	DMF	150 ˚C	5 d	Traces (< 0.1%)
b	20 equiv. KF	18-crown-6	DMF	150 ˚C	5 d	-
c	20 equiv. KOPh	18-crown-6	DMF	125 ˚C	5 d	-
d	100 mM NH_4HCO_3	-	H_2O	125 ˚C	3 d	-

It is evident from these data that the traditional base-mediated Hofmann elimination was limited by temperature. Conducting the Hofmann elimination of trimethyl-(4-phenylbutyl)-ammonium iodide [**31**] at temperatures below 150 ˚C did not lead to the removal of trimethylamine and the generation of the terminal alkene **32**. The incorporation of different non-nucleophilic bases to improve the Hofmann elimination did not have an impact on the yield of the reaction. Even an increase in temperature to 200 ˚C only resulted in marginal

generation of the olefin **32**. Since the next steps towards promoting the Hofmann elimination to form the desired alkene would be either to perpetually increase the temperature of the reaction or to use harshly basic and water sensitive superbases[146] or the combination of both, the further optimisation of the classical Hofmann elimination to achieve a successful transformation to the alkene usable in a biological environment was deemed impractical. At this stage of the project, an alternative approach to the classical Hofmann elimination was sought to catalyse the elimination of quaternary ammonium functionalities without increasing the reaction temperature and the base strength. In the search for possible ways of enhancing the Hofmann elimination, a publication from 1978 sparked our interest in applying micelles to catalyse the Hofmann elimination, which will be discussed in the following subchapter.

2.1.4 Micelle-catalysed Hofmann elimination of quaternary ammonium groups in small molecules

Peters and co-workers demonstrated that cationic surfactants containing a *N*-hydroxyalkyl ammonium functionality have a positive influence on the rate of the Hofmann elimination of 4-nitrophenethyltrimethylammonium iodide to 4-nitrostyrene (see Scheme 2.1.14).[147]

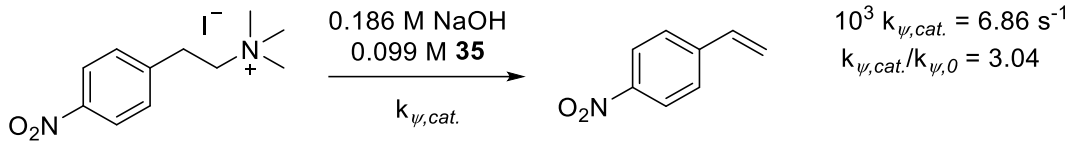

Scheme 2.1.14 Hofmann elimination of 4-nitrophenethyltrimethylammonium iodide catalysed by *N,N*-dimethyl-*N*-hexadecyl-*N*-(2-hydroxyethyl) ammonium bromide [35] in NaOH solution. The reactions (published by Peters *et al.*) were followed spectrophotometrically to determine the first-order rate constants of the elimination reactions in the presence ($k_{\Psi,cat.}$) and the absence ($k_{\Psi,0}$) of the investigated surfactant.

Peters *et al.* analysed the first-order rate constants of the investigated Hofmann elimination reaction spectrophotometrically in the presence and the absence of different surfactants. As shown in Scheme 2.1.14, catalytic effects of *N,N*-dimethyl-*N*-hexadecyl-*N*-(2-hydroxyethyl) ammonium bromide [**35**] (see structure in Figure 2.1.5) on the Hofmann elimination were observed in the presence of sodium hydroxide (pH > 12) at 39 ˚C, which was hypothesised to be based on the generation of the zwitterions and their subsequent role as the base in the elimination. In contrast, when cetyltrimethylammonium bromide (CTAB) [**34**] was used at high concentrations as the cationic surfactant in the reaction, the elimination of 4-nitrophenethyltrimethylammonium iodide was also accelerated, however, to a lesser extent. Peters *et al.* argued that the catalysis by CTAB was solely based on the incorporation of the starting material into the cationic micelles, but since CTAB did not possess a zwitterionic character, meaning that the basic environment closely to the starting material was lowered, only a slight rate increase was observed. Similar statements were made by Bunton and co-workers, who discovered that the 3-bromo-3-phenyl propionate ion was undergoing E2

elimination upon treatment with 1-hydroxyethyl-2-dimethylalkylammonium bromides and sodium hydroxide at 25 ℃.[148] In the absence of the zwitterionic surfactant, E2 elimination only appeared when the concentration of the sodium hydroxide base was significantly increased. Building on these discoveries, many studies appeared on the catalytic effect of cationic surfactants on elimination reactions in the presence of hydroxide anions.[149–151]

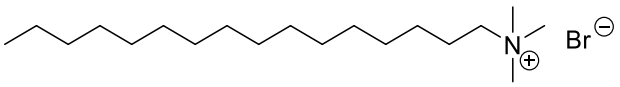

cetyltrimethylammonium bromide (CTAB) [**34**]

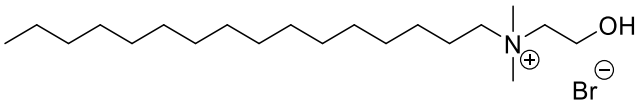

N,*N*-dimethyl-*N*-hexadecyl-*N*-(2-hydroxyethyl) ammonium bromide [**35**]

Figure 2.1.5 Structure of the discussed cationic surfactants.

The role of micelles in the catalysis or inhibition of organic reactions has been discovered relatively early on and was investigated extensively, which was firstly summarised by Fendler in 1970.[152] Many reviews followed highlighting a great interest in the application of micellar catalysis to organic reactions to date.[153–159] A major contribution to the acceleration of organic reactions is made by the capability of micelles to compartmentalize organic reagents and form an effective microreactor. Similar to enzymes, micelles are able to isolate the reactants from the bulk of the solvent enhancing their localised concentration compared to the overall aqueous solution. Since micelles possess an amphiphilic character, organic reagents are able to insert into the micellar environment and interact with the polar head groups depending on their structure. Micelles additionally improve solubilisation of the organic reagents in water and the resulting solvent effect can then influence a reaction's outcome. In case of elimination reactions, micelles formed by cationic surfactants attract the hydroxide ions of the base, significantly increasing the basicity directly on the surface of the micelles in contrast to the rest of the aqueous solution. The proximity of the basic anions to the substrate and their increased concentration on the surface of the micelles impact the rate of the elimination reaction. In some cases, the cationic surfactant can be further functionalised to be actively involved in the

transformation of interest. The above given example by Peters and co-workers displayed this phenomenon by utilising *N,N*-dimethyl-*N*-hexadecyl-*N*-(2-hydroxyethyl) ammonium bromide [**35**] as the cationic surfactant in the Hofmann elimination, which is involved in the reaction as the base.[147] In conclusion, the structure and the physicochemical properties of cationic surfactants have a significant influence on the micellisation process and its catalytic impact.

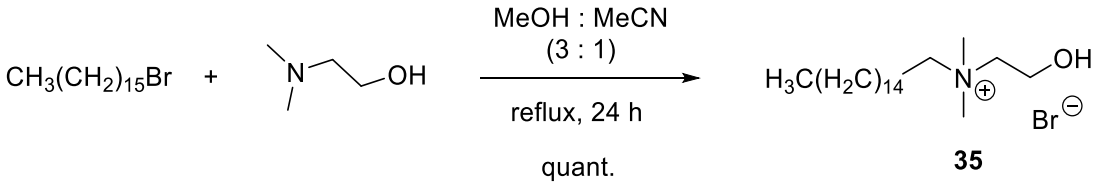

Scheme 2.1.15 Synthesis of *N,N*-dimethyl-*N*-hexadecyl-*N*-(2-hydroxyethyl) ammonium bromide [35].

With this knowledge in hand, we decided to investigate the effect of micellar catalysis on the Hofmann elimination using our model system. Our goal was to achieve the conversion of the trimethyl ammonium starting material **31** to the alkene product **32** at low temperatures using micellar systems made from the cationic surfactants with a *N*-hydroxyalkyl ammonium functionality. Consequently, *N,N*-dimethyl-*N*-hexadecyl-*N*-(2-hydroxyethyl) ammonium bromide [**35**] was synthesised according to the protocol by Li *et al.* (see Scheme 2.1.15).[160] 1-Bromo-hexadecane was reacted with 2-dimethylaminoethanol under reflux for 24 hours to give the desired cationic surfactant **35** in quantitative yield.

Peters *et al.* reported that the most efficient catalytic system they have discovered for the Hofmann elimination of their substrate consisted of *N,N*-dimethyl-*N*-hexadecyl-*N*-(2-hydroxyethyl) ammonium bromide [**35**] and sodium hydroxide in 0.099 M and 0.186 M concentrations, respectively. Therefore, trimethyl-(4-phenylbutyl)-ammonium iodide [**31**] was exposed to *N,N*-dimethyl-*N*-hexadecyl-*N*-(2-hydroxyethyl) ammonium bromide [**35**] (0.099 M) and sodium hydroxide (0.186 M) in water at 39 °C as shown in Scheme 2.1.16. The reaction progress was monitored via TLC, which confirmed a slow transformation of the starting material to the alkene. After 13 days of stirring at 39 °C, the reaction was processed and analysed via quantitative ^{1}H NMR to confirm the formation of the terminal alkene **32**, however, in only 2% yield.

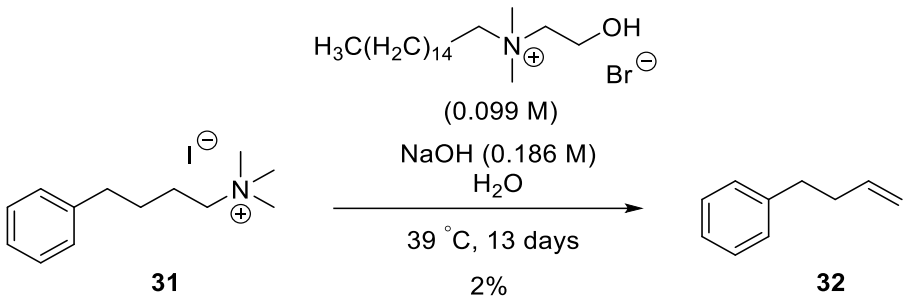

Scheme 2.1.16 The initial example of the micelle-catalysed Hofmann elimination of trimethyl-(4-phenylbutyl)-ammonium iodide [31]. The conversion was calculated using quantitative ^{1}H NMR with trimethyl benzene-1,3,5-tricarboxylate in DMSO (0.1 M) as internal standard.

Even though a low yield was obtained, this reaction confirmed the capability of a micellar system to reduce the temperature of the Hofmann elimination reaction from initially over 150 °C to 39 °C. With this initial success of a low temperature Hofmann elimination, it was believed that the yield of the reaction could be increased with further optimisation. Consequently, the micelle-catalysed Hofmann elimination was repeated with an increased amount of sodium hydroxide (2 M) in order to elevate the basicity of the system and to ensure the deprotonation of the cationic surfactant **35** (see Scheme 2.1.17). Unfortunately, increasing the amount of sodium hydroxide resulted in traces of the desired alkene (< 1%). Taking a closer look on the structure and properties of the cationic surfactant **35**, the amount of base used in combination with **35** has an impact on both the structural stability and the surface potential of the micellar system. Micellisation of *N,N*-dimethyl-*N*-hexadecyl-*N*-(2-hydroxyethyl) ammonium bromide [**35**] is based on hydrophobic and electrostatic interactions such as CTAB [**34**], but because of the hydroxyl group in the head of the surfactant, it is additionally stabilised by intermolecular hydrogen bonding interactions.[161] Upon deprotonation, the electrostatic properties of the surfactant changes, since the generation of zwitterions reduces its cationic character. Even though it has been reported that surfactants containing a zwitterionic head can form stabilised micellar structures at lower concentrations due to the decreased Coulombic repulsions of the head groups[162], the change of its surface potential effects its interaction with ionic reagents.[163] The decrease in cationic character of the surfactant might increase its interactions of the positively charged trimethyl ammonium substrate **31**, however, its interactions with the hydroxide anions of the base might be lowered leading to a decreased concentration of the basic ions in the micellar system. In addition, it is noteworthy that it has been observed by Bunton *et al.* that the catalytic effect of micelles is not directly proportional to the base concentration.[148]

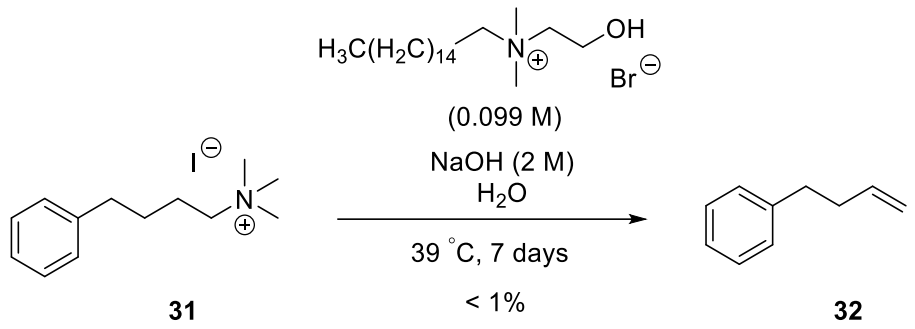

Scheme 2.1.17 Micelle-catalysed Hofmann elimination of trimethyl-(4-phenylbutyl)-ammonium iodide [31] using an increased amount of NaOH (2 M). The conversion was calculated using quantitative ^{1}H NMR with trimethyl benzene-1,3,5-tricarboxylate in DMSO (0.1 M) as internal standard.

Since the increase in base concentration reduced the yield of the micelle-catalysed Hofmann elimination, an alternative approach was taken with the goal of enhancing the efficiency of the elimination. As illustrated in Scheme 2.1.18, the amount of the cationic surfactant **35** was increased to a concentration of 0.5 M while keeping the base-to-surfactant ratio the same as in the original reaction condition. By increasing the concentration of the cationic surfactant, it was hypothesised that higher-order structures of micelles such as bilayers would be formed, which might be able to incorporate an increased amount of the trimethyl ammonium starting material **31** and thus increase the yield of the elimination. Nevertheless, the reaction resulted in the formation of the alkene **32** in only 3% yield after heating it for 7 days at 39 ℃.

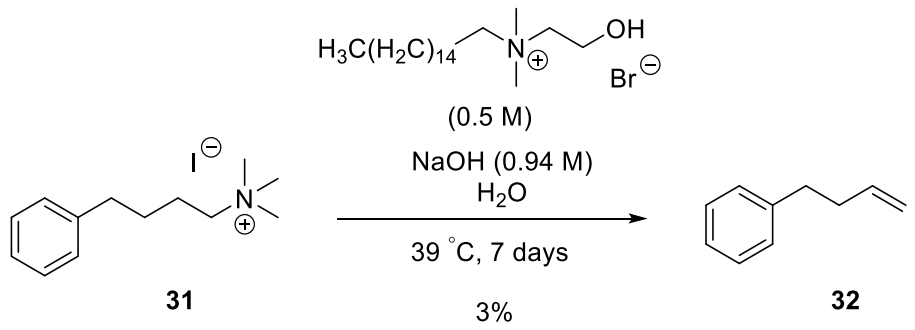

Scheme 2.1.18 Micelle-catalysed Hofmann elimination of trimethyl-(4-phenylbutyl)-ammonium iodide [31] using an increased amount of cationic surfactant 35 (0.5 M). The conversion was calculated using quantitative ^{1}H NMR with trimethyl benzene-1,3,5-tricarboxylate in DMSO (0.1 M) as internal standard.

The investigation of the micelle-catalysed Hofmann elimination was continued with the effect of temperature on the elimination reaction. Moulik *et al.* extensively studied the micellisation of *N,N*-dimethyl-*N*-hexadecyl-*N*-(2-hydroxyethyl) ammonium bromide [**35**] (the cationic surfactant investigated herein) in relation to the temperature.[164] As shown in Table 2.1.8, Moulik and colleagues stated that the cmc of **35** increased alongside the temperature confirming firstly that micelles are still being formed at higher temperatures and secondly that the micelle concentration needs to be adjusted according to the temperature used in the reaction.

Table 2.1.8 CMC values in relation to temperature reported by Moulik and co-workers for 35.[164]

Temperature [°C]	CMC [M] values determined via	
	conductometry	microcalorimetry
19.9	0.0078	0.0083
24.9	0.0083	0.0091
39.9	0.0095	0.0097
49.9	0.0107	0.0113

With these observations in mind, the micelle-catalysed Hofmann elimination of trimethyl-(4-phenylbutyl)-ammonium iodide [**31**] was performed with an increased amount of the cationic surfactant **35** at 60 °C as shown in Scheme 2.1.19 (Entry a). Unfortunately, the reaction did not yield any alkene product. To verify if an alternative cationic surfactant would lead to a similar reaction outcome at this reaction temperature, the reaction was repeated with CTAB (see Entry b). However, the same result was observed with CTAB meaning that no formation of the desired olefin **32** was detected.

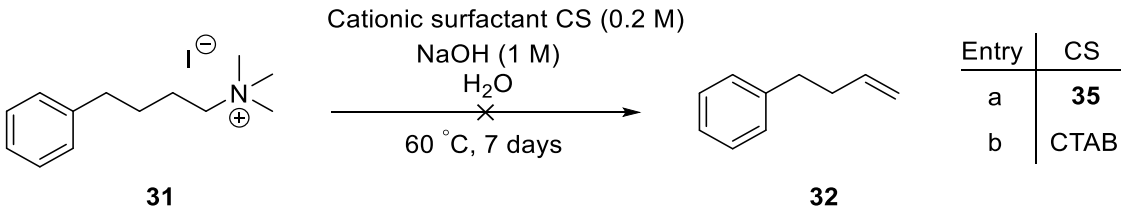

31 **32**

Scheme 2.1.19 Micelle-catalysed Hofmann elimination of trimethyl-(4-phenylbutyl)-ammonium iodide [31] at 60 °C.

To verify if the cationic surfactant **35** was forming micellar structures and to understand the effect of the base on these systems, preliminary dynamic light scattering (DLS) measurements were conducted using the conditions shown in Table 2.1.9. The DLS measurements confirmed that micelles were formed in the given conditions. When 0.186 M sodium hydroxide was included in the sample, the size of the measured micelles decreased from 31.5 nm (without a base, Entry b) to 10.9 nm (Entry a). This decrease in size confirmed the formation of the zwitterions reducing the Coulombic repulsion of the head groups of **35**. As expected, an increase in size was detected, when the concentration of **35** was increased to 0.2 M due to the formation of aggregates (see Entry c). Surprisingly, an increase in base concentration to 1 M also increased the size of the micellar structures (see Entry d), which might be the reason for the decreased yield received from the elimination in Scheme 2.1.17.

Table 2.1.9 DLS measurements to confirm the formation of micelles and the to determine the size of the micellar systems.

Entry	Cationic surfactant CS	Concentration of CS	Concentration of NaOH	Solvent	Z-Average diameter [nm]	Polydisperity Index
a	**35**	0.099 M	0.186 M	H_2O	10.9	0.154
b	**35**	0.099 M	-	H_2O	31.5	0.225
c	**35**	0.2 M	0.372 M	H_2O	368.5	0.341
d	**35**	0.099 M	1 M	H_2O	206.4	0.348

One of the remarks made during the experimental procedure of the micelle-catalysed Hofmann elimination was the low solubility of the starting material in water. The use of organic solvents in micellar catalysis is known to induce reverse micellisation, which have been used for the catalysis of distinct reactions.[155] In addition, the ability of the cationic surfactant to act as a phase transfer catalyst was believed to increase the solubility of the inorganic base in the organic solvent. Therefore, trimethyl-(4-phenylbutyl)-ammonium iodide [**31**] was exposed to *N,N*-dimethyl-*N*-hexadecyl-*N*-(2-hydroxyethyl) ammonium bromide [**35**] (0.099 M) and sodium hydroxide (0.186 M) in acetonitrile at 39 ˚C (see Scheme 2.1.20). The reaction performed in acetonitrile resulted in the generation of the terminal alkene **32** in 2% yield.

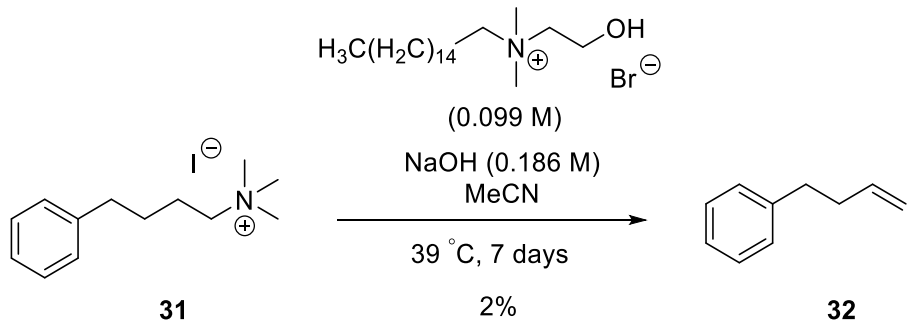

Scheme 2.1.20 Micelle-catalysed Hofmann elimination of trimethyl-(4-phenylbutyl)-ammonium iodide [31] in acetonitrile. The conversion was calculated using quantitative ^{1}H NMR with trimethyl benzene-1,3,5-tricarboxylate in DMSO (0.1 M) as internal standard.

The application of micellar catalysis on the Hofmann elimination of trimethyl-(4-phenylbutyl)-ammonium iodide [**31**] showed success in reducing the reaction temperature to 39 ̊C. Traces of the desired alkene **32** were discovered after the reactions at that temperature, confirming the catalytic effects of micelles on the Hofmann elimination. In comparison, the original solely base-mediated Hofmann elimination did not result in the formation of the alkene **32** at even 70 ̊C. Nevertheless, the sensitivity of the micellar structures to changes in reaction conditions challenged the optimisation of the micelle-catalysed Hofmann elimination. Since an alternative, more versatile approach to induce the elimination of trimethylamine was discovered, which is discussed in the subsequent chapter, we decided to discontinue our research on the micelle-catalysed Hofmann elimination.

2.2 Pd-catalysed Hofmann-type elimination of quaternary ammonium groups in organic small molecules

The use of the original Hofmann elimination presented a limitation for the progression of the project. The idea of incorporating the concept of catalysis into the Hofmann elimination was initially sparked by a publication by Peters *et al.*, in which the use of cationic surfactants surprisingly led to the elimination of trimethylamine at 39 °C.[147] As described in Subchapter 2.1.4, the impact of micelle catalysis in the Hofmann elimination was investigated, however, the low conversation rate to the olefin product and the sensibility of micelles towards changes of the reaction conditions (*e.g.* temperature) depicted the limiting criteria of the micelle-catalysed Hofmann elimination.

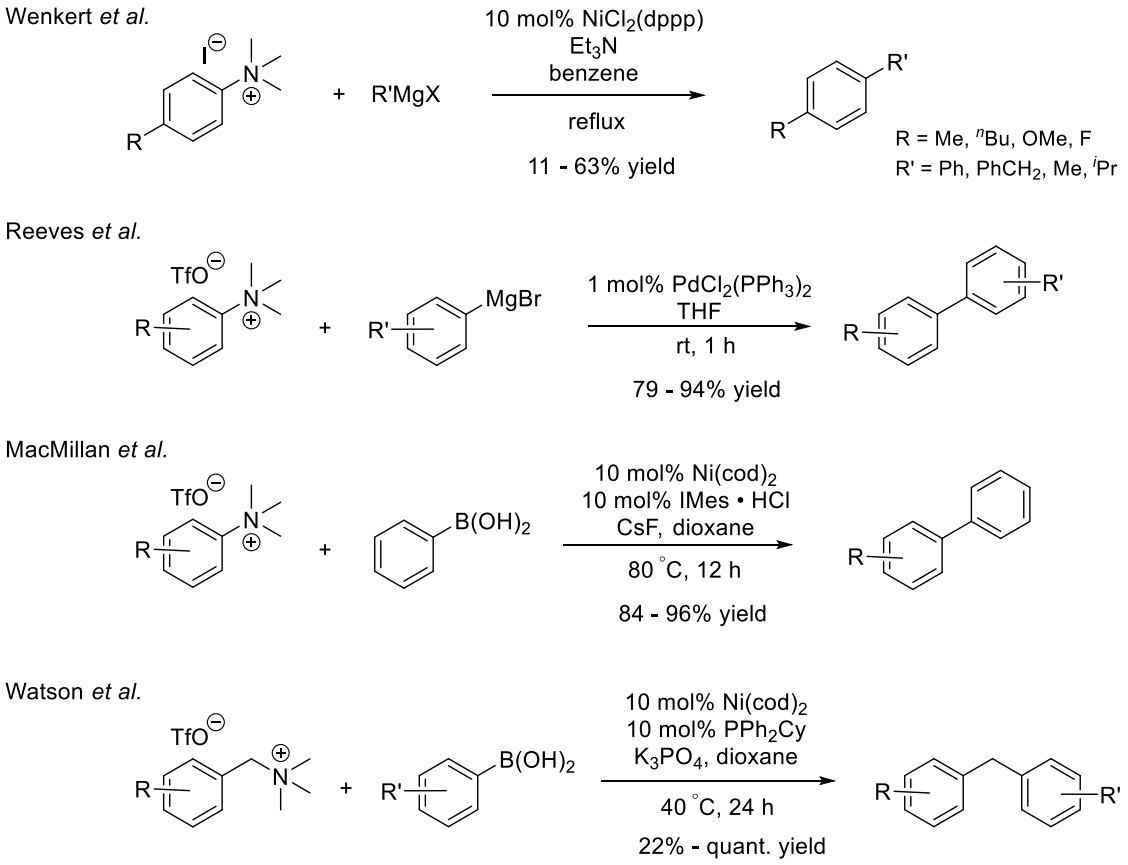

Scheme 2.2.1 Transition-metal-catalysed cross coupling of trimethyl ammonium substrates.

With the objective of finding inspiration to construct a new reaction to induce the elimination of trimethylamine, the literature was reviewed for methods of breaking a carbon-nitrogen bond. A publication from 1984 by Maier *et al.* reported the selective cleavage of carbon-nitrogen bonds via hydrogenolysis with the aid of platinum catalysts.[165] Based on this research, the idea of using transition-metals (TMs) to break the carbon-nitrogen bond of the trimethyl ammonium substrate was further investigated (Prior Art displayed in Scheme 2.2.1). In 1988, Wenkert *et al.* applied nickel catalysts to break the carbon-nitrogen bond in aryl trimethylammonium iodide via the oxidative addition of the active Ni^0 species for the Kumada-Corriu cross coupling reaction with Grignard reagents.[166] Decades later, Reeves *et al.* updated this reaction by using a palladium catalyst to couple aryl trimethylammonium triflates with Grignard reagents at room temperature.[167] Following the discovery by Wenkert, MacMillan presented the first Suzuki coupling of aryl trimethylammonium salts using $Ni[cod]_2$ as the catalyst to undergo oxidative addition upon activation. Analogously, Wang *et al.* expanded the application of the Ni-catalysed cross-coupling reactions of aryl trimethylammonium salts to perform Negishi cross-couplings[168,169] and Buchwald-Hartwig aminations[170]. The first transition-metal catalysed cross-coupling reaction on benzylic ammonium salts was published by Watson *et al.* in 2013.[171] By using $Ni[cod]_2$ and a phosphine-based ligand in the presence of aryl boronic acids, Watson and his team achieved the Suzuki cross-coupling of benzylic ammonium triflates to afford diarylmethanes. Concluding from these previous studies, the application of transition-metals to break the carbon-nitrogen bond in our substrate seemed plausible, however, several uncertainties had to be clarified to choose the suitable catalytic system to perform the elimination of trimethylamine and the subsequent generation of the terminal alkene.

Firstly, the main goal of this project is the discovery of water- and protein-compatible conditions to perform the desired chemical modification. The use of $Ni[cod]_2$, which has been applied for the cross-coupling reactions of aryl and benzyl trimethylammonium salts, is not suitable for this purpose due to its sensitivity to air and moisture. $Ni[cod]_2$ must be handled under glovebox conditions to undergo the desired oxidative addition prior to its decay. With the rise of palladium reactions performed in aqueous media, palladium catalysts have been applied to complex biological systems[172,173], which makes it an ideal candidate to use for the screening of the TM-catalysed elimination reactions.

Secondly, the goal of the TM-catalysed elimination is the generation of a terminal alkene. Since the examples given above demonstrated the use of TMs for the cross-coupling of aryl trimethylammonium salts, the design of these reactions needed to be changed to ensure

the generation of a terminal alkene instead of the cross-coupling of the substrate with another reagent. To achieve the formation of an olefin, the Heck reaction was appointed as the starting point for the design of the Pd-catalysed elimination. The Heck reaction is the palladium-catalysed arylation of olefins, which is based on the regeneration of the substituted olefin within the catalytic cycle (known as the *β*-hydride elimination). An overview of the key features of the Heck reaction is given in Subchapter 2.2.1 and the design of the Pd-catalysed elimination is discussed in Subchapter 2.2.2.

Thirdly and lastly, the examples in the literature demonstrated the use of aryl trimethylammonium salts to undergo oxidative addition. In contrast, our substrate is an alkyl ammonium salt. In the field of palladium catalysis, alkyl electrophiles are known to be unactivated substrates, which are reluctant to undergo oxidative addition.[174] This observation is due to the fact that the carbon-heteroatom bond (such as iodide, bromide) of alkyl electrophiles are more electron rich than those of aryl or vinyl electrophiles. Nevertheless, there are examples of the use of alkyl electrophiles in palladium-catalysed reactions, which have been through catalyst and reaction optimisation.[175,176]

Taking these propositions into consideration, we were optimistic to design a new reaction, which was based on the oxidative addition of an activated palladium catalyst into the carbon-nitrogen bond of the alkyl ammonium substrate. We believed that the diversity of palladium chemistry would make it possible to find convenient palladium catalysts to achieve the elimination of trimethylamine under mild conditions.

2.2.1 Background: The Heck reaction as the foundation for the Pd-catalysed Hofmann-type elimination

In the beginning of the 1970s, Heck[177] and Mizoroki[178,179] independently discovered that organic halides react with catalytic amounts of palladium forming the organopalladium precursors for vinylic substitution reactions. These reactions were conducted in the presence of a base at elevated temperature. Heck and colleagues developed this reaction further[180], which throve to become one of the most widely used C – C cross coupling reactions and thus a powerful tool in organic synthesis. Today, the Heck reaction is known as the palladium-catalysed arylation or alkenylation of olefins using aryl, alkenyl and alkyl (no β-hydrogen atoms present) electrophiles. Scheme 2.2.2 displays the standard Heck reaction. The reactivity of the Heck catalysis is based on the ability of the active Pd^0 to insert into various R – X bonds via an oxidative addition step and the addition of the resulting organopalladium intermediate to unsaturated bonds.

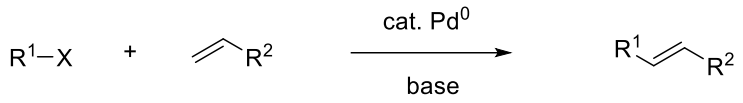

R^1 = aryl, benzyl, alkenyl, alkyl (without a β-hydrogen atom)
X = I, Br, Cl, OTf, OTs, N_2^+ etc.

R^2 = large variety of functional groups

Scheme 2.2.2 Standard Heck reaction.

Over decades of optimisation, the Heck reaction has expanded its applicability from the traditional organic halides to more diverse electrophiles such as organic triflates, aryldiazonium ions and aromatic carboxylic acids, anhydrides and active esters.[181,182] Numerous reviews have been published to cover different aspects of the Heck reaction, which provide the reader with further detail.[182–187] To implement palladium catalysis into the elimination of quaternary ammonium salts and to further optimise the resulting Pd-catalysed Hofmann-type elimination, it is important to recognise key determinants of Pd-catalysed cross coupling reactions such as the Heck reaction and to understand their function:

1. *Palladium precatalyst*: A vast range of palladium sources have been used for palladium catalysis, *i. a.* the widely known $Pd(OAc)_2$ and $Pd_2(dba)_3$.[188] Nevertheless, the choice

of palladium precursor used for specific transformations is important due to its influence on the catalytic rates of the reaction.[189]

2. *Solvent*: Palladium-catalysed reactions tolerate a variety of solvents, but mainly polar aprotic solvents such as NMP and dioxane are being used frequently due to their σ-donating property.

3. *Base*: The nature of the base for palladium-catalysed reactions is versatile and both organic bases including tertiary amines (Et_3N, Cy_2NMe etc.) and inorganic bases such as K_2CO_3 and K_3PO_4 can be used. However, it is essential to use at least a stoichiometric amount of base to neutralize the strong acid released in palladium-catalysed reactions.

4. *Ligand*: A massive library of ligands ranging from bulky tertiary phosphines to palladacycles to carbene etc. has been employed in palladium catalysis.[190,191] The role of the ligand is the *in situ* generation of the active Pd^0 catalyst and its stabilization throughout the reaction. The modification of the steric and electronic properties of the ligand allows the fine-tuning of the catalytic system and thus it generates a platform to regulate the reaction according to the substrates used. The first examples of the Heck reaction have shown that the use of ligands is not a requirement for this transformation, but they are used to increase the reactivity and longevity of the catalyst. To overcome the stability issues of a ligand-free catalytic system, Jefferey introduced the use of quaternary ammonium salts, which is now referred to as the Jefferey conditions.[192–194] De Vries *et al.* adopted the Jefferey conditions and demonstrated that the ligandless Heck reaction can still be efficiently used with extremely low Pd-loading.[195] Herrmann *et al.* combined the use of phase-transfer agents with a catalytic system consisting of both the Pd-catalyst and the phosphine ligand. The to date known Herrmann-Beller conditions were first shown in the Heck olefination of chloro- and bromoarenes using palladacycles in the presence of quaternary ammonium salts.[196]

5. *Additives*: In some cases, such as in asymmetric Heck reactions, the use of silver(I) additives plays a major role in the success of the reaction. Silver(I) additives have been used as halide scavengers to prevent the deactivation of the catalyst and enhance the reaction by forming 16-electron, cationic palladium intermediates, which transform the mechanism of the reaction from the neutral to the cationic pathway.[197]

The influence of all these reactants on the Pd-catalysed Hofmann-type elimination was studied, and the results are discussed in the subsequent subchapters.

The General Mechanism of the Heck Reaction

Scheme 2.2.3 illustrates a generic Heck catalytic cycle, which has been used to introduce the major steps of the Heck reaction. Yet, it is only a simplified approximation, since the mechanism of the Heck reaction varies depending on the substrate, the catalytic system and the reaction conditions used. The first step in the basic mechanism is the activation of the Pd precatalyst to the active Pd^0 (**A**) *in situ*, which is usually performed by phosphines if they are being used as ligands. The active Pd^0 catalyst inserts into the carbon – heteroatom bond of the electrophile via oxidative addition (**B**) cleaving that bond and forming an organopalladium(II) complex. The oxidative addition is accepted to be the rate-determining step of the Heck reaction. Coordination of an alkene to the Pd-complex followed by the migratory insertion (**C**) of the organopalladium(II) intermediate to the alkene occurs next. Prior to the *syn* β-hydride elimination (**E**) leading to the substituted alkene product, the organopalladium(II) complex rotates around the C – C bond (**D**) to facilitate a co-planar structure of the hydrogens to the palladium. Finally, the catalytic cycle is completed by the deprotonation of the hydrinopalladium(II) complex by means of a base reforming the active Pd^0 catalyst in the reductive elimination step (**F**).

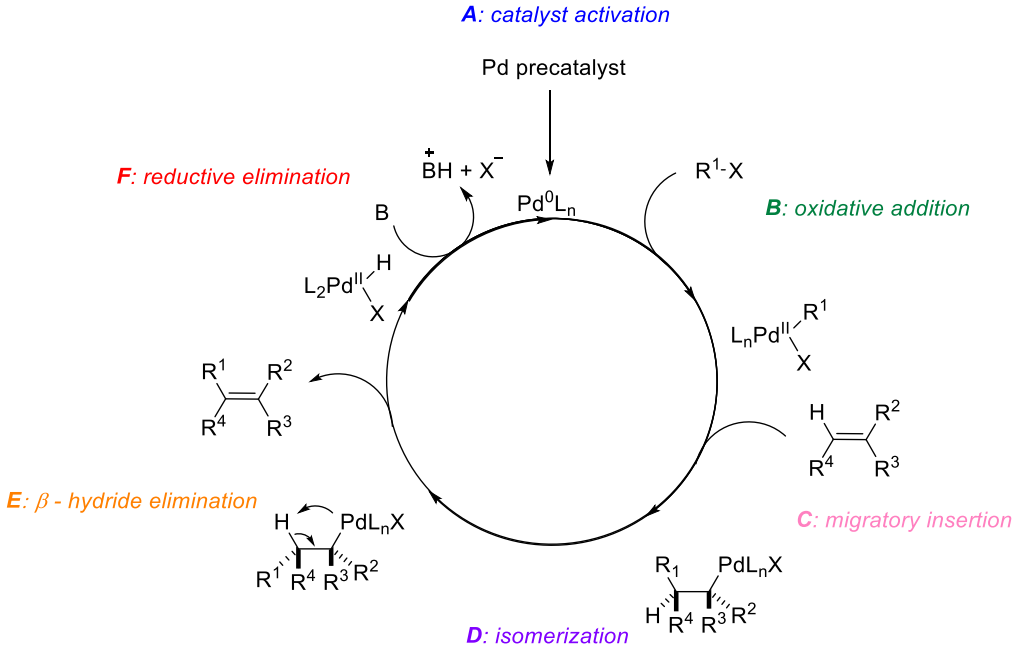

Scheme 2.2.3 The general mechanism of the Heck reaction.

2.2.2 Pd-catalysed Hofmann-type elimination

The Heck reaction was chosen as a template, from which the Pd-catalysed Hofmann-type elimination reaction could be developed. As described in the previous subchapter, the objective of the Heck reaction is the Pd-catalysed substitution of alkenes using aryl electrophiles, *i.e.* the migratory insertion of the organopalladium complex to the alkene is a key step in the Heck catalytic cycle. In contrast, the aim of the Pd-catalysed Hofmann-type elimination is the cleavage of the C(sp^3) – N bond, followed by the formation of a terminal alkene and the elimination of trimethylamine. Consequently, the Heck catalytic cycle had to be altered, eliminating the migratory insertion step, to meet the distinct objectives of the Pd-catalysed Hofmann-type elimination.

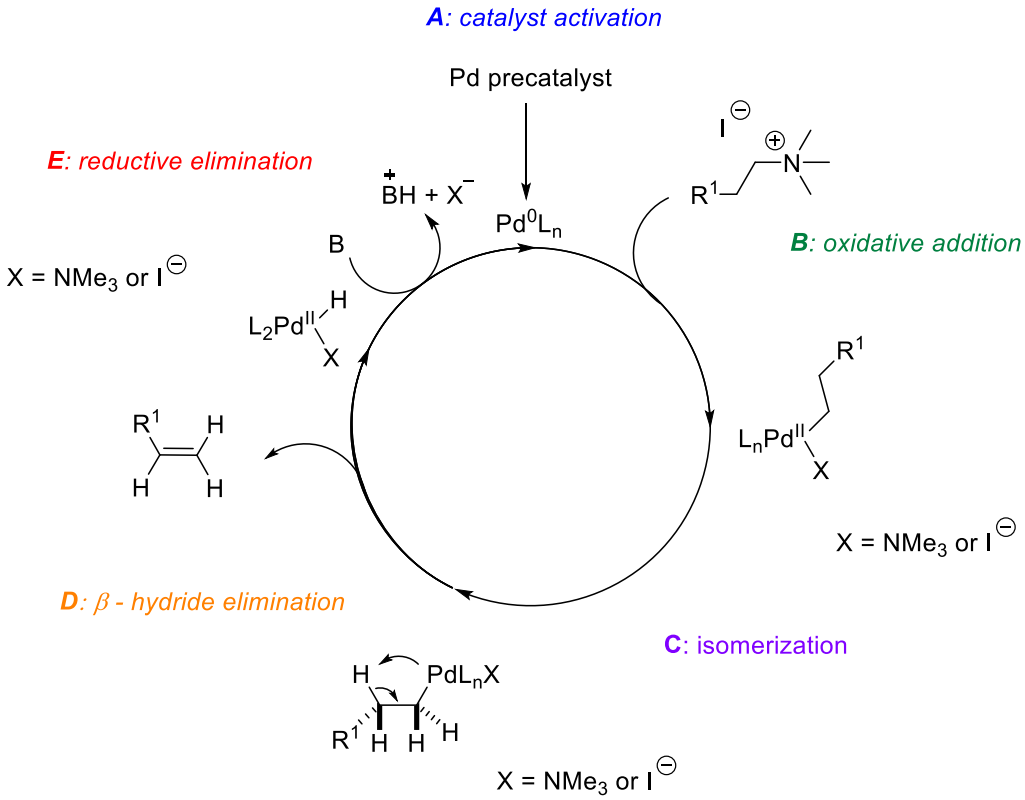

Scheme 2.2.4 Proposed general mechanism of the Pd-catalysed Hofmann type elimination.

Scheme 2.2.4 displays the modified catalytic cycle to describe the Pd-catalysed Hofmann-type elimination of trimethylammonium electrophiles. Identical to the Heck reaction, the Pd-

catalysed elimination starts with the activation of the palladium precatalyst to the active Pd^0 (**A**). The active Pd^0 species can now insert into the $C(sp^3)$ – $N(Me_3)$ bond leading to the alkylpalladium(II) intermediate (**B**). Since the electrophile used in the Pd-catalysed elimination is an ammonium salt, a counterion is present and can be bound to the metal. Consequently, it is important to consider the effect of the counterion on the reactivity of this reaction. The next step in the Pd-catalysed elimination is the isomerization of the alkylpalladium(II) complex (**C**) to guarantee coplanarity of the hydrogens prior to the *β*-hydride elimination (**D**). After the formation of the terminal alkene, the hydrinopalladium(II) complex can undergo base-assisted reductive elimination resulting in the regeneration of the active Pd^0 catalyst (**E**).

The following remarks resulting from the proposed catalytic cycle of the Pd-catalysed Hofmann-type elimination can be incorporated into the strategy of the reaction screening:

(1) A choice of different precatalysts and ligands can induce different mechanisms, on which the oxidative addition occurs.
(2) The activity of the Pd-catalyst can be tuned by means of ligands; however, it is noteworthy that the effect of the ligand can be contradictory within different parts of the catalytic cycle, *e.g.* electron-donating, less sterically-hindered ligands favour oxidative addition, whereas electron-withdrawing, sterically-hindered ligands favour reductive elimination. Therefore, it is important to find an optimum balance.
(3) Due to the presence of ions in the reaction, it is important to make sure that the metal has free coordination sites, which can facilitate oxidative addition and *β*-hydride elimination.
(4) High nucleophilicity of the Pd-complex is necessary to induce *β*-hydride elimination.

Hence, the strategy of the Pd-catalysed Hofmann-type elimination screening is to investigate each step of the proposed catalytic cycle to both increase their efficiency and identify possible obstacles impeding the catalysis of the elimination. Once these obstacles are identified, they can then be rectified by modifying the reaction conditions accordingly.

Since no prior evidence was found on the oxidative addition of a Pd-complex into a $C(sp^3)$ – $N(Me_3)$ bond connected to an alkyl chain and on the subsequent elimination of trimethylamine, this proposed transformation, if successful, would represent a novel reaction for all future eliminations of quaternary ammonium functionalities and formations of terminal alkenes.

2.2.3 Initial investigation of the Pd-catalysed Hofmann-type elimination

To test the newly designed Pd-catalysed Hofmann-type elimination reaction, one of the original Heck conditions using palladium(II) acetate and tri(*o*-tolyl)phosphine as the catalytic system was applied to our model system. After Heck introduced the use of tri(*o*-tolyl)phosphine as a potential ligand[180], Spencer displayed the efficiency of tri(*o*-tolyl)phosphine in the arylation of olefin with aryl bromides reaching high turnover numbers with low catalyst loading in polar aprotic solvents.[198] Consequently, trimethyl-(4-phenylbutyl)-ammonium iodide [**31**] was reacted with palladium(II) acetate, tri(*o*-tolyl)phosphine and triethylamine in acetonitrile at 60 °C for 24 h as shown in Scheme 2.2.5. The quantitative ^{1}H NMR analysis of the reaction using trimethyl benzene-1,3,5-tricarboxylate as the internal standard displayed a minimal conversion (1%) of the starting material **31** to the desired product **32** confirming the feasibility of our hypothesis. Additionally, starting material **31** was only identified in the obtained complex proton spectrum, however, its exact absolute concentration value could not be determined due to a possible loss of the ionic compound in the post-reaction work-up.

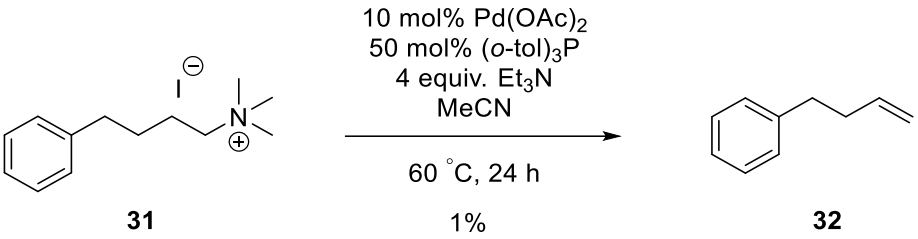

Scheme 2.2.5 Initial Pd-catalysed Hofmann-type elimination of the alkyl trimethylammonium iodide substrate 31. The conversion was calculated using quantitative ^{1}H NMR with trimethyl benzene-1,3,5-tricarboxylate in DMSO (0.1 M) as internal standard.

The initial result of the reaction provided a new opportunity for the continuity of the project. Even though the low conversion of 1% was not sufficient, it was believed that through screening of suitable reaction conditions for the Pd-catalysed Hofmann-type elimination, an improvement in yield could be achieved. With the primary aim of increasing the yield of the reaction to minimum 20%, the screening of the Pd-catalysed elimination was commenced by

investigating the effect of the ligand onto the reaction outcome (see Table 2.2.1). Through the ligand it should be possible to fine-tune the catalyst's activity towards specific parts of the catalytic cycle by alternating its steric and electronic properties.[186]

Table 2.2.1 The influence of a range of ligands on the Pd-catalysed Hofmann-type elimination.

*4.5 equiv. of base was used for this reaction. †The conversion was calculated using quantitative ^{1}H NMR with trimethyl benzene-1,3,5-tricarboxylate in DMSO (0.1 M) as internal standard.

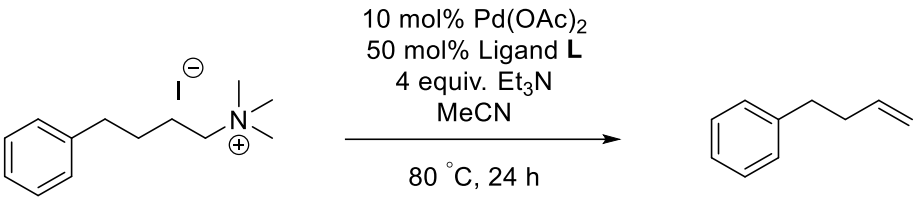

31 **32**

Entry	**Ligand L**	Conversion to **Product**†
a	(*o*-tol)$_3$P	2%
b	CyPh$_2$P	1%
c*	^{t}Bu$_3$PH • BF$_4$	< 1%
d	(*p*-OMePh)$_3$P	5%
e	*rac*-BINAP	1%
f	dppf	< 1%
g	BrettPhos	1%
h	SPhos	2%
i	^{t}BuDavePhos	1%

Palladium(II) acetate and tri(*o*-tolyl)phosphine form a dimeric, extremely thermally stable (up to 250 °C) palladacycle *in situ* prolonging the lifetime of the palladium complex compared to the conventional Pd/PPh$_3$ catalytic complex.[199] Consequently, the reaction shown in Scheme 2.2.5 was repeated, however, the temperature was increased from 60 °C to 80 °C with the goal of increasing the formation of the product **32**. The elevation of temperature led to a 2% conversion of the trimethylated ammonium substrate **31** to the terminal alkene **32** (see Entry a, Table 2.2.1). Next, a range of ligands, which are deployed in common Pd-catalysed cross-coupling reactions, were investigated. Table 2.2.1 summarises the ligand screening and its outcome. Entries b – d present a small library of monodentate tertiary phosphine ligands, which are most commonly used in the traditional Heck reaction.[184] In contrast to the conventionally

used triphenylphosphine, the replacement of the aromatic substituents by alkyl substituents increases the electron-donating character of the monodentate phosphine ligands resulting in more active catalytic systems. Nevertheless, the use of cyclohexyldiphenylphosphine (Entry b) and tri-*tert*-butylphosphine (Entry c) did not result in an improvement in yield. Hii *et al.* showed that compared to the traditional triphenylphosphine an addition of a *para*-substituent (MeO- or Me_2N-) on the phenyl ring increased the relative rates of the reaction by making the ligand-metal complex more electron-rich.[200] Consequently, tris(2,4,6-trimethoxyphenyl)phosphine was included in the library of ligands (Entry d), which led to an increase in conversion to the olefin product **32** to 5%. In the search for active ligands to overcome the struggles in using more unreactive electrophiles such as aryl bromides and aryl chlorides, Buchwald and Hartwig, respectively, introduced the application of chelating ligands in Pd-catalysed cross-coupling reactions. The early examples of chelating ligands in Pd-catalysed reactions were the use of (±)-2,2′-bis(diphenylphosphino)-1,1′-binaphthalene (*rac*-BINAP) by Buchwald *et al.*[201] and the use of 1,1-bis(diphenyl-phoshino)ferrocene (dppf) by Hartwig *et al.*[202]. Both ligands were investigated in the Pd-catalysed elimination of trimethyl-(4-phenylbutyl)-ammonium iodide [**31**] as listed in Entry e and Entry f (Table 2.2.1). Unfortunately, both reactions did not improve the conversion rate to the desired product. Inspired by the effect of chelating ligands on Pd-catalysed cross coupling reactions, Buchwald *et al.* introduced a new class of phosphine ligands in 1998, whose unique design is based on a dialkylbiaryl phoshine backbone.[203] Ever since their discovery, these phosphines have had a massive impact on many TM-catalysed reactions including the Heck reaction.[204] A small selection of Buchwald ligands has been investigated in the Pd-catalysed Hofmann-type elimination reaction and their structures are displayed in Figure 2.2.1.

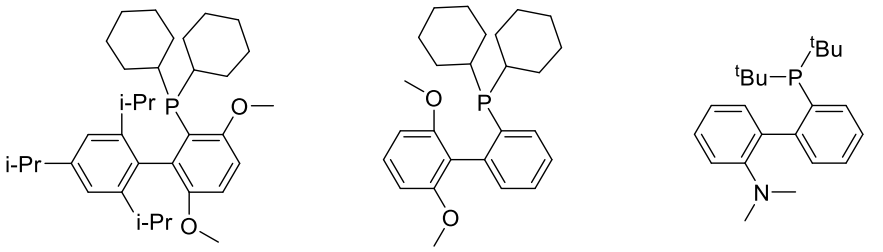

Figure 2.2.1 Structure of the Buchwald-ligands screened for the Pd-catalysed elimination reactions.

Unfortunately, the use of these Buchwald ligands did not result in an increase in elimination of the trimethylammonium functionality to give the terminal alkene **32**. The results of these reactions are shown in Entries g – i. The screening of the selection of ligands listed in Table 2.2.1 did not result in a significant increase in yield. The Pd-catalysed elimination using tris(2,4,6-trimethoxyphenyl)phosphine as the ligand (Entry d) gave the highest yield of the screening with a conversion rate of 5%. At this early stage of the screening, it was not clear why the reaction only resulted in a minimal conversion of the quaternary ammonium substrate **31** to the alkene **32**. Preliminary mechanistic studies were conducted using ^{31}P NMR spectroscopy to identify which step of the catalytic cycle was impeded in the conducted Pd-catalysed elimination of trimethyl-(4-phenylbutyl)-ammonium iodide [**31**]. However, the complex ^{31}P NMR spectra obtained in these experiments were inconclusive and the cause for the low conversion rate of these reactions could not be determined by means of ^{31}P NMR spectroscopy. Therefore, it was decided to continue the investigation of the Pd-catalysed Hofmann-type elimination with a more traditional approach by analysing each parameter of the catalytic cycle individually with the ligand, which afforded the highest conversion rate.

2.2.4 Investigation of the solvent effects on the Pd-catalysed Hofmann-type elimination

The first step towards improving the conversion rate of the Pd-catalysed Hofmann-type elimination was taken by analysing the effect of the solvent on the catalysis. In transition-metal-catalysed cross coupling reactions, the solvation effect of the solvent can manipulate the efficiency of the catalyst by entering the coordination sphere of the metal and possibly competing with the ligand.[205] Clark *et al.* demonstrated that the initial rate in the Heck reaction was proportional to the dipolarity of the solvent.[206] A preference on σ-donating dipolar aprotic solvents for the Heck reaction is reported throughout the literature.[207,208] Acetonitrile was initially used for the screening of the ligands, since the starting material **31** was completely soluble in it and nitrile solvents have been frequently used in the Heck reaction. Table 2.2.2 displays the summary of the investigated solvents for the Pd-catalysed elimination reaction.

Table 2.2.2 The influence of distinct solvents on the Pd-catalysed Hofmann-type elimination.
†The conversion was calculated using quantitative ^{1}H NMR with trimethyl benzene-1,3,5-tricarboxylate in DMSO (0.1 M) as internal standard.

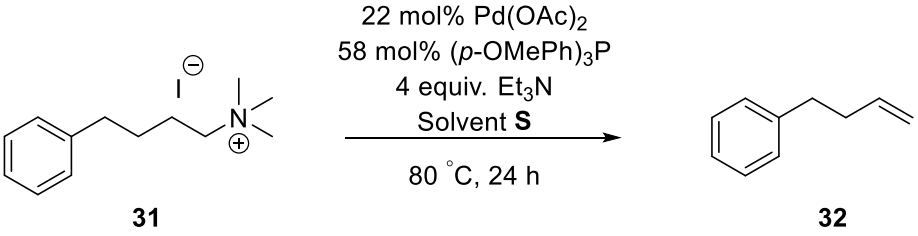

31 **32**

Entry	**Solvent S**	Conversion to **Product**†
a	DMSO	< 1%
b	NMP	1%
c	H_2O : MeCN, (1 : 1)	2%
d	Toluene	1%
e	Dioxane	1%
f	THF	1%

The reactions were conducted with the catalytic system consisting of palladium(II) acetate, tris(2,4,6-trimethoxyphenyl)phosphine and triethylamine. The use of DMSO (Entry a) as the solvent only gave traces of the desired product **32** (< 1%). NMP (Entry b), toluene (Entry d), dioxane (Entry e) and THF (Entry f) resulted in a conversion rate of 1%. The effect of water has been explored in Pd-catalysed cross coupling reactions. Hayashi *et al.* first reported that water was necessary for the reduction of $Pd(OAc)_2$ to the active catalyst in the presence of BINAP.[209] Ever since then, the importance of water on the activation of the $Pd(OAc)_2$ precatalyst has been discussed in several publications.[210–212] Thus, the addition of water to acetonitrile was hoped to have an impact on the Pd-catalysed elimination. However, the use of the co-solvent water-acetonitrile (1 : 1, Entry c) only resulted in the formation of the product **32** in comparably low yield (2%).

Table 2.2.3 Investigation of the activity of the Pd-catalyst at different time points t in the Pd-catalysed elimination. †The conversion was calculated using quantitative ^{1}H NMR with trimethyl benzene-1,3,5-tricarboxylate in DMSO (0.1 M) as internal standard.

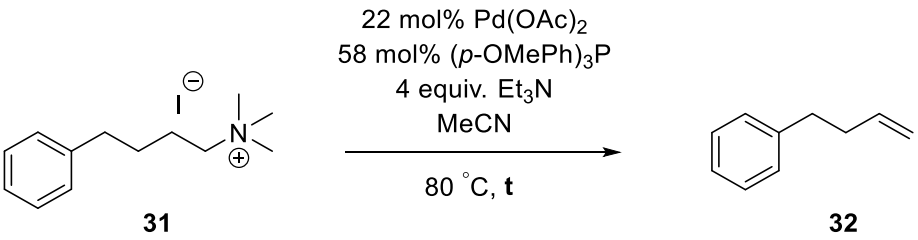

Entry	**t**	Conversion to **Product**†
a	24 h	2%
b	18 h	1%
c	12 h	1%
d	9 h	1%
e	6 h	2%

Since the investigation of different solvents did not result in an increase in yield, the screening was continued using acetonitrile as the solvent. At this point in the investigation, it was believed that the lifetime of the active catalyst might have be a reason why the reaction was not leading

to a full conversion. Palladium black was detected after the reaction disputing the stability of the Pd^0 catalyst, which could undergo metal aggregation and precipitate. In order to confirm if the catalyst was inactive for the substantial part of the 24 h reaction time, a time study was conducted. The reaction using palladium(II) acetate, tris(2,4,6-trimethoxyphenyl)phosphine and triethylamine was repeated at 80 °C. Thereby, the reaction time was decreased stepwise from 24 h to 6 h to determine when the reaction reached its plateau (see Table 2.2.3). As a starting point for the time study, the original reaction, which initially gave a conversion of 5% after 24 h (see Table 2.2.1, Entry d) was repeated, however, this time it resulted in a conversion of 2% as shown in Table 2.2.3, Entry a. Even a fourfold decrease in reaction time (Entry e), *i.e.* a total reaction time of 6 h, resulted in a conversion of 2%. These results confirm that there was no further turnover of product beyond the earliest time point.

The results demonstrated in Table 2.2.3 supported our suspicion that the deterioration of the active catalyst might be the reason for the low conversion rates of the reaction. A closer analysis of the reductive elimination in the Pd-catalysed Hofmann-type elimination was conducted to investigate the efficiency of the regeneration of the Pd^0 from the Pd-H catalyst. The results of this investigation are presented in the following subchapter.

2.2.5 Analysis of the Reductive Elimination step in the catalytic cycle

The reductive elimination in the Pd-catalysed Hofmann-type elimination is responsible for the reduction of the *in situ* generated palladium(II) hydride to the active Pd^0 catalyst completing the catalytic cycle. In case the reductive elimination is inhibited, the catalytic cycle can come to a halt and the effective palladium catalyst can be captured as palladium(II) hydride, which can add into olefins causing double bond isomerization and migration and thus the formation of possible side products.[213,214] The base plays a major role in the reductive elimination of palladium(II) hydride, since it induces dehydrohalogenation via deprotonation of the hydrinopalladium(II) complex and generation of the zero-valent palladium catalyst. In addition, it has been reported that the base affects the overall rate of the Heck reaction by stabilising the anionic $[Pd^0(Ar_3P)_2(OAc)]^-$ catalytic species during catalyst activation and oxidation addition.[215] Depending on the nature of the base, it can also influence the stability of the catalytic complex by coordinating to the metal or inducing ligand exchange. Consequently, it was decided to test a selection of bases with varying electronic and steric properties to improve the efficiency of the reductive elimination and thus increase the catalyst's turnover number. Table 2.2.4 lists a range of inorganic and organic bases, which have been commonly used in Pd-catalysed cross coupling reactions and thus were investigated in the Pd-catalysed Hofmann-type elimination of trimethyl-(4-phenylbutyl)-ammonium iodide [**31**] using palladium(II) acetate and tris(2,4,6-trimethoxyphenyl)phosphine in acetonitrile at 80 °C for 24 h. Parameters including base strength, solubility and solvation effects, sterics and ionic dissociation have an impact on the efficiency of the base in the reductive elimination step. In contrast to sodium acetate (Entry c) and potassium phenolate (Entry d), which did not result in the formation the desired alkene **32**, potassium carbonate (Entry a) gave a 2% conversion to the product. Potassium *tert*-butoxide (Entry b) only generated traces of the desired olefin **32** (< 1%). Comparing the results of the inorganic bases to the organic bases, DBU (Entry e), proton sponge (Entry f) and *N,N*-dicyclohexylmethylamine (Entry g) yielded the product **32** in similar rates (2%, 2% and 1%). Concluding from these results, the change in base did not have an apparent impact on the conversion rate of the Pd-catalysed Hofmann-type elimination. The base study therefore did not provide conclusive evidence that the reductive elimination was in fact the limiting factor of the catalytic cycle. Consequently, the examination of the regeneration of Pd^0 was continued and the initial base study was expanded concentrating on inorganic bases.

Table 2.2.4 The influence of the base on the Pd-catalysed Hofmann-type elimination. †The conversion was calculated using quantitative ^{1}H NMR with trimethyl benzene-1,3,5-tricarboxylate in DMSO (0.1 M) as internal standard.

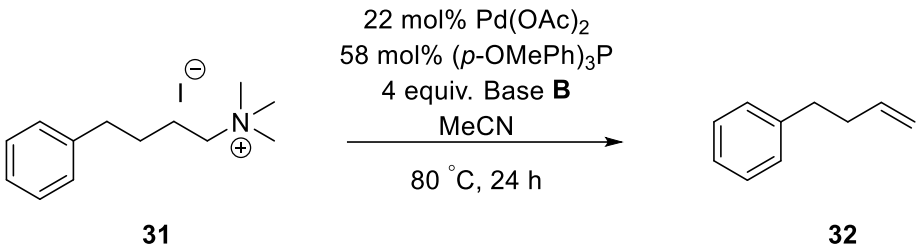

31 **32**

Entry	**Base B**	Conversion to **Product**†
a	K_2CO_3	2%
b	KO^{t}Bu	< 1%
c	NaOAc	-
d	KOPh	-
e	DBU	2%
f	Proton Sponge	2%
g	Cy_2NMe	1%

As mentioned in Table 2.2.4, the use of potassium carbonate in acetonitrile in the Pd-catalysed elimination resulted in a 2% conversion of the trimethylammonium substrate **31** to the terminal alkene **32**. A possible reason behind the low conversion rate was believed to be the low solubility of potassium carbonate in acetonitrile. It was hypothesized that an increase in solubility of the inorganic base in the reaction solvent might improve the efficiency of the catalyst's regeneration. In addition, the effect of water on the activation of catalyst (see Subchapter 2.2.4) might influence the overall success of the reaction. Hence, the Pd-catalysed Hofmann-type elimination of trimethyl-(4-phenylbutyl)-ammonium iodide [**31**] using palladium(II) acetate and tris(2,4,6-trimethoxyphenyl)phosphine was repeated and water was added as a co-solvent to acetonitrile (1 : 4) to ensure a better solubility of potassium carbonate in the reaction solvent (see Table 2.2.5, Entry b). As a control to compare the outcome of this reaction, trimethyl-(4-phenylbutyl)-ammonium iodide [**31**] was also reacted with palladium(II)

acetate and tris(2,4,6-trimethoxyphenyl)phosphine in the co-solvent system of water : acetronitrile (1 : 4) using triethylamine as the base (Entry a). Both reactions only yielded traces of the desired product **32** (< 1%).

Caesium carbonate was added to the library of bases examined in the Pd-catalysed Hofmann-type elimination, since it is known to have a higher solubility in organic solvents compared to potassium carbonate.[216] Entries c – d display the use of caesium carbonate as the base in the Pd-catalysed elimination of trimethyl-(4-phenylbutyl)-ammonium iodide [**31**]. The reaction using caesium carbonate in acetonitrile resulted in the minimal formation of the product **32** (< 1%, Entry c). The change in solvent from the polar, aprotic acetonitrile to the polar, protic *n*-butanol did not improve the yield of the reaction (Entry d). With the attempt to increase the stabilisation of the active catalyst as well as to improve the efficiency of the reductive elimination, tetrabutylammonium bromide was added to the reaction using caesium carbonate in water : acetonitrile (1 : 4) as shown in Entry e.

There are many advantages of encompassing quaternary ammonium salts in palladium catalysis (see Subchapter 2.2.13). It was believed that the addition of tetrabutylammonium bromide would improve the overall solubility of the reagents by acting as a phase transfer catalyst. Additionally, it was presumed that tetrabutylammonium bromide would further stabilise the Pd^0 catalyst increasing its longevity and it would exchange the more ligating iodide counterion with bromide. Even with the reported benefits of the quaternary ammonium additive, this reaction only gave traces of the desired olefin **32** (< 1%, see Entry d).

An alternative additive for Heck reactions is the use of silver(I) salts, whose advantages are listed in Subchapter 2.2.1.[197] As displayed in Entry f, silver(I) carbonate was added to the reaction using potassium carbonate as the base in water : acetonitrile (1 : 4). It was aimed that the use of silver(I) carbonate would lead to the trapping of the iodide counterion as silver(I) iodide precipitate leaving the weakly coordinating carbonate ion in the reaction mixture. The oxidative addition and the *β*-hydride elimination steps in the catalytic cycles require a free coordination site on the catalyst to function. By trapping the iodide counterion with silver(I) carbonate, it was ensured that the lack of coordination site on the metal was not the cause for the low yielding Pd-catalysed elimination. Unfortunately, the addition of silver(I) carbonate did not improve the yield of the reaction and only traces of the olefin **32** were detected (Entry f).

Table 2.2.5 Closer examination of inorganic bases used on the Pd-catalysed Hofmann-type elimination. †The conversion was calculated using quantitative ^{1}H NMR with trimethyl benzene-1,3,5-tricarboxylate in DMSO (0.1 M) as internal standard.

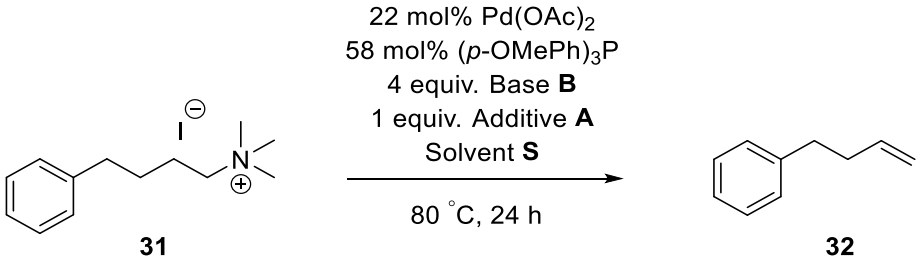

Entry	**Base B**	**Additive A**	**Solvent S**	Conversion to **Product**†
a	Et_3N	-	H_2O : MeCN (1 : 4)	< 1%
b	K_2CO_3	-	H_2O : MeCN (1 : 4)	< 1%
c	Cs_2CO_3	-	MeCN	< 1%
d	Cs_2CO_3	-	*n*-butanol	< 1%
e	Cs_2CO_3	$^nBu_4NBr$	H_2O : MeCN (1 : 4)	< 1%
f	K_2CO_3	Ag_2CO_3	H_2O : MeCN (1 : 4)	< 1%

To compare the results of the interplay of base and the used catalytic system to an alternative catalytic system, the base study was repeated using palladium(II) acetate and BrettPhos. Fu *et al.* observed that the reductive elimination is sensitive to the structure of the ligand, which they postulated to be based on the L – Pd – L geometry of the palladium(II) hydride complex.[217] Upon reductive elimination, the steric tension of the L_2PdHX complex is relieved, which is the driving force for the generation of the Pd^0 catalyst. By incorporating the more sterically demanding BrettPhos ligand in our base study, we believed to further improve the reductive elimination. In addition, the increased stability of the Buchwald ligands in comparison to the tertiary aryl phosphine ligands was believed to stabilise the active Pd^0 more efficiently preventing the generation of the inactive palladium black. The effect of the base using palladium(II) acetate and BrettPhos as the catalytic system is summarised in Table 2.2.6.

Table 2.2.6 Closer examination of inorganic bases used for the Pd-catalysed Hofmann-type elimination using an alternative catalytic system. †The conversion was calculated using quantitative ^{1}H NMR with trimethyl benzene-1,3,5-tricarboxylate in DMSO (0.1 M) as internal standard.

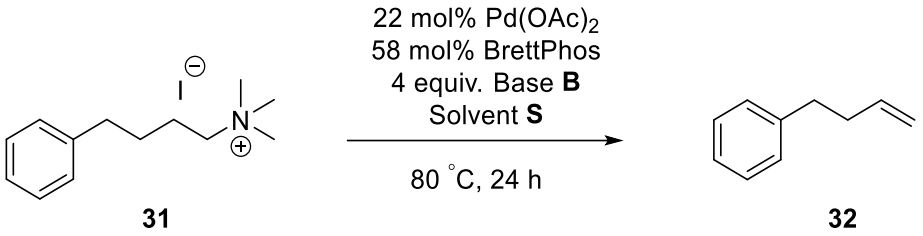

31 **32**

Entry	**Base B**	**Solvent S**	Conversion to **Product**†
a	Et_3N	MeCN	1%
b	K_2CO_3	H_2O : MeCN (1 : 4)	< 1%
c	Cs_2CO_3	MeCN	< 1%
d	Cs_2CO_3	*n*-butanol	< 1%

As shown in Entries b – d, a change in base and solvent did not lead to an increase in yield compared to the originally investigated reaction condition using triethylamine in acetonitrile (Entry a). All three reactions resulted in a minimal formation of the desired product **32** (< 1%). These results verified that the limited conversion to the product remained even after alternating the base in a diverse catalytic system using BrettPhos, which provided a different stabilising effect to the catalyst. Since the excessive screening of the base in the Pd-catalysed Hofmann-type elimination did not enhance the conversion of the quaternary ammonium starting material **31** to the terminal alkene **32**, it was presumed that the limiting factor may not be the catalyst's regeneration process in catalytic cycle. Consequently, alternative pathways, which might have caused the deterioration of the catalyst were investigated and they are discussed next.

2.2.6 Oxygen as the destroyer of the active catalyst?

Pd-catalysed cross coupling reactions are performed under an inert, oxygen-free environment, because the presence of oxygen can cause the ligand to oxidize leading to a decrease in stability of the active catalyst and hence to the formation of palladium clusters and eventually to the precipitation of palladium black.[218,219] All the reactions performed hitherto were conducted under inert condition degassing each reagent individually prior to their addition to a sealed reaction vessel. In order to confirm if the presence of remaining oxygen was the cause for the decay of the catalyst, the Pd-catalysed elimination reactions using palladium(II) acetate, tris(2,4,6-trimethoxyphenyl)phosphine and caesium carbonate were repeated under the presence of oxygen (see Table 2.2.7, Entries a – e). Compared to the previously performed reactions, the order of addition of the reagents were also changed. Instead of adding the reagents successively to the reaction tube, the precatalyst and the ligand were combined, dissolved in the solvent and pre-stirred for 10 min to form the active catalyst prior to the addition of the trimethylammonium starting material **31** and the base.

To obtain a first indication of the effect of oxygen onto the reaction, trimethyl-(4-phenylbutyl)-ammonium iodide [**31**] was treated with the pre-actived catalytic system consisting of palladium(II) acetate and tris(2,4,6-trimethoxyphenyl)phosphine in non-degassed acetonitrile for 30 minutes at room temperature in the presence of caesium carbonate in open-air (see Entry a). To our surprise, the reaction still resulted in a 1% conversion of the starting material **31** to the alkene **32** performing the elimination as quickly as 30 minutes and at room temperature. Temperature can be a contributing parameter for the success of the Heck reaction. The common temperature range used for the Heck reaction is 70 – 100 °C.[184] However, high temperatures can also cause the collapse of the catalytic system as a result of the cleavage of the stabilising phosphine ligands.[220] Consequently, the performance of the Pd-catalysed elimination at room temperature is an additional control to ensure that the decay of the catalytic system is not temperature-based. The detection of the alkene after the reaction at room temperature encouraged our hypothesis on the applicability of the Pd-catalysed Hofmann-type elimination to complex biological systems. The reaction was repeated at room temperature using *n*-butanol instead of acetonitrile as displayed in Entry b and it also led to the formation of the alkene **32** in 1% yield. Next, the amount of the ligand was increased from 2.6 equiv. to 3.5 equiv. relative to the precatalyst and the reaction was repeated in acetonitrile (see Entry c).

The adjustment of the precatalyst : ligand ratio did not lead to an increase in yield (< 1%). Repeating the reaction in Entry c in water : acetonitrile (1 : 10) instead of 100% acetonitrile did not result in a higher conversion rate to the product **32** either (1%, see Entry d). In addition, increasing the reaction time from 30 minutes to 24 hours did not give the product **32** in higher yield either (Entry e).

Table 2.2.7 The influence of oxygen and temperature on the Pd-catalysed Hofmann-type elimination. †The conversion was calculated using quantitative ^{1}H NMR with trimethyl benzene-1,3,5-tricarboxylate in DMSO (0.1 M) as internal standard.

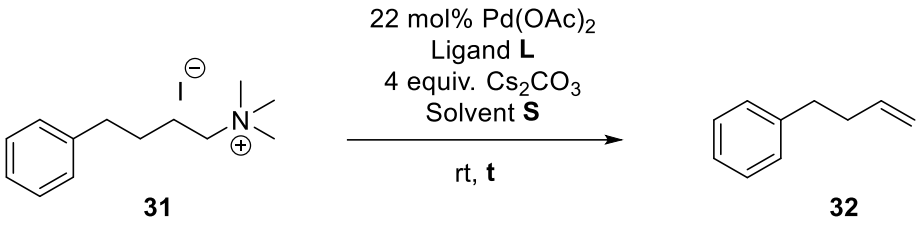

Entry	**Ligand L**	**Solvent S**	Presence of **Oxygen**	**Reaction time t**	Conversion to **Product**†
a	58 mol% (p-OMePh)$_3$P	MeCN	Yes	10 min + 30 min	1%
b	58 mol% (p-OMePh)$_3$P	n-butanol	Yes	10 min + 30 min	1%
c	77 mol% (p-OMePh)$_3$P	MeCN	Yes	10 min + 30 min	< 1%
d	77 mol% (p-OMePh)$_3$P	H_2O : MeCN (1 : 10)	Yes	10 min + 30 min	1%
e	77 mol% (p-OMePh)$_3$P	MeCN	Yes	10 min + 24 h	< 1%
f	77 mol% (p-OMePh)$_3$P	MeCN	No	10 min + 15 h	< 1%
g	55 mol% BrettPhos	MeCN	No	10 min + 15 h	1%

Although the experiments displayed in Table 2.2.7 (Entries a – e) suggested that the Pd-catalysed elimination could run in the presence of oxygen, nevertheless, all the subsequent reactions were performed under inert conditions since the reason behind the low conversion rates of the elimination was yet to be determined. In contrast to the room temperature reactions, which were exposed to oxygen, the eliminations displayed in Entry f and g (Table 2.2.7) were conducted under inert atmosphere. However, the Pd-catalysed Hofmann-type elimination of trimethyl-(4-phenylbutyl)-ammonium iodide [**31**] using either tris(2,4,6-trimethoxyphenyl)-phosphine (Entry f) or BrettPhos (Entry g) as the ligand, performed under inert atmosphere at room temperature, did not lead to a higher yield in the alkene product **32** compared to the reactions conducted open to air.

2.2.7 The investigation of the metal-to-ligand ratio and the catalyst loading

The investigation of the reductive elimination in combination with our efforts in both discovering the cause for the catalyst's demise and incorporating stabilising additives to increase the catalyst's lifetime was unfortunately not effective in accelerating the Pd-catalysed Hofmann-type elimination. In order to further improve the stabilisation of the zero-valent palladium centre and prevent the aggregation of the palladium catalyst to eventually form inactive palladium black, a closer examination of the interaction between ligand and metal was carried out. As discussed in the ligand study in Subchapter 2.2.3, the ligand plays a vital role in the Pd-catalysed reactions, as it is responsible for the stabilisation of the metal centre and exerts influences on all the steps throughout the catalytic cycle. One consideration for the use of a ligand is the exact metal-to-ligand ratio. Even though one might assume that an excess in ligand might maximise the stabilisation around the metal centre, it has been reported that a metal-to-ligand ratio in the range of 0.5 – 1 has positive impacts on palladium catalysis. Due to the ligand's function in the catalyst activation step, a slight excess of ligand (2 – 3 equiv. relative to the precatalyst) established a higher rate in the oxidative addition step.[221] However, examples in the literature also demonstrated that adjusting the metal-to-ligand ratio to 1 : 1 can exhibit a higher activity than the use of a 1 : 2 ratio.[222,223] Hartwig *et al.* suggested that the presence of free phosphine decreases the rate of the reaction, which can be avoided by lowering the metal-to-ligand ratio to 1 : 1.[222] Fu *et al.* discussed that a palladium monophosphine adduct may be the active catalyst in the Suzuki reaction conducted with $Pd_2(dba)_3$ and $P((t\text{-}Bu)_3)_2$, since the use of the preformed $Pd(P(t\text{-}Bu)_3)_2$ catalyst only resulted in a low conversion to the desired product.[223]

With the goal of investigating this phenomenon, the impact of the metal-to-ligand ratio on the Pd-catalysed Hofmann-type elimination was explored. Table 2.2.8 displays the results of this investigation. To test the influence of a significant excess of ligand on the longevity of the active catalyst, the metal-to-ligand ratio of 1 : 5 was included in the screening. On top of the decelerating effect of an excess of ligand (see above), it was also disputed if it would block the coordination sites of the catalyst, so that the metal would not be able to perform the oxidative addition and/or the β-hydride elimination. Therefore, the metal-to-ligand ratio of 1 : 1 and 1 : 2 were simultaneously investigated. Similar conversion rates to the alkene were received in the elimination reactions using 10 mol% palladium(II) acetate with an increasing amount of

tris(2,4,6-trimethoxyphenyl)phosphine including 10 mol% (1 : 1, Entry a), 20 mol% (1 : 2, Entry b) and 50 mol% (1 : 5, Entry c). Doubling the catalyst loading to 20 mol% palladium(II) acetate with either 20 mol% (1 : 1, Entry d) or 40 mol% (1 : 2, Entry e) tris(2,4,6-trimethoxyphenyl)phosphine did not lead to any differences in the conversion rate to the alkene **32** compared to the previously obtained results.

Table 2.2.8 The influence of the metal-to-ligand ratio and catalyst loading on the Pd-catalysed Hofmann-type elimination. †The conversion was calculated using quantitative ^{1}H NMR with trimethyl benzene-1,3,5-tricarboxylate in DMSO (0.1 M) as internal standard.

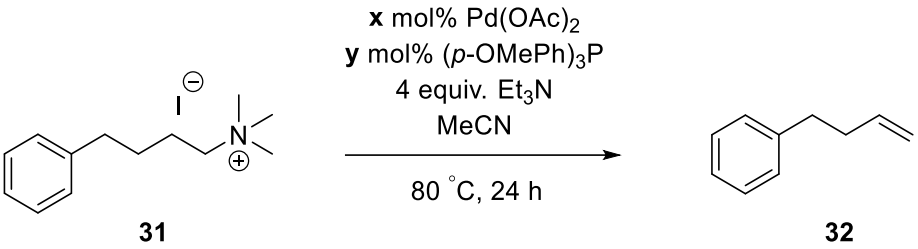

31 **32**

Entry	**x** mol%	**y** mol%	Conversion to **Product**†
a	10	10	1%
b	10	20	< 1%
c	10	50	1%
d	20	20	< 1%
e	20	40	< 1%

Since the investigation of the metal-to-ligand ratio did not give any indications regarding the limiting factor of the Pd-catalysed Hofmann-type elimination, an alternative approach was taken to abolish the formation of inactive palladium black. While we investigated the stabilisation of the palladium centre using a range of ligands, solvents, bases and supporting additives such as quaternary ammonium salts, Spencer *et al.* firstly introduced the use of the so-called 'homeopathic' (*i.e.* very low) amount of palladium catalysts to prevent the generation of palladium sediments in the Heck reaction. By decreasing the catalyst loading of the reaction to as low as 0.005 mol%, Spencer and his colleagues achieved to significantly increase the

turnover number of the catalytic system.[198] It is important in the Heck reaction to establish a balance between the correlation of the use of an increasing amount of catalyst to produce more product versus the rate of aggregation of the catalyst inhibiting the progression of the reaction (see Figure 2.2.2).

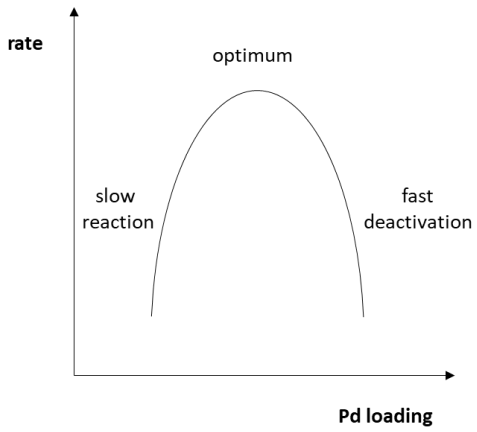

Figure 2.2.2 The relation between palladium loading and the reaction rate in catalytic reactions.

Consequently, the concept of using low loadings of palladium catalyst, so that the oxidative addition outruns the aggregation process opened new possibilities in guaranteeing an efficient catalytic system. Scheme 2.2.6 displays the Pd-catalysed Hofmann-type elimination of trimethyl-(4-phenylbutyl)-ammonium iodide [**31**] using a homeopathic amount of palladium(II) acetate (3.3 mol%) in the presence of tris(2,4,6-trimethoxyphenyl)phosphine and caesium carbonate in acetonitrile. The reduction in the quantity of the palladium catalyst did not improve the yield of the Pd-catalysed elimination, but it resulted in only traces of the desired product **32** (< 0.1%, see Scheme 2.2.6).

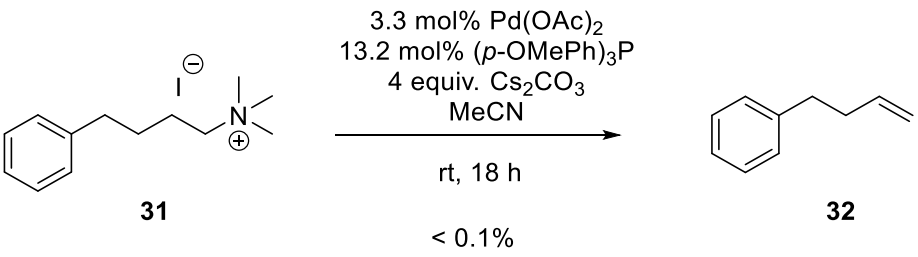

Scheme 2.2.6 Homeopathic amount of palladium catalyst used in the Pd-catalysed Hofmann-type elimination. The conversion was calculated using quantitative ^{1}H NMR with trimethyl benzene-1,3,5-tricarboxylate in DMSO (0.1 M) as internal standard.

After Spencer *et al.* introduced the theory of homeopathic quantities of catalyst in the Heck reaction, many studies followed on applying this concept on various systems. De Vries *et al.* used this theory to further improve the efficiency of ligand-free Heck reactions.[224–226] Since ligandless systems are in need of alternative ways of stabilising the active catalyst, De Vries *et al.* showed that by lowering the Pd-loading in a ligandless system, a similar kinetic profile was achieved compared to a catalytic system consisting of a palladacycle.[224] The approach by De Vries was adopted to our system as shown in Scheme 2.2.7. Unfortunately, the reaction did not result in the formation of the desired terminal alkene **32**.

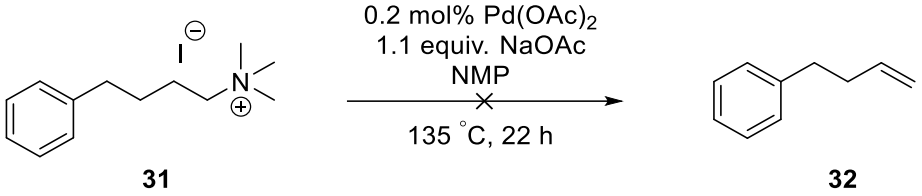

Scheme 2.2.7 The ligandless conditions by De Vries were adopted to the Pd-catalysed Hofmann-type elimination.

Since all our efforts towards increasing the activity of the catalytic system thus far could not accelerate the Pd-catalysed Hofmann-type elimination, a different direction was taken in the next set of experiments and is discussed in the subsequent subchapter.

2.2.8 Pd-catalysed Hofmann-type elimination with stoichiometric amount of catalyst

Since no enhancement of the reaction was achieved by attempting to improve other parts of the catalytic cycle, we next decided to concentrate on the oxidative addition step of the catalyst into the C – N bond of the ammonium functionality. It was envisioned that by increasing the amount of catalyst and performing the Pd-catalysed Hofmann-type elimination stoichiometrically, any issues with catalytic turnover could be avoided.

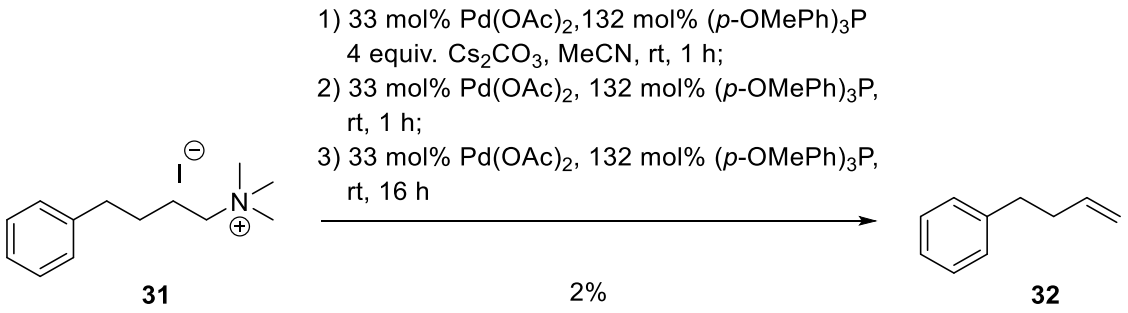

Scheme 2.2.8 Continuous addition of the activated catalyst to the Pd-catalysed Hofmann-type elimination. The conversion was calculated using quantitative ^{1}H NMR with trimethyl benzene-1,3,5-tricarboxylate in DMSO (0.1 M) as internal standard.

To start, the Pd-catalysed Hofmann-type elimination of trimethyl-(4-phenylbutyl)-ammonium iodide [**31**] was repeated with a continuous addition of a fresh batch of palladium(II) acetate and tris(2,4,6-trimethoxyphenyl)phosphine every hour (see Scheme 2.2.8). After the third addition of the pre-activated catalytic complex, the reaction was stirred for 16 hours at room temperature. By this approach, it was anticipated that the conversion rate to the desired alkene **32** would improve. Since the stability of the catalyst was questioned, a continuous addition of catalyst throughout the reaction time was thought to overcome these concerns. A threefold addition of 33 mol% palladium(II) acetate was conducted to reach a total amount of 1 equiv. of catalyst in relation to the starting material **31**. Unfortunately, the use of an increase amount of catalyst still only led to the formation of the alkene **32** in low yield (2%). The expected increase in conversion rate was not achieved.

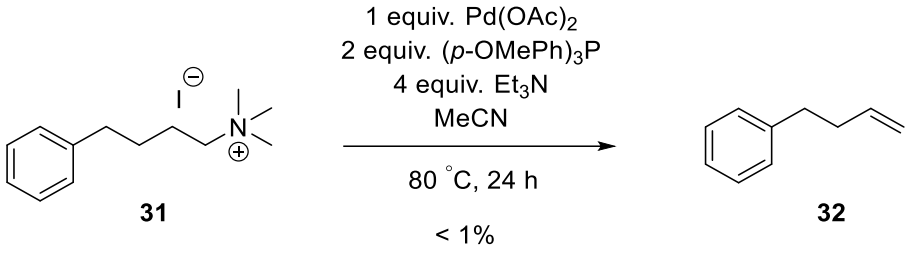

Scheme 2.2.9 Stoichiometrically performed Pd-catalysed Hofmann-type elimination. The conversion was calculated using quantitative ^{1}H NMR with trimethyl benzene-1,3,5-tricarboxylate in DMSO (0.1 M) as internal standard.

In order to further investigate if stoichiometrically performed Pd-catalysed Hofmann-type elimination could increase the conversion rate to the alkene **32**, trimethyl-(4-phenylbutyl)-ammonium iodide [**31**] was treated with 1 equiv. palladium(II) acetate and 2 equiv. tris(2,4,6-trimethoxyphenyl)phosphine using triethylamine as the base in acetonitrile. Even though a stoichiometric amount of catalyst was used, the reaction only resulted in traces of the alkene **32** (< 1%) as shown in Scheme 2.2.9. Repeating the stoichiometric reaction with a change in base to caesium carbonate and in solvent to the polar protonic *n*-butanol (see Scheme 2.2.10) also gave the product **32** in low yield (< 1%).

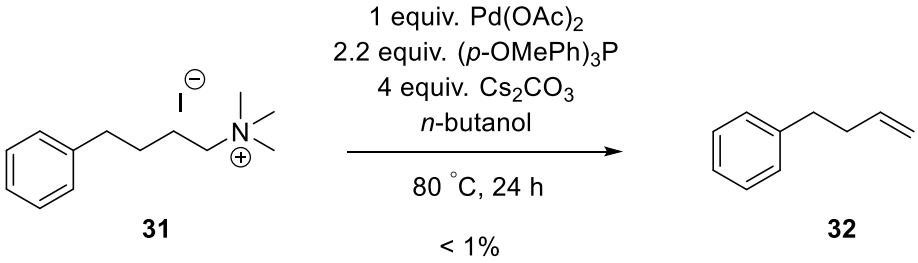

Scheme 2.2.10 Stoichiometrically performed Pd-catalysed Hofmann-type elimination with an alternative solvent and base. The conversion was calculated using quantitative ^{1}H NMR with trimethyl benzene-1,3,5-tricarboxylate in DMSO (0.1 M) as internal standard.

As displayed in Scheme 2.2.11, we next increased the amount of ligand to 4 equiv. and changed the base to silver(I) carbonate to not only deprotonate the catalyst but to simultaneously trap the iodide counterion of the starting material **31** and ensure a free coordination site of the

catalyst for the oxidative addition and the *β*-hydride elimination. Even including these changes, the stoichiometrically conducted Pd-mediated elimination of trimethyl-(4-phenylbutyl)-ammonium iodide [**31**] only gave a minimal conversion to the desired alkene **32** (< 1%).

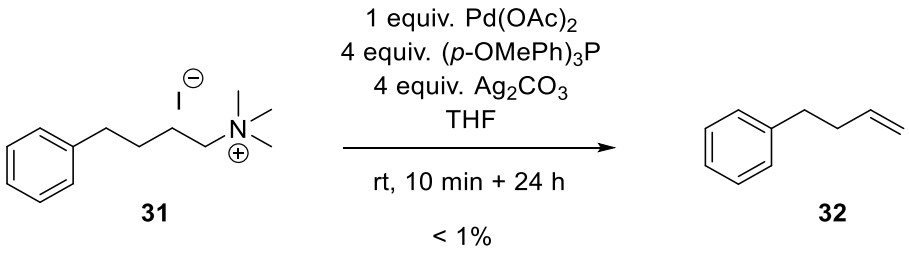

Scheme 2.2.11 The addition of silver(I) carbonate in the stoichiometrically performed Pd-catalysed Hofmann-type elimination. The conversion was calculated using quantitative ^{1}H NMR with trimethyl benzene-1,3,5-tricarboxylate in DMSO (0.1 M) as internal standard.

These stoichiometric experiments strongly suggest that the limiting factor of the Pd-catalysed Hofmann-type elimination is the oxidative addition of the active catalyst into the C(sp^3) – N bond of the starting material **31**. At the same time, we questioned if the formation of the alkene **32** was in fact the outcome of the proposed Pd-catalysed elimination or if it was based on a possible side reaction. In case of the latter, the outcome of the stoichiometric study would be explained, since the non-involvement of the palladium catalyst in the elimination reaction would clarify the invariant yields obtained in the reactions, in which an increased amount of catalyst was used. Consequently, a series of control reactions were conducted to verify the involvement of the catalyst in the formation of the desired alkene **32** in the proposed Pd-catalysed Hofmann-type elimination, which are discussed next.

2.2.9 Is the formation of the alkene based on the oxidative addition of the Pd-catalyst?

At this stage of the project, it was questioned if the cause for the low yielding elimination might have been the result of the trimethyl ammonium substrate reacting with any of the other reagents resulting in a side reaction. Consequently, an array of control reactions was conducted to eliminate any suspicion that the formation of the alkene was caused due to side reactions and not the hypothesised catalytic pathway proposed in Scheme 2.2.4 (Subchapter 2.2.2). One of the possible side reactions was believed to be the standard Hofmann elimination due to the use of base in the reaction. Consequently, the elimination of trimethyl-(4-phenylbutyl)-ammonium iodide [**31**] was repeated using 1 equiv. palladium(II) acetate and 4 equiv. tris(2,4,6-trimethoxyphenyl)phosphine in the absence of a base as displayed in Table 2.2.9. The use of stoichiometric amounts of catalyst does not require the reductive elimination step of the conventional catalytic cycle making the primary function of the base, which is the regeneration of the active palladium(0), obsolete. As seen in Entry a, the base-free reaction resulted in the formation of the desired elimination product **32** in 2% yield confirming that the standard Hofmann elimination was not the cause for the detection of the alkene.

Table 2.2.9 Base-free Pd-catalysed Hofmann-type elimination. †The conversion was calculated using quantitative ^{1}H NMR with trimethyl benzene-1,3,5-tricarboxylate in DMSO (0.1 M) as internal standard.

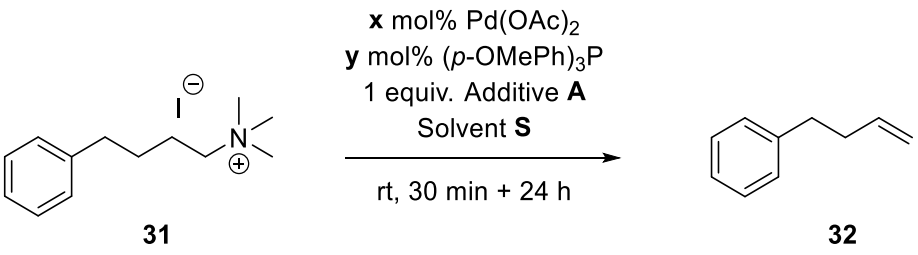

31 **32**

Entry	**x** mol%	**y** mol%	**Additive A**	**Solvent S**	Conversion to **Product**†
a	100	400	-	THF	2%
b	33	132	-	MeCN	1%
c	33	132	AgBr	MeCN	1%
d	33	132	AgOTf	MeCN	2%

Continuing the idea of a base-free Pd-catalysed elimination, the reaction was repeated using catalytic amounts of palladium(II) acetate (see Entry b). This experiment was conducted to both investigate the overall importance of the base in the Pd-catalysed elimination and determine its key functions in the catalytic cycle when compared to the stoichiometric reaction shown in Entry a. In addition, it was hypothesised that trimethylamine, which is removed from the starting material during the oxidative addition of the catalyst, might be sufficient to deprotonate the inactive catalyst, which would suggest that an addition of a base is not essential for the Pd-catalysed Hofmann-type elimination of quaternary ammonium substrates. The base-free elimination with catalytic amounts of palladium(II) acetate seen in Entry b resulted in the formation of the desired alkene **32** in 1% yield. Simultaneously, it was believed that an exchange in counterion to a less nucleophilic and thus less coordinating counterion would be beneficial for the base-free elimination reaction. Entries c and d display the base-free Pd-catalysed elimination using catalytic amounts of palladium(II) acetate and silver-based additives to exchange the iodide counterion to bromide (Entry c) and triflate (Entry d). Yet both reactions did not lead to an increase in yield compared to the base-free Pd-catalysed elimination using solely the iodide starting material **31** without counterion exchange. Even though the results of the base-free eliminations did not provide conclusive evidence that the addition of an external base is dispensable, it important to investigate this hypothesis further, once the efficiency of the Pd-catalysed Hofmann-type elimination is improved.

Table 2.2.10 Control reaction in the absence of a palladium catalyst. †The conversion was calculated using quantitative ^{1}H NMR with trimethyl benzene-1,3,5-tricarboxylate in DMSO (0.1 M) as internal standard.

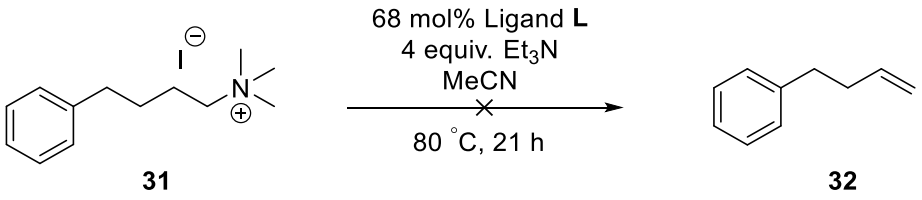

Entry	**Ligand L**	Conversion to **Product**†
a	(*p*-OMePh)$_3$P	0%
b	BrettPhos	0%

Since the formation of the alkene was not caused because of the base, the importance of the catalyst was investigated next. The proposed pathway of the Pd-catalysed Hofmann-type elimination starts with the oxidative addition of the active Pd-catalyst into the carbon-nitrogen bond of the starting material. Accordingly, the absence of catalyst should not lead to the elimination of trimethylamine and thus to the generation of the alkene. To confirm the role of the catalyst in the Pd-catalysed elimination, trimethyl-(4-phenylbutyl)-ammonium iodide [**31**] was treated with either tris(2,4,6-trimethoxyphenyl)phosphine (Entry a) or BrettPhos (Entry b) in the presence of triethylamine in acetonitrile, but in the absence of palladium(II) acetate (see Table 2.2.10). Both reactions did not give any elimination product confirming the importance of the Pd-catalyst on the cleavage of the carbon-nitrogen bond in the Pd-catalysed Hofmann-type elimination. Concluding from these control reactions, the Pd-catalyst appears important to obtain the alkene **32** (albeit in low conversion). Further investigation towards understanding the reasons behind the low yielding Pd-catalysed elimination was conducted to exclude any alternative side reactions that might interfere with the outcome of this reaction.

2.2.10 Possible side reactions of the formed alkene

To verify that the formed alkene **32** was not involved in any side reactions, which might explain the low yield of the elimination through product degradation, possible reactions with olefins in the presence of palladium were explored. Since the Heck reaction is the Pd-catalysed arylation of alkenes, it was questioned if the generated terminal alkene would participate in the catalytic Heck cycle and couple with the electrophile in the migratory insertion step (see the general mechanism in Scheme 2.2.3) to give the substituted diphenyl olefin. Consequently, a standard Heck reaction was performed using trimethyl-(4-phenylbutyl)-ammonium iodide [**31**] as the electrophile and 4-phenyl-1-butene [**32**] as the alkene (see Scheme 2.2.12). Depending on the regioselectivity of the *β*-hydride elimination by the carbopalladium, two possible products **36** and **37** were expected. NMR analysis of the reaction outcome verified that mainly starting material was recovered after the reaction. There were no new peaks in the alkene region of the ^{1}H NMR spectrum corresponding to the alkene protons of the products.

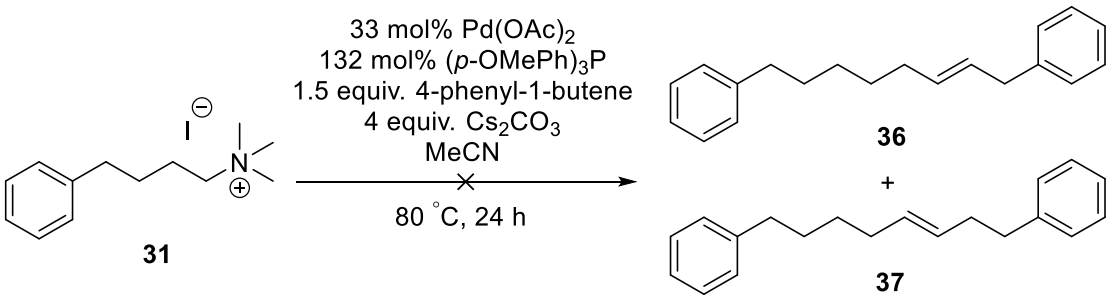

Scheme 2.2.12 Pd-catalysed cross coupling reaction of the trimethylammonium electrophile 31 with 4-phenyl-1-butene.

Alternative reactions known for the transition-metal-catalysed modification of alkenes are hydroamination[227] and hydroaminoalkylation[228]. Whereas hydroamination is the addition of R_2N – H across an unsaturated C – C bond forming a new N – C bond, hydroaminoalkylation is the *α*-alkylation of dialkylamines forming a new C – C bond. A general scheme is displayed in Scheme 2.2.13. The following reviews are given for further information on the mechanism and application of these transformations.[227–233]

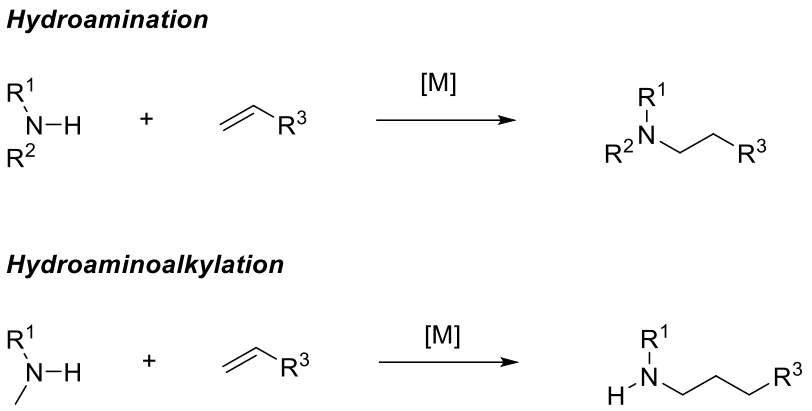

Scheme 2.2.13 A general scheme for the hydroamination and hydroaminoalkylation reactions.

Hartwig and Kawatsura introduced the use of palladium catalysts in the intramolecular hydroamination of vinylarenes using aromatic amines.[234] Since then, palladium catalysts have been involved in various hydroaminations.[235,236] Considering our model system, we debated if the generated alkene **32** could undergo either a hydroamination-type or a hydroaminoalkylation-type transformation with the eliminated trimethylamine. In the search of similar transformations in the literature, an example was found, in which a tertiary *N*-methylamine was added into an alkene via a hydroaminoalkylation reaction using a cationic scandium catalyst.[237] The methyl group on the tertiary amine was involved in the catalytic cycle leading to the formation of an alkylated tertiary amine. In addition, a palladium-catalysed hydroamination-type reaction was discovered, which demonstrated the addition of a trialkylamine to a terminal alkene with electron-withdrawing groups via a C – N bond activation step.[238] Consequently, a control reaction was conducted, in which 4-phenyl-1-butene [**32**] was exposed to trimethylamine in the presence of a palladium-based catalytic system (see Scheme 2.2.14). Depending on the type of reaction, either dimethyl-(4-phenylpentyl)-amine [**38**] (hydroaminoalkylation) or dimethyl-(4-phenylbutyl)-amine [**39**] (hydroamination-type reaction) was expected. Additionally, since triethylamine was used in the original Pd-catalysed Hofmann-type elimination condition, it was also included in this control reaction creating the possibility of the formation of diethyl-(4-phenylbutyl)-amine [**40**] as a possible product.[236] As displayed in Scheme 2.2.14, the control reactions using palladium(II) acetate with either tris(2,4,6-trimethoxyphenyl)phosphine (Entry a) or BrettPhos (Entry b) as the catalytic system did not result in the formation of the alkylated tertiary amines **38**, **39** and **40**.

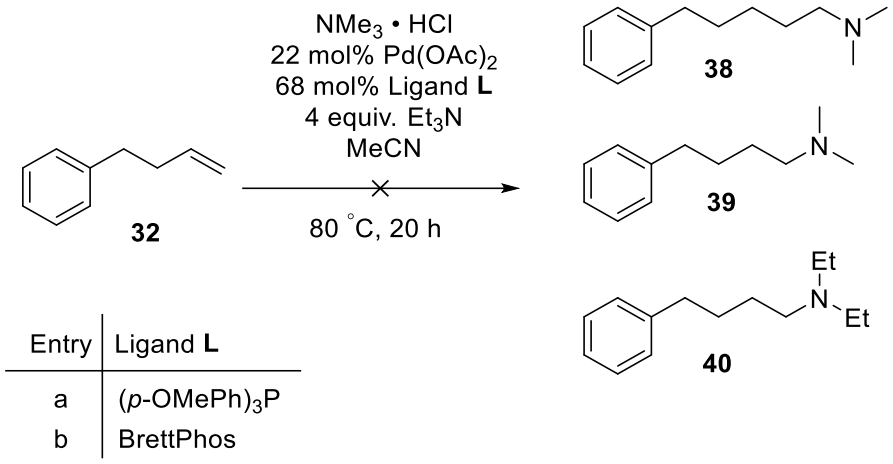

Scheme 2.2.14 Control reaction to investigate a possible hydroamination or hydroalkylamination side reaction of the alkene product [32].

The above conducted control reactions confirmed that the obtained low yields of the Pd-catalysed elimination reactions were not explained by possible side reactions of the terminal alkene product.

2.2.11 Investigation of the electrophile – the effect of the counterion

The synthesis of the electrophile was conducted via the trimethylation of 4-phenylbutyl amine [**30**] using methyl iodide in excess as displayed in Scheme 2.1.13. The resulting trimethyl-(4-phenylbutyl)-ammonium iodide [**31**] was then used for the investigation of the Pd-catalysed Hofmann-type elimination. In some cases, silver(I) salts were added to the reaction mixture to trap the iodide counterion of the electrophile **31**. However, no alternative electrophiles were synthesised via a different pathway and analysed in the Pd-catalysed Hofmann-type elimination up until now. Consequently, it was decided to synthesise trimethyl-(4-phenylbutyl)-ammonium triflate [**41**] to test the effect of the less coordinating triflate anion compared to the iodide counterion without the influence of precipitated silver salts. The synthesis of trimethyl-(4-phenylbutyl)-ammonium triflate [**41**] is displayed in Scheme 2.2.15. 4-Phenylbutyl amine [**30**] was exposed to Eschweiler-Clarke conditions to give *N*,*N*-dimethyl-4-phenylbutan-1-amine [**39**] in good yield (81%). Monomethylation with methyl triflate (1.2 equiv.) in diethyl ether resulted in the desired trimethyl-(4-phenylbutyl)-ammonium triflate [**41**] in quantitative yield. Direct trimethylation was substituted by this stepwise methylation approach to avoid the use of excess reagents.

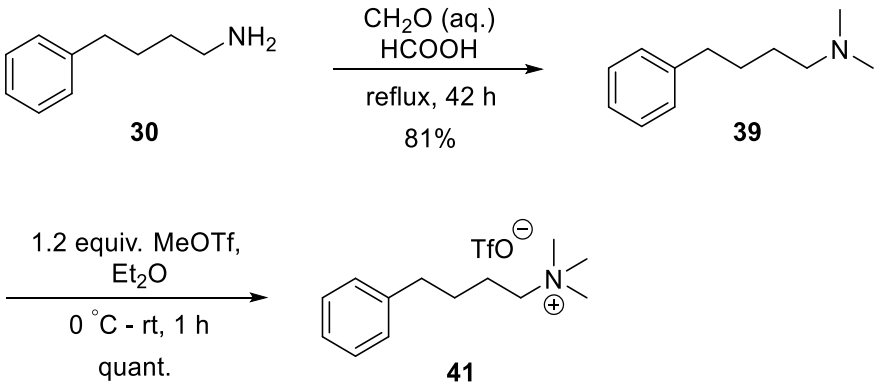

Scheme 2.2.15 Synthesis of trimethyl-(4-phenylbutyl)-ammonium triflate [41].

As displayed in Table 2.2.11, trimethyl-(4-phenylbutyl)-ammonium triflate [**41**] was then exposed to catalytic and stoichiometric amounts of palladium(II) acetate in combination with either tris(2,4,6-trimethoxyphenyl)phosphine (Entries a – d) or BrettPhos (Entries e – h) in the

presence of a base (Et_3N or Cs_2CO_3) at 80 °C. The change in counterion from iodide to triflate was believed to induce an alternative mechanistic pathway for the activated Pd^0 catalyst, since triflate as a less coordinating counterion would not be as closely bound to the palladium as iodide. However, the use of triflate as the counterion of the ammonium substrate did not improve the yield of the Pd-catalysed elimination reaction confirming that the hitherto observed blockade of the reaction was not due to the coordination of the iodide counterion.

Table 2.2.11 The influence of the counterion on the Pd-catalysed Hofmann-type elimination. †The conversion was calculated using quantitative ^{1}H NMR with trimethyl benzene-1,3,5-tricarboxylate in DMSO (0.1 M) as internal standard.

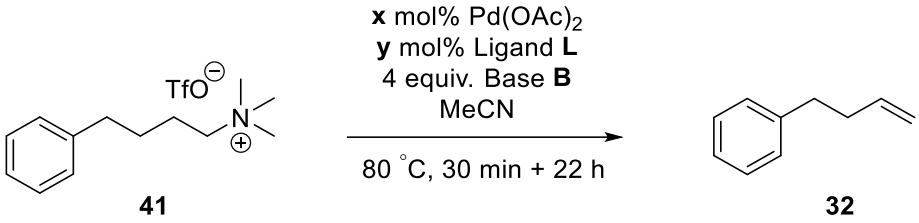

41 **32**

Entry	**x** mol%	**y** mol%	**Ligand L**	**Base B**	Conversion to **Product**†
a	22	68	(*p*-OMePh)$_3$P	Et_3N	< 1%
b	22	68	(*p*-OMePh)$_3$P	Cs_2CO_3	1%
c	100	310	(*p*-OMePh)$_3$P	Et_3N	< 1%
d	100	310	(*p*-OMePh)$_3$P	Cs_2CO_3	-
e	22	68	BrettPhos	Et_3N	-
f	22	68	BrettPhos	Cs_2CO_3	< 1%
g	100	310	BrettPhos	Et_3N	-
h	100	310	BrettPhos	Cs_2CO_3	< 1%

To test the Pd-catalysed elimination on an alternative functionality and compare the results to the elimination of trimethylamine, 4-phenyl-1-iodobutane [**43**] was synthesised (see Scheme 2.2.16). 4-Phenylbutanol [**42]** was treated with Appel conditions using iodine and triphenylphosphine to give 4-phenyl-1-iodobutane [**43**] in excellent yield (91%).

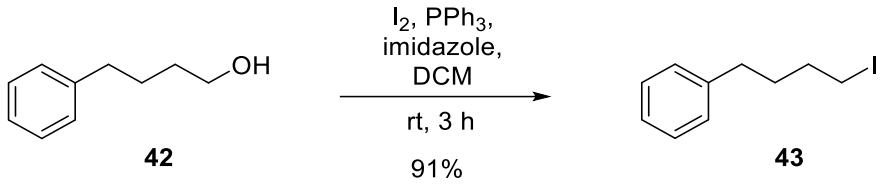

Scheme 2.2.16 Synthesis of 4-phenyl-1-iodobutane [43].

Alkyl iodides are considered to be unactivated substrates in contrast to aryl or vinyl iodides in the field of palladium catalysis.[176] Therefore, it was believed that a comparison of the efficiency of the oxidative addition into a C(sp^3) – I bond against a C(sp^3) – N bond might give additional information on the difference in bond strength and the reactivity of the chosen catalytic system. Consequently, 4-phenyl-1-iodobutane [**43**] was reacted with palladium(II) acetate and tris(2,4,6-trimethoxyphenyl)phosphine in the presence of triethylamine in acetonitrile as shown in Scheme 2.2.17. The Pd-catalysed elimination of 4-phenyl-1-iodobutane [**43**] resulted in a minimal formation of the terminal alkene (1%). This experiment raised questions on the efficiency of the used catalytic system. It became clear that the reactivity of the catalytic system had to be enhanced to perform the oxidative addition effectively and thus to increase the overall success of the elimination reaction.

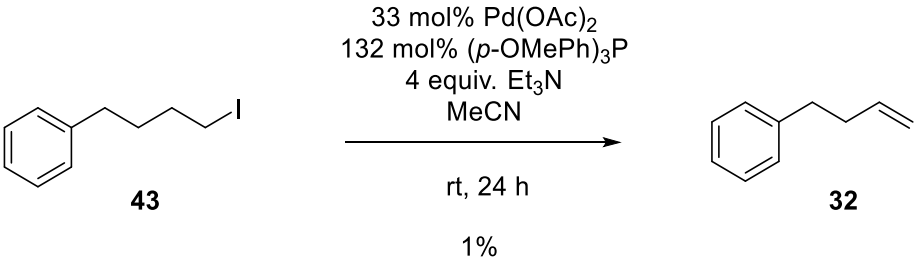

Scheme 2.2.17 Pd-catalysed Hofmann-type elimination on 4-phenyl-1-iodobutane [43]. The conversion was calculated using quantitative ^{1}H NMR with trimethyl benzene-1,3,5-tricarboxylate in DMSO (0.1 M) as internal standard.

In order to confirm the observations made on the inefficiency of the catalytic system to perform the oxidative addition and to break the C(sp^3) – N bond, the Pd-catalysed Hofmann-type elimination was performed in deuterated acetonitrile to monitor the reaction via NMR spectroscopy, which will be presented next.

2.2.12 Examination of the Pd-catalysed Hofmann-type elimination in deuterated acetonitrile

The Pd-catalysed Hofmann-type elimination of trimethyl-(4-phenylbutyl)-ammonium iodide [**31**] was performed in deuterated acetonitrile using palladium(II) acetate and tris(2,4,6-trimethoxyphenyl)phosphine as the catalytic system. The reaction was prepared in a J. Young NMR tube including trimethyl benzene-1,3,5-tricarboxylate as the internal standard to follow the progress of the reaction via quantitative ^{1}H NMR spectroscopy. The first spectrum was taken after 2.5 hours into the reaction and another one after leaving the reaction progressing overnight (15.5 hours). Triethylamine (Entry a) and caesium carbonate (Entry b) were investigated as the base of the reaction (see Scheme 2.2.18).

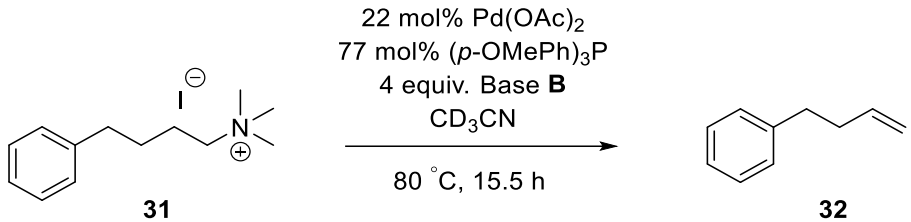

Entry	Base **B**
a	Et_3N
b	Cs_2CO_3

Scheme 2.2.18 Pd-catalysed Hofmann-type elimination in deuterated acetonitrile.

These experiments were designed to identify the substrates after the reaction without processing the mixture post-reaction. Quantitative ^{1}H NMR analysis of both reactions at the two given time points revealed that nearly quantitative amounts of starting material were present after the reaction. As demonstrated in Figure 2.2.3, there were no distinguishable side products detected in the proton spectrum after 15.5 hours into the reaction. Including the starting material **31**, proton peaks belonging to the internal standard, the ligand/ligand-metal complex, the base and the NMR solvent were identified. Consequently, these reactions confirmed that the starting material was not consumed during the reaction indicating that the oxidative addition was *de facto* the limitation of the Pd-catalysed Hofmann-type elimination.

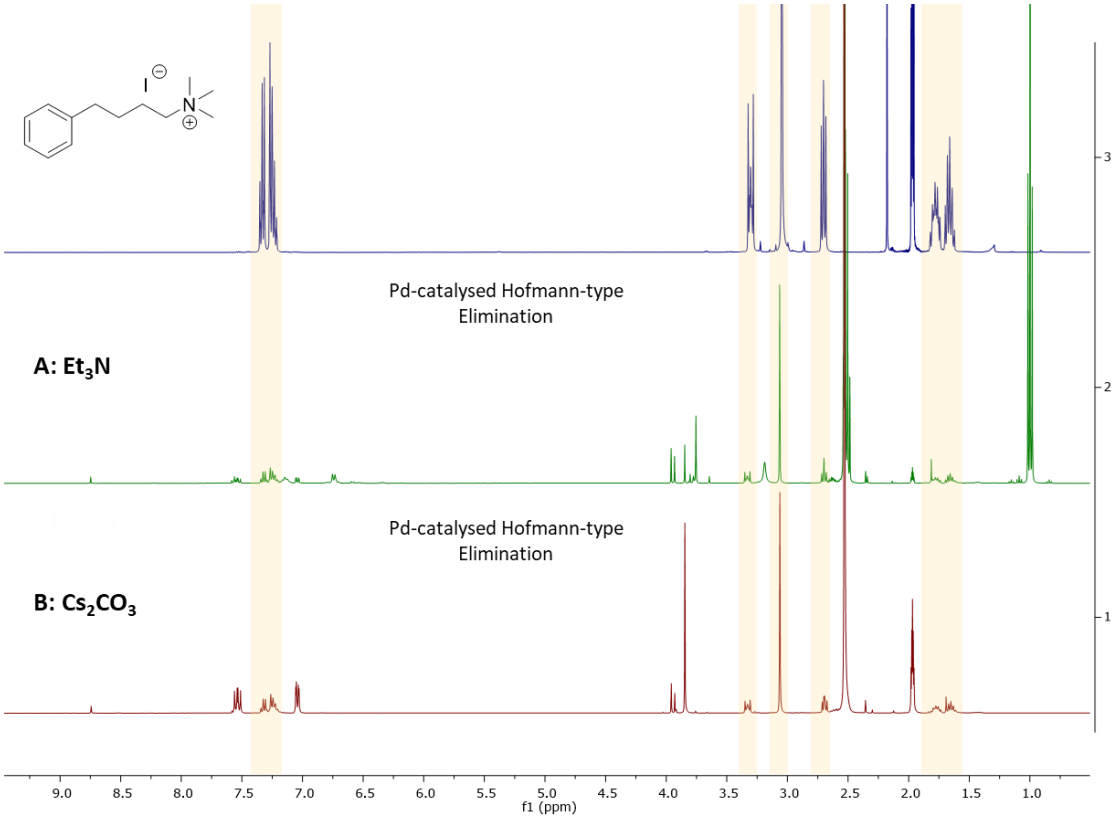

Figure 2.2.3 ^{1}H NMR spectra of the Pd-catalysed Hofmann-type elimination in deuterated acetonitrile using either Et_3N (A) or Cs_2CO_3 (B) as the base compared to ^{1}H NMR spectrum of the starting material 31.

2.2.13 Ligandless Pd-catalysed Hofmann-type elimination – oxidative addition by stabilised Pd^0 nanoparticles

In the search of alternative ways for a palladium catalyst to insert into the C(sp^3) – N bond of the starting material **31**, the ligandless Jeffery conditions were investigated next. The ligand-free Heck reaction undergoes a dissimilar mode-of-action than the traditional Heck reaction using tertiary phosphines. The reduction of the palladium(II) acetate is established by either amines, which are used as a base[239] or by thermolytic decomposition in the presence of quaternary ammonium salts (Jeffery conditions[192–194]), which are used to further stabilise the palladium(0) complex.[240] Scheme 2.2.19 displays the reduction of the palladium(II) acetate to the active Pd^0 catalyst. Reetz and Westermann reported that the oxidative addition of iodobenzene is performed by Pd^0 nanoparticles leading to the formation of either PhPdI or $PhPdX_3^{2-}$.[240]

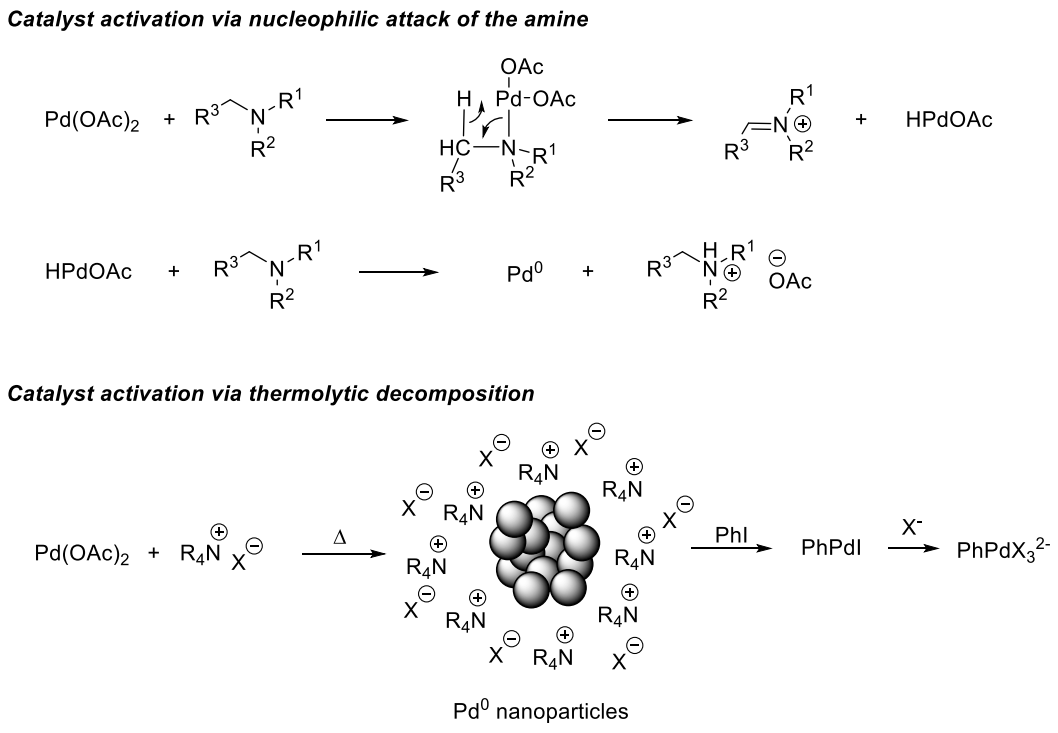

Scheme 2.2.19 Mechanism of the ligandless Heck reaction using Jeffrey conditions.

Next to their stabilising property, the use of quaternary ammonium salts in the ligandless Heck reaction has additional advantages, which are as follows: (i) they can act as a solid-liquid phase-transfer catalysts in case solid inorganic bases are used in the reaction, (ii) they can act as a liquid-liquid phase-transfer catalysts when two phase solvent systems (aqueous : organic) are being used and (iii) they can exchange the ions during the reaction, which is beneficial for the iodide substrate since iodide can be replaced by less ligating ions such as acetate transforming the neutral Pd species to the more reactive cationic Pd species.[182] Alternatively to the Jeffery condition, De Vries displayed the mechanism of the homeopathic ligand-free Heck reaction, which can be found in detail in the referenced publications.[226,241]

Table 2.2.12 Ligandless Pd-catalysed Hofmann-type elimination. †The conversion was calculated using quantitative ^{1}H NMR with trimethyl benzene-1,3,5-tricarboxylate in DMSO (0.1 M) as internal standard.

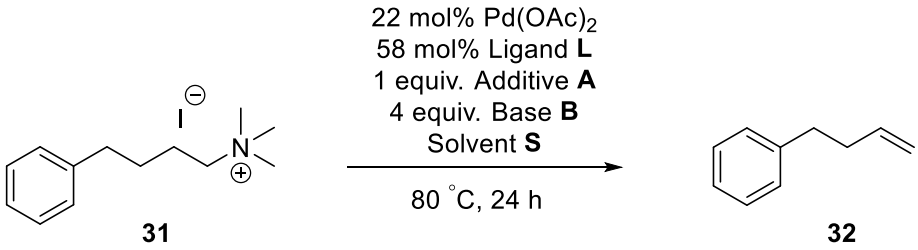

Entry	**Ligand L**	**Additive A**	**Base B**	**Solvent S**	Conversion to **Product**†
a	(*p*-OMePh)$_3$P	^{n}Bu$_4$NBr	Et$_3$N	MeCN	1%
b	-	^{n}Bu$_4$NBr	Et$_3$N	MeCN	< 1%
c	-	^{n}Bu$_4$NBr	Et$_3$N	H_2O : MeCN (1 : 1)	< 1%
d	-	^{n}Bu$_4$NBr	K_2CO_3	H_2O : MeCN (1 : 1)	< 1%
e	-	Ph$_4$PCl	Et$_3$N	H_2O : MeCN (1 : 1)	< 1%

Table 2.2.12 summarises the investigation of ligandless conditions for the Pd-catalysed Hofmann-type elimination of trimethyl-(4-phenylbutyl)-ammonium iodide [**31**]. As shown in Entry a, trimethyl-(4-phenylbutyl)-ammonium iodide [**31**] was firstly treated with

palladium(II) acetate and tris(2,4,6-trimethoxyphenyl)phosphine in the presence of tetrabutylammonium bromide (TBAB) in acetonitrile to test the supporting effects of the quaternary ammonium salt in addition to the stabilising properties of the phosphine ligand. Although TBAB is another tetraalkylammonium substrate, which might compete with **31**, there is no prevalent evidence that the Pd catalyst undergoes oxidative addition to TBAB. Unfortunately, the reaction only gave the desired alkene **32** in 1% yield.

Moving on to the Jeffery conditions, trimethyl-(4-phenylbutyl)-ammonium iodide [**31**] was then exposed to palladium(II) acetate and tetrabutylammonium bromide in acetonitrile as displayed in Entry b. This reaction resulted in the marginal formation of the terminal alkene **32** (< 1%). Next, the solvent system was changed to a mixture of acetonitrile and water (1 : 1) to increase the homogeneity of the reaction and to investigate the role of water in the activation of the catalyst, as proposed by De Vries.[226] In addition, Jeffery highlighted the importance of water in the ligandless Heck reaction, especially when alkali carbonates were used as a base, since it may induce a change from the solid-liquid phase to a liquid-liquid phase.[242] Amatore *et al.* demonstrated the multifaceted role of the hydroxide anions including the acceleration of the rate of the Heck reaction by their ability to act as a ligand for the palladium catalyst.[243] Both triethylamine (Entry c) and potassium carbonate (Entry d) were tested in the ligandless Pd-catalysed elimination reaction using tetrabutylammonium bromide in acetonitrile : water (1 : 1), however, both reactions only gave traces of the desired alkene **32** (< 1%).

In addition to quaternary ammonium salts, Reetz *et al.* introduced the use of tetraphenylphosphonium salts to increase the catalytic activity of simple palladium precatalysts in the ligandless Heck reaction.[244] Consequently, the Pd-catalysed Hofmann-type elimination of trimethyl-(4-phenylbutyl)-ammonium iodide [**31**] was repeated in the presence of tetraphenylphosphonium chloride (Entry e). Unfortunately, the change to the tetraphenylphosphonium salt as the stabilising additive of the ligandless Pd-catalysed elimination did not improve the yield of the reaction (< 1%).

After the investigation of ligand-free Pd-catalysed elimination conditions, it became clear that the suggested active Pd^0 nanoparticles were not able to increase the efficiency of the $C(sp^3)$ – N bond cleavage. Alternative palladium-based catalytic systems were therefore surveyed for the Pd-catalysed Hofmann-type elimination to drive the oxidative addition step into the $C(sp^3)$ – N bond.

2.2.14 $Pd_2(dba)_3$ – an alternative palladium source

In the search for an efficient catalytic system to perform a Suzuki reaction on unactivated aryl chlorides, Littke and Fu discovered the use of $Pd_2(dba)_3$, tris(dibenzylideneacetone)-dipalladium(0), in their catalytic system to successfully cross-couple aryl chlorides with arylboronic acids.[245] While screening various palladium precursors for this transformation, they have repeatedly reported the superiority of $Pd_2(dba)_3$ to $Pd(OAc)_2$.[190,223,245,246] Compared to $Pd(OAc)_2$, the activation of the zero-valent $Pd_2(dba)_3$ is not based on reduction but on ligand exchange at elevated temperature.[247–249] However, a complicating factor of the generation of the active Pd^0L_2 species during activation of $Pd_2(dba)_3$ is the competing ligation of free dba to the palladium forming $Pd(dba)_xL_y$ complexes, which can impede the reactivity of the catalyt.[250,251] Due to the successful applications of $Pd_2(dba)_3$ on unreactive electrophiles and the difference in the formation of the active catalytic species, $Pd_2(dba)_3$ was applied to our system as the source of the palladium catalyst. As displayed in Scheme 2.2.20, trimethyl-(4-phenylbutyl)-ammonium iodide [**31**] was exposed to tris(dibenzylideneacetone)dipalladium(0) and tris(2,4,6-trimethoxyphenyl)phosphine in the presence of triethylamine at 80 °C. Despite the change in the palladium precursor used for the Pd-catalysed Hofmann-type elimination, the reaction only gave the desired alkene **32** in 1% yield.

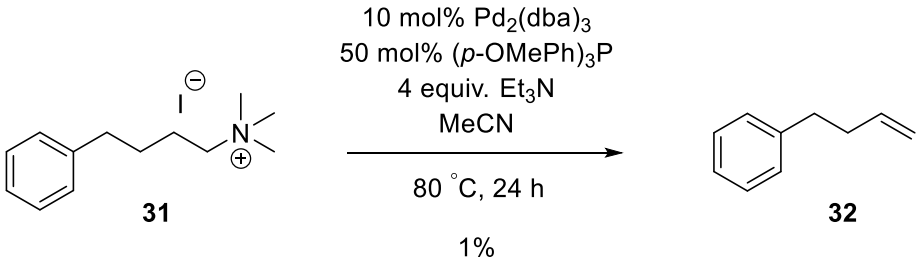

Scheme 2.2.20 Tris(dibenzylideneacetone)-dipalladium(0) as an alternative palladium precursor for the Pd-catalysed Hofmann-type elimination. The conversion was calculated using quantitative ^{1}H NMR with trimethyl benzene-1,3,5-tricarboxylate in DMSO (0.1 M) as internal standard.

While following the work by Fu on Pd-catalysed cross-coupling reactions of challenging electrophiles using $Pd_2(dba)_3$, we became aware of his publication on the Pd-catalysed dehydrohalogenation of alkyl bromides to form terminal alkenes.[252] Inspired by the generation

of olefin side products in the Suzuki coupling of alkyl electrophiles[253], Fu *et al.* developed optimised conditions to eliminate hydrogen bromide from a range of alkyl bromides to form terminal alkenes at room temperature with the use of $Pd(P(^tBu)_2Me)_2$ in excellent yields (see Scheme 2.2.21). No elimination product was detected upon treating primary alkyl chlorides with these conditions.

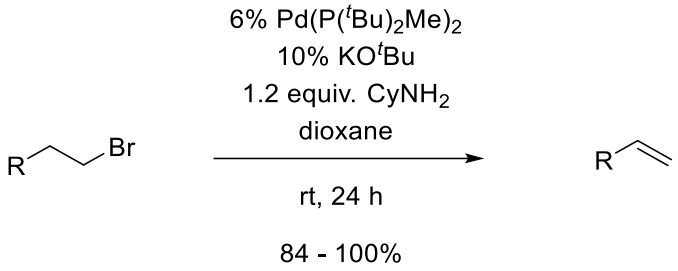

Scheme 2.2.21 Dehydrohalogenation of alkyl bromides published by Fu *et al.*.

With the hope of improving the Pd-catalysed Hofmann-type elimination, trimethyl-(4-phenylbutyl)-ammonium iodide [**31**] was treated with the conditions reported by Fu and colleagues (see Table 2.2.13). The active catalyst was prepared *in situ* after combining $Pd_2(dba)_3$ with $P(^tBu)_2Me$ in the presence of both bases prior to the addition of the starting material. Fu confirmed that no difference in yield was detected between the use of the pre-formed $Pd(P(^tBu)_2Me)_2$ catalyst and the use of $Pd_2(dba)_3$ and $P(^tBu)_2Me$.[252] As shown in Entry a, the Pd-catalysed Hofmann-type elimination using the 'standard' Fu conditions resulted in the formation of the product **32** in 1% yield. Changing the solvent to acetonitrile to ensure a better solubility of the starting material did not improve the yield of the reaction (1%, Entry b). Unfortunately, the 'standard' Fu conditions used for the dehydrohalogenations of alkyl bromides could not be adopted to our model system. Elevating the temperature from room temperature to 100 °C to enforce the elimination of trimethyl-(4-phenylbutyl)-ammonium iodide [**31**] did not increase the yield of the reaction (see Entry c, Table 2.2.13). As displayed in Entries d and e (Table 2.2.13), silver(I) salts were added to the reaction to trap the iodide counterion of the starting material and to exchange it for the less ligating bromide (Entry d) and triflate (Entry e) anions. It was believed that this modification may improve the efficiency of the active Pd-species. However, both reactions did not enhance the formation of the terminal alkene **32**.

Table 2.2.13 Pd-catalysed Hofmann-type elimination of alkyl trimethylammonium iodide 31 using the Fu conditions. †The conversion was calculated using quantitative ^{1}H NMR with trimethyl benzene-1,3,5-tricarboxylate in DMSO (0.1 M) as internal standard.

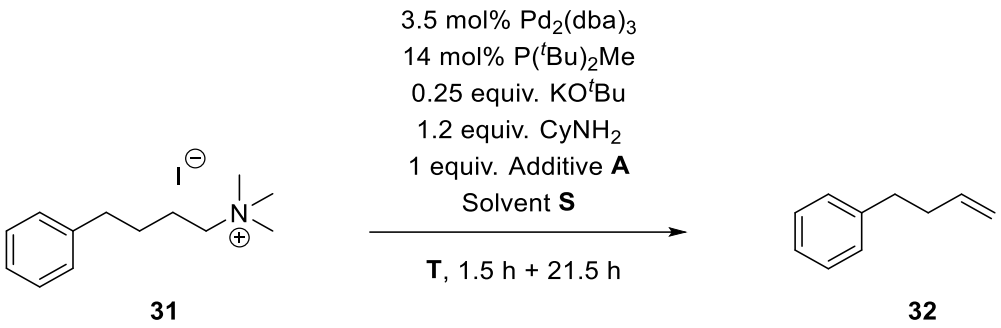

Entry	**Solvent S**	**Temperature T**	**Additive A**	Conversion to **Product**†
a	dioxane	rt	-	1%
b	MeCN	rt	-	1%
c	dioxane	100 °C	-	< 1%
d	dioxane	rt	AgBr	1%
e	dioxane	rt	AgOTf	< 1%

The reaction by Fu was then repeated with a 10-fold increase of catalyst loading (see Scheme 2.2.22). Nevertheless, no product was detected after the reaction. It became clear that the conditions published by Fu were not applicable to primary alkyl ammonium salts, presumably because of the high energy barrier to break the C(sp^3) – N bond in the oxidative addition step. Therefore, no further optimisation of the Fu conditions was conducted.

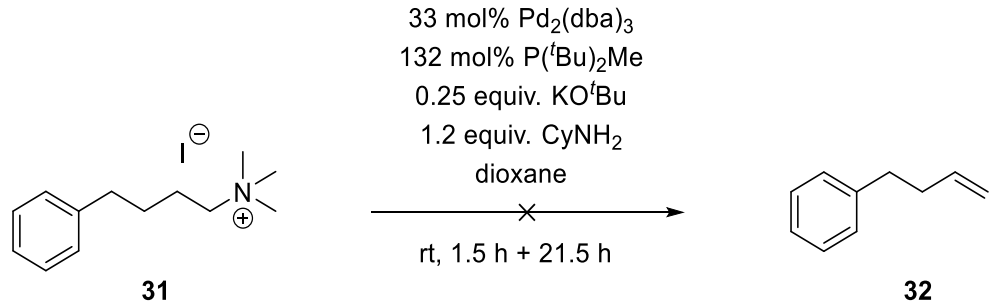

Scheme 2.2.22 Increasing the catalyst loading to improve the Pd-catalysed Hofmann-type elimination using the catalytic system published by Fu.

2.2.15 Investigation of Suzuki cross-coupling of alkyl trimethylammonium substrates

During our research on the oxidative addition of activated palladium catalysts into C(sp^3) – N bonds, Zhao *et al.*[254] and Phipps *et al.*[255], respectively, published a successful protocol for the Suzuki coupling of benzyl trimethylammonium salts with boronic acids. To our knowledge, these two protocols were the first palladium catalysed cleavage of a C(sp^3) – N bond via the release of trimethylamine. Zhao *et al.* demonstrated the Suzuki cross coupling of benzyl trimethylammonium triflates with a wide range of boronic acids using palladium(II) chloride and triphenylphosphine in the presence of sodium carbonate at high temperature. In contrast, Phipps *et al.* successfully demonstrated the Suzuki cross coupling of benzyl trimethylammonium tosylates with boronic acids under mild conditions (T < 60 °C) with the reagents displayed in Scheme 2.2.23. In addition, they have verified that halide counterions such as bromide and chloride were compatible with their conditions. Consequently, the reaction by Phipps and colleagues was carried out with our model system.

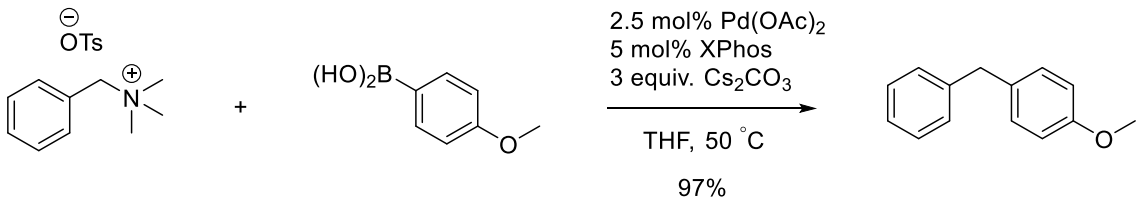

Scheme 2.2.23 Suzuki cross-coupling of benzylic trimethylammonium triflate according to the protocol by Phipps *et al.*.

As shown in Scheme 2.2.24, trimethyl-(4-phenylbutyl)-ammonium iodide [**31**] was exposed to the exact conditions published by Phipps and his team. In order to test these conditions on our substrate and to investigate the importance of the boronic acid for the efficiency of the reaction, the Pd-catalysed Hofmann-type elimination was changed to a Suzuki cross coupling reaction. Nevertheless, the use of the Phipps conditions with either *para*- or *ortho*-methoxyphenyl boronic acid did not give the desired transformation to the coupled products **44** or **45**, but only the starting material **31** was identified in the proton spectrum. GC-MS analysis additionally confirmed that no product was formed during these reactions.

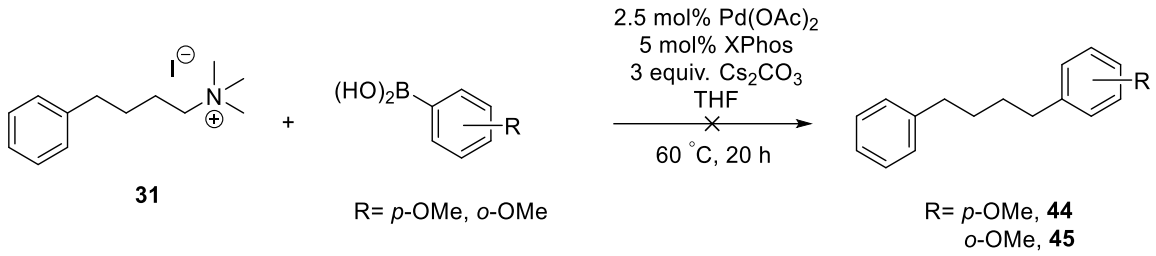

Scheme 2.2.24 Suzuki cross-coupling reaction of alkyl trimethylammonium iodide according to the Phipps protocol.

Since this Suzuki cross coupling has been proven to work for benzylic ammonium salts, but it could not be applied to alkyl ammonium salts, it became increasingly evident that the limiting factor of the reaction is the strength of the carbon-nitrogen bond in our substrate. The hitherto tested catalysts were not able to break this bond, which ultimately lead to the observed low yielding conversions to the desired product. Compared to alkyl trimethylammonium substrates, benzyl trimethylammonium salts are activated due to the benzylic position of the ammonium functionality. When the Suzuki coupling was repeated on the 4-phenyl-1-iodobutane [**43**], the alkene product **32** was formed in 5% yield. This result confirms that the carbon-nitrogen bond strength of our substrate is also higher than the carbon-iodo bond strength in the 4-phenyl-1-iodobutane [**43**], which is considered as an unreactive, challenging electrophile. However, compared to our initial investigation of the 4-phenyl-1-iodobutane [**43**] substrate to undergo Pd-catalysed elimination (see Scheme 2.2.17, Subchapter 2.2.11), an increase in yield from 1% to 5% was achieved confirming that the reactivity of this catalytic system is more enhanced.

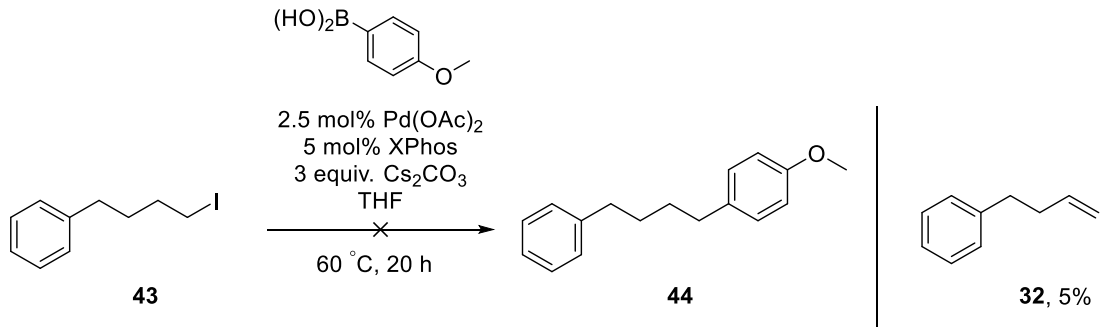

Scheme 2.2.25 Suzuki cross-coupling of 4-phenyl-1-iodobutane [43]. The conversion was calculated using quantitative ^{1}H NMR with trimethyl benzene-1,3,5-tricarboxylate in DMSO (0.1 M) as internal standard.

Next, an array of ligands, which were tested and proven successful in varies degrees for the reported Suzuki reaction of benzyl trimethylammonium tosylates, were investigated for the Pd-catalysed Hofmann-type elimination. The structure of the tested ligands is given in Figure

2.2.4. The boronic acid was omitted to increase the *β*-hydride elimination by avoiding the competing transmetalation. As shown in Table 2.2.14, the screening of the ligands in Entries a – f did not lead to the formation of the desired terminal alkene **32**.

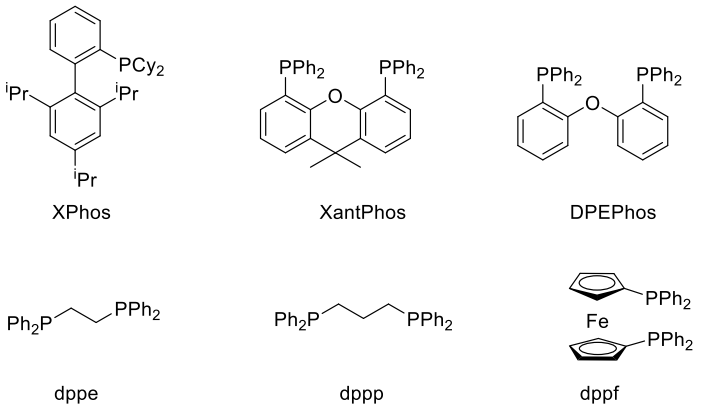

Figure 2.2.4 Expanding the library of ligands screened for the Pd-catalysed Hofmann-type elimination.

Zhao *et al.*[254] and Phipps *et al.*[255] have both shown that the oxidative addition of palladium complexes into a C(sp^3) – N bond of a trimethylammonium functionality is possible. However, our study clarified that this phenomenon is only applicable to activated substrates having the ammonium functionality on the benzylic position. When the published conditions were applied to our butyl ammonium substrate **31**, the palladium complexes failed to insert into the alkyl-C(sp^3) – N bond. This investigation highlighted that more reactive palladium catalysts were needed to break the unactivated C(sp^3) – N bond in the oxidative addition step.

Table 2.2.14 Expanding the ligand library for the Pd-catalysed Hofmann-type elimination.

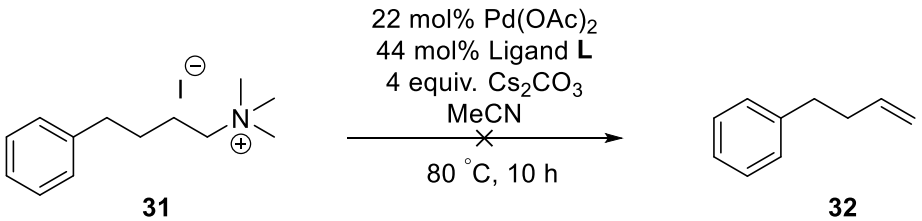

Entry	**Ligand L**	Reaction outcome	Entry	**Ligand L**	Reaction outcome
a	XPhos	only SM, no P	d	dppe	only SM, no P
b	XantPhos	only SM, no P	e	dppp	only SM, no P
c	DPEPhos	only SM, no P	f	dppf	only SM, no P

2.2.16 NHC complexes for the Pd-catalysed Hofmann-type elimination – an attempt to improve oxidative addition

In the search of challenging cross-coupling reactions represented in the literature, examples of Suzuki-Miyaura cross-couplings of amides were found. Inspired by Garg *et al.*, who used Ni[cod]$_2$ to break the C – N bond in amides[256], Szostak *et al.* described successful cross-couplings of a range of amides by N – C bond activation using Pd-NHC complexes as catalyst of the reaction.[257,258] As shown in Scheme 2.2.26, Szostak and his team exposed amides to low loadings of either Pd-PEPPSI-IPr[257] or (IPr)Pd(cinnamyl)Cl[258] in the presence of potassium carbonate. Even though amide bonds are perceived as strong bonds due to their amidic resonance, Szostak *et al.* showed that Suzuki-Miyaura cross-couplings of amides can be achieved in high yields when using highly active Pd-NHC catalysts.

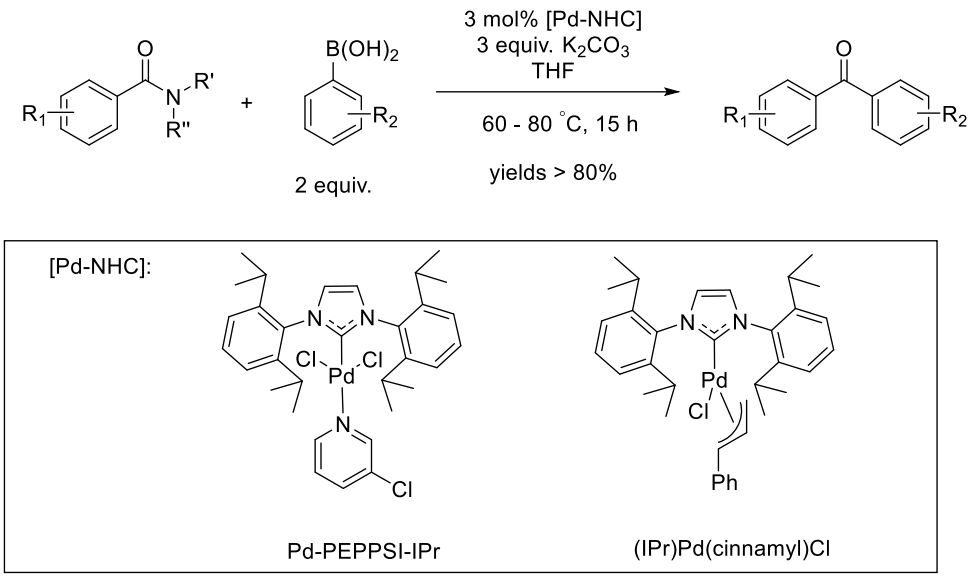

Scheme 2.2.26 Suzuki-Miyaura cross-coupling of amides using Pd-PEPPSI-IPr and (IPr)Pd(cinnamyl)Cl.

Compared to tertiary phosphines, the electronic and steric properties of the NHC compounds are quite different. NHCs are stronger σ-electron donors than tertiary phosphines[259,260] making the Pd-NHC complexes more reactive towards oxidative addition, which is beneficial for the more challenging substrates.[261] Details on the electronic and steric effects of the NHCs on catalysis can be found in these reviews.[262–266]

The reaction conditions used for the cross-coupling of amides by Szostak *et al.* were adopted to our model system.[257,258] Trimethyl-(4-phenylbutyl)-ammonium iodide [**31**] was treated with 3 mol% of either Pd-PEPPSI-IPr (Entry a) or (IPr)Pd(cinnamyl)Cl (Entry b) with 2 equiv. of *p*-tolylboronic acid in the presence of potassium carbonate in THF at 60 °C for 22.5 h (see Scheme 2.2.27). The aim of this reaction was to achieve successful oxidative addition into the C(sp^3) – N bond followed by the coupling of the organopalladium with the boronic acid to give 1-methyl-4-(4-phenylbutyl)benzene [**46**]. It was believed that the increased reactivity of the Pd-NHC catalyst would enhance the oxidative addition into the alkyl ammonium electrophile. The crude ^{1}H NMR spectra for both reactions displayed a similar reaction outcome confirming that mostly starting material **31** was recovered after the reaction. The most prominent peaks in the product to follow the reaction are the C<u>H</u>$_2$ peaks adjacent to the phenyl ring and C<u>H</u>$_3$ peak of the tolyl group. Traces of both peaks were detected in the crude ^{1}H NMR spectra, however, it was not clear enough if they belonged to the product since other peaks were overlapping the detected peaks. Prep TLC was conducted with the goal of removing the starting material **31** and residual boronic acid. The isolated band was analysed via various NMR techniques. To our surprise, the ^{1}H NMR spectra displayed proton peaks around 4.9 ppm and 5.8 ppm corresponding to a terminal alkene **32**.

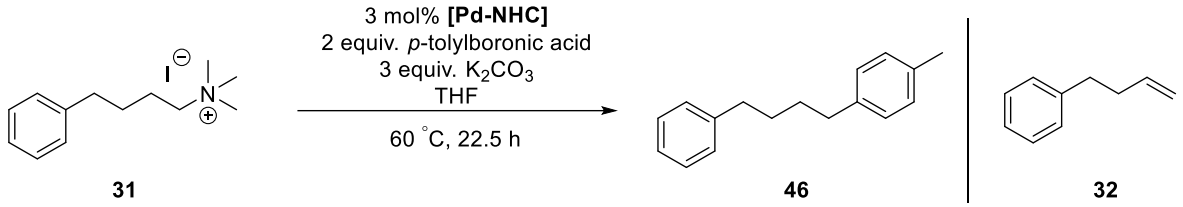

Entry	[Pd-NHC]	Reaction outcome
a	Pd-PEPPSI-IPr	Mainly SM, traces of **32**
b	(IPr)Pd(cinnamyl)Cl	Mainly SM, traces of **32**

Scheme 2.2.27 Investigation of the Suzuki-Miyaura cross-coupling of alkyl ammonium iodide 31 using catalytic amounts of Pd-PEPPSI-IPr and (IPr)Pd(cinnamyl)Cl.

In order to confirm that the detected terminal alkene peaks were in fact from the elimination product **32** and to identify the substrates produced in this reaction, a DOSY experiment was run. Unfortunately, a clear diffusion spectrum was not obtained due to the low amount of sample. At this stage of the investigation the following insights to the reaction were made: (i) starting material was mainly recovered indicating that the oxidative addition was not as

efficient as hoped, (ii) a terminal alkene was discovered pointing out that *β*-hydride elimination was present and it was competing with the transmetalation step in the Suzuki-Miyaura reaction, (iii) there were some indications that the coupling product **46** was present as well, however, only in traces, (iv) both reactions gave similar results. In order to increase the consumption of the starting material and confirm the formation of the terminal alkene **32** and the coupling product **46**, the Suzuki-Miyaura reaction was repeated with stoichiometric amount of the Pd-NHC precatalysts (see Scheme 2.2.28). The amount of *p*-tolylboronic acid and potassium carbonate used in the reaction were adjusted accordingly. The stoichiometric Suzuki-Miyaura reaction using either Pd-PEPPSI-IPr (Entry a) or (IPr)Pd(cinnamyl)Cl (Entry b) gave similar results as seen in the previously described catalytic reactions. Mainly starting material **31** was detected after the reaction with traces of a terminal alkene, presumably **32**. After prep TLC, an excessive NMR analysis of the isolated band was conducted, however, the abovementioned NMR techniques did not give any further information on the observed reaction outcome.

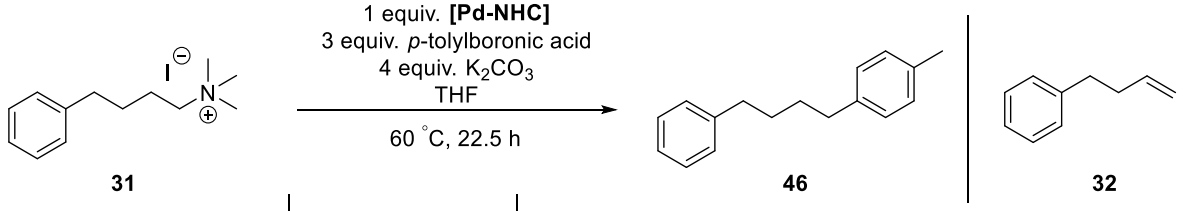

Entry	[Pd-NHC]	Reaction outcome
a	Pd-PEPPSI-IPr	Mainly SM, traces of **32**
b	(IPr)Pd(cinnamyl)Cl	Mainly SM, traces of **32**

Scheme 2.2.28 Investigation of Suzuki-Miyaura cross-coupling of alkyl ammonium iodide 31 using stoichiometric amounts of Pd-PEPPSI-IPr (Entry a) and (IPr)Pd(cinnamyl)Cl (Entry b).

With the aim of confirming the formation of the desired alkene product **32**, a selective TOCSY experiment was performed exploring the $^{1}H - {}^{1}H$ connectivity of the detected alkene peaks. When the proton peak around 5.8 ppm was excited, a connectivity to a peak at around 2.0 ppm was found indicating the alkene's connectivity to an alkyl proton. When the alkyl peak around 2.0 ppm was excited, a connectivity to a peak in the aromatic region was detected supporting that the elimination product **32** was formed during this reaction. No further study towards the verification of the coupled product **46** was made, since the formation of the alkene was the preferred product. The next objective of this screening was to increase the *β*-hydride elimination to form the terminal alkene **32** and at the same time to avoid the transmetalation

step in the catalytic cycle. The use of *p*-tolylboronic acid had a two-fold purpose in the Suzuki-Miyaura reaction: (1) it was involved in the activation of the Pd-NHC precatalyst and (2) it was the coupling partner for the transmetalation step. By removing the boronic acid from the reaction, the transmetalation step could be prevented. However, an alternative way of catalyst activation was then needed if the Pd-NHC precatalysts were used in the Pd-catalysed Hofmann-type elimination reaction.

Table 2.2.15 Pd-catalysed Hofmann-type elimination by means of the *in situ* generated NHC-Pd^0 catalyst.

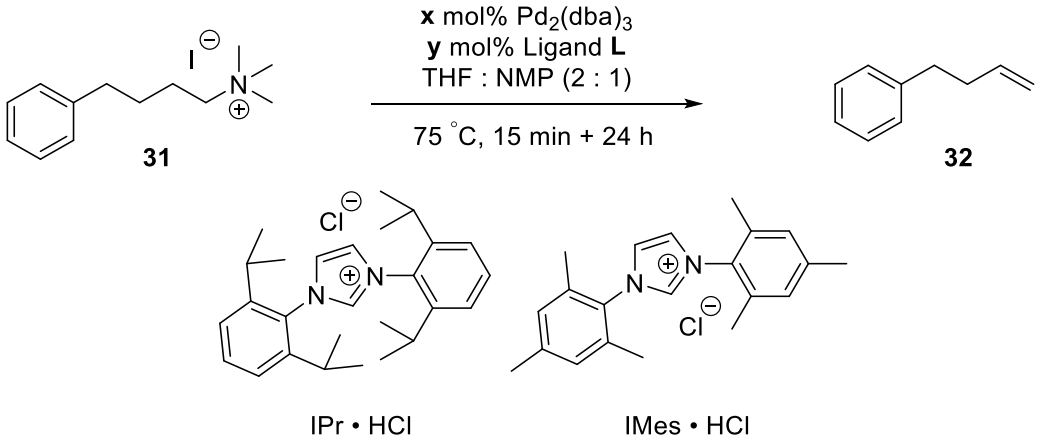

Entry	**x** mol%	**y** mol%	**Ligand L**	Reaction outcome
a	2	8	IPr	SM, no P
b	50	200	IPr	SM, no P
c	2	8	IMes	SM, no P
d	50	200	IMes	SM, no P

As an alternative to the use of Pd-NHC precatalysts in the Pd-catalysed elimination is the *in-situ* generation of the active Pd-NHC catalyst using a palladium source and imidazolium salts as ligand precursors. An example in the literature was found, in which Organ *et al.* described the Negishi coupling of alkyl bromides using 2 mol% $Pd_2(dba)_3$, tris(dibenzylideneacetone)dipalladium(0) and 8 mol% IPr, 1,3-bis-(2,6-diisopropylphenyl)imidazolinium chloride, in THF : NMP (2 : 1).[267] In this publication, they have reported that the use of NMI as base of the reaction was not necessary for this

transformation, yet, when NMP was replaced with alternative solvents the yield of the reactions was significantly decreased. Since the reported Negishi coupling starts with the oxidative addition of the catalyst to the alkyl electrophile, the reported reaction conditions were adopted to our model system, however, the organozinc substrate was left out to avoid transmetalation. Table 2.2.15 displays the modified conditions to achieve the elimination of trimethylamine and the generation of the desired alkene **32**. Trimethyl-(4-phenylbutyl)-ammonium iodide [**31**] was exposed to low (Entry a) and high (Entry b) loadings of $Pd_2(dba)_3$ in the presence of IPr • HCl in the co-solvent system THF : NMP (2 : 1) at 75 °C for 24 h. Quantitative ^{1}H NMR analysis of both reactions showed that the alkene product **32** was not formed during this reaction. Mainly starting material **31** was present in the collected ^{1}H NMR spectra.

Upon analysing the reaction spectra and searching the literature for possible explanations for the outcome of these reactions, it was discovered that even though IPr has been known to be an efficient ligand for cross-coupling reactions, the steric bulk of the ligand disfavours Pd/H interactions obstructing the *β*-hydride-elimination step in the proposed catalytic cycle.[268] In a later publication, Organ *et al.* confirmed this theory investigating the structure-property relationship of Pd-PEPPSI complexes in the Negishi coupling of alkyl electrophiles.[269] Organ and his colleagues demonstrated that the use of Pd-PEPPSI-IPr and -IPr derivatives did not lead to the formation of the terminal alkene side product in the Negishi coupling of (3-bromopropyl)benzene. However, by minimizing the steric bulk on the *N*-substituents of the NHC ligand, the *β*-hydride-elimination pathway was activated competing with the transmetalation step in the Negishi reaction and generating the terminal alkene as a side product of the reaction in about 30 – 35% yield. Thereby, the isopropyl moiety on the phenyl rings of the IPr ligand were substituted by methyl groups creating both Pd-PEPPSI-IXy (xylyl *N*-substituents) and Pd-PEPPSI-IMes (mesityl *N*-substituents).

With this knowledge in mind, the reactions described in Table 2.2.15 were repeated and the initially used IPr ligand was substituted by IMes (see Entries c + d). Unfortunately, the olefin product **32** was not detected even after an increase in catalyst loading. As seen in the reactions before, only the starting material **31** was detected in the proton spectra. An explanation may be that the deprotonation of the imidazolium salt and/or the *in situ* coordination of the free carbene to the Pd-centre to form the active Pd^0 have not been efficient.[268] Comparing the use of a Pd-PEPPSI-IPr to the *in situ* formed IPr-Pd^0 catalyst from $Pd_2(dba)_3$ and IPr • HCl, Organ *et al.* reported that the active catalyst generated from the Pd-PEPPSI-IPr precatalyst had a 40-fold higher turnover-number at 0.1 mol% loading after 1 h

into the reaction than the *in situ* generated active catalyst at 4 mol% loading implying that only a fraction of the added $Pd_2(dba)_3$ and IPr • HCl formed the active IPr-Pd^0 catalyst *in situ*.[270] In order to avoid negative and low yielding results of the Pd-catalysed elimination due to the inefficient generation of the active IMes-Pd^0 catalyst, it was decided to substitute the use of $Pd_2(dba)_3$ and IMes • HCl as the catalytic system to the Pd-PEPPSI-IMes precatalyst [**47**]. Since Pd-PEPPSI-IMes is not commercially available, a literature protocol was followed to synthesise **47** from $PdCl_2$ and IMes • HCl in 3-choloropyridine in the presence of potassium carbonate.[271] The reaction resulted in the dehalogenation of the chloro-pyridine ligand and a mixture of Pd-PEPPSI-IMes [**47**] and pyr-Pd-PEPPSI-IMes [**48**] was obtained (see Scheme 2.2.29).

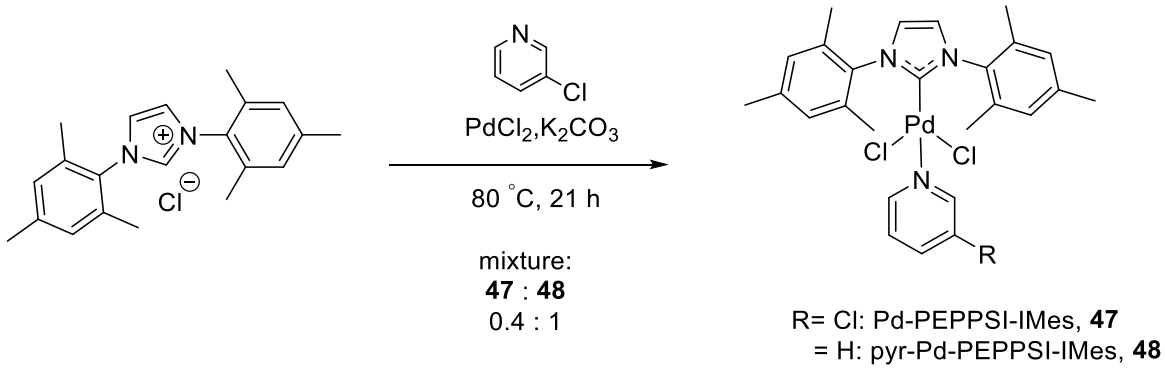

Scheme 2.2.29 Attempted synthesis of the Pd-PEPPSI-IMes [47] precatalyst.

At this stage, a closer investigation of the structure-property relationship of Pd-PEPPSI precatalysts was undertaken. There are three major components to the ligands of the Pd-PEPPSI precatalysts, the imidazolium ring (red) and the *N*-substituents (blue) of the NHC ligand and the dummy ligand (green), which is needed to stabilise and isolate the precatalyst.

The effect of the *N*-substituents was discussed above, which led to the substitution of the IPr ligand to the IMes ligand. By decreasing the steric bulk of the *N*-substituents, it was believed to enhance the *β*-hydride elimination, an important step of the proposed Pd-catalysed elimination. However, it is worth mentioning that the general trend in the literature regarding the effect of the steric bulk of the *N*-substitutents on the catalytic cross coupling reactions using organometallic reagents is that an increase in size of these substituents advances the reductive elimination of the catalytic cycle making challenging cross coupling reactions more efficient.[272–274] Consequently, it is important to incorporate reactions using stoichiometric

amount of IMes-based catalysts into our screening in order to contemplate for possible negative reaction outcomes, which might emerge due to errors in the reductive elimination step of the catalytic cycle.

The imidazolium core possesses the carbene centre of the NHC ligand with two nitrogen adjacent to it, through which the electron is delocalised. Since the imidazolium core is the centre for electron donation to the metal, it has a great influence on the oxidative addition step in the catalytic cycle. By modifying the backbone of the imidazolium ring (see Figure 2.2.5, in red) and thus changing the overall electronic properties of the catalyst, it is possible to tune the Pd-NHC complex towards improving the oxidative addition step. The addition of substituents onto the imidazolium ring does not have a direct steric effect on the metal centre, because they would be outside of the coordination sphere of metal catalyst.

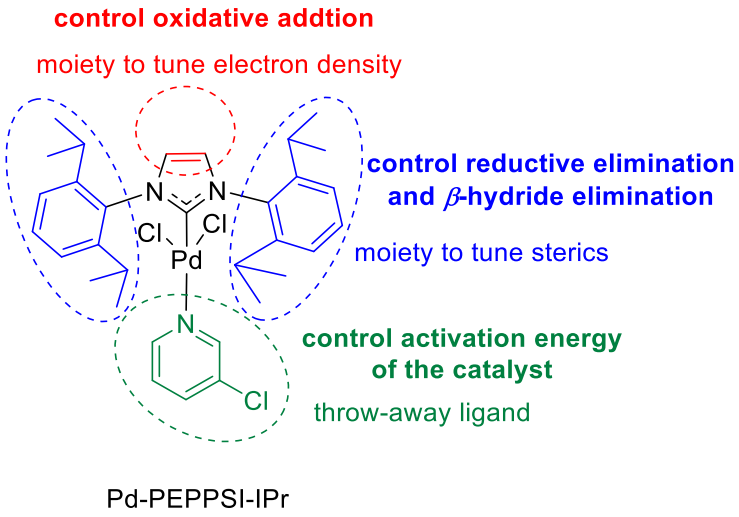

Figure 2.2.5 Structure-property analysis of Pd-PEPPSI-IPr.

The 3-chloropyridine throw-away ligand was introduced by Organ *et al.*[270] to stabilise the PEPPSI-Pd precatalyst making it easier to isolate and to use even when it is exposed to air and moisture. Next to its stabilising function, 3-chloropyridine was chosen to be used as the throw-away ligand due to its electron-withdrawing properties making it more prone to dissociate from the metal centre upon catalyst activation. However, recent studies have shown that the 3-chloropyridine ligand undergoes a Pd-mediated hydrodehalogenation forming the pyridine ligated Pd-NHC precatalyst prior to the actual activation of the precatalyst to give the active NHC-Pd^0.[275] Organ *et al.* reported that the replacement of the 3-chloropyridine ligand by

pyridine lowered the temperature required to activate the precatalyst. In addition, Organ and co-workers observed an increased yield in the cross-coupling of aryl chlorides when pyridine-ligated PEPPSI-Pd was used instead of the 3-chloropyridine-ligated PEPPSI-Pd precatalyst.[269] They hypothesised that the more electron-donating character of pyridine would continuously support the active NHC-Pd^0 catalyst slowing down its decomposition.

Based on the discussion above, a small library of Pd-PEPPSI-IMes derivatives was assorted to investigate the structure-property relation of these precatalysts in the Pd-catalysed Hofmann-type elimination (displayed in Figure 2.2.6). The mesityl rings on the imidazolium core were maintained as before, however, the backbone of the imidazolium ring was modified and 3-chloropyridine was replaced by pyridine as the throw-away ligand on the Pd-complex, which simultaneously avoided the issue of dehalogenation experienced in the synthesis of Pd-PEPPSI-IMes [**47**] (displayed in Scheme 2.2.29).

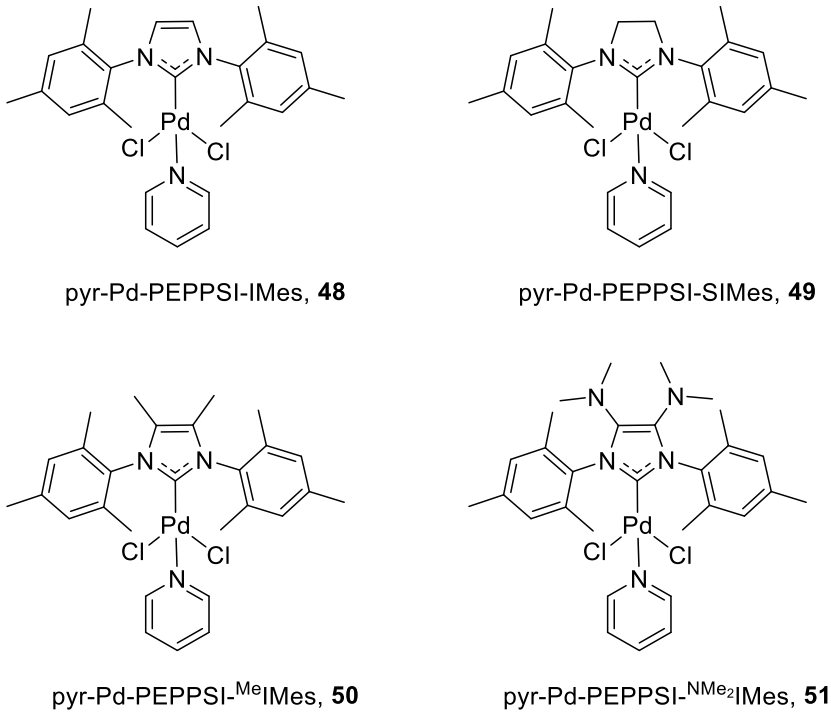

Figure 2.2.6 A small library of Pd-PEPPSI precatalysts to investigate their structural effect on the Pd-catalysed Hofmann-type elimination.

Pyr-Pd-PEPPSI-IMes [**48**] was synthesised to compare the efficiency of the active catalyst generated from the activation of **48** in the Pd-catalysed Hofmann-type elimination compared the reactions conducted with the *in situ* generated NHC-Pd^0 catalysts (as displayed in Table

2.2.15). In addition, the activity of pyr-Pd-PEPPSI-IMes [**48**] was used as a baseline to compare the effect of the electronic changes in the imidazolium core. As demonstrated in Scheme 2.2.30, pyr-Pd-PEPPSI-IMes [**48**] was synthesised from the commercially available IMes • HCl and $PdCl_2$ in the presence of potassium carbonate and pyridine at 80 °C for 21 h. After the reaction, pyr-Pd-PEPPSI-IMes [**48**] was isolated in good yield (86%).

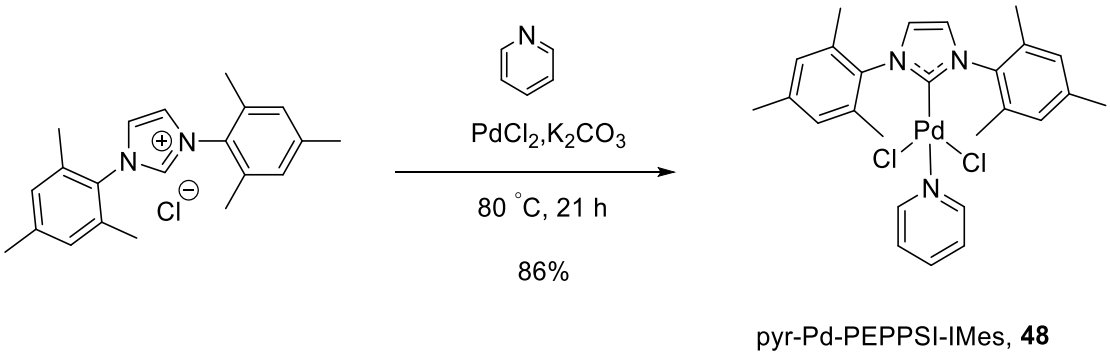

Scheme 2.2.30 Synthesis of pyr-Pd-PEPPSI-IMes [48].

In the Suzuki-Miyaura reaction, described in Scheme 2.2.27, the role of the *p*-tolylboronic acid is not only to act as the coupling partner in the transmetalation step, but it is also responsible for the activation of the Pd-PEPPSI-IPr precatalyst. Experimental evidence by Organ *et al.* indicated that the reduction of the Pd-PEPPSI-IPr precatalyst to Pd^0 by means of an organometallic reagent may be the rate-determining step of the precatalyst activation, which is followed by a fast dissociation of the throw-away ligand.[269] Since our goal for the following experiments using the synthesised pyr-Pd-PEPPSI-IMes is the increase in efficiency of the *β*-hydride elimination in the catalytic cycle, an alternative way of precatalyst activation is necessary to avoid the use of organometallic reagents and thus to hinder the competing transmetalation step. Instead of using organometallic reagents, which are able to activate the precatalyst under mild conditions, it was suggested by the literature to incorporate strong bases and/or elevated temperatures to achieve the activation of the precatalyst forming the active NHC-Pd^0.[275] Consequently, trimethyl-(4-phenylbutyl)-ammonium iodide [**31**] (Entries a + c) and trimethyl-(4-phenylbutyl)-ammonium triflate [**41**] (Entries b + d) were both exposed to catalytic and stoichiometric amounts of pyr-Pd-PEPPSI-IMes [**48**] in the presence of caesium carbonate in acetonitrile at 80 °C for 22 h, respectively (see Table 2.2.16). Since triflate is a

less ligating anion than iodide, it was expected that the triflate ion would not occupy a free coordination site of the Pd centre preventing a possible poisoning of the active catalyst. All four reactions resulted in the formation of the desired alkene **32**, however, in low yield (≤ 1%). Nevertheless, the alkene product **32** was marginally produced with the use of the pyr-Pd-PEPPSI-IMes precatalyst [**48**] in contrast to the elimination reactions catalysed by the *in situ* generated NHC-Pd^0 from $Pd_2(dba)_3$ and IMes • HCl, which did not result in the formation of the desired alkene **32**.

Table 2.2.16 Pd-catalysed Hofmann-type elimination of alkyl ammonium electrophiles using pyr-Pd-PEPPSI-IMes [48]. †The conversion was calculated using quantitative ^{1}H NMR with trimethyl benzene-1,3,5-tricarboxylate in DMSO (0.1 M) as internal standard.

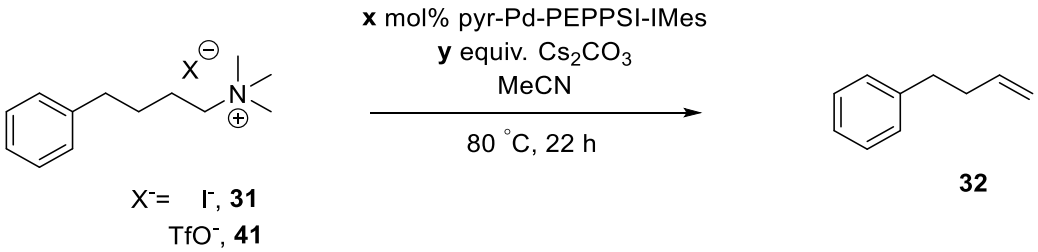

Entry	X^-	x mol%	y equiv.	Conversion to **Product**†
a	I^-	3	3	< 1%
b	^-OTf	3	3	1%
c	I^-	100	4	< 1%
d	^-OTf	100	4	< 1%

The investigation of the Pd-catalysed Hofmann-type elimination was continued with the synthesis of the three remaining Pd-PEPPSI precatalysts, which were displayed in Figure 2.2.6. Since SIMes • HCl is commercially available, the synthesis of pyr-Pd-PEPPSI-SIMes was conducted with the same reaction conditions as reported before using SIMes • HCl as the NHC ligand (see Scheme 2.2.31) to give pyr-Pd-PEPPSI-SIMes [**49**] in decent yield (52%). Pyr-Pd-PEPPSI-SIMes [**49**] was included in the structure-property relationship study of distinct Pd-PEPPSI-IMes precatalysts, because there are examples in the literature, which showed a higher

efficiency of the saturated version of a certain precatalyst compared to its unsaturated version.[276,277] The loss of unsaturation on the imidazolium ring shifts the mesityl rings closer to the metal centre occupying a greater volume of the coordination sphere of the metal.[266]

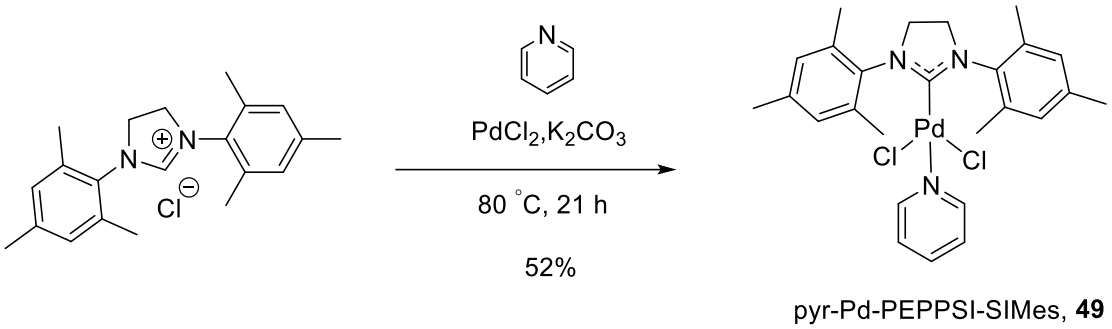

Scheme 2.2.31 Synthesis of pyr-Pd-PEPPSI-SIMes [49].

For the synthesis of pyr-Pd-PEPPSI-^{Me}IMes [**50**] and pyr-Pd-PEPPSI-^{NMe2}IMes [**51**] the imidazolium salt precursors were not commercially available. Consequently, the imidazolium salts of ^{Me}IMes and ^{NMe2}IMes were synthesised prior to their ligation to the palladium to form the desired NHC-Pd complexes. Both imidazolium salts are synthesised from *N,N*-dimesitylformimidamide [**52**], a common starting material for the synthesis of substituted NHC ligands.[278] 2,4,6-Trimethylaniline was reacted with triethylorthoformate in acetic acid at 160 ˚C to give *N,N*-dimesitylformimidamide [**52**] in excellent yield (99%) as shown in Scheme 2.2.32.

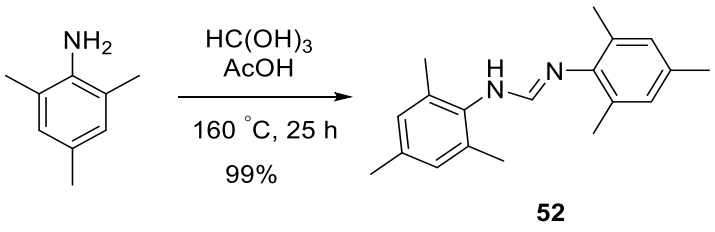

Scheme 2.2.32 Synthesis of *N,N*-dimesitylformimidamide [52].

For the synthesis of the ^{Me}IMes • HCl ligand, *N,N*-dimesitylformimidamide [**52**] was treated with 2-chloro-3-butanone in the presence of diisopropylethylamine to give the hydroxyimidazolidinium chloride upon substitution of the chloride and the subsequent

intramolecular cyclization (see Scheme 2.2.33). Dehydration of the hydroxyimidazolidinium chloride using acetic anhydride resulted in the formation of the desired ^{Me}IMes • HCl ligand [**53**] in moderate yield (33%).

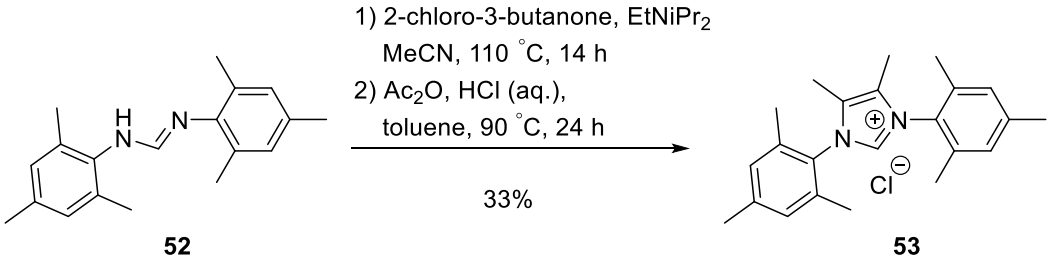

Scheme 2.2.33 Synthesis of ^{Me}IMes • HCl [53].

The synthesis of the ^{NMe2}IMes • HOTf ligand [**55**] is illustrated in Scheme 2.2.34. Deprotonation of *N,N*-dimesitylformimidamide [**52**] by *n*BuLi followed by the addition of the *in situ* generated dichlorodiaminoethene led to the formation of the formamidine intermediate [**54**]. Abstraction of the chloride with trimethylsilyl trifluoromethanesulfonate (TMSOTf) formed a keteneiminium species, which was immediately cyclised to give the desired ^{NMe2}IMes • HOTf NHC ligand [**55**] in low yield (13%).

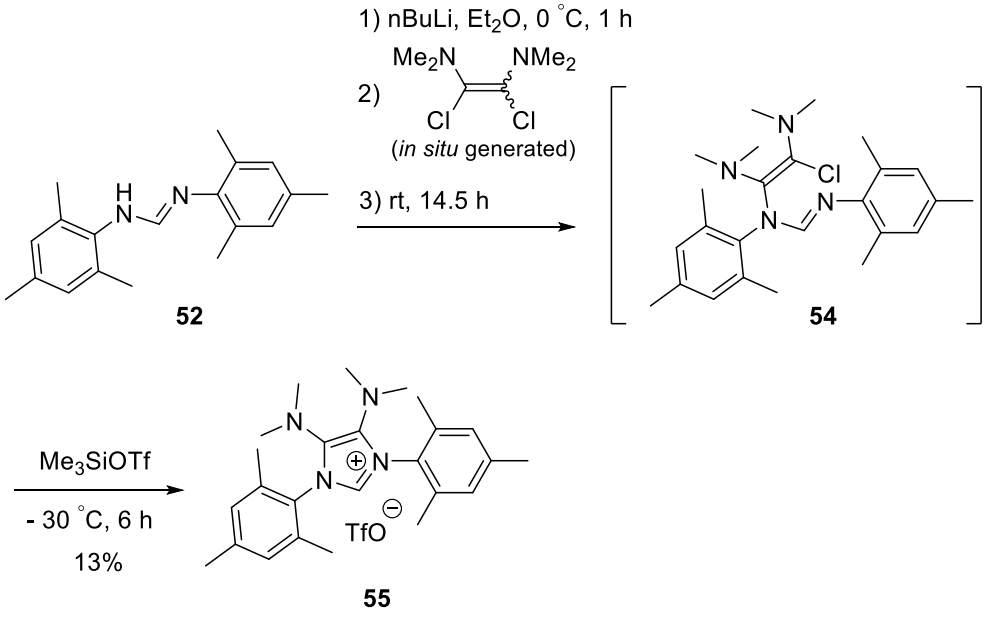

Scheme 2.2.34 Synthesis of ^{NMe2}IMes • HOTf [55].

With these two modified NHC ligands in hand, the synthesis of their corresponding PEPPSI-Pd precatalysts was conducted using the same protocol as previously reported (see Scheme 2.2.35), however, only pyr-Pd-PEPPSI-^{Me}IMes [**50**] was isolated in good yield (57%). The reaction using ^{NMe2}IMes • HOTf [**55**] as ligand resulted in a complex mixture and pyr-Pd-PEPPSI-^{NMe2}IMes [**51**] could not be isolated after column chromatography. MS analysis of the collected mixture suggested that pyr-Pd-PEPPSI-^{NMe2}IMes [**51**] was not formed in this reaction.

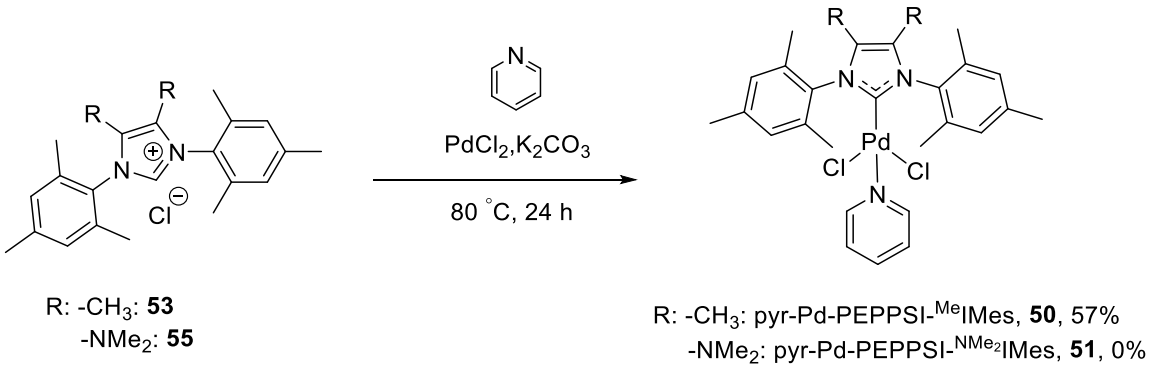

Scheme 2.2.35 Synthesis of Pd-PEPPSI-IMes analogues.

Consequently, three (**48**, **49** and **50**) of the four PEPPSI-Pd-IMes precatalysts listed in Figure 2.2.6 were investigated for the Pd-catalysed Hofmann-type elimination of both trimethyl-(4-phenylbutyl)-ammonium iodide [**31**] and triflate [**41**]. For these experiments, stoichiometric amounts of precatalysts were used and since the activation of these precatalysts was accomplished with the use of strong bases and elevated temperatures, caesium carbonate was used at 80 °C. Table 2.2.17 summarises the outcome of these reactions. Unfortunately, the modification of the NHC ligands did not have an impact on the yield of the elimination reaction. Even though the Pd-NHC precatalysts were designed to improve the oxidative addition and the *β*-hydride elimination, only marginal formation of the desired terminal alkene **32** (≤ 1%) was detected.

Table 2.2.17 Pd-catalysed Hofmann-type elimination using the tailored Pd-PEPPSI-IMes precatalysts in combination with caesium carbonate. †The conversion was calculated using quantitative ^{1}H NMR with trimethyl benzene-1,3,5-tricarboxylate in DMSO (0.1 M) as internal standard.

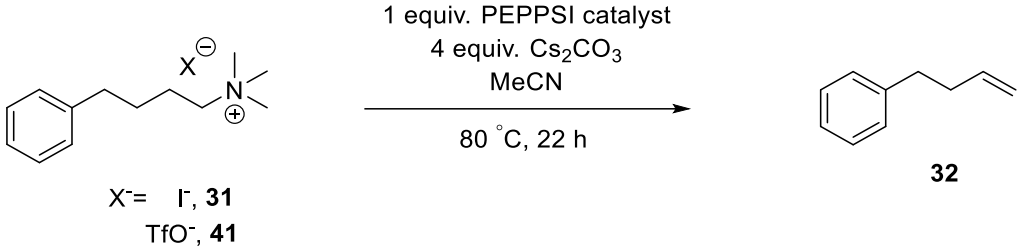

X⁻= I⁻, **31**
TfO⁻, **41**

Entry	X^-	PEPPSI catalyst	Conversion to **Product**†
a	I^-	pyr-Pd-PEPPSI-IMes	< 1%
b	^-OTf	pyr-Pd-PEPPSI-IMes	< 1%
c	I^-	pyr-Pd-PEPPSI-SIMes	< 1%
d	^-OTf	pyr-Pd-PEPPSI-SIMes	< 1%
e	I^-	pyr-Pd-PEPPSI-^{Me}IMes	1%
f	^-OTf	pyr-Pd-PEPPSI-^{Me}IMes	1%

To ensure that the catalyst activation was not the reason for the low yields obtained above, the Pd-catalysed Hofmann-type elimination of both trimethyl-(4-phenylbutyl)-ammonium iodide [**31**] and triflate [**41**] were repeated using the modified NHC-Pd precatalysts in the presence of potassium-*tert*-butoxide, an alternative strong base to generate the active NHC-Pd^0 species. As displayed in Table 2.2.18, a change in base did not improve the yield of the experiments either.

A recent study by Ananikov *et al.* revealed a different mode of action of Pd-NHC systems.[279] They challenged the widely accepted assumption that the catalytic activity of the Pd-NHC complex was based on a stable metal-ligand binding stabilising the active Pd^0 species throughout the reaction. Ananikov and colleagues argued that the catalytic activity was based on the dissocation of the Pd-NHC complex leading to the formation of Pd clusters and nanoparticles, which can be further stabilised using quaternary ammonium salts by preventing the agglomeration of these Pd particles. After studying 19 different NHC-Pd precatalysts in a typical Heck-Mizoroki reaction, they have inferred that small substituents on the imidazolium ring and weakly bound ligands facilitate the 'fast-release' of the active Pd clusters. In addition,

the use of high temperatures (140 °C) also increased the rate of these reactions. The stabilising impact of ionic liquids on Pd nanoparticles in combination with high temperatures have also been reported in earlier studies.[280,281] To test this theory, the Pd-catalysed Hofmann-type elimination was conducted in TBAB using the modified Pd-NHC precatalysts at 140 °C. The results of this study are listed in Table 2.2.19. Even with the use of the stabilising TBAB and the significant increase in temperature, only traces of the desired olefin **32** were determined.

Table 2.2.18 Pd-catalysed Hofmann-type elimination using the tailored Pd-PEPPSI-IMes precatalysts in combination with potassium-*tert*-butoxide. †The conversion was calculated using quantitative ^{1}H NMR with trimethyl benzene-1,3,5-tricarboxylate in DMSO (0.1 M) as internal standard.

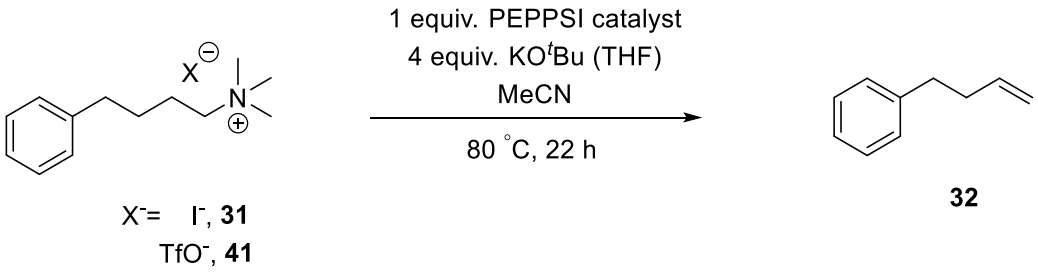

X^-= I^-, **31**
TfO^-, **41**

Entry	X^-	PEPPSI catalyst	Conversion to **Product**†
a	I^-	pyr-Pd-PEPPSI-IMes	< 1%
b	$^-$OTf	pyr-Pd-PEPPSI-IMes	< 1%
c	I^-	pyr-Pd-PEPPSI-SIMes	< 1%
d	$^-$OTf	pyr-Pd-PEPPSI-SIMes	< 1%
e	I^-	pyr-Pd-PEPPSI-^{Me}IMes	< 1%
f	$^-$OTf	pyr-Pd-PEPPSI-^{Me}IMes	< 1%

While we were conducting our research on the application of Pd-NHC catalysts on the cleavage of the C(sp^3) – N bond in our alkyl trimethylammonium substrate, a publication from Jia *et al.* surfaced in early 2019, which described the first application of a PEPPSI-Pd complex on the Suzuki cross coupling of benzylic trimethylammonium bromides with aryl boronic acids to obtain diarylmethanes.[282] Next to the two protocols published by Zhao *et al.*[254] and Phipps *et al.*[255], which were discussed in Subchapter 2.2.15, this protocol by Jia and colleagues is the

third example of using palladium catalysts to perform an oxidative addition into a C(sp^3) – N bond of benzylic trimethylammonium compounds. Although the application of the reported PEPPSI-Pd complexes did not give the desired results in our model system, this publication by Jia and co-workers has confirmed that the right approach towards the cleavage of the carbon-ammonium bond was taken in this research, but further optimisation was needed to induce the oxidative addition into the less activated alkyl ammonium substrates.

Table 2.2.19 Pd-catalysed Hofmann-type elimination using the tailored Pd-PEPPSI-IMes precatalysts in combination with caesium carbonate and TBAB. †The conversion was calculated using quantitative ^{1}H NMR with trimethyl benzene-1,3,5-tricarboxylate in DMSO (0.1 M) as internal standard.

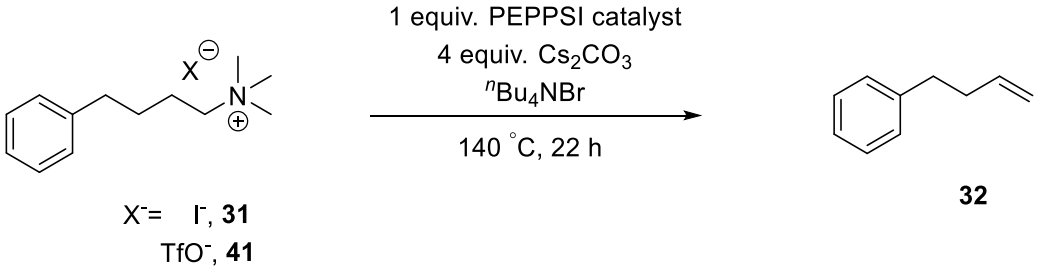

X⁻= I⁻, **31**
TfO⁻, **41**

Entry	**X**$^-$	**PEPPSI catalyst**	Conversion to **Product**†
a	I^-	pyr-Pd-PEPPSI-IMes	< 1%
b	$^-$OTf	pyr-Pd-PEPPSI-IMes	< 1%
c	I^-	pyr-Pd-PEPPSI-SIMes	< 1%
d	$^-$OTf	pyr-Pd-PEPPSI-SIMes	< 1%
e	I^-	pyr-Pd-PEPPSI-^{Me}IMes	< 1%
f	$^-$OTf	pyr-Pd-PEPPSI-^{Me}IMes	< 1%

2.3 Pd-catalysed Hofmann-type elimination screening on model synthetic peptide

The overall aim of the project is the site-specific modification of histone proteins to develop a chemical biological tool to analyse post-translational modifications and their relation to epigenetic diseases. As a start, we decided to focus on the investigation of trimethyllysine marks on histone tails by chemically modifying these marks to olefins in order to attach affinity tags for their enrichment. Over the course of the project, we took several approaches to design a chemical reaction to convert the trimethylammonium functionality to a terminal alkene on model systems (see Chapter 2.1 for Hofmann elimination and Chapter 2.2 for Pd-catalysed Hofmann-type elimination). A major drawback to using a model system might be encountered when applying the optimised reaction conditions to the actual target: proteins. Since the Pd-catalysed Hofmann-type elimination is to be performed on the trimethyllysine moiety in peptides and proteins containing other natural amino acids, it was questioned whether any catalytic system developed for model small molecules would be compatible for biomolecules. The exploration of the Pd-catalysed elimination on synthetic peptides was therefore performed in parallel to our efforts in improving the reaction on model small molecules. We started our study of the Pd-catalysed Hofmann-type elimination on peptides by adopting similar experimental settings to those published in the literature. The use of palladium-mediated chemical modifications in biological systems reported in the literature is summarised in the subsequent subchapter.

2.3.1 Background: Palladium chemistry in protein modifications

The field of chemical protein modification has emerged as an important tool for understanding biological systems both *in vitro* and *in vivo*.[283] With the introduction of biorthogonal chemistry to biological systems, the use of transition-metal catalysis became more prominent in protein modification.[284,285] Next to copper, which has revolutionized the labelling of proteins via the widely known Cu(I)-catalysed azide–alkyne cycloaddition (CuAAC) reaction, palladium has gained importance in targeting both natural and synthetically incorporated unnatural amino acids *in vitro* and in living cells.[173,286–288] The initial limitations in applying the traditional Pd-catalysed reactions to biological systems such as the use of organic solvents, the potential catalyst poisoning by surrounding nucleophiles and the need of elevated temperatures have been overcome. The emergence of air- and moisture-stable catalytic systems enabled the

optimisation of palladium catalysis in biological media (aqueous buffers with a certain pH range) leading to the development of efficient, chemoselective and mild (close to room temperature) protocols.

An early example of the use of palladium catalysts in protein modification was published by Kodadek *et al.*, who successfully achieved the photoinduced cross-linking of two interacting proteins in the presence of palladium(II)-5,10,15,20-tetra-(methylpyridinium)-porphyrin (Pd(II)TMPyP) and ammonium persulfate.[289] Tilley and Francis introduced the site-selective tyrosine modification based on a Tsuji-Trost reaction. The tyrosine residue of the protein of interest was reacted with the *in situ* generated π-allylpalladium complex in either triethylammonium carbonate or phosphate buffer (pH = 8.6).[290] The catalytic system was prepared using palladium(II) acetate and water-soluble triphenylphosphine tris(sulfonate) (TPPTS) in degassed distilled water. Most of the examples on the application of palladium chemistry for the modification of natural amino acids are based on the nucleophilicity of the side chains, which attack the pre-formed organopalladium complex. In addition to tyrosine and lysine[291], cysteine has been a favoured site for Pd-mediated modifications due to its low abundance in proteins.[286] Buchwald *et al.* displayed the arylation of cysteine residues in various proteins using the pre-developed (RuPhos)Pd(Ar)OTf reagent in Tris buffer (pH 7.5).[292] Building on the work by Buchwald, Messaoudi and colleagues reported the arylation of cysteine-containing biomolecules without the need of the pre-formed organopalladium complex.[293] By using the palladacycle Pd-G3-XantPhos catalyst (1.25 equiv. per thiol), Messaoudi and co-workers achieved cysteine conjugation with aryl halides in the presence of a variety of functional groups. An inspiring discovery was made by Davis *et al.*, who have reported the selective *S*-arylation of proteins by guiding the metal complex towards the reactive amino acid with the help of a metal-binding motif present in the protein.[294] Davis and co-workers used an excess (80 equiv.) of palladium(II) acetate ligated with the disodium salt of *N*,*N*-dimethyl-2-amino-4,6-dihydroxypyrimidine (ADHP) in the presence of aryl iodide (500 equiv.) in Tris buffer (pH 7.6) at 65 °C.

A more ‘classical’ approach to ensure chemoselectivity in protein modifications is the incorporation of unnatural amino acids, which can be installed genetically, enzymatically or chemically.[295–298] These unnatural amino acids are equipped with reactive functional groups for certain modifications. In case of palladium-mediated cross coupling reactions, unnatural amino acids such as aryl halides, aryl boronates and alkynes have been installed into proteins or polypeptides. With the integration of these functional groups, protocols have surfaced, in

which the palladium catalyst was directly interacting with the target protein to undergo oxidative addition instead of using the nucleophilic sites of the protein to attack the organopalladium complex as previously described. The first reported Mizoroki-Heck reaction on proteins was published in 2007, in which Kodama *et al.* modified the 4-iodo-l-phenyl-alanine residue of the Ras protein using palladium(II) acetate and triphenylphosphine-trisulfonate (TPPTS).[299] This work by Kodama and colleagues has proven that the oxidative addition of a palladium complex directly into the target functional group on a protein is feasible, however, further improvement of the conditions is needed, since only a low yield was observed (2%). Davis *et al.* revolutionized the Suzuki-Miyaura coupling of proteins by introducing 2-amino-4,6-dihydroxypyrimidine (ADHP, L1 in Figure 2.3.1) as a viable ligand to use for palladium catalysis in a biological setting.[300] Davis and his team managed to successfully couple a chemically incorporated iodobenzyl residue of a protein with a range of boronic acids in an aqueous buffer (pH = 8.0) at low temperature (37 ˚C) and open to air, giving the desired modified proteins in excellent yields (> 95%). Founded on this publication by Davis and co-workers, many studies followed using ADHP and alternative amine-based ligands, which are displayed in Figure 2.3.1, to successfully modify proteins bearing an iodophenyl handle to undergo Suzuki cross coupling reactions with boronic acids.[301–303]

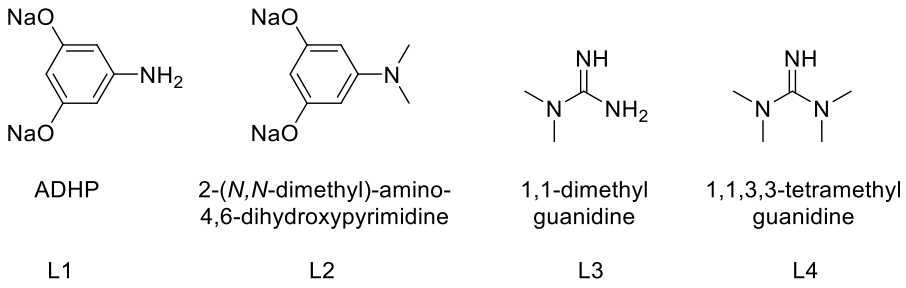

Figure 2.3.1 Amine-based ligands commonly used for the Pd-catalysed cross-coupling reactions of proteins.

Due to the advantages in the use of amine-based ligands (moisture- and air-stable) and the effective interactions of the palladium complexes formed from these ligands with the reported proteins, it was decided to start our investigation of the Pd-catalysed Hofmann-type elimination of trimethyllysine residues in peptides using the conditions published by Davis *et al.*[300]. This chapter will demonstrate our efforts in applying complex palladium catalysis into a biological experimental setting utilising synthetic peptides in aqueous buffers at physiological temperature.

2.3.2 The design of the synthetic peptide used for the Pd-catalysed Hofmann-type elimination

The application of the Pd-catalysed Hofmann-type elimination reaction to peptides and proteins was commenced using the peptide sequence **56** shown in Figure 2.3.2. Since our collaborators had purchased this peptide prior to our experiments, it was available in our laboratory and used for the Pd-mediated elimination experiments. As illustrated in Figure 2.3.2, the synthetic peptide consists of 19 amino acids with a variety of functional groups including the requisite trimethylammonium functionality on lysine K9, which can undergo the expected elimination upon treatment with the Pd-based catalytic system. Due to the versatility of the peptide side chains ranging from nucleophilic amines and alcohols to acidic carboxylic acids and less coordinating free amides to the sterically demanding alkyl and aryl groups, it was believed that the use of this peptide sequence might give additional information on the interaction of the palladium catalyst with functionalities other than the quaternary ammonium group.

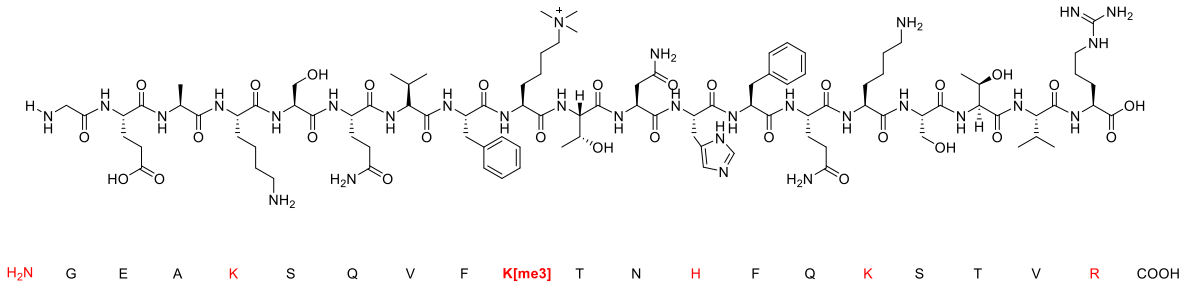

56

Figure 2.3.2 Synthetic peptide sequence GEAKSQVFK[me3]TNHFQKSTVR [56] for the investigation of the Pd-catalysed Hofmann-type elimination.

There are six basic groups present in the synthetic peptide **56** making it highly charged (see Figure 2.3.2 in red). The total monoisotopic mass of the sextuple positively charged peptide **56** is 2233.20 Da resulting in the calculated mass-to-charge ratios listed in Figure 2.3.3. As shown in the mass spectrum of **56** in Figure 2.3.3, four major peaks are detected representing the double (m/z 1117.64), triple (m/z 745.53), quadruple (m/z 559.61) and quintuple (m/z 447.85) positively charged ions of **56**.

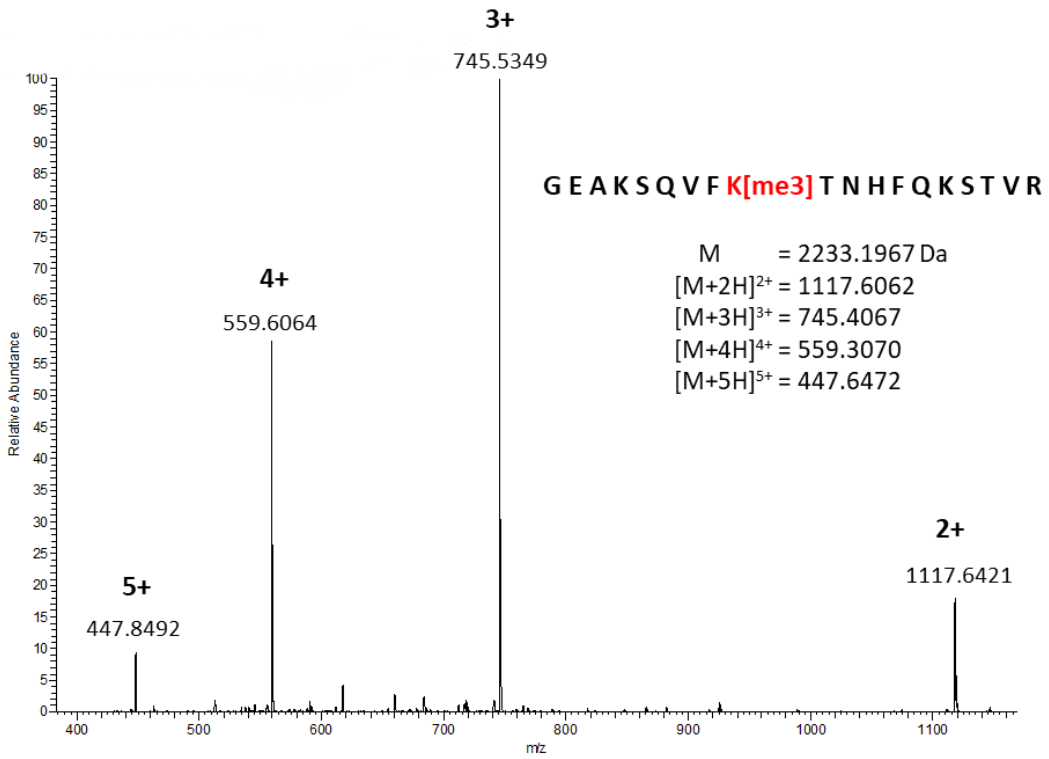

Figure 2.3.3 Mass spectrum of GEAKSQVFK[me3]TNHFQKSTVR [56].

Due to the size of the peptide sequence, the complexity of the Pd-catalysed elimination reaction and the resulting uncertainty of the possible reaction outcomes, it was decided to analyse the experiments using tandem mass spectroscopy. In case of complex mixtures obtained after the reaction, tandem mass spectroscopy would provide an additional information layer to decipher the structure of the resulting peptides. Figure 2.3.4 displays the MS2 spectrum of the synthetic peptide **56**. The identified fragment ions are annotated in green for b ions and blue for y ions. The MS2 spectrum in Figure 2.3.4 suggests that a successful fragmentation pattern of the peptide **56** was achieved.

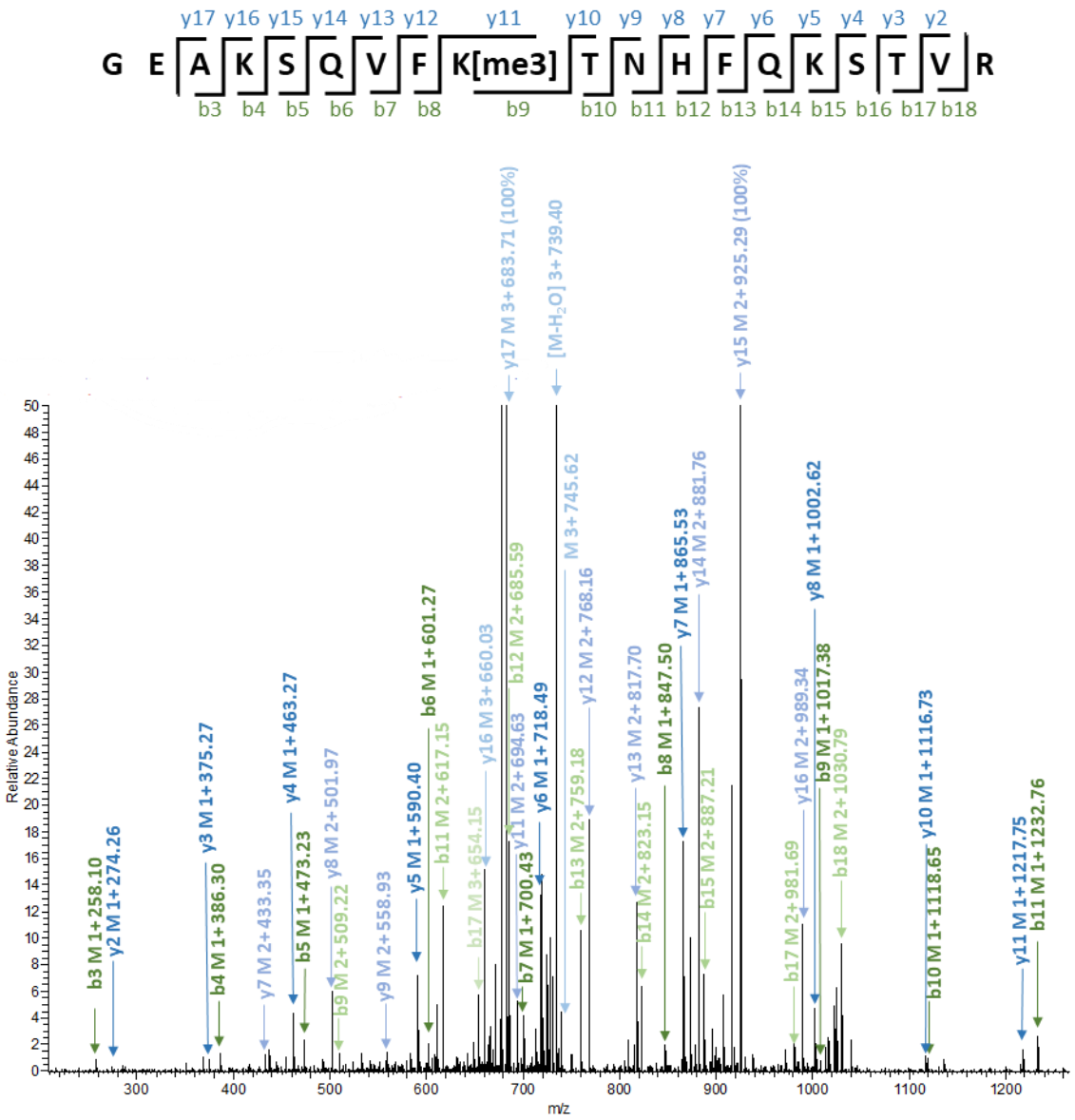

Figure 2.3.4 MS2 spectrum of the synthetic peptide 56 (precursor ion: [M/3] 745.62). Spectrum is zoomed in, *i.e.* 100% in bracket stands for signal intensity of that peak.

The initial design of the Pd-catalysed Hofmann-type elimination experiments is shown in Figure 2.3.5. The main features of the setup were the formation of the palladium catalyst in a solvent prior to its addition to the buffer solution, in which the peptide was pre-dissolved. The Lo-Bind Eppendorf tube including the reaction mixture was sealed and heated overnight. The next day the samples were dried and desalted using C18 spin columns in order to remove palladium residues. After purification, the samples were analysed via tandem mass spectroscopy.

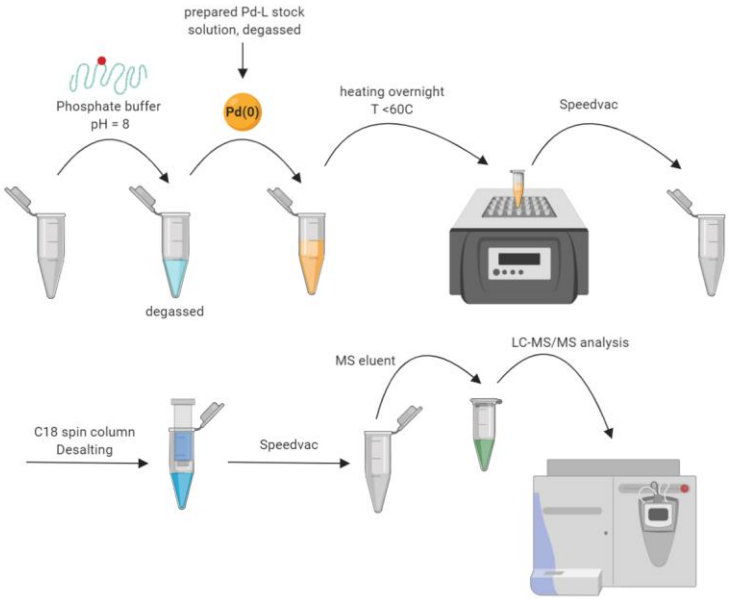

Figure 2.3.5 Experimental setup of the investigation of the Pd-catalysed Hofmann-type elimination of the synthetic peptide 56.

Upon treatment of the synthetic peptide **56**, it was expected for the Pd-based catalytic system to target the trimethylammonium lysine residue at position 9 of the peptide sequence to undergo oxidative addition and eliminate trimethylamine leading to the formation of the product peptide **57** (Figure 2.3.6).

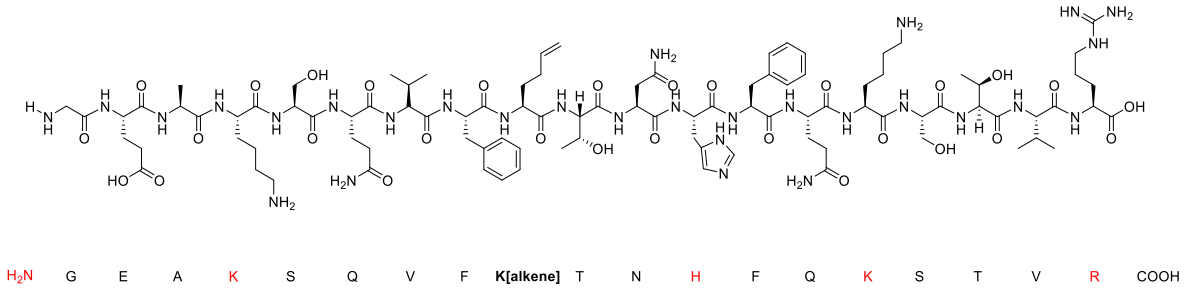

57

Figure 2.3.6 The peptide sequence of the product 57 including the desired alkene functionality at lysine K9.

Consequently, the analysis of these experiments by tandem mass spectroscopy is based on the loss of 60.0813 Da compared to the starting peptide **56**. The calculated monoisotopic mass of the product peptide **57** and the expected m/z ratios are listed in Table 2.3.1.

Table 2.3.1 Calculated monoisotopic masses for the peptide 56 and the desired peptide product 57 and their corresponding m/z ratios.

GEAKSQVFK[me3]TNHFQKSTVR		GEAKSQVFK[alkene]TNHFQKSTVR	
2233.1967 Da		2173.1154 Da	
$[M+1H]^{1+}$	2234.2045	$[M+1H]^{1+}$	2174.1232
$[M+2H]^{2+}$	1117.6062	$[M+2H]^{2+}$	1087.5655
$[M+3H]^{3+}$	745.4067	$[M+3H]^{3+}$	725.3796
$[M+4H]^{4+}$	559.3070	$[M+4H]^{4+}$	544.2867
$[M+5H]^{5+}$	447.6472	$[M+5H]^{5+}$	435.6309
	Δ	**-60.0813 Da**	

The investigation of the Pd-catalysed Hofmann-type elimination was commenced using the protocol by Davis and co-workers[300], which will be presented in the subsequent subchapter.

2.3.3 Attempted Pd-catalysed Hofmann-type elimination on the model peptide using amine-based ligands

The Pd-L complexes shown in Figure 2.5.5 were investigated for the Pd-catalysed Hofmann-type elimination of the trimehyllysine residue of **56**. They were prepared according the protocols published by Davis and co-workers.[302]

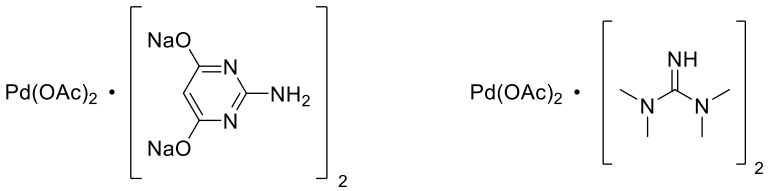

58 **59**

Figure 2.3.7 Palladium-ligand complexes investigated for the Pd-catalysed Hofmann-type elimination of 56.

As displayed in Scheme 2.3.1, the synthetic peptide **56** (1.5 nmol) was treated with both Pd-complexes **58** and **59** (75 nmol, 50 equiv.), respectively, in sodium phosphate buffer (50 mM, pH = 8.00) at 37 ˚C for 18 h. After the reaction, the samples were desalted using C18 spin columns and the outcome was analysed via LC-MS/MS.

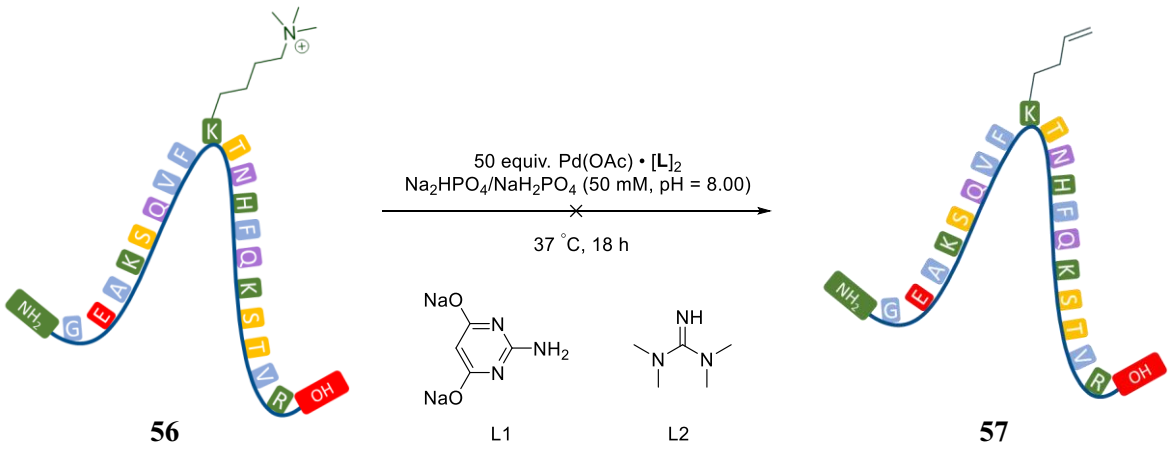

56 L1 L2 **57**

Scheme 2.3.1 Investigation of the amine-ligated palladium complexes 58 and 59 on the Pd-catalysed Hofmann-type elimination of 56.

The collected MS data from the described reactions in Scheme 2.3.1 revealed a dramatic loss of signal intensity, which made the examination and monitoring of these reactions by mass spectroscopy difficult. According to the literature, one possible cause for the signal loss could be residual palladium coordinating to the peptide.[301] In order to overcome this problem, scavengers were introduced to the reaction, to which the palladium metal can coordinate more strongly than to the peptide. As shown in Scheme 2.3.2, the nucleophilic thiols 3-mercaptopropionic acid (MPA) and 1,4-dithiothreitol (DTT) were investigated as possible scavengers to prevent palladium ions from binding to the peptide. The peptide **56** (5 nmol) was exposed to either one of the palladium complexes **58** or **59** (250 nmol, 50 equiv.) in sodium phosphate buffer (50 mM, pH = 8.00) at 37 °C for 20 h. The reaction mixture was then treated with the scavengers DTT (Entries I + III) or MPA (Entries II + IV) at 37 °C for 1.5 h.

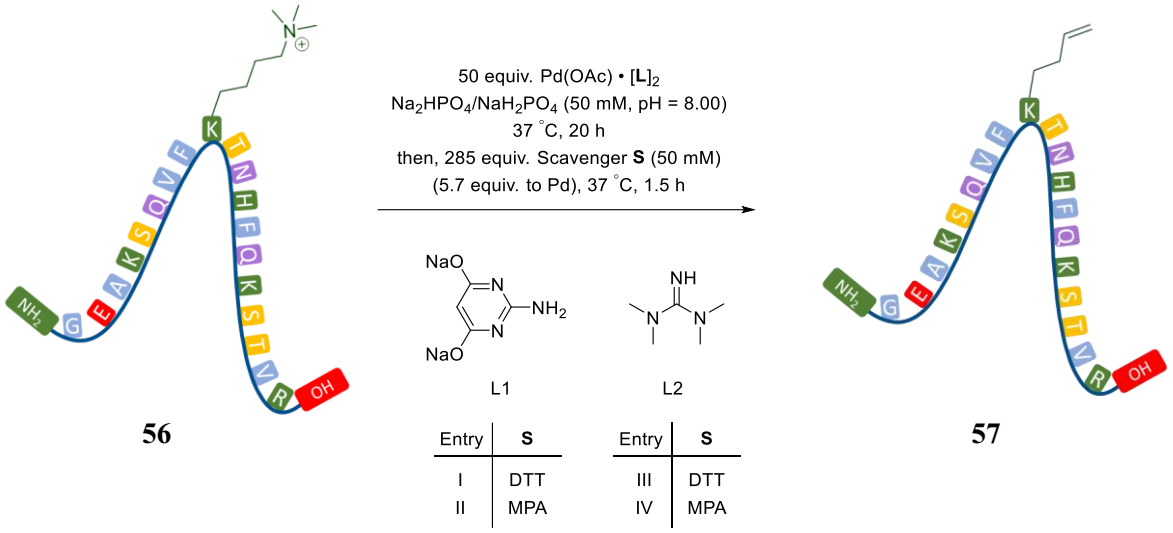

Scheme 2.3.2 Investigation of MPA and DTT as possible metal scavenger for the Pd-catalysed Hofmann-type elimination of 56 using the amine-ligated palladium complexes 58 and 59.

The total ion chromatograms (TICs) of the reactions in Scheme 2.3.1 and Scheme 2.3.2 are displayed in Figure 2.3.8. Chromatograms A and B demonstrate the results of the reactions from Scheme 2.3.1 highlighting the generation of numerous adducts without the use of a scavenger. As seen in the chromatograms C – F, the incorporation of scavengers drastically reduced the amount of these adducts. Comparing the efficiency of the investigated scavengers,

it is evident that DTT (see chromatograms C + D) is a more efficient in generating a clean chromatogram than MPA (see chromatograms E + F). Therefore, it was decided to use DTT as the scavenger for further Pd-catalysed elimination reactions.

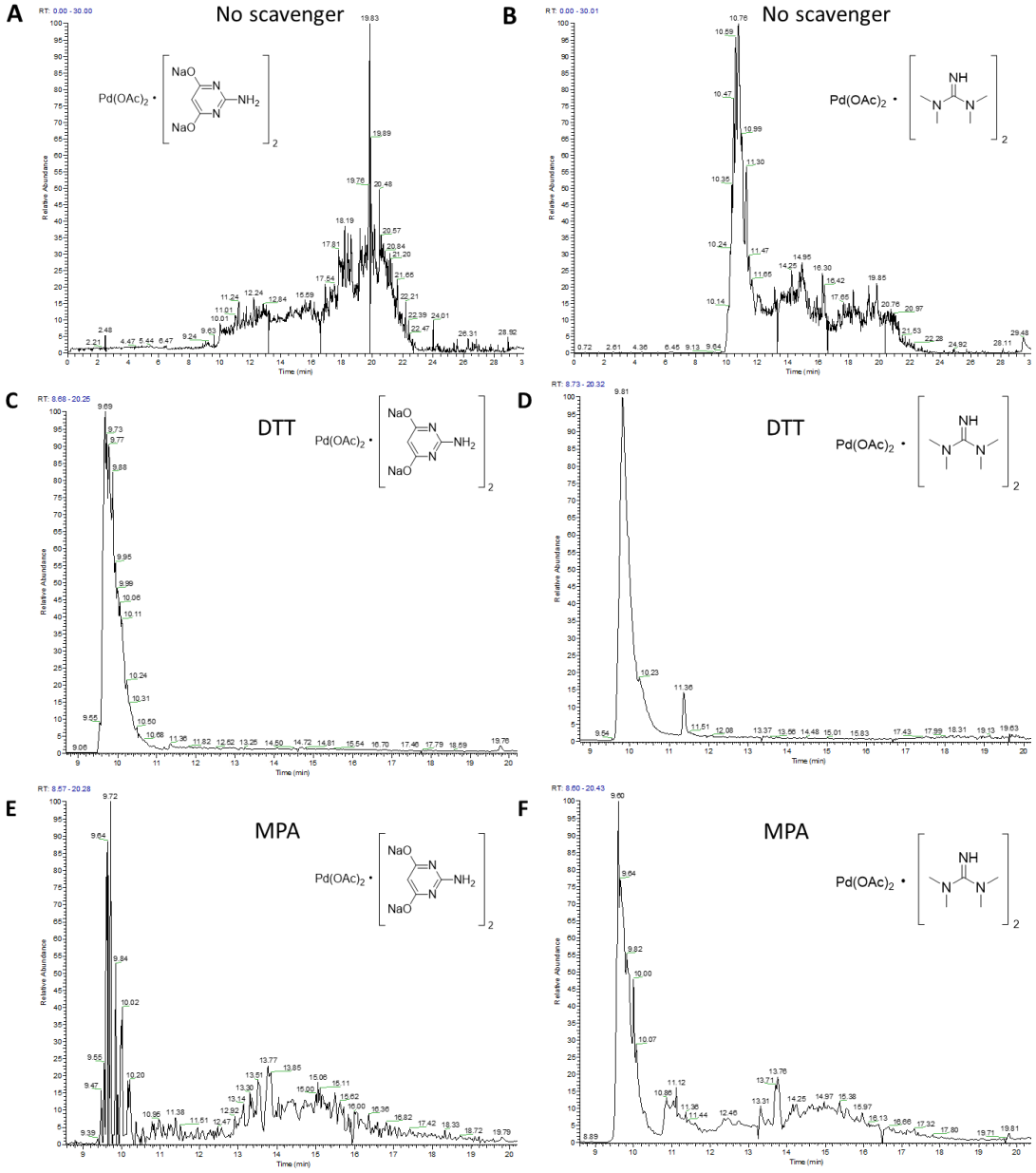

Figure 2.3.8 Total ion chromatograms (TICs) collected after the reactions with the Pd-complexes 58 (A) and 59 (B) with no scavenger; with DTT as scavenger (58, C + 59, D) or with MPA as scavenger (58, E + 59, F).

A closer examination of the MS peaks detected from the reactions in Entry I and Entry III (Scheme 2.3.2) are demonstrated in Figure 2.3.9. As seen in Figure 2.3.9 **A**, the Pd-catalysed elimination reaction using the palladium complex **58** and DTT as the scavenger only detected the initial peptide **56** (starting material, SM). Similarly, the Pd-catalysed elimination reaction using the palladium complex **59** and DTT as the scavenger (Figure 2.3.9 **B**) mainly showed the initial peptide **56**. However, an additional peak was detected in the TIC at 11.36 min, which was determined to have a mass of 1306.1092 Da (Δ to SM: 927.0875 Da).

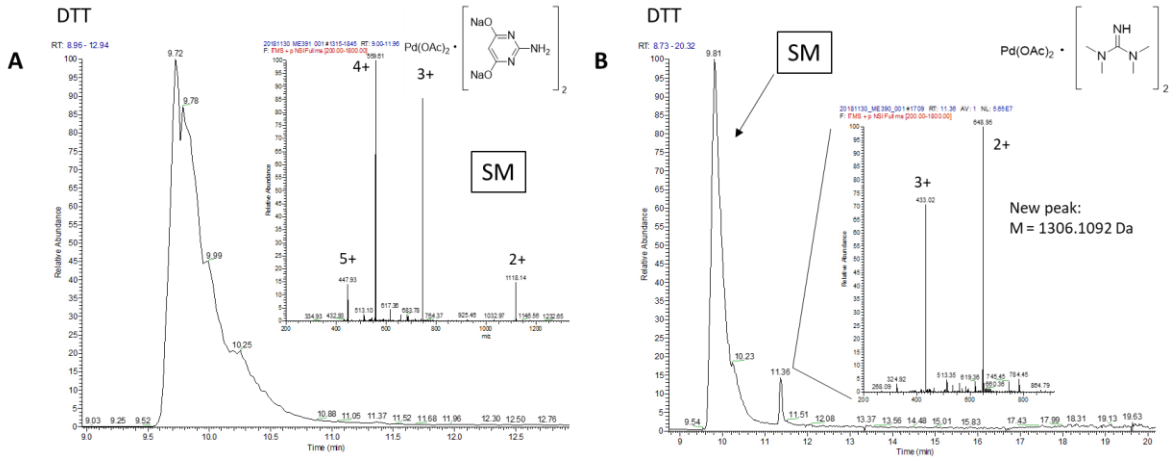

Figure 2.3.9 MS analysis of the results from the Pd-catalysed Hofmann-type elimination reactions of 56 using the Pd-complexes 58 (A) and 59 (B) with DTT as scavenger.

In order to clarify if this new peak was in fact a result of the palladium complex interacting with the peptide, a control reaction was performed, which did not include the palladium complex (see Scheme 2.3.3). Only the initial peptide **56** was recovered after the control reaction verifying the stability of the peptide to the used reagents and therefore confirming that the detected new peak in Figure 2.3.9 **B** was caused due to the presence of the palladium complex in the protocol. The detected mass of about 1306 Da suggested the fragmentation of the peptide **56** to a shorter peptide. Since the detected peak was not representative for the desired alkene product **57** and it did not appear to be caused by any obvious side reactions, it was disregarded at this point without further analysis.

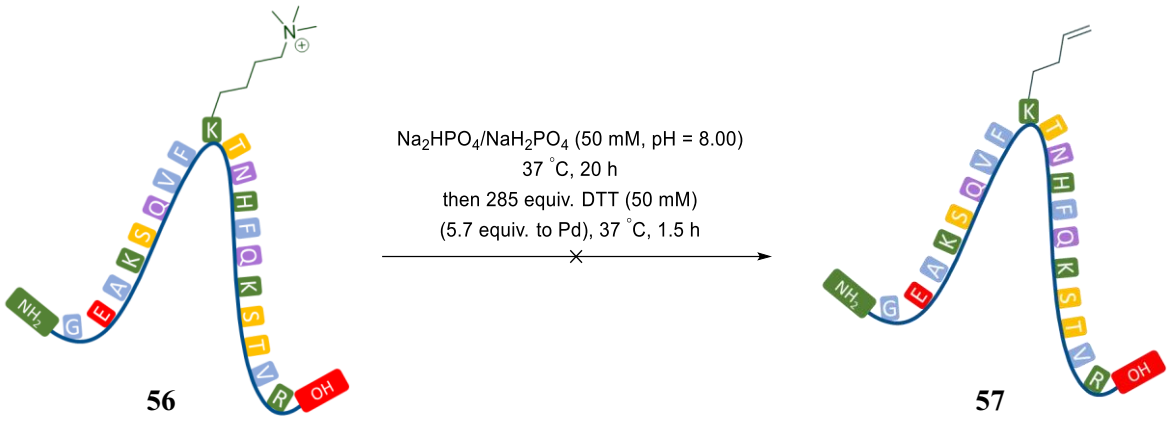

Scheme 2.3.3 Control reaction using DTT in sodium phosphate buffer without the use of a palladium catalyst.

Since the initial reactions using the palladium catalysts with the amine-based ligands primarily resulted in the recovery of the starting peptide **56**, it was decided to attempt to force the desired Pd-catalysed elimination of the quaternary ammonium functional group by increasing the reaction temperature. As shown in Scheme 2.3.4, the Pd-catalysed Hofmann-type elimination was repeated with both palladium catalysts **58** and **59** at 100 ˚C. Both reactions, however, led to the decomposition of the peptide **56** forming smaller fragments and confirming the sensitivity of peptide substrates to higher temperatures.

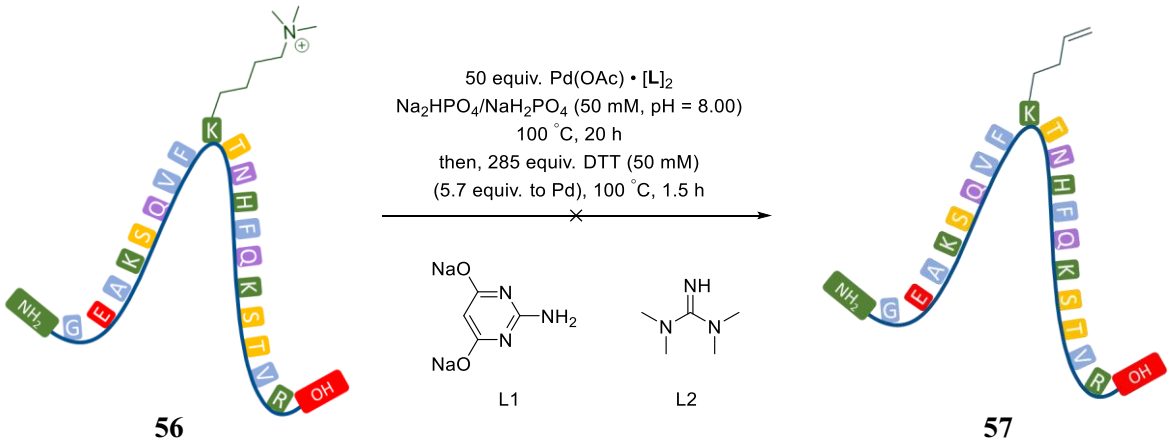

Scheme 2.3.4 Investigation of the stability of the peptide substrate 56 to high reaction temperatures.

2.3.4 Attempted Pd-catalysed Hofmann-type elimination on the model peptide using phosphine ligands

During our investigation of the Pd-catalysed Hofmann-type elimination on model small molecules (see Chapter 2.2) the generation of the terminal alkene **32** was achieved using phosphine ligands including tris(2,4,6-trimethoxyphenyl)phosphine and BrettPhos (albeit in a very low yield). Even though marginal yields of the Pd-catalysed elimination were determined, it was important to confirm whether these catalytic systems could also target the trimethylammonium functionality within peptide **56**. First, the synthetic peptide **56** dissolved in sodium phosphate buffer (50 mM, pH = 8.00, degassed) was exposed to the pre-formed catalytic complex (50 equiv.) consisting of palladium(II) acetate and tris(2,4,6-trimethoxyphenyl)phosphine at 37 ˚C for 20 h (see Scheme 2.3.5). The reaction mixture was then treated with DTT (5.7 equiv. to Pd) to prevent any residual palladium ions to bind to the peptide.

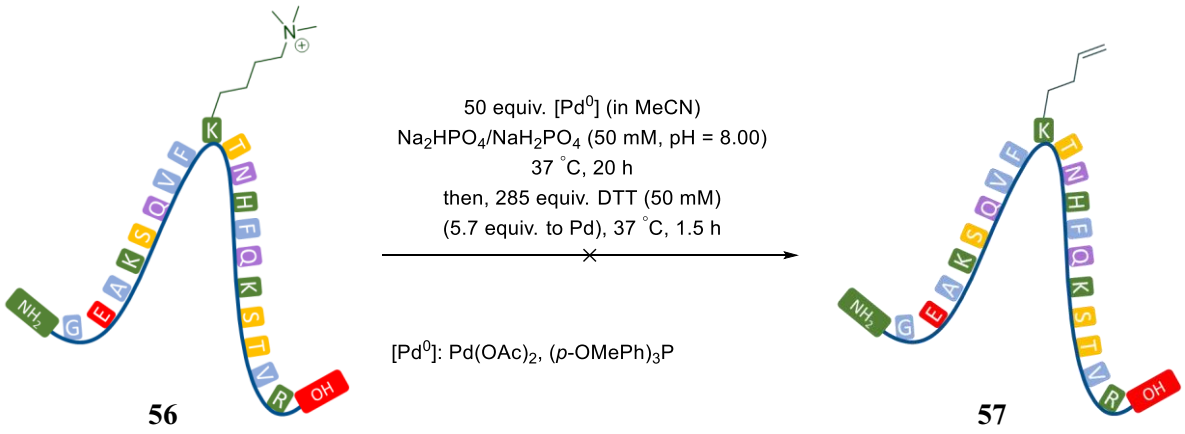

Scheme 2.3.5 Investigating the Pd-catalysed Hofmann-type elimination of 56 using palladium(II) acetate and tris(2,4,6-trimethoxyphenyl)phosphine.

The MS examination of the reaction outcome confirmed that the desired peptide product **57** was not formed and that mainly starting material was still present. However, a variety of novel peaks were also detected in the mass chromatogram (see Figure 2.3.10 **A**), potentially suggesting the higher activity of the palladium-phosphine catalysts compared to the palladium-pyrimidine and palladium-guanidine complexes.

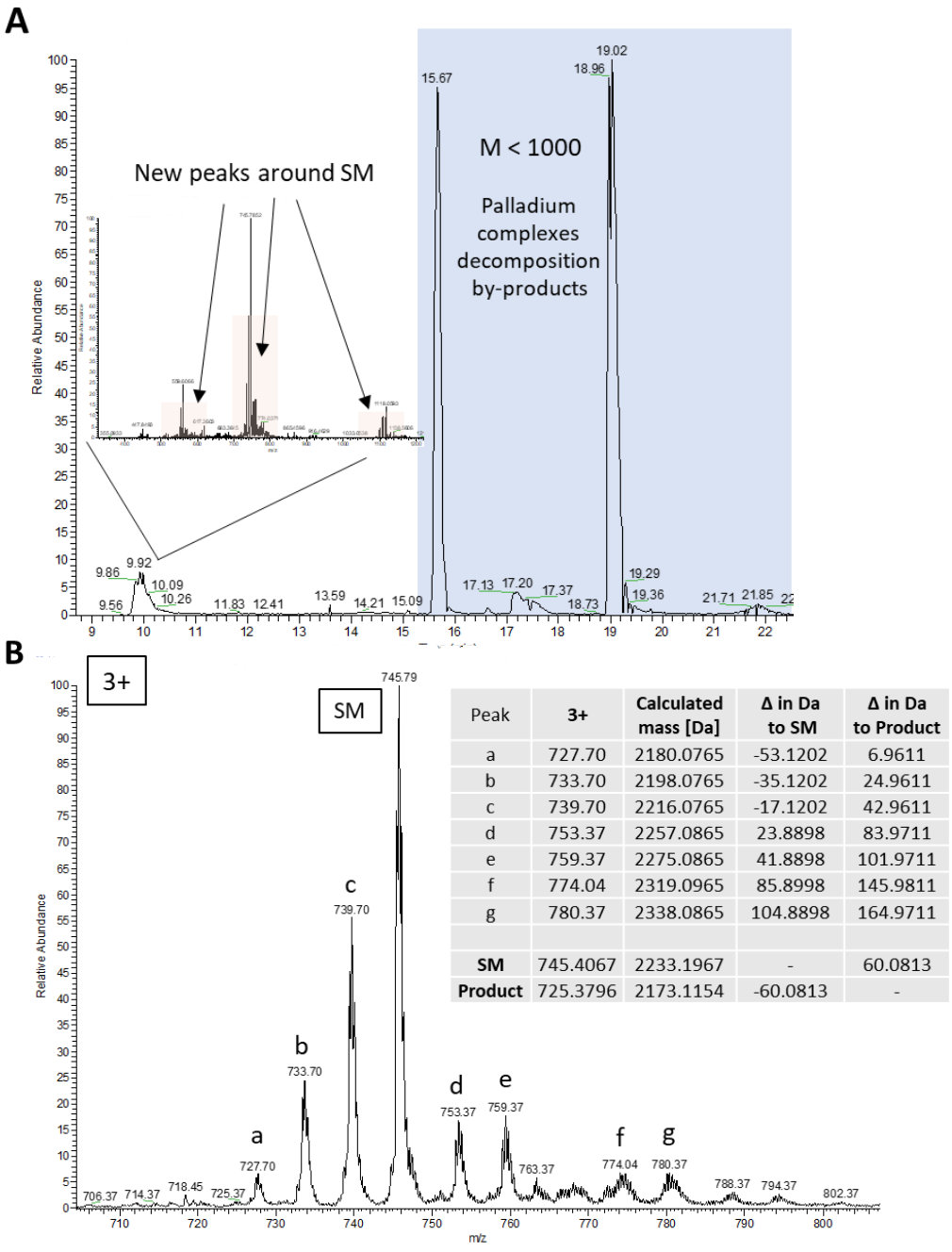

Peak	3+	Calculated mass [Da]	Δ in Da to SM	Δ in Da to Product
a	727.70	2180.0765	-53.1202	6.9611
b	733.70	2198.0765	-35.1202	24.9611
c	739.70	2216.0765	-17.1202	42.9611
d	753.37	2257.0865	23.8898	83.9711
e	759.37	2275.0865	41.8898	101.9711
f	774.04	2319.0965	85.8998	145.9811
g	780.37	2338.0865	104.8898	164.9711
SM	745.4067	2233.1967	-	60.0813
Product	725.3796	2173.1154	-60.0813	-

Figure 2.3.10 Analysis of the TIC (A) and the mass spectrum of the triply charged ions (B) detected after the reaction shown in Scheme 2.3.5.

A closer examination of the collected mass spectrum (see Figure 2.3.10 **B**) revealed that the detected compounds exhibited both a decrease in mass (see compounds a – c) and an increase in mass (see compounds d – g) compared to the starting material **56**. The desired product **57** with the expected decrease in total mass of about 60 Da was, however, not present suggesting that the Pd-catalysed elimination of the trimethylammonium functionality using the tertiary

phosphine ligand was not successful. Evaluating the mass differences of the detected compounds to the alkene product **57** did not give any conclusive information on the formation of apparent adduct isomers such as the existence of residual palladium (M = 106 Da) on the surface of the peptide. Due to the limited fragmentation of the compounds, the analysis of the MS2 spectrum did not give any evidence on the structure of the detected compounds either.

The synthetic peptide **56** was also treated with an alternative catalytic system consisting of palladium(II) acetate and BrettPhos in sodium phosphate buffer (50 mM, pH = 8.00, degassed) at 37 °C for 20 h (see Entry I, Scheme 2.3.6). Unfortunately, the desired peptide product **57** was not detected in the MS analysis of the reaction and mainly peptide **56** was recovered. Similar compounds as observed in the reaction above using the tertiary phosphine as the ligand were also formed during this reaction (see Figure 2.3.11 **A**). However, no clear analysis of the identity of these side products could be made from the gathered MS data.

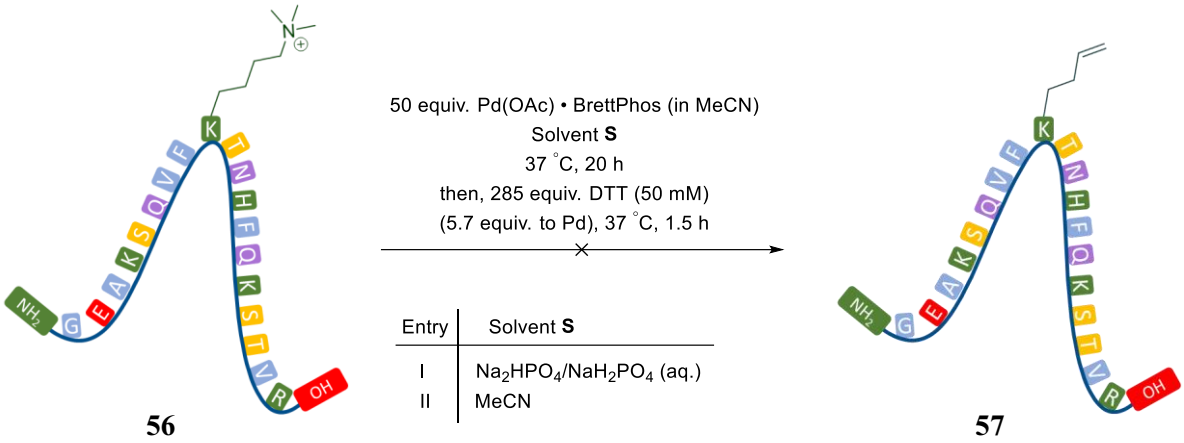

Scheme 2.3.6 Investigating the Pd-catalysed Hofmann-type elimination of 56 using palladium(II) acetate and BrettPhos.

In order to eliminate any possible adducts formed due to the high salt content of the aqueous buffer and to investigate its effect on the catalytic efficiency of the Pd-catalyst, the Pd-catalysed elimination reaction of the peptide **56** using palladium(II) acetate and BrettPhos was repeated in acetonitrile (see Entry II, Scheme 2.3.6). The desired alkene peptide was not formed during this reaction as confirmed by the observed MS spectrum (see Figure 2.3.11 **B**). In contrast to the reaction in the aqueous sodium phosphate buffer, the reaction in acetonitrile resulted in the

formation of different compounds, which presented a higher total mass than the starting peptide **56** as listed in the table in Figure 2.3.11 **B**. These results confirmed the influence of the solvent system on the activity of the Pd-catalyst and subsequently, the generation of distinct products. Nevertheless, these experiments confirmed that the formation of the alkene product, which was observed for alkyl ammonium iodide **31** in low yield (discussed in Chapter 2.2), could not be replicated in this setting using the peptide **56**. It was believed that, as was the case for the model small molecule systems, oxidative addition of the palladium catalyst to the strong $C(sp^3) – N(Me_3)$ bond was limiting.

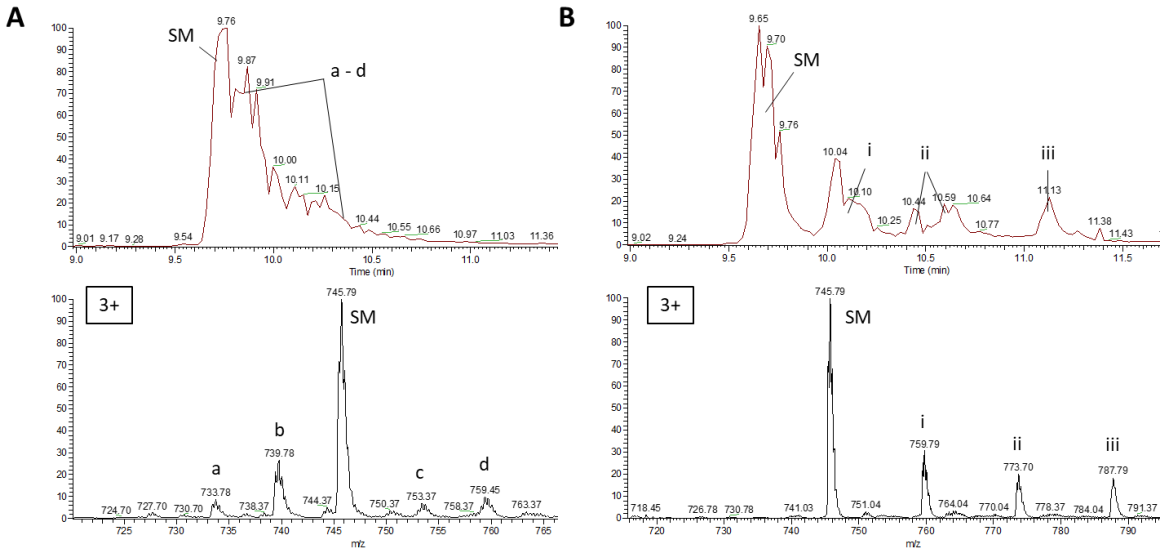

Peak	3+	Calculated mass [Da]	Δ in Da to SM	Δ in Da to Product
a	733.78	2198.3165	-34.8802	25.2011
b	739.78	2216.3165	-16.8802	43.2011
c	753.37	2257.0865	23.8898	83.9711
d	759.45	2275.3265	42.1298	102.2111
SM	745.4067	2233.1967	-	60.0813
Product	725.3796	2173.1154	-60.0813	-

Peak	3+	Calculated mass [Da]	Δ in Da to SM	Δ in Da to Product
i	759.79	2276.3465	43.1498	103.2311
ii	773.70	2318.0765	84.8798	144.9611
iii	787.79	2360.3465	127.1498	187.2311
SM	745.4067	2233.1967	-	60.0813
Product	725.3796	2173.1154	-60.0813	-

Figure 2.3.11 MS analysis of the Pd-catalysed Hofmann-type elimination reaction using BrettPhos in both the sodium phosphate buffer (A) and acetonitrile (B).

2.3.5 Attempted Pd-catalysed cleavage of the C(sp^3) – N(Me_3) bond in the model peptide using NHC ligands

In parallel to our work on model small molecules, we were searching for more reactive palladium catalysts to undergo oxidative addition into the strong carbon-nitrogen bond of the alkyl trimethylammonium electrophile. As described in detail in Subchapter 2.2.16, Szostak *et al.* described the successful cross-coupling of a range of amides by N – C bond activation using Pd-PEPPSI-IPr[257] or (IPr)Pd(cinnamyl)Cl[258] (structures are given in Figure 2.3.12). It was therefore decided to investigate these catalysts for the Pd-catalysed cleavage of the C(sp^3) – N bond of the trimethylammonium functionality in the synthetic peptide **56**, in addition to our model small molecule system (see Subchapter 2.2.16).

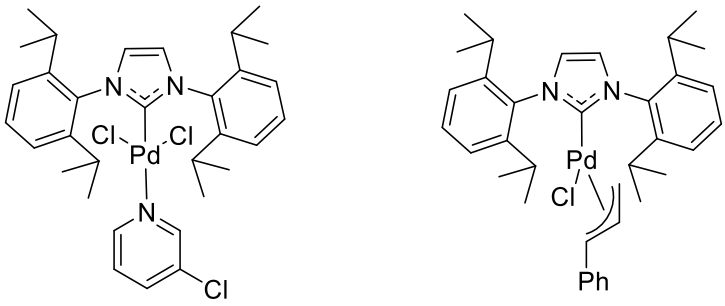

Pd-PEPPSI-IPr (IPr)Pd(cinnamyl)Cl

Figure 2.3.12 Structure of the investigated Pd-NHC precatalysts.

Since Szostak and colleagues used these catalytic systems for the Suzuki coupling of amides, the initial reaction attempted on peptide **56** was a Suzuki cross coupling between the trimethylammonium lysine residue and *p*-tolylboronic acid. The structure of the resulting peptide **60** bearing a tolyl functional group at position 9 is given in Figure 2.3.13. The calculated mass of peptide **60** is 2266.1858 Da leading to a difference in mass of +31.9813 Da to the starting peptide **56**.

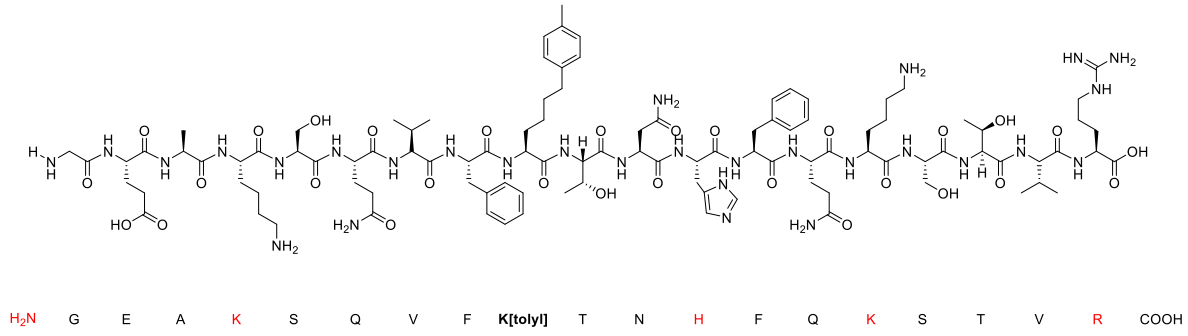

60

GEAKSQVFK[me3]TNHFQKSTVR		GEAKSQVFK[tolyl]TNHFQKSTVR	
2233.1967 Da		2265.1780 Da	
$[M+1H]^{1+}$	2234.2045	$[M+1H]^{1+}$	2266.1858
$[M+2H]^{2+}$	1117.6062	$[M+2H]^{2+}$	1133.5968
$[M+3H]^{3+}$	745.4067	$[M+3H]^{3+}$	756.0672
$[M+4H]^{4+}$	559.3070	$[M+4H]^{4+}$	567.3023
$[M+5H]^{5+}$	447.6472	$[M+5H]^{5+}$	454.0434

Δ	**+31.9813 Da**

Figure 2.3.13 The structure of peptide 60 bearing a tolyl functionality at position 9 (above) and the calculated mass of 60 and the expected m/z ratios (below).

Similar to the use of the phosphine-based catalytic system, the NHC-precatalysts Pd-PEPPSI-IPr (Entry I) and (IPr)Pd(cinnamyl)Cl (Entry II) were firstly preactivated using *p*-tolylboronic acid in tetrahydrofuran (degassed) prior to their addition (50 equiv.) to the peptide **56** in sodium phosphate buffer (50 mM, pH = 8.00, degassed). The sealed reactions were heated at 60 ˚C for 20 h and processed as previously reported (see Scheme 2.3.7). The results of both reactions are summarised in Figure 2.3.14. The TICs for these reactions using Pd-PEPPSI-IPr (Figure 2.3.14 **A**) and (IPr)Pd(cinnamyl)Cl (Figure 2.3.14 **B**) illustrate the formation of new peaks after the reactions, potentially confirming the interaction of the palladium complex with the peptide **56**. The peaks in the blue-annotated area of the chromatograms represent the decomposition products of the palladium catalysts after the reactions. The MS chromatograms of the red-annotated area of the TICs confirmed that the starting peptide **56** was still present after the reactions, however, new compounds with total masses higher than the mass of the starting peptide **56** were also generated.

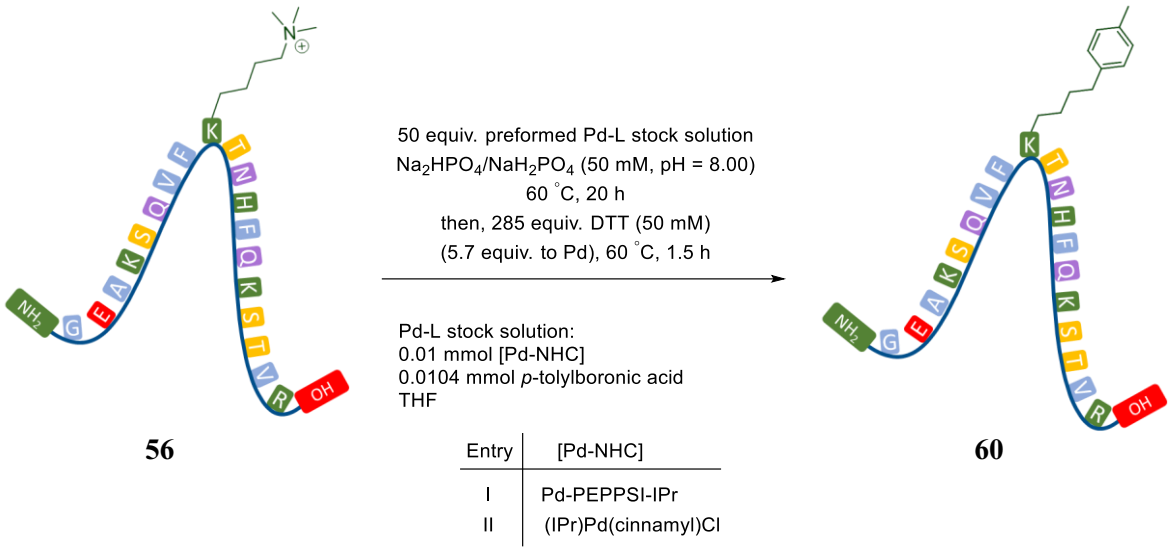

Scheme 2.3.7 Suzuki cross coupling of peptide 56 with *p*-tolylboronic acid using Pd-PEPPSI-IPr (Entry I) and (IPr)Pd(cinnamyl)Cl (Entry II).

A closer examination of the obtained MS chromatograms is given in Figure 2.3.14 **C** and **D**. This data shows the triply charged ions of the detected compounds due to their high signal intensity. As listed in the table in Figure 2.3.14 **C**, six triply charged ions (a – f) representing six novel products were detected in the MS chromatogram of the Suzuki reaction using Pd-PEPPSI-IPr in addition to the one representing the starting peptide **56**. Upon calculating the total masses of these products and determining their mass differences to the SM **56** and the desired peptide **60** bearing the tolyl handle, it was discovered that all these detected products had total masses higher than both the SM and the desired product **60**. Comparing these results to the reaction outcome of the Suzuki reaction using (IPr)Pd(cinnamyl)Cl (Figure 2.3.14 **D**), four main products (a – d) were detected, of which three had similar masses as the products shown in Figure 2.3.14 **C** suggesting that both reactions had similar reaction outcomes. One of the compounds detected in both MS chromatograms had a total mass of 2288 Da (**61**, see compound a in **C** and b in **D**, Figure 2.3.14) and a mass difference of about 23 Da to the product peptide **60**. With the mass of sodium being 22.99 Da, it was inferred that the detected compound **61** might be the sodium adduct of the desired peptide **60**. The MS2 spectrum of the detected compound was investigated to gain additional information on the structure of the peptide, however, the analysis of the MS2 spectrum was inconclusive due to the poor fragmentation of the observed peptide.

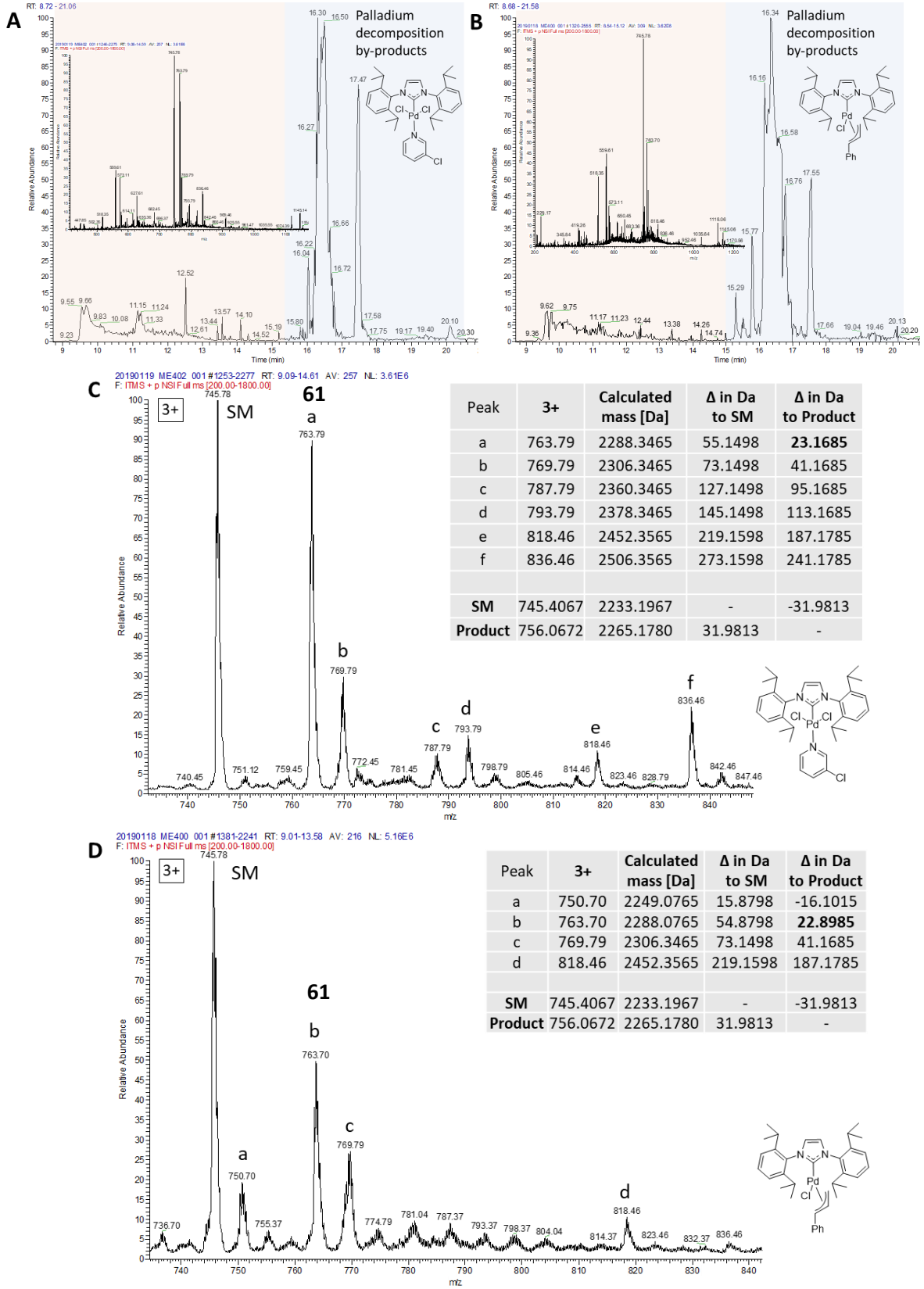

Peak	3+	Calculated mass [Da]	Δ in Da to SM	Δ in Da to Product
a	763.79	2288.3465	55.1498	**23.1685**
b	769.79	2306.3465	73.1498	41.1685
c	787.79	2360.3465	127.1498	95.1685
d	793.79	2378.3465	145.1498	113.1685
e	818.46	2452.3565	219.1598	187.1785
f	836.46	2506.3565	273.1598	241.1785
SM	745.4067	2233.1967	-	-31.9813
Product	756.0672	2265.1780	31.9813	-

Peak	3+	Calculated mass [Da]	Δ in Da to SM	Δ in Da to Product
a	750.70	2249.0765	15.8798	-16.1015
b	763.70	2288.0765	54.8798	**22.8985**
c	769.79	2306.3465	73.1498	41.1685
d	818.46	2452.3565	219.1598	187.1785
SM	745.4067	2233.1967	-	-31.9813
Product	756.0672	2265.1780	31.9813	-

Figure 2.3.14 MS analysis of the Pd-catalysed Suzuki reaction of peptide 56 using both Pd-PEPPSI-IPr (A + C) and (IPr)Pd(cinnamyl)Cl (B + D). Compound 61 was detected with a mass difference of 22.99 Da to the desired product 60.

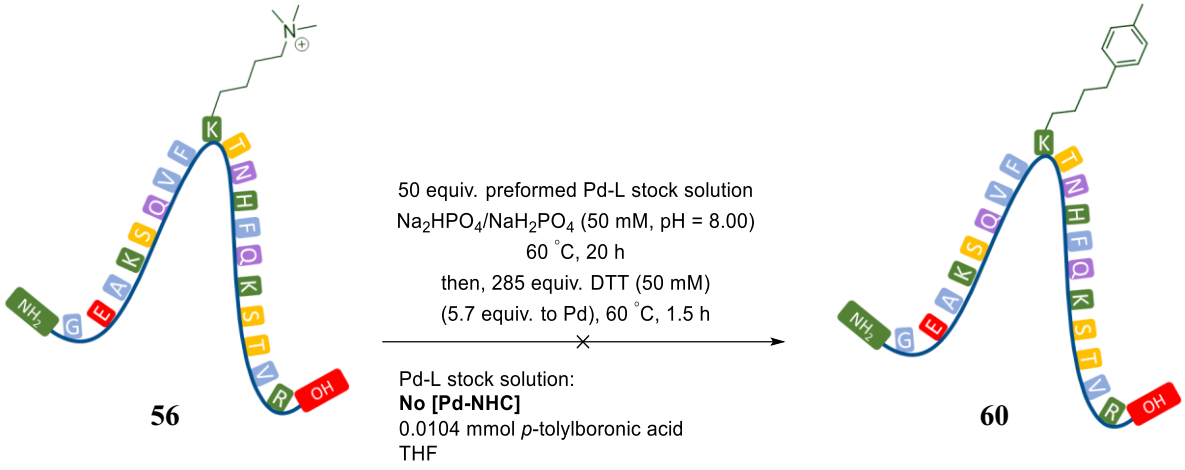

Scheme 2.3.8 Control reaction using *p*-tolylboronic acid in THF/sodium phosphate buffer and DTT without the use of a palladium catalyst.

To verify if the observed key product **61** of the Pd-catalysed Suzuki reactions in Scheme 2.3.7 was based on the interaction of the palladium catalyst with the target functional group of the peptide **56**, a control reaction without the addition of a palladium catalyst was performed (see Scheme 2.3.8). Peptide **56** was solely treated with *p*-tolylboronic acid (THF) in sodium phosphate buffer (50 mM, pH = 8.00) without the presence of a palladium catalyst.

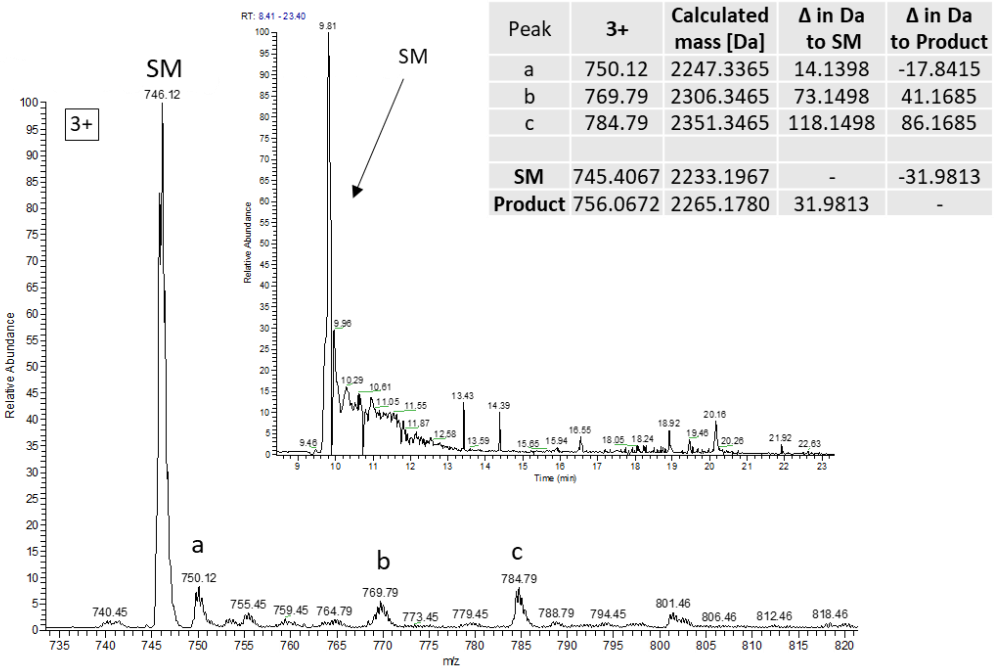

Peak	3+	Calculated mass [Da]	Δ in Da to SM	Δ in Da to Product
a	750.12	2247.3365	14.1398	-17.8415
b	769.79	2306.3465	73.1498	41.1685
c	784.79	2351.3465	118.1498	86.1685
SM	745.4067	2233.1967	-	-31.9813
Product	756.0672	2265.1780	31.9813	-

Figure 2.3.15 MS analysis of the control reaction in the absence of a palladium catalyst.

The results of the control reaction are shown in Figure 2.3.15. As seen in the TIC, mainly the starting peptide **56** was detected after the reaction. The beforementioned key product **61**, which was observed after the Pd-catalysed Suzuki reactions was not present in the MS chromatogram confirming that the formation of **61** was in fact based on the presence of the Pd-catalyst.

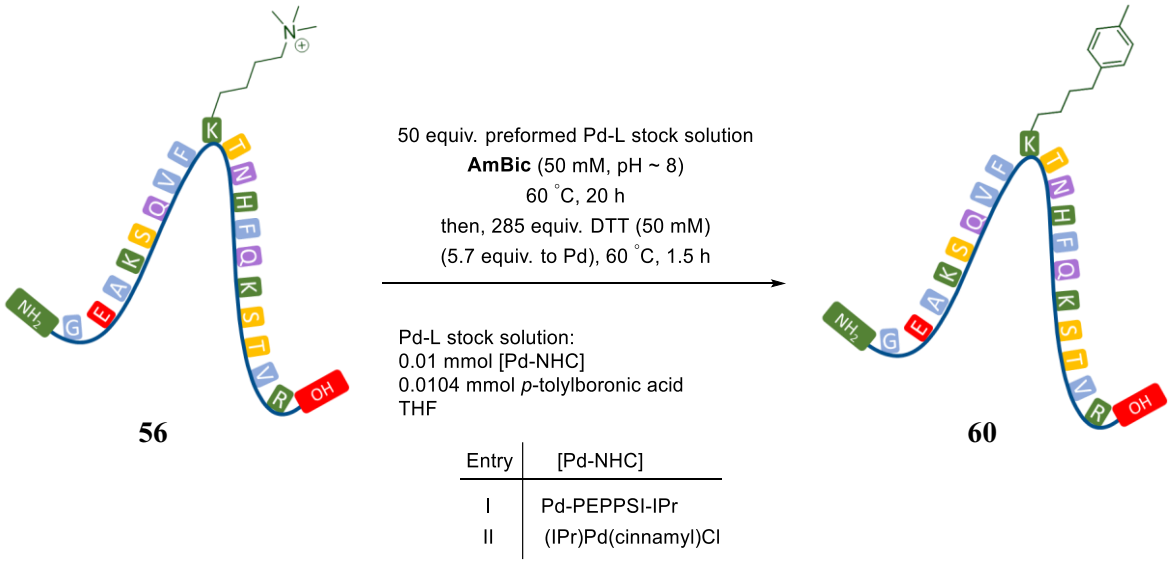

Scheme 2.3.9 Suzuki cross coupling of peptide 56 using Pd-PEPPSI-IPr (Entry I) and (IPr)Pd(cinnamyl)Cl (Entry II) in ammonium bicarbonate buffer.

With the aim of reducing the amount of sodium ions present in the sample and thus to avoid the generation of sodium adducts, the Pd-catalysed Suzuki cross-coupling reactions were repeated in ammonium bicarbonate buffer (50 mM, pH ~ 8.00, AmBic) instead of the previously used sodium phosphate buffer (see Scheme 2.3.9). Both reactions in AmBic mainly resulted in the starting peptide **56** and only a reduced number of new compounds were detected compared to the reactions in Scheme 2.3.7. However, the previously observed product **61** was still present even after eliminating the use of a sodium-based buffer. Consequently, it was questioned if the previously observed product **61** with a total mass of 2288 Da was in fact the sodium adduct of the desired peptide product **60** bearing a tolyl functionality.

The involvement of the boronic acid in the Pd-catalysed Suzuki cross-coupling reaction of peptide **56** and thus in the generation of the observed product **61** was investigated. By using (4-pentylphenyl)boronic acid, it was expected to observe a mass shift of +56 Da compared to the use of *p*-tolylboronic acid. As displayed in Scheme 2.3.10, peptide **56** was exposed to a

catalytic system consisting of a Pd-NHC precatalyst (either Pd-PEPPSI-IPr (Entry I) or (IPr)Pd(cinnamyl)Cl (Entry II)) and (4-pentylphenyl)boronic acid. The MS examination of the reaction outcomes showed that the expected mass shift of +56 Da was not observed and that the previously detected product **61** with a mass of 2288 Da was still present. These experiments confirmed that observed product was not dependent on the boronic acid meaning that the boronic acid was not involved in the formation of this product. In addition, no novel peaks were detected in the MS chromatogram. Consequently, these results verified that a Suzuki cross coupling reaction with the boronic acid was not occurring and that product **61** had a different origin.

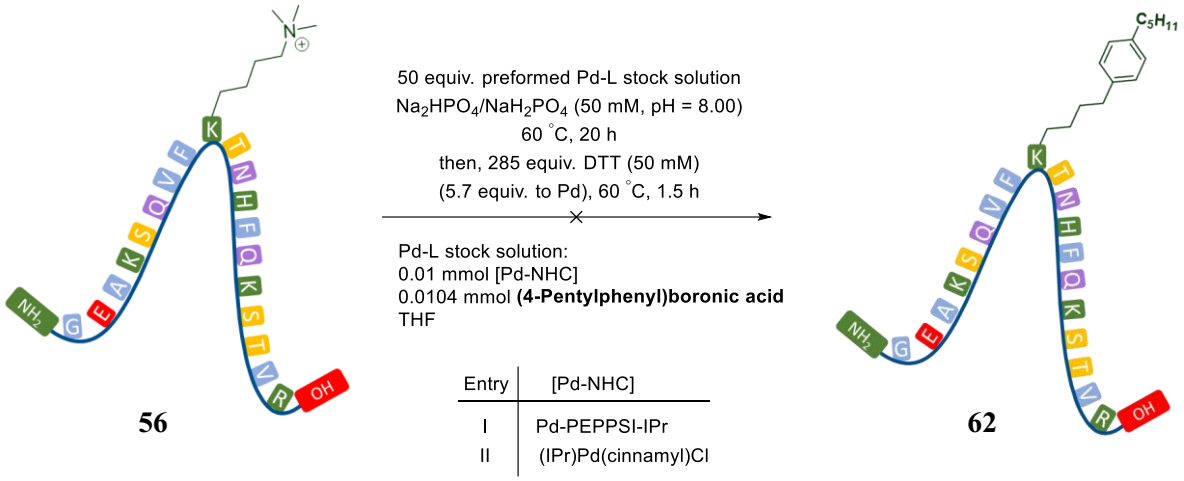

Scheme 2.3.10 Suzuki cross coupling of peptide 56 with (4-pentylphenyl)boronic acid using Pd-PEPPSI-IPr (Entry I) and (IPr)Pd(cinnamyl)Cl (Entry II).

In order to investigate if the trimethylammonium functionality of the lysine residue in peptide **56** was involved in the Pd-mediated generation of the observed products, an alternative starting material was exposed to the reaction conditions (see Scheme 2.3.11). The trimethylammonium lysine residue at position 9 was replaced by a dimethyllysine residue, thus evaluating the importance of the trimethylammonium group in the generation of the observed products. The MS spectrum of peptide **63** with the observed and calculated mass-to-charge ratios is given in Figure 2.3.16.

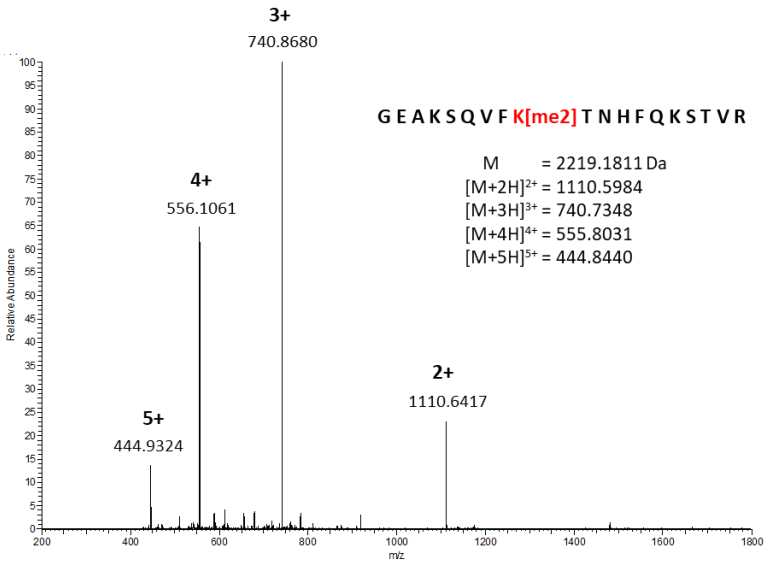

Figure 2.3.16 The MS spectrum of peptide 63 with the dimethyllysine residue at K9.

The observed triply charged mass ions from both reactions (Entries I + II, Scheme 2.3.11) and the corresponding calculated total masses of the detected products are displayed in Figure 2.3.17. As previously observed, the Pd-catalysed reactions led to the formation of compounds with an increased total mass compared to the starting peptide **63**. A closer examination of the mass differences of these compounds to the SM revealed that the reaction using peptide **63** resulted in similar products to those identified using peptide **56** bearing the trimethylammonium functional group.

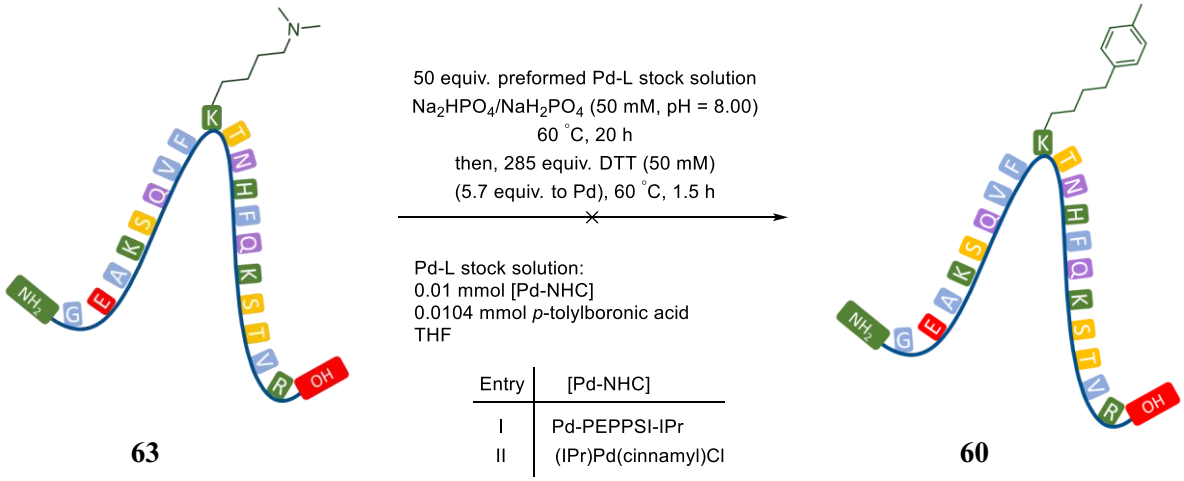

Scheme 2.3.11 Control reaction using peptide 63 without an trimethylammonium functionality in combination with Pd-PEPPSI-IPr (Entry I) and (IPr)Pd(cinnamyl)Cl (Entry II).

The resulting compounds with the mass increase of +55 Da and +73 Da were also observed in the MS analysis of the reactions starting from peptide **56** (see Figure 2.3.14) indicating that the trimethylammonium group was not involved in the generation of these compounds and therefore that the palladium catalyst was not interacting with the target functional group.

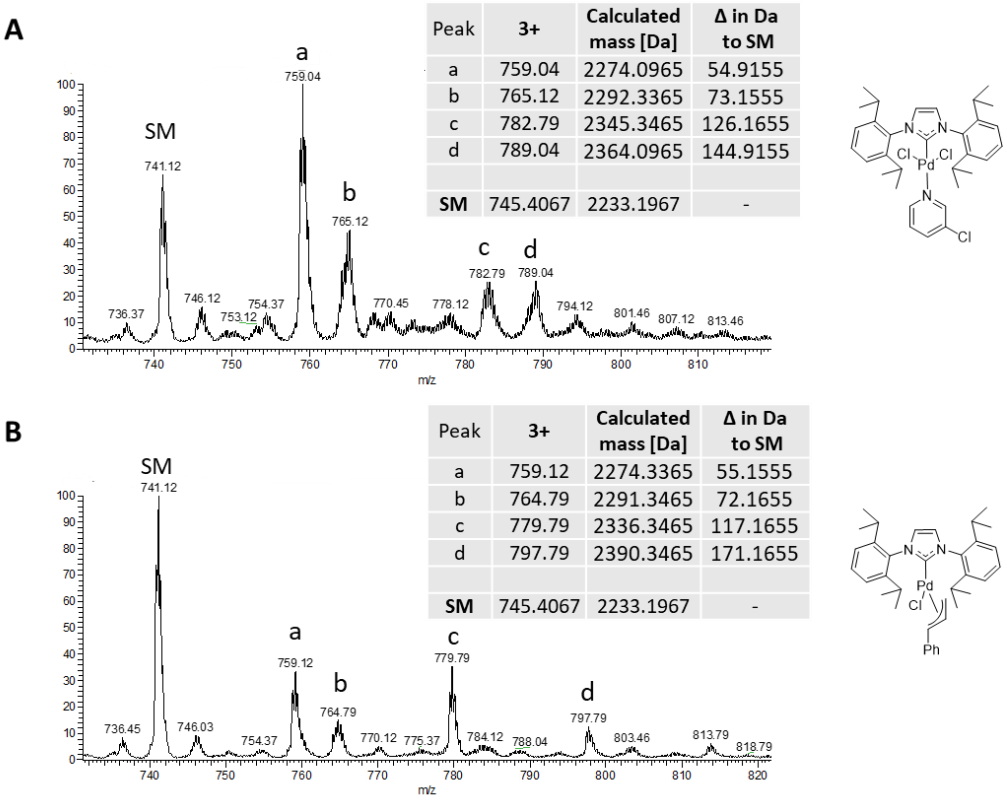

Figure 2.3.17 MS chromatograms showing the triply charged mass ions detected from the reaction of peptide 63 with Pd-PEPPSI-IPr (A) and (IPr)Pd(cinnamyl)Cl (B).

Due to the vast number of functional groups present in peptide **56**, which can interact with the palladium catalyst and undergo a chemical modification, it was challenging to determine which residue of the peptide was modified to result in the formation of the observed products. Consequently, it was decided to digest the resulting peptide products obtained from the initial reactions in Scheme 2.3.7 using trypsin in order to narrow down which residue of peptide **56** was responsible for the detected masses. Trypsin digestion resulted in cleavage of the peptides at the carboxylic side of both unmodified lysine residues leading to the formation of the three fragment peptides A, B and C shown in Scheme 2.3.12. After the fragmentation procedure, the obtained samples from both reactions were examined using mass spectroscopy. The MS analysis of the reaction using Pd-PEPPSI-IPr is given in Figure 2.3.18.

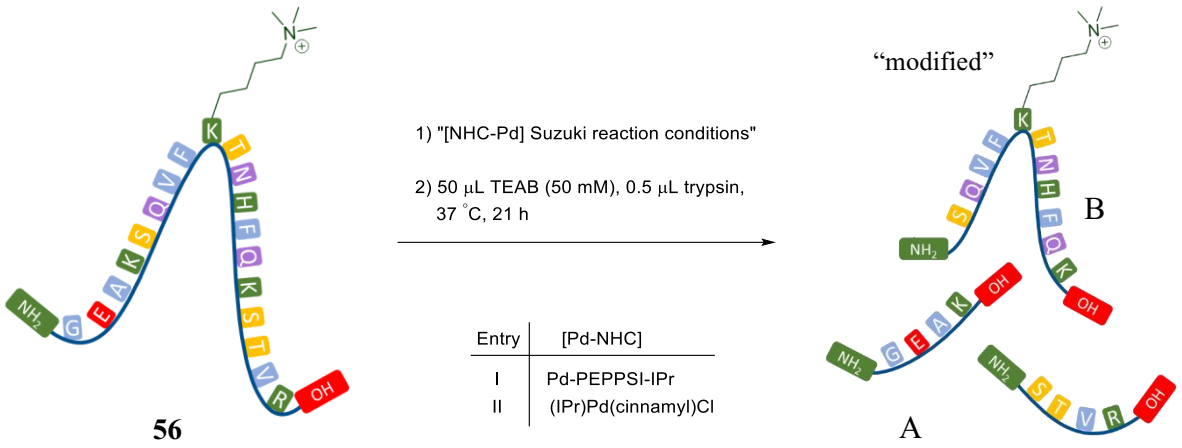

Fragment	M	$[M+1H]^{1+}$	$[M+2H]^{2+}$	$[M+2H]^{3+}$
A	403.2067	404.2145	202.6034	-
B	1404.7510	1405.7588	703.3755	469.2503
C	461.2598	462.2676	231.6299	-

Scheme 2.3.12 Fragmentation of the resulting peptide products after the Suzuki reaction using trypsin. The calculated m/z ratios of the fragments are given in the table.

Since the starting material **56** was recovered after the reaction, all three unmodified fragments A, B and C were also present as a result from the fragmentation of the starting peptide **56** (see the TIC in Figure 2.3.18 **A**). The detected ions representing these fragments are also annotated in the MS chromatograms in Figure 2.3.18 **B**. The MS chromatograms were examined to discover the fragment ions representing the obtained products with the detected mass increases to the SM [**56**], which were listed in the table in Figure 2.3.14 **C**. As seen in the MS chromatogram of the peptide fragment A, only the unmodified fragment was discovered, *e.g.* that the increase in mass of the products was not based on the modification of the four starting amino acids (GEAK) of peptide **56**. The analysis of the other short peptide fragment C revealed that next to the unmodified fragment, the fragment ions with a mass increase of +55 Da, +73 Da, +127 Da and +145 Da were also present proving that the obtained products of the Pd-mediated reaction using Pd-PEPPSI-IPr were in fact based on the modification of either one or more of the last four amino acids (STVR) of peptide **56**. Since valine (V) consists of an unreactive isopropyl side chain, it is presumably stable against a Pd-mediated chemical modification. Therefore, serine (S), threonine (T), arginine (R) or the C-terminus are the possible sources for detected increase in mass after the reaction. Since the middle fragment B also possesses a serine and a threonine residue, it was questioned why these residues were not

modified after the reaction, since no mass ions with the reported mass differences were found in the MS chromatogram of fragment B. In addition, fragment A possesses a carboxylic acid in the side chain (glutamic acid E), which also did not possess a mass ion with the reported mass differences indicating that the carboxylic acid at the C-terminus might not have been modified. This experiment raised suspicion that the arginine residue was modified during the Pd-mediated reaction, however, it could not be resolved with absolute certainty. The same conclusions were made from the MS analysis of the fragmentation experiment from the obtained products using (IPr)Pd(cinnamyl)Cl (Entry II, Scheme 2.3.12) as the catalyst of the reaction.

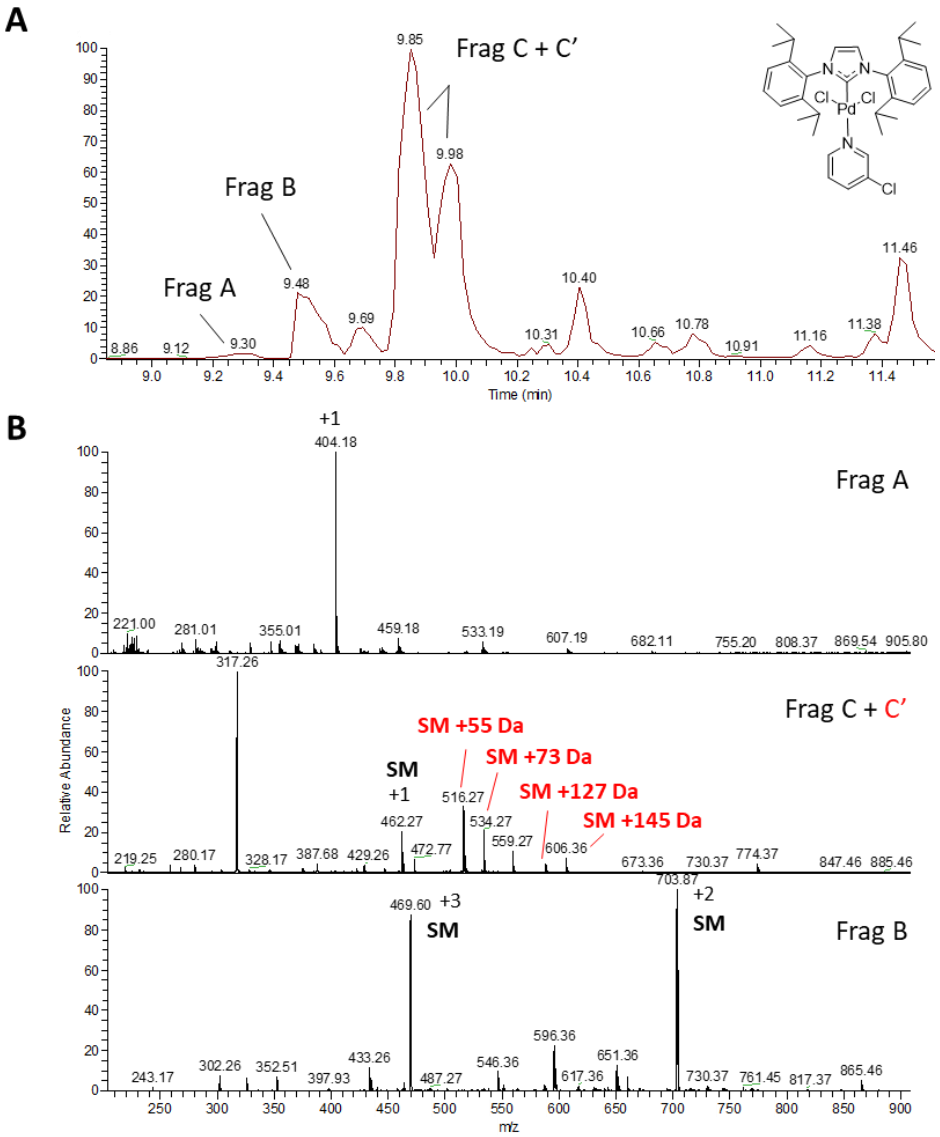

Figure 2.3.18 MS analysis of the fragmentation of the obtained peptide products from the Suzuki cross-coupling reaction using Pd-PEPPSI-IPr.

In order to limit the interaction of the palladium catalyst with other nucleophilic residues and thus to increase the efficiency of the catalyst to target the trimethyllysine residue, it was decided to treat the peptide **56** with propionic anhydride to block some of the nucleophilic sites (see Scheme 2.3.13). Propionylation with propionic anhydride is a known chemical modification for the capping of unmodified *N*-terminal amines and unmodified and/or mono-methylated lysine residues with propionyl groups. It is a chemical derivatization method to reduce the overall charge of hydrophilic peptides and thus to ensure homogeneity throughout their MS analysis, which has been used in the profiling of histone lysine methylation (see Subchapter 1.3.2.3 for more details). With the following three basic nucleophilic sites - the *N*-terminus and the two unmodified lysine residues, the peptide **56** could undergo tripropionylation resulting in the peptide **64** with a total mass of 2404 Da. In addition, over-propionylation has been reported using this protocol, in which residues bearing an alcohol side chain such as serine (S), threonine (T) and tyrosine (Y) have also been propionylated, which is beneficial to block further nucleophilic sites.[304]

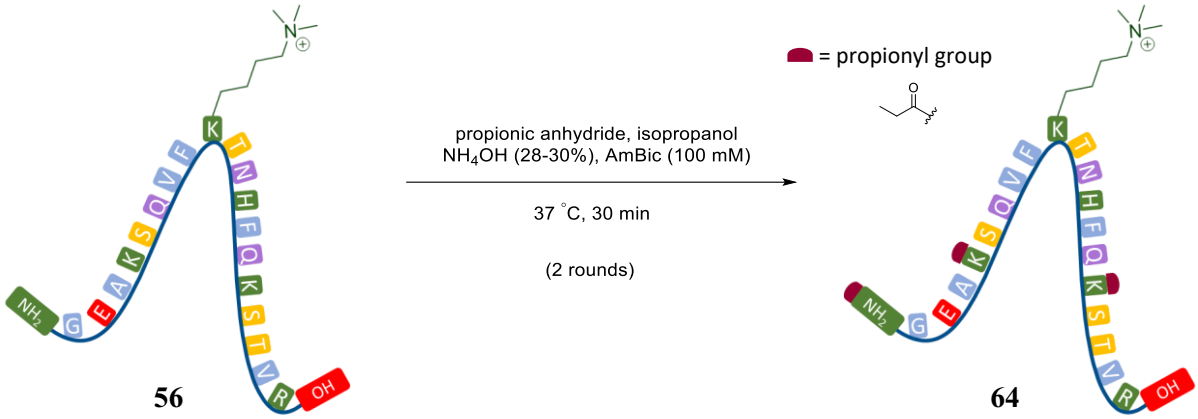

	Propionylation			
	Mono-	**Di-**	**Tri-**	**Tetra-**
M	2290.2307	2347.2648	2404.2988	2461.3329
$[M+2H]^{2+}$	1146.1232	1174.6402	1203.1572	1231.6743

Scheme 2.3.13 Propionylation of peptide 56. The calculated m/z ratios of the expected products are given in the table.

The result of the propionylation of peptide **56** is given in Figure 2.3.19. As seen in the MS spectrum in Figure 2.3.19 **B**, peptide **56** underwent di-, tri- and tetrapropionylation resulting in the formation of the propionylated peptides with the corresponding total masses. Next to the SM [**56**], an additional peak **X** was observed with a calculated total mass of about 2504 Da,

which could not be identified. As expected, peptide **64** was formed confirming the propionylation of the *N*-terminal amine and the two unmodified lysine residues. The formation of the tetrapropionylated peptide additionally confirmed the theory of overpropionylation, which is due to the presence of many alternative nucleophilic groups in peptide **56**.

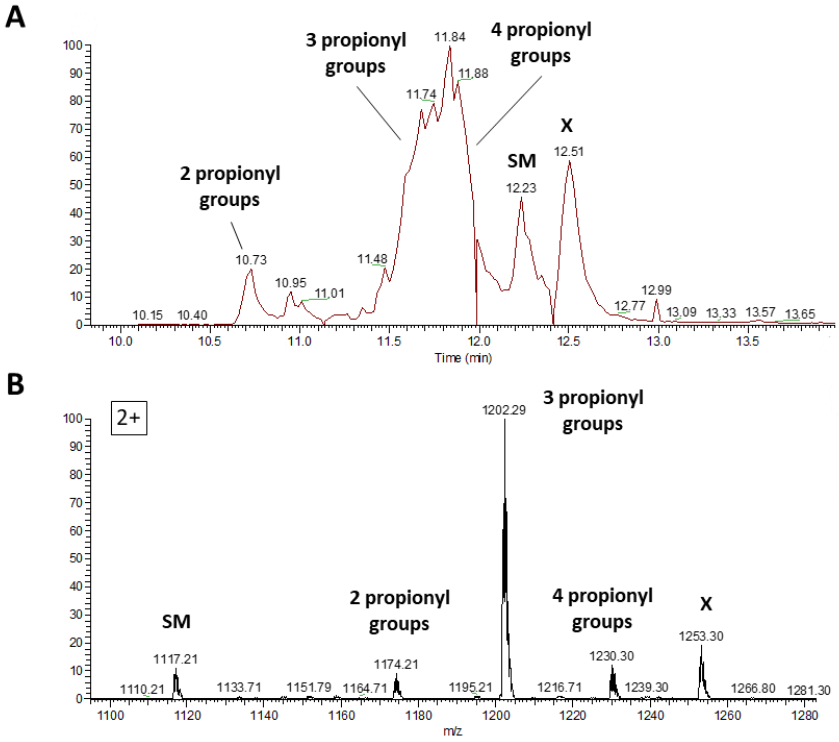

Figure 2.3.19 The obtained TIC (A) and MS spectrum of the doubly charged ions (B) resulting from the propionylation experiment of peptide 56.

Next, the propionylated peptides were exposed to the Suzuki cross-coupling conditions using Pd-PEPPSI-IPr as displayed in Scheme 2.3.14. The amount of *p*-tolylboronic acid was increased to improve both the catalyst activation and the transmetalation step of the reaction. The MS analysis of the reaction revealed that mainly the propionylated starting peptides were recovered after the reaction. The expected peptide **65** bearing a tolyl handle was not detected in the MS spectrum. When the investigated Suzuki reaction was applied to trimethyl-(4-phenylbutyl)-ammonium iodide [**31**] (see Subchapter 2.2.16), the reaction resulted in the formation of the terminal alkene **32** instead of the expected tolyl product **46**. Consequently, the MS spectrum was examined for any evidence of the formation of the propionylated modification of peptide **57** bearing an alkene handle, however, no proof was found that the elimination of trimethylamine occurred.

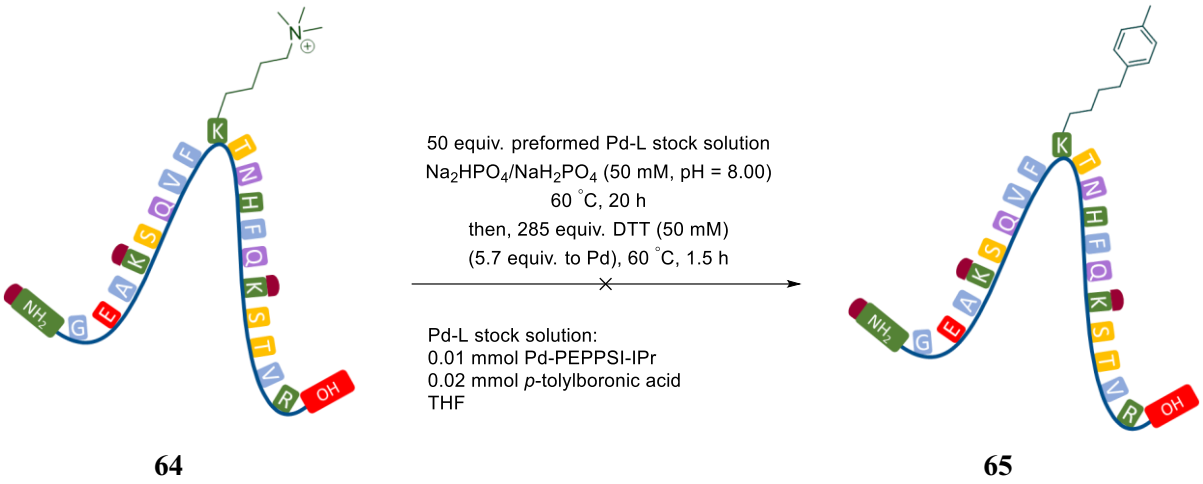

Scheme 2.3.14 Suzuki cross coupling of the propionylated peptide 64 using Pd-PEPPSI-IPr.

The results from the application of the Suzuki cross-coupling reaction using either Pd-PEPPSI-IPr or (IPr)Pd(cinnamyl)Cl on peptide **56** were not conclusive regarding the ability of the active NHC-Pd^0 catalyst to react with the trimethylammonium functionality in this substrate. At this stage of the project, we decided to concentrate our efforts in the optimisation of the NHC precatalyst to potentially increase its activity towards the cleavage of the $C(sp^3) – N(Me_3)$ bond. A detailed analysis of the structure of the NHC precatalyst and the subsequent efforts in redesigning the catalyst to ensure a Pd-catalysed Hofmann-type elimination of the trimethylammonium functionality is given in detail in Subchapter 2.2.16. As a result, three alternative NHC precatalysts were synthesised, which were primarily based on both the reduction of the steric bulk of the *N*-substituents of the imidazolium ring to improve the *β*-hydride elimination step and the increase of the electronic donor character of the NHC ligand. The prepared IMes-Pd catalysts were tested on trimethyl-(4-phenylbutyl)-ammonium iodide [**31**], which only resulted in the marginal formation of the terminal alkene **32** (≤ 1% yield).

Nevertheless, these precatalysts were also investigated in the Pd-catalysed elimination of peptide **56** using both caesium carbonate and potassium-*tert*-butoxide to activate the catalyst prior to their interaction with the peptide. In addition, they were also tested with the propionylated substrate **64**. Unfortunately, the sudden breakdown of the MS instrument during the last couple weeks of laboratory work and the resulting time constraint did not allow a MS examination of these experiments. Nevertheless, preliminary results from the Pd-catalysed Hofmann-type elimination reaction of peptide **56** using pyr-Pd-PEPPSI-IMes [**48**] confirmed that the desired peptide **57** bearing an alkene handle was not formed during this reaction and

that mainly the starting peptide **56** was present. Taking into consideration the beforementioned low yields of the Pd-catalysed Hofmann-type elimination of trimethyl-(4-phenylbutyl)-ammonium iodide [**31**], it is apparent that more reactive catalysts are needed to achieve the formation of the alkene functional group on the peptide substrate. While the major challenge of this reaction is the cleavage of the strong $C(sp^3)$ – N bond, the efficiency of the palladium catalyst is depleted with the presence of numerous functional groups in the peptide substrate. However, with the discovery of an efficient catalyst to form the desired alkene in good yields, this problem could potentially be diminished in the MS protocol by optimising the treatment of the peptide (such as propionylation or alternative chemical modifications) prior to its reaction with the active palladium catalyst.

2.4 Conclusion and Future Work

The desired chemical modification of trimethylated ammonium substrates to the terminal alkene has proven to be a challenging step in the design of the proposed novel enrichment tool CLICK-seq to monitor trimethyllysine marks on histones. The original strategy of applying the known Hofmann elimination reaction to achieve the removal of trimethylamine resulted in minimal success of the alkene formation at temperatures higher than 150 ˚C. The incorporation of micelle catalysis into the Hofmann elimination showed initial success in the generation of the alkene at low temperature (39 ˚C), yet only in low yields (≤ 3%). The sensitivity of the micellar structures to changes in reaction conditions further challenged the optimisation of the micelle-catalysed Hofmann elimination, nevertheless, a possible expansion of the research on this reaction could be the use of different functionalised cationic surfactants such as the incorporation of a tris(hydroxyethyl) head group.

With the design of the Pd-catalysed Hofmann-type elimination, a novel reaction based on the oxidative addition of an activated palladium catalyst into the $C(sp^3) – N(Me_3)$ bond of the alkyl ammonium substrate, we were able to induce partial elimination of trimethylamine under mild conditions. However, even after an excessive optimisation process of the Pd-catalysed Hofmann-type elimination, the generation of the desired alkene was only achieved in low yields (≤ 5%) on our model small molecules. Concluding from the research conducted on the Pd-catalysed Hofmann-type elimination, the limiting step of the reaction is potentially associated with the oxidative addition step in the catalytic cycle. Considering the bond dissociation energies published by Luo[305], carbon-nitrogen bonds have relatively high bond energies making them more challenging for the catalytic system to insert into and commence the cleavage of these bonds. For example, the following trend displayed in Figure 2.4.1 was established according to the values published by Luo, in which the bond dissociation energies of phenyl-nitrogen bonds are higher than those of phenyl iodide and phenyl bromide, the commonly used electrophiles in Pd-catalysed cross coupling reactions.

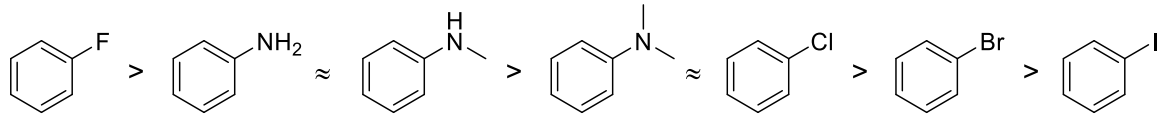

Figure 2.4.1 Trend established by bond dissociation energies published by Luo[305].

The bond dissociation energies of both $C(sp^2) – N(Me_3)$ and $C(sp^3) – N(Me_3)$ bonds could not be found in the literature. Therefore, computational studies in future work might be beneficial to gain insight on the actual bond strength of quaternary ammonium compounds and to determine the energies needed to break the carbon-nitrogen bond in our model systems. Taking the observed bond energies also into consideration, more reactive Pd – L complexes are presumably needed to induce the oxidative addition of the active catalyst to the unactivated alkyl ammonium electrophiles. A first step towards the synthesis of more electron-rich palladium complexes was taken in this project, nevertheless, more optimisation is needed to further enhance their activity towards oxidative addition in future work.

To investigate the underlying mechanism of the Pd-catalysed Hofmann-type elimination of quaternary ammonium substrates and to understand the occurring challenges, ^{31}P NMR spectroscopy was used in this project. However, the formation of numerous Pd/P complexes and the resulting complexity of the obtained spectra hindered the successful application of this technique. Consequently, trimethyl-(4-(4-fluorophenyl)butyl)-ammonium iodide was synthesised during this project in overall 5 steps to follow the progress of the reaction by means of ^{19}F NMR spectroscopy in future work. By using this approach, it was expected that the analysis of the resulting fluorine spectrum might become less challenging. Once the efficiency of the Pd-catalysed Hofmann-type elimination is improved, mechanistic studies using either experimental techniques such as ^{19}F NMR spectroscopy or computational methods might be valuable for the advancement of this reaction.

The investigation of alternative metals to perform the desired elimination reaction on quaternary ammonium substrates would also be useful. Next to palladium, metals including *e.g.* nickel[171,306], copper[307,308], iron[309], rhodium[310,311] and ruthenium[312] have been studied in the metal-catalysed breakage of carbon-nitrogen bonds in recent publications.[313] Since nickel has been primarily used in previous studies for the cross coupling reactions of trimethylammonium substrates (see Subchapter 2.2 for further details), we tested $Ni[cod]_2$ on our model substrate and obtained preliminary results using the Watson protocol[171] confirming the formation of the desired alkene product (albeit in low yield ≤ 3%). However, we did not perform an elaborate optimisation of this protocol due to the sensitivity of $Ni[cod]_2$ against air and water. We also tested 3 different air-stable Jamison nickel(II) precatalysts (see structures in Figure 2.4.2), which would overcome the issue of sensitivity seen with $Ni[cod]_2$. Our initial study did not result in the generation of the desired olefin, however, a further investigation of these catalysts and a further optimisation of the used Jamison protocol[314] would be beneficial, since nickel is

more electropositive than palladium facilitating oxidative addition more readily.[315,316] In addition, we briefly investigated copper(I) iodide according to the protocol by Gao *et al.*[307], which was successful in the coupling of benzyl trimethylammonium substrates with thiols, but not when using our alkyl trimethylammonium substrate. Nevertheless, a vast amount of metals can be investigated to overcome the obstacles experienced with Pd-catalysed Hofmann-type elimination of alkyl trimethylammonium electrophiles.

An investigation of photoredox catalysis on the desired elimination on alkyl trimethylammonium electrophiles was also planned in this project and could be investigated in the future. Yu e*t al.* demonstrated the possibility of the visible-light-driven cross coupling of benzyl trimethylammonium triflates by means of an iridium complex making photoredox catalysis an alternative reaction to the investigated Pd-catalysed elimination for the removal of trimethylamine.[317]

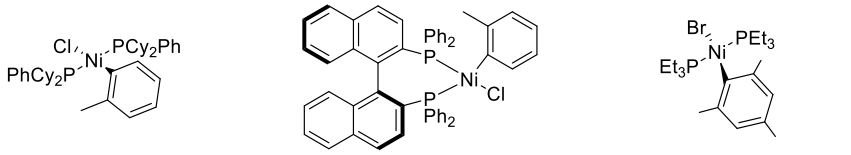

trans-$(PCy_2Ph)_2Ni(o\text{-tolyl})Cl$ *cis*-((*S*)-BINAP)Ni(*o*-tolyl)Cl *trans*-$(PEt_3)_2Ni(mesityl)Br$

Figure 2.4.2 Commercially available, air-stable Jamison nickel catalysts.

With the discovery of efficient catalytic systems to perform the desired elimination on quaternary ammonium substrates, the MS protocol for the chemical modification of peptides can be further improved. Furthermore, the optimised MS protocol can then be applied for the metal-catalysed modification and the subsequent analysis of tryptic histone peptides. Preliminary examination of commercially available human native nucleosomes using the bottom-up MS approach was conducted confirming the existence of trimethyllysine marks on tryptic histone peptides such as H3K9(me_3)K14 (area % of total: ~ 16%) and H3K27(me_3)K36 (area % of total: ~ 15%).

The screening of biocompatible and efficient Hofmann-type elimination conditions to chemically modify trimethylammonium substrates has proven to be more challenging than initially anticipated impeding the development of the original CLICK-seq protocol. Over the course of this project, alternative concepts originated to achieve the cleavage of the desired

carbon-nitrogen bond, one of which is the possible incorporation of enzymes. As displayed in Subchapter 1.2, certain lysine demethylases can selectively target trimethyllysine residues to remove a methyl group via oxidative cleavage. Hence, a future concept for the selective modification of trimethyllysine residues might be to alter lysine demethylases to perform the desired modification without influencing their selectivity towards trimethyllysine. Alternatively, artificial metalloenzymes, which consist of an abiotic metal cofactor incorporated into a protein scaffold, have been successfully used in Pd-catalysed cross coupling reactions.[318] By taking advantage of both homogenous catalysis and enzymatic catalysis, the integration of artificial metalloenzymes might also be a prospective method to selectively and efficiently modify the target trimethylammonium substrate. In addition, distinct calixarene compounds have been developed for various applications such as for the encapsulation of methylated lysine residues or for metal-based catalysis.[319,320] Consequently, the development of novel calixarene compounds combining both characteristics, might be an alternative approach to achieve the elimination of quaternary ammonium substrates at mild conditions in future work.

3 RESULTS AND DISCUSSION II – ACID-CLEAVABLE CROSS-LINKER FOR BOTTOM-UP MS ANALYSIS OF HISTONE INTERACTIONS

3.1 Background: Cross-linking mass spectroscopy

Cross-linking mass spectroscopy (XL-MS) is a powerful tool for the investigation of protein structures and interactions in complex biological systems.[321–323] In order to covalently-link otherwise non-covalent protein-protein interactions (PPIs) or protein complexes, a wide range of bifunctional cross-linkers have been developed preserving the structural integrity of the biological system for further processing prior to MS evaluation. A general outline for the cross-linking mass spectroscopy procedure is given in Figure 3.1.1.

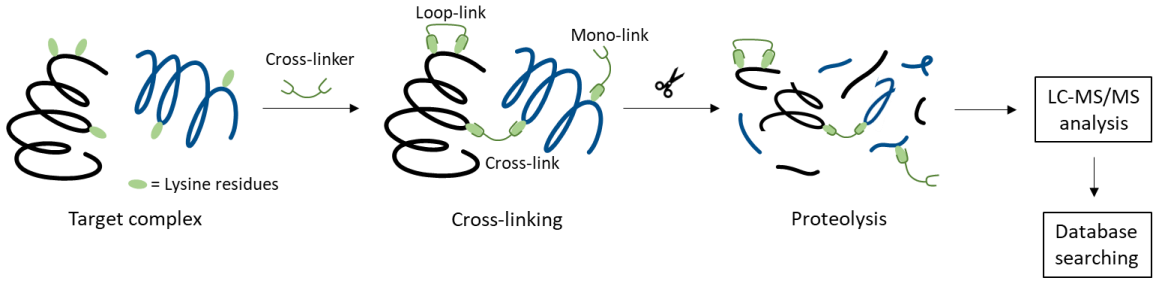

Figure 3.1.1 Procedure of cross-linking mass spectroscopy (XL-MS) to analyse protein complexes.

The high abundance of lysine residues and the specificity of the side chain amino group towards cross-linker reagents bearing activated esters makes lysine side chains the most commonly used targets for cross-linking experiments. Under controlled pH, reaction time and amount of reagent, side reactions with alternative residues within the proteins can be minimised or prevented. Upon cross-linking, the proteins are analysed via the bottom-up MS approach, in which they are firstly digested using trypsin and then investigated and identified by LC-MS/MS in combination with bioinformatics (see Figure 3.1.1). The digestion of the cross-linked proteins generates a complex mixture of peptides including mono-, loop- and cross-linked peptides as well as unmodified peptides. Consequently, the overall abundance of the target cross-linked peptides is low in the complex mixture and hence the cross-linked peptides need to be enriched before their MS analysis. Dong *et al.* applied cross-linking mass spectroscopy

to analyse PPIs in both E. *coli* and C. *elegans*.[324] By using the non-cleavable cross-linker BS^3 (see Figure 3.1.2), Dong and colleagues identified 394 cross-links from E. *coli* lysates and 39 cross-links from more complex C. *elegans* lysates. However, a major drawback of the use of non-cleavable cross-linkers is the complexity of the obtained MS/MS fragmentation pattern from the peptides containing the cross-linking bridge, or even incomplete fragmentation, which greatly complicates the analysis and characterisation of these peptides. Since the cross-linked peptides consist of two linear peptides, the data analysis algorithms need to consider all possible peptide pair combinations from the linear peptide databases, which leads to a tremendous increase in computational search space (known as the 'n-square problem').[325]

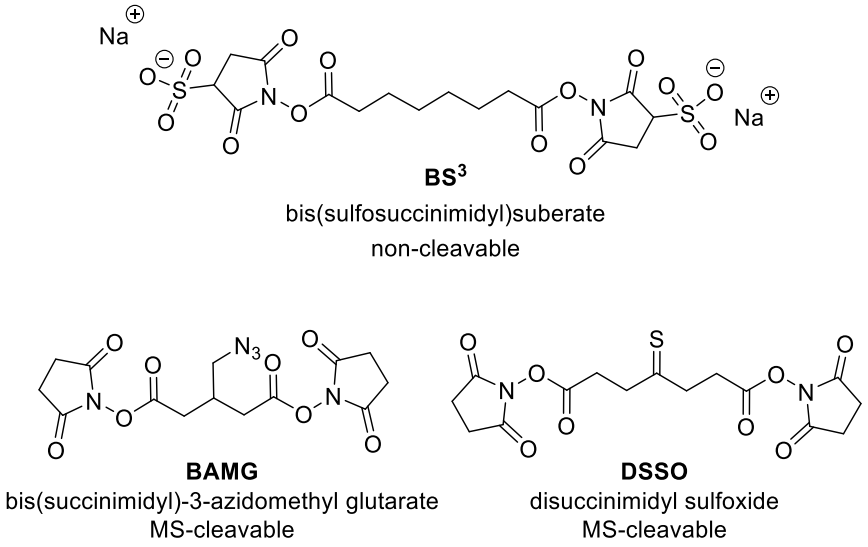

Figure 3.1.2 Structure of common cross-linkers used in *in vitro* XL-MS experiments.

To overcome these challenges, MS-cleavable cross-linkers have been developed and incorporated into XL-MS experiments, which are cleaved by low-energy CID leading to the formation of two individual peptides and thus to a more simplified MS/MS fragmentation spectrum. For example, Jong *et al.* employed the MS-cleavable cross-linker BAMG (see Figure 3.1.2) to analyse nuclear extracts from HeLa cells.[326] After cross-linking and protease digestion, the azido group was reduced by TCEP to an amine to enrich the cross-linked peptides using strong cation exchange (SCX) chromatography. Next, the enriched cross-linked peptides were analysed via MS/MS, in which the cross-linked peptides were cleaved by CID, resulting in the successful identification of 247 cross-links. Heck *et al.* also demonstrated the feasibility of MS-cleavable cross-linkers for the large-scale proteome-wide analysis of PPIs. With the use

of the MS-cleavable cross-linker DSSO (see Figure 3.1.2) in combination with SCX purification, Heck and his group identified 1822 cross-links at 1% FDR (false discovery rate) indicating the identification of 134 PPIs in HeLa cell lysates.[325] In addition, Heck *et al.* applied this approach to study PPIs in intact human cell nuclei identifying about 8700 cross-links at 1% FDR and thus gaining insight on protein interactions involving histone proteins and on the influence of PTMs on PPIs.[327]

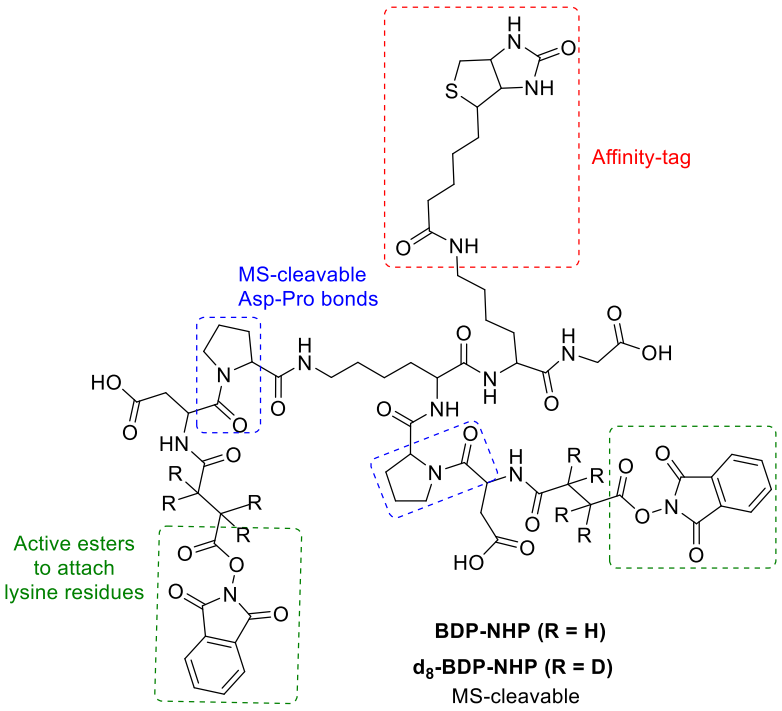

Figure 3.1.3 Structure of BPD-NHP cross-linkers used for *in vivo* XL-MS experiments.

With the development of a novel MS-cleavable and enrichable cross-linker – BDP-NHP (see Figure 3.1.3), Bruce and his group applied the XL-MS approach to study dynamic PPIs in living human cells.[328,329] After the treatment of HeLa cells with the BDP-NHP cross-linker, the proteins were extracted and digested to give a complex peptide mixture, which included the cross-linked peptides. Enrichment of the cross-linked peptides via affinity chromatography followed by MS/MS analysis led to the identification of 368 cross-links including intra- and interprotein cross-links for histone proteins, of which several contained PTMs.[328] By synthesising heavy d_8-BDP-NHP (see Figure 3.1.3) and combining *in vivo* cross-linking with SILAC, Bruce *et al.* quantified nearly 1000 cross-linked peptide pairs from 382 interacting proteins in E. *coli* demonstrating the feasibility of quantitative XL-MS for the proteome-wide analysis of PPIs *in vivo*.[329]

As displayed in the examples given above, the introduction of MS-cleavable cross-linkers enabled the proteome-wide large-scale analysis of PPIs *in vitro* and *in vivo* using cross-linking mass spectroscopy. However, since each peptide is required to undergo CID fragmentation in order to obtain a clear identification of the cross-linked peptides, incomplete fragmentation, especially due to the low abundance of the cross-linked peptides in the obtained complex peptide mixture, might lead to loss of information.[322] Consequently, a series of fragmentation methods are acquired to ensure sufficient sequence coverage, yet the disadvantages of multistage MS methods are diminished scan rate and lower sensitivity.[330] In addition, advanced MS instrumentations are needed to achieve optimal fragmentation and identification of the cross-linked peptides, since *e.g.* different fragmentation energies are required to simultaneously cleave the cross-linker and fragment the peptides due to differences in bond strengths. Trypsin has been preferably used in most proteomic experiments including XL-MS due to its robustness and efficiency to produce digested peptides beneficial for MS/MS fragmentation. However, the distinct modifications present in the protein complexes upon cross-linking (mono-, loop- and cross-links) challenges the trypsin digestion process leading to the generation of cross-linked peptides with varying lengths.[331] As a result, the obtained tryptic peptides are difficult to purify and separate by reverse-phase chromatography thus leading to a decrease in overall sensitivity. In order to reduce the size of large tryptic peptides, protocols have surfaced, which incorporated additional proteases (AspN, chymotrypsin and Glu-C) to further digested tryptic peptides via sequential digestion processes[332], however, the generation of heterogeneous proteomic peptides by protease digestion still remains an obstacle in the XL-MS method.

Here we propose an acid-cleavable cross-linker used for XL-MS experiments to analyse PPIs of histone proteins. Due to the cleavage of the cross-linker prior to proteolysis, we aimed to overcome the challenges observed with the use of common MS-cleavable cross-linkers. The design of the proposed cross-linking mass spectroscopy technique using an acid-cleavable cross-linker is presented next.

3.2 The development of an acid-cleavable cross-linker for XL-MS analysis of histone proteins

With the design of a homobifunctional cross-linker, which upon cleavage transfers a chemical group onto lysine residues of histones, it was believed that the cross-linking MS approach could be further improved by providing homogenous linear peptide sequences for the MS/MS fragmentation process. As previously discussed, a major challenge in the common XL-MS protocols is the generation of cross-linked peptides with varying lengths upon proteolysis, which makes their fragmentation and subsequent identification additionally challenging. The cleavage of the cross-linker prior to protease digestion was proposed to improve the efficiency of this process. Chemical derivatisation, such as propionylation, has been used to ensure the generation of homogenous tryptic peptides by chemically modifying basic lysine residues prior to trypsin digestion (see Subchapter 1.3.2.3 for more details). Consequently, by labelling lysine residues upon acid-catalysed cleavage, the proposed cross-linker would also act as a derivatising reagent. Hydroxy butanoate was chosen as the chemical modification to be transferred onto the lysine residues, which was functionalised with an active ester for the amines to attach to the cross-linker (see structure in Figure 3.2.1). Yi *et al.* developed a novel protocol for the specific and efficient derivatisation of histones using *N*-hydroxysuccinimidyl propionate (NHS-propionate), which laid the foundation for the possibility of the cleavable cross-linker functionalised with reactive *N*-hydroxysuccinimide esters to be also used as a derivatising reagent for the modification of histone lysine residues.[113]

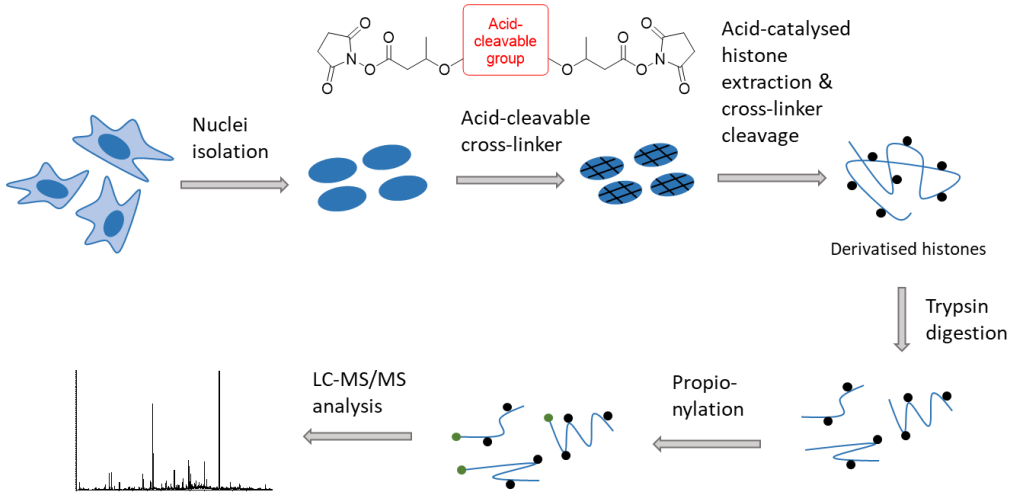

Figure 3.2.1 Proposed protocol for XL-MS experiments using the acid-cleavable cross-linker to investigate interactions and PTMs of histone proteins.

With the aim of incorporating the cross-linker into the developed protocols for the analysis of histones proteins with minimal disruption of the workflow, the choice of the bridging group in the cross-linker fell on the use of acid-labile functional groups, since the extraction of histone proteins from the cell nucleus is performed using sulfuric acid (0.4 N).[333] The proposed protocol for the optimised XL-MS technique incorporating the acid-cleavable cross-linker is shown in Figure 3.2.1. After the isolation of the nuclei, the protein complexes are fixed using the acid-cleavable cross-linker. Next, the histone proteins are extracted by means of sulfuric acid, which simultaneously cleaves the cross-linker to give the derivatised histone proteins. Upon trypsin digestion and propionylation, the peptide fragments can then be analysed by LC-MS/MS.

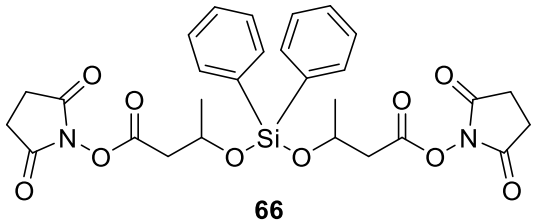

66

Figure 3.2.2 Original design of the acid-cleavable cross-linker.

The decision on the acid-labile group for the cross-linker fell on a bifunctional silyl ether linker (see Figure 3.2.2). Silyl ethers are one of the most widely used alcohol protecting groups in organic synthesis. One major advantage of silyl ethers is that the rate of deprotection via acid hydrolysis can be tuned by adjusting the substituents on the silicon atom. Consequently, it was decided to incorporate a silyl functionality into the design of the acid-cleavable cross-linker. DeSimone *et al.* developed polymeric biomaterials including a bifunctional dialkyl silyl cross-linker and demonstrated the degradation of various dialkyl silyl cross-linkers under mild acidic conditions (pH = 5 – 7).[334] In a later publication, DeSimone and his group expanded the use of bifunctional silyl ethers to produce prodrugs and regulated the rate of drug release by changing the steric bulk on the silicon atom.[335] The synthesis of the acid-cleavable cross-linker was started with the design displayed in Figure 3.2.2, which included the acid-labile diaryldialkoxysilyl group connected to *N*-hydroxysuccinimidyl butanoate groups to give the cross-linker **66**. Our synthetic effects towards the formation of an acid-cleavable cross-linker is displayed in the subsequent subchapters.

3.3 Synthetic efforts towards generation of the acid-cleavable cross-linker

3.3.1 Towards the synthesis of the diaryldialkoxysilyl cross-linker

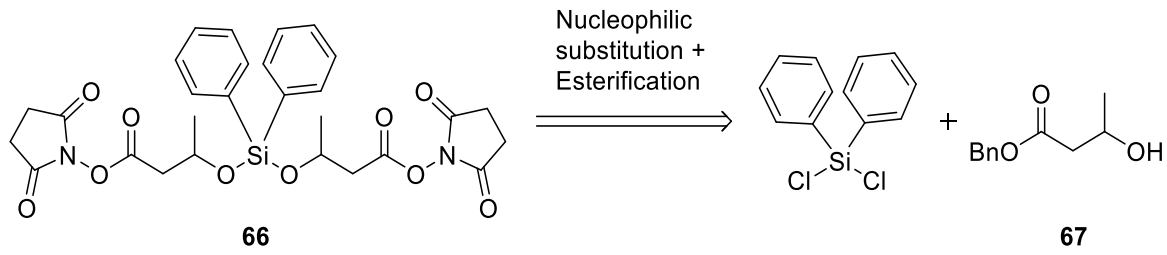

Scheme 3.3.1 Synthesis of diaryldialkoxysilyl cross-linker via nucleophilic substitution.

As shown in Scheme 3.3.1, a double nucleophilic substitution of dichlorodiphenylsilane with benzyl 3-hydroxybutanoate [**67**] followed by a dual debenzylation and esterification with *N*-hydroxysuccinimide should lead to the formation of the desired acid-cleavable diaryldialkoxysilyl cross-linker **66**. This formed our initial plan for the synthesis of the acid-cleavable cross-linker.

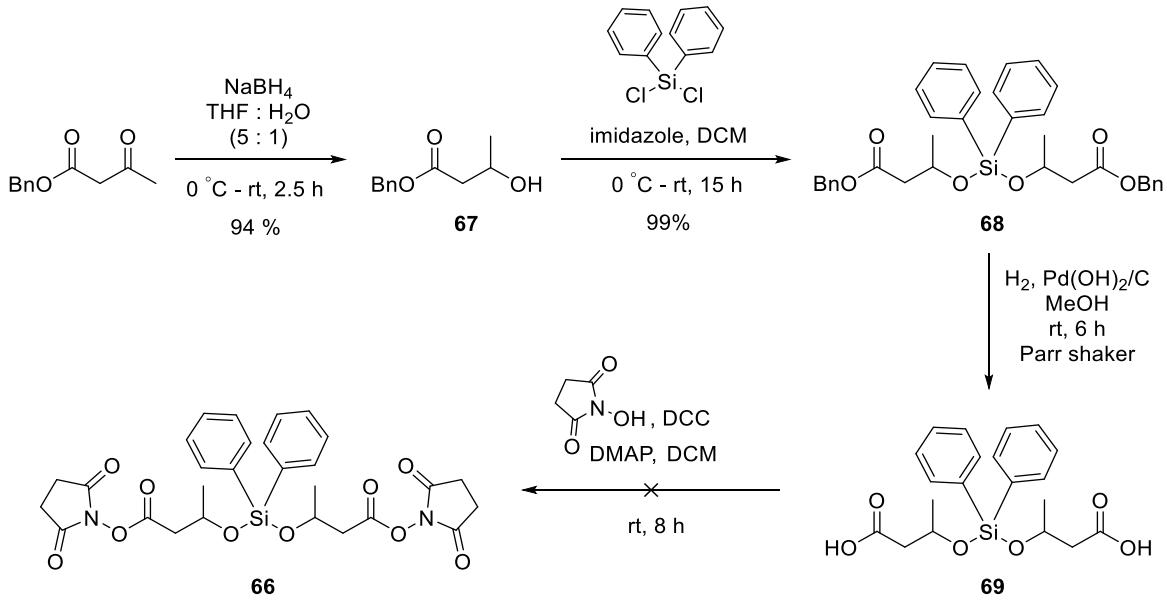

Scheme 3.3.2 The attempted forward synthesis of the diaryldialkoxysilyl cross-linker.

The forward synthesis of the diaryldialkoxysilyl cross-linker **66** is shown in Scheme 3.3.2. To synthesize the hydroxyester **67**, benzyl 3-oxobutanoate was reduced with sodium borohydride in THF : water (5 : 1) to give benzyl 3-hydroxybutanoate [**67**] in excellent yield (94%). Dual nucleophilic substitution of dichlorodiphenylsilane with benzyl 3-hydroxybutanoate [**67**] gave the dialkoxysilane **68** in excellent yield (99%). 2-D TLC of the dialkoxysilane **68** confirmed its instability towards silica gel column chromatography. Hence, the synthesis was continued without further purification of **68**. Debenzylation of the dialkoxysilane **68** with hydrogen and catalytic amounts of palladium hydroxide in a Parr Shaker (3.5 atm) gave the dialkoxysilyl diacid **69**. The obtained proton NMR spectrum confirmed the removal of the benzyl groups. The crude diacid **69** was treated with *N*-hydroxysuccinimide, DCC and catalytic amounts of DMAP in dichloromethane at room temperature. However, NMR analysis confirmed the decomposition of the molecule. A possible reason for the decomposition may be the instability of the free diacid **69**, since the molecule simultaneously possesses an acid-labile group. Consequently, the benzyl ester protecting group was substituted for a methyl ester with the aim of performing a base-catalysed deprotection and isolating the carboxylate salt of the diaryldialkoxy silyl substrate **69**.

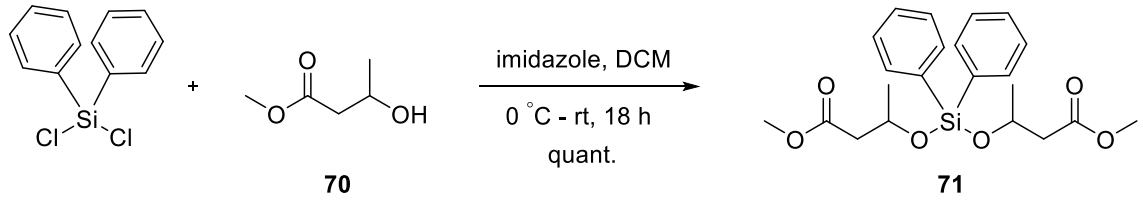

70 **71**

Scheme 3.3.3 Synthesis of the dialkoxysilane 71.

Methyl 3-hydroxybutanoate [**70**] was reacted with dichlorodiphenylsilane in the presence of imidazole in dichloromethane for 18 h to give the methyl ester bearing dialkoxysilane **71** in quantitative yield. However, this molecule was unstable and decomposed to the alcohol starting material **70**. Since the synthesis towards the formation of the dialkoxydiphenylsilyl cross-linker **66** was challenging due to its instability, a step towards increasing the stability of the silyl linker group was additionally taken. It was hypothesised that an increase in bulk of the phenyl substituents would decelerate the hydrolysis of the dialkoxysilyl linker group and thus it would increase the overall stability of the molecule. Consequently, dichlorodimesitylsilane [**72**] was reacted with methyl 3-hydroxybutanoate [**70**] in the presence of imidazole in dichloromethane

both at room temperature (Entry a) and under reflux (Entry b) as shown in Scheme 3.3.4. However, both reactions did not lead to the formation of the dialkoxydimesitylsilane **73**, but only starting material was recovered after the reaction.

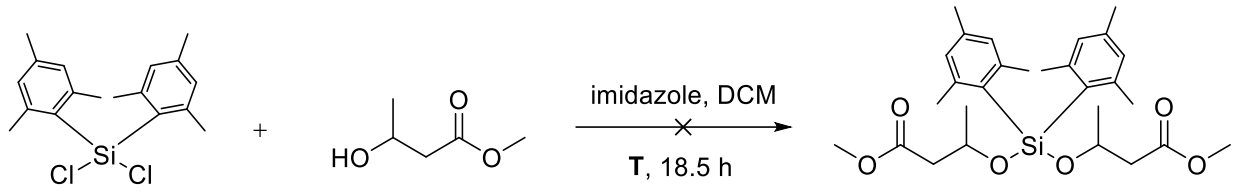

72 **70** **73**

Entry	T	Reaction outcome
a	rt	SM
b	reflux	SM

Scheme 3.3.4 Formation of the dialkoxydimesitylsilane 73.

Since the formation of the bulkier dialkoxydimesitylsilane **73** was impeded under the used reaction conditions, it was clear that harsher conditions were needed to overcome the steric hindrance and achieve the dual nucleophilic substitution reaction. At this stage of the project, it was believed that the difficulty in forming the dialkoxydimesitylsilane **73** might make the subsequent cleavage of the silyl linker under the required mild acidic conditions, when used as cross-linker, problematic. We therefore sought to design alternative acid-cleavable cross-linkers.

3.3.2 New design of the acid-cleavable cross-linker

The main aim for the design of the acid-cleavable cross-linker was to find a sweet spot between a functional group, which is stable enough to be able to be synthesised, purified and employed for the cross-linking of the protein complexes but labile enough to break when exposed to the mild acidic protocol used for cross-linking experiments. Figure 3.3.1 shows an exemplary summary of acid-cleavable functionalities used previously for general cross-linking experiments.[336,337]

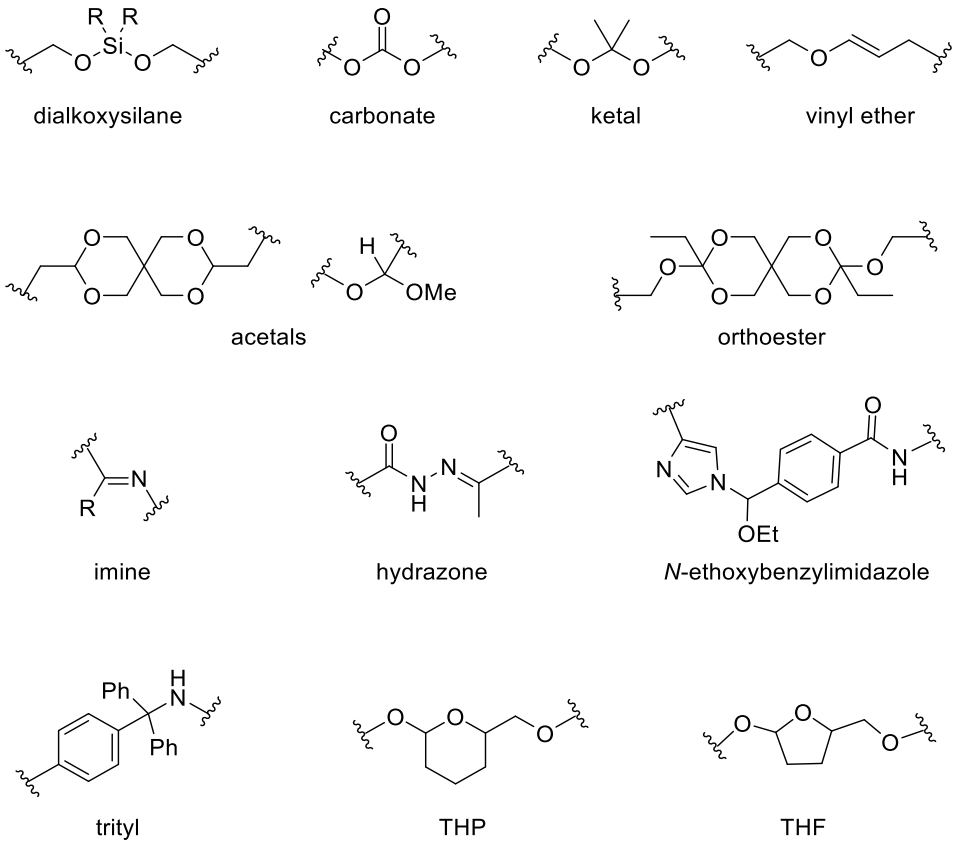

Figure 3.3.1 Summary of acid-labile functional groups used in common cross-linkers.

We decided on a novel, 'out-of-the-box' design of an acid-cleavable functional group to be used for the desired cross-linker. The designs of the core structure shown in Figure 3.3.2 were chosen for the synthesis of the cross-linker.

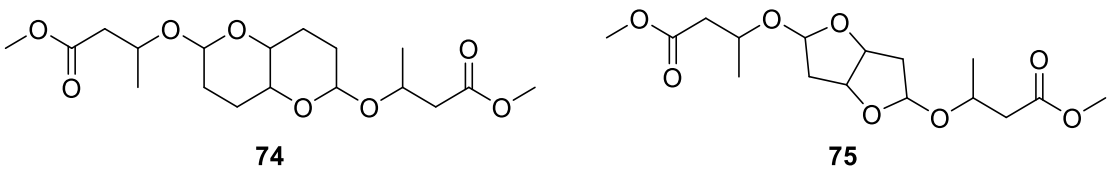

74 **75**

pyrano[3,2-*b*]pyran furo[3,2-*b*]furan

ring-fused THP linker ring-fused THF linker

Figure 3.3.2 Core structures to be used for the novel acid-cleavable cross-linkers.

Tetrahydropyran (THP) and tetrahydrofuran (THF) are known protecting groups for hydroxyl groups, which are widely used in organic synthesis due to their ease of installation, their general stability to most nonacidic compounds and their ease of removal. Numerous mild acidic protocols have been reported to cleave THP- and THF-ethers at room temperature and in high yield making them ideal candidates to use in a biological setting.[338] In addition, a study by Funhoff *et al.* has demonstrated that the relative stability of THP is higher than other known acetals[339], which is promising to overcome the stability issues seen in the synthesis of the diaryldialkoxysilyl cross-linker. Nevertheless, they have been scarcely exploited in the generation of acid-sensitive cross-linkers.[340,341] In order to assure that the adduct on each target peptide is homogenous in the MS analysis, the design of the novel cross-linkers were required to be symmetric. Consequently, our design was based on the ring fusion of either two THP molecules leading to the pyrano[3,2-*b*]pyran core **74** or two THF molecules forming the furo[3,2-*b*]furan core **75** as demonstrated in Figure 3.3.2. The ring-fused THF design was included in the synthesis of the acid-cleavable cross-linker, since the cleavage of the THF functionality can be performed under much milder acidic conditions and it is known to be faster than the cleavage of the THP group.[338,340] As shown in Scheme 3.3.5, the main precursors for the synthesis of the coupled ring-fused THP [**74**] and THF [**75**] cores are the corresponding bis-lactones, which can be reduced to the hemi-acetal prior to their coupling with the hydroxyester **70** to give the coupled bicyclic precursors **74** and **75**, which can then be functionalised with *N*-hydroxysuccinimidyl esters.

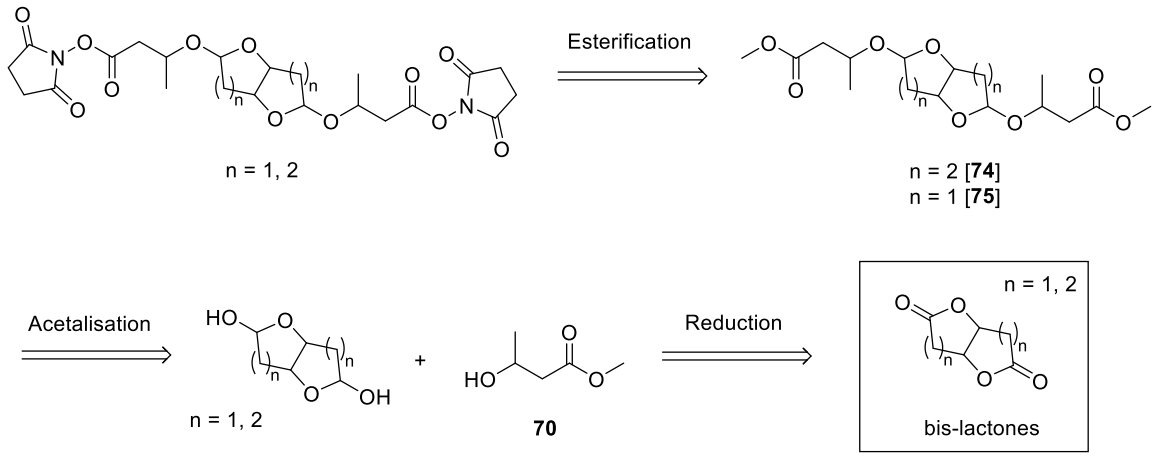

Scheme 3.3.5 Bis-lactones as precursors for the synthesis of the ring-fused THP and THF cross-linkers.

Two main approaches have been taken for the synthesis of the bis-lactone precursors: either Baeyer-Villiger oxidation or the iodine-catalysed lactonisation. Both were attempted in our synthetic efforts towards the formation of the bis-lactone precursors, which are discussed in the following subchapter.

3.3.3 Synthesis of the bis-lactone precursors

3.3.3.1 Baeyer-Villiger approach for the synthesis of the pyrano[3,2-*b*]pyran lactone

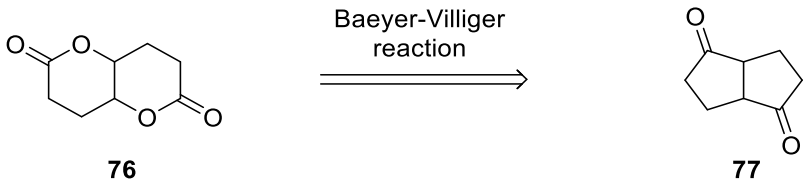

Scheme 3.3.6 Baeyer-Villiger approach for the synthesis of the bis-lactone 76.

The main step in the first approach for the synthesis of the pyrano[3,2-*b*]pyran lactone **76** was based on the Baeyer-Villiger oxidation of the cyclic diketone **77** as shown in Scheme 3.3.6. The Baeyer-Villiger reaction is the oxidative cleavage of the carbon-carbon bond next to the C=O bond by means of a peracid resulting in the formation of esters or lactones.[342] A synthetic route was developed for the formation of the pyrano[3,2-*b*]pyran lactone **76** in overall four steps including the Baeyer-Villiger oxidation step (see Scheme 3.3.7). Cycloocta-1,5-diene [**78**] was converted into 2,6-diacetoxybicyclo[3,3,0]octane [**79**] by undergoing a transannular Pd-catalysed ring closure with lead(IV) acetate in acetic acid.[343] After stirring at room temperature for 6 days, **79** was isolated in good yield (64%). The removal of the acetyl group by potassium hydroxide in methanol gave the diol **80** in 39% yield. Swern oxidation of the diol **80** led to the formation of the cyclic diketone **77** in moderate yield (55%). A change in oxidation conditions from Swern to DMP oxidation increased the yield of the generated cyclic diketone **77** to 91%. The cyclic diketone **77** was reacted with *meta*-chloroperbenzoic acid in the presence of catalytic amounts of bismuth(III) triflate in dichloromethane at room temperature.[344] Even though the full consumption of the starting material was confirmed via TLC, it was inferred from the NMR spectra that the bis-lactone **76** was not isolated, since the proton peaks (expected around ~ 4.5 ppm) characteristic for the hydrogens at the ring junction were not detected. Since a parallel route for the synthesis of the furo[3,2-*b*]furan lactone **89** was successful, no further analysis of the reaction outcome was conducted and no alternative Baeyer-Villager oxidation conditions were tested.

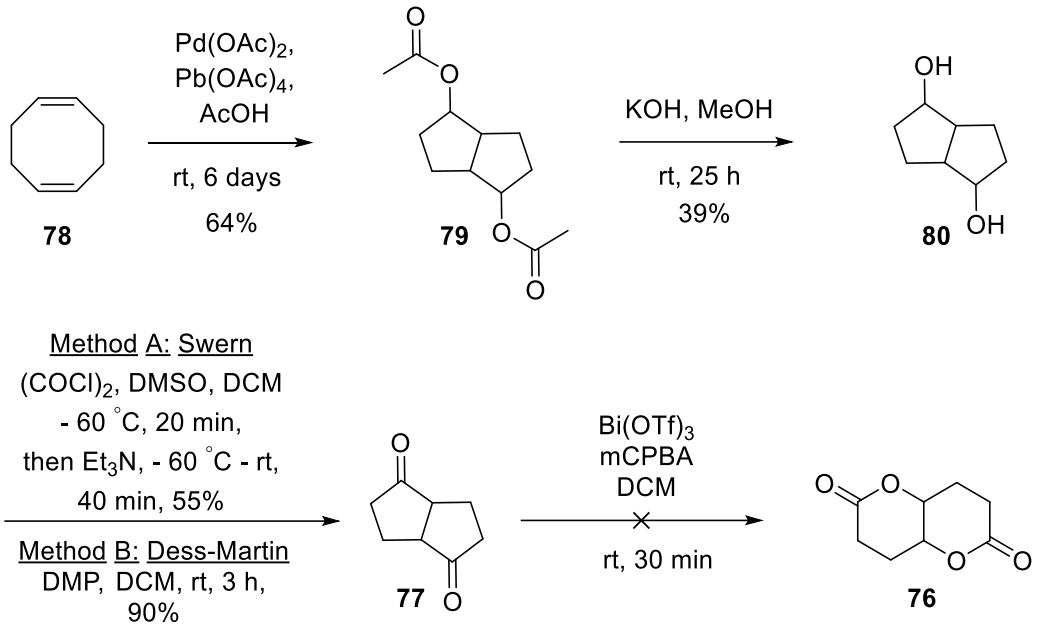

Scheme 3.3.7 Attempted synthesis of the bis-lactone 76 via the Baeyer-Villiger reaction.

3.3.3.2 Synthesis of the pyrano[3,2-*b*]pyran lactone via iodine-catalysed lactonisation

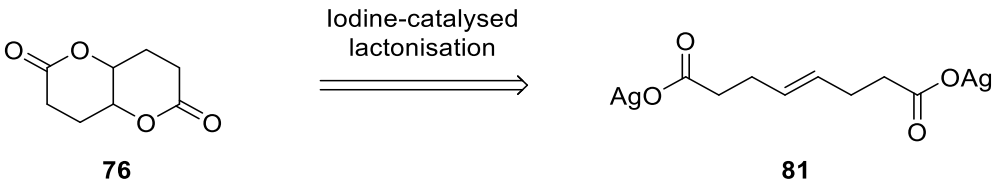

76 **81**

Scheme 3.3.8 Iodine-catalysed lactonisation approach to synthesise the bis-lactone 76.

While the Baeyer-Villager approach was explored for the synthesis of the pyrano[3,2-*b*]pyran lactone **76**, a protocol by Sakai *et al.* was applied for the synthesis of the furo[3,2-*b*]furan lactone **89**.[345] Sakai and colleagues used iodine-catalysed double lactonisation to achieve the formation of the furo[3,2-*b*]furan lactone **89** in overall two steps starting from the commercially available *trans*-3-hexene-1,6-dioic acid [**91**]. Upon replication of this protocol, we successfully synthesised the furo[3,2-*b*]furan lactone **89** in good yield (81%) (see Subchapter 3.3.3.3 for further details). Since the iodine-catalysed lactonisation was successful in the synthesis of the furo[3,2-*b*]furan lactone **89**, it was decided to continue the synthesis of the pyrano[3,2-*b*]pyran lactone **76** using the procedure demonstrated by Sakai *et al.* starting from *trans*-4-octene-1,8-dioic acid [**85**]. Since **85** is not commercially available, we attempted the synthesis of this compound according to the literature (see Scheme 3.3.9).[346] Benzylation of pent-4-enoic acid [**82**] with benzyl bromide and potassium carbonate in dimethylformamide gave the benzyl pent-4-enoate [**83**] in excellent yield (88%). The benzyl-protected olefin **83** was next treated with the Grubbs' 2nd generation catalyst in dichloroethane under reflux to undergo cross-metathesis resulting in the formation of the diester **84**. The Grubbs' metathesis reaction resulted in a mixture of compounds and after several purification attempts the diester **84** was isolated in 22% yield. When the reaction was repeated in gram-scale, the yield dropped to 11%, however, enough material was brought through to continue the synthesis. The removal of the benzyl group via base-catalysed hydrolysis was performed with lithium hydroxide firstly at room temperature as the literature procedure suggested.[346] Even after increasing the reaction time and heating the reaction to 90 °C, mainly starting material **84** was recovered. After 7 days of heating at 90 °C, the diacid **85** was only formed in 25% yield.

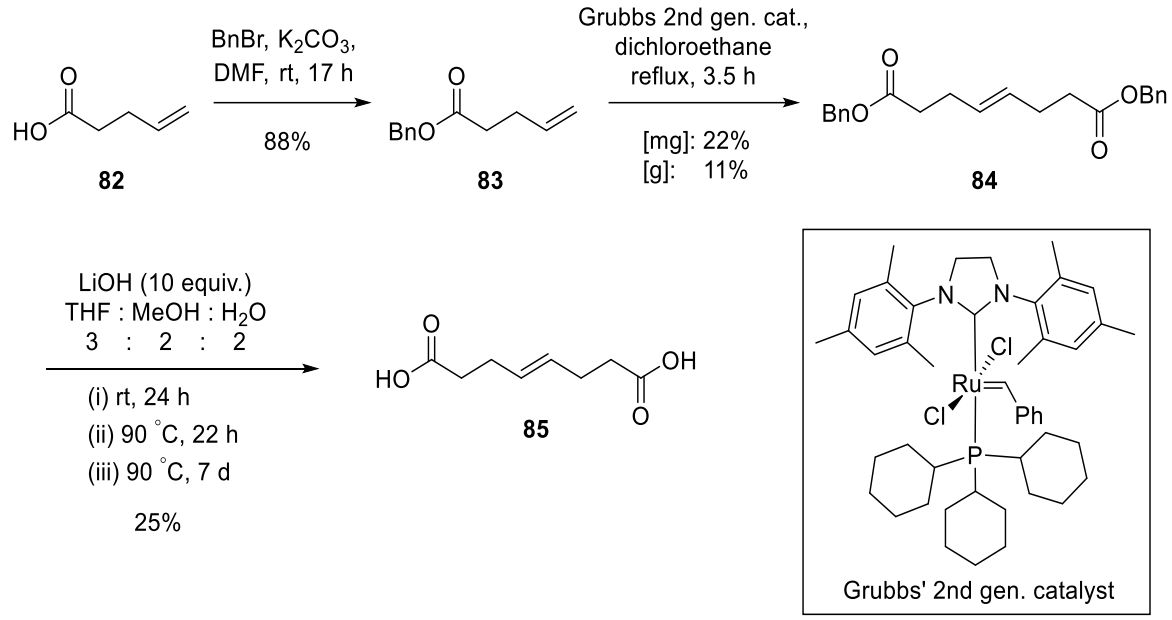

Scheme 3.3.9 Synthesis of the *trans*-4-octene-1,8-dioic acid [85].

Nevertheless, the synthesis was continued with the low amount of the diacid **85** in hand to determine if the iodine-catalysed lactonisation by Sakai *et al.* could be applied for the synthesis of the pyrano[3,2-*b*]pyran lactone **76**. As demonstrated in Scheme 3.3.10, the diacid **85** was converted to the disilver dicarboxylate **81** in good yield (95%). Substrate **81** was then treated with iodine in dichloromethane at room temperature for 16 h. In the synthesis of the furo[3,2-*b*]furan lactone **89**, the product was isolated via recrystallisation due to its instability towards column chromatography. Consequently, several recrystallisation approaches were conducted to isolate the pyrano[3,2-*b*]pyran lactone **76**, including ethyl acetate/pentane, ethyl acetate/diethyl ether and 100% pentane. Because of the small scale of the reaction, the pyrano[3,2-*b*]pyran lactone **76** could not be isolated via recrystallisation. Nevertheless, the analysis of the crude product using NMR and GC-MS techniques (*m/z* 170.1 $(M+H)^+$, see Experimental, Subchaper 5.3.2 for more details) confirmed the formation of the pyrano[3,2-*b*]pyran lactone **76**. Concluding from the initial application of the Sakai protocol, the iodine-catalysed lactonisation can be applied for the synthesis of the pyrano[3,2-*b*]pyran lactone **76**, however, further optimisation, especially for the synthesis of the diacid precursor **85**, was needed.

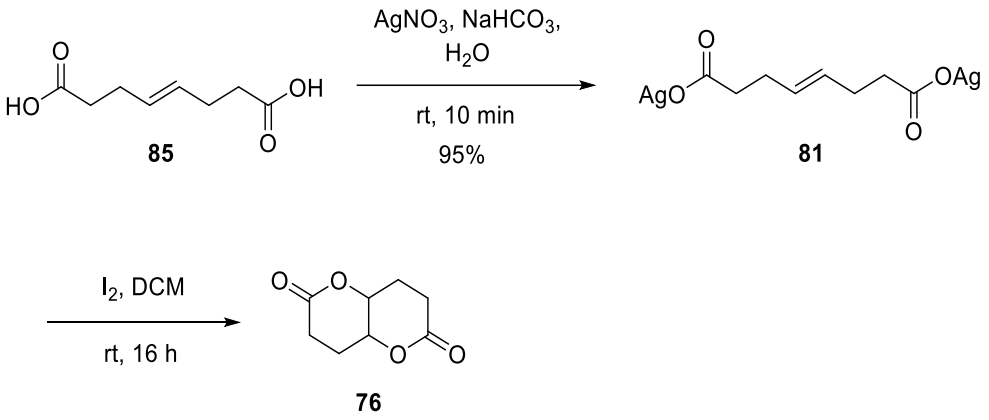

Scheme 3.3.10 Synthesis of the pyrano[3,2-*b*]pyran lactone 76 using the Sakai protocol.

In parallel to the investigation of the Sakai protocol, an alternative approach for the synthesis of the *trans*-4-octene-1,8-dioic acid [**85**] was taken. Instead of using the low yielding Grubbs' metathesis for the formation of the 1,8- diester olefin **84**, which led to product mixtures difficult to purify, a protocol by Lipinski[347] was investigated (see Scheme 3.3.11). *Tert*-butyl acetate was treated with the *in situ* formed LDA prior to its addition to 1,4-dibromobut-2-ene [**86**] undergoing a double nucleophilic substitution to give the 1,8-diester olefin **87**. The use of *tert*-butyl protecting groups was believed to overcome the challenges encountered in the hydrolysis step to obtain the desired diacid **85**. After the full consumption of the starting material, a product was isolated from the reaction after column chromatography. However, the obtained experimental data for the compound recovered from the reaction did not comply with the data reported by Lipinski.

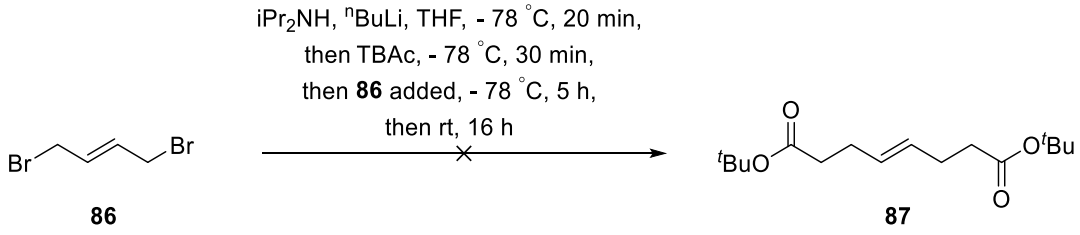

Scheme 3.3.11 Synthesis of the diester 97 using a protocol by Lipinsky[347].

In order to compare the results obtained from reaction in Scheme 3.3.11 to the di-*tert*-butyl ester of interest [**87**], the Grubbs' metathesis approach was revisited using an alternative catalyst. Starting from pent-4-enoic acid [**82**], the carboxylic acid was protected using *tert*-

butanol, DCC and DMAP in dichloromethane to give the olefin bearing a *tert*-butyl ester [**88**] in moderate yield (39%). Next, Grubbs' metathesis using the 2nd generation Hoveyda-Grubbs catalyst in the presence of *p*-benzoquinone to prevent isomerisation[348] was performed, which led to the formation of the desired di-*tert*-butyl ester **87**, however, in low yield (24%). A comparison of the obtained experimental data to one from the previous reaction (Scheme 3.3.11) confirmed, that the isolated compound from the Lipinski protocol was in fact not the di-*tert*-butyl ester **87**. Unfortunately, the use of an alternative Grubbs' catalyst did not increase the yield of the reaction.

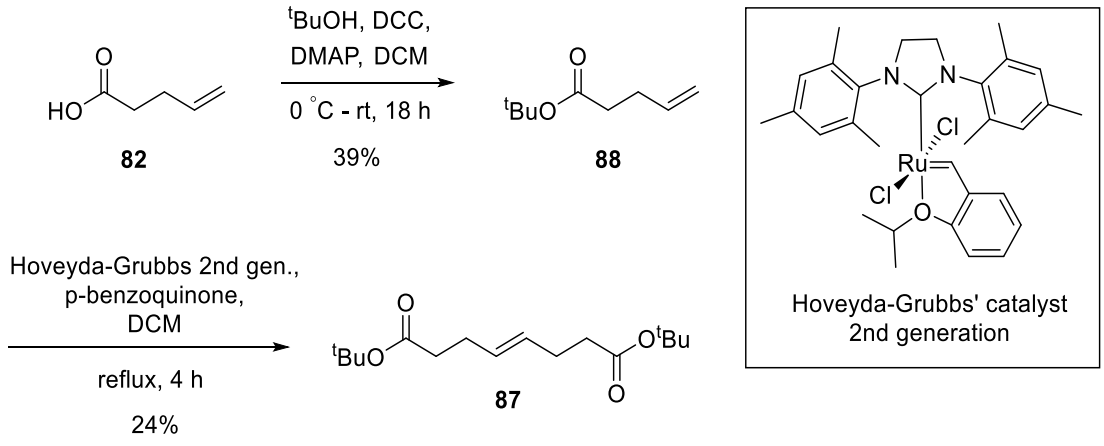

Scheme 3.3.12 Synthesis of the diester 87 via Grubbs metathesis.

At this stage of the research, it was decided to pause the synthesis of the pyrano[3,2-*b*]pyran cross-linker and to mainly concentrate on the synthesis and application of the furo[3,2-*b*]furan cross-linker, since the THF-based bis-lactone precursor **89** could be reproduced quicker and more efficiently in overall two steps from a commercially available starting material.

3.3.3.3 Synthesis of the furo[3,2-*b*]furan lactone via iodine-catalysed lactonisation

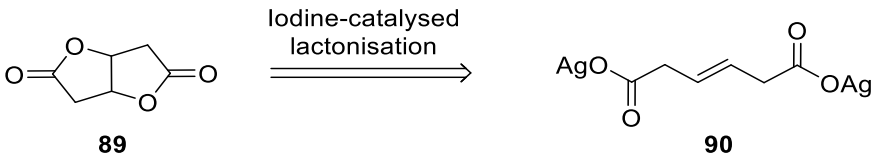

Scheme 3.3.13 Iodine-catalysed lactonisation approach for the synthesis of the bis-lactone 89.

A key factor for the progression of the acid-cleavable cross-linker synthesis was the discovery of the iodine-catalysed lactonisation protocol by Sakai and colleagues.[345] By forming the silver salt of the diacid [**90**] first, Sakai *et al.* have confirmed the formation of the cyclic bis-lactone **89** via a double lactonisation in excellent yield. When the reaction was repeated starting directly from the diacid **91**, only mono-lactonisation was observed. Subsequently, the synthesis of furo[3,2-*b*]furan lactone **89** was commenced with the commercially available *trans*-3-hexene-1,6-dioic acid [**91**] as shown in Scheme 3.3.14.

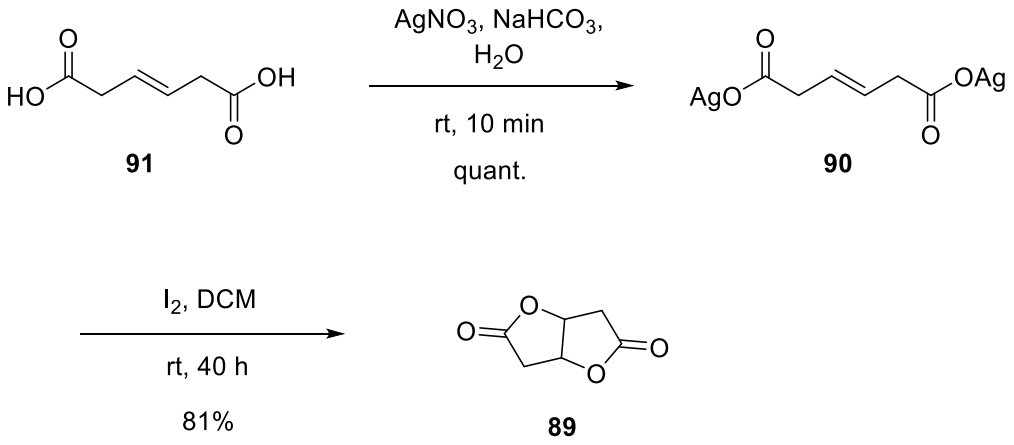

Scheme 3.3.14 Synthesis of the furo[3,2-*b*]furan lactone 89 using the protocol by Sakai[345].

The treatment of the diacid **91** with silver(I) nitrate and sodium bicarbonate in water led to the formation of the disilver dicarboxylate **90** in quantitative yield, which was excessively dried and stored in an amber glass container. The dried disilver dicarboxylate **90** was then exposed to iodine in dichloromethane undergoing double lactonisation to provide the furo[3,2-*b*]furan lactone **89** in excellent yield (81%). The bis-lactone **89** was isolated via recrystallisation, since 2D TLC confirmed its instability towards silica gel chromatography.

3.3.4 Acetalisation of the furo[3,2-*b*]furan lactone

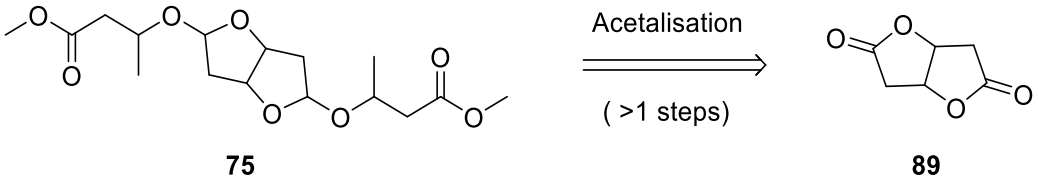

Scheme 3.3.15 Acetalisation of the bis-lactone 89 to give the desired disubstituted acetal 75.

The first approach taken for the acetalisation of the furo[3,2-*b*]furan lactone **89** is shown in Scheme 3.3.16. Double reduction of the bis-lactone **89** using DIBAL (3 equiv., 1 M in toluene) at – 78 °C gave the hemiacetal **92** in good yield (63%). Transetherification of the hemiacetal **92** with methyl 3-hydroxybutanoate catalysed by rhenium(VII) oxide according to the protocol published by Dussault[349] led to the formation of the disubstituted acetal **75** in moderate yield (45%).

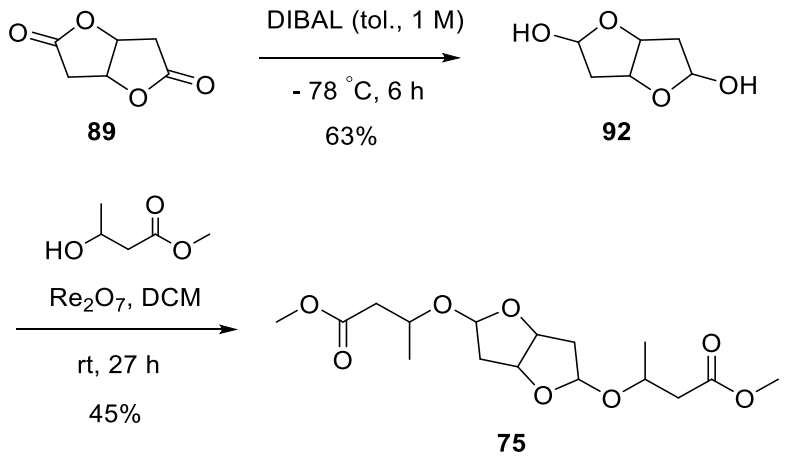

Scheme 3.3.16 Formation of the disubstituted acetal 75 via the reduction of the bis-lactone 89 to the hemiacetal 92 and the subsequent rhenium (VII) oxide catalysed acetalisation of 92.

Since only a small amount of the desired acetal **75** was isolated, which was not enough for the continuity of the synthesis of the desired cross-linker, the reactions were repeated on a larger scale. Upon repeating the reduction of the bis-lactone **89** to obtain the hemiacetal **92** on a 15-fold increase in scale (see Entry b, Table 3.3.1), the reaction mainly showed starting material after exposure to 3 equiv. of DIBAL for 4.5 h. After adding an extra 1 equiv. of DIBAL and

leaving the mixture for another 5 h to react, the reaction did not result in the formation of the hemiacetal **92**, but NMR analysis suggested the decomposition of the bicyclic compound to the tetrahydroxyl compound **93**, which has been reported in the literature as a possible side product.[350] When the reduction of the bis-lactone **89** was repeated on a slight increase in scale (almost 4-fold), a similar observation was made as mainly starting material was observed after reacting it for 5 h with DIBAL with traces of the side product **93** detected in the NMR spectrum (see Entry c).

Table 3.3.1 Reduction of the bis-lactone 89 to the hemiacetal 92.

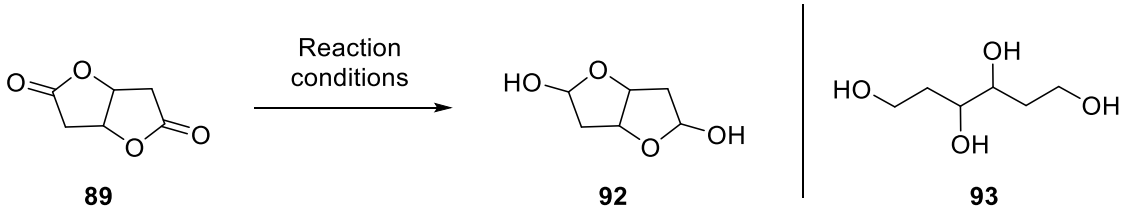

89 **92** **93**

Entry	**Reaction scale**	**Reaction conditions**	**Reaction outcome**
a	0.3 mmol	3 equiv. DIBAL (1 M, tol.) 6 h, - 78 °C	63%
b	4.7 mmol	3 equiv. DIBAL (1 M, tol.), 4.5 h, - 78 °C + 1 equiv. DIBAL (1 M, tol.), 5 h, - 78 °C	mainly starting material, then decomposition to give **93**
c	1.1 mmol	3 equiv. DIBAL (1 M, tol.), 5 h, - 78 °C	mainly starting material, traces of **93**
d	0.5 mmol	Et_2O (0.05 mM), - 78 °C; then 2.1 equiv. DIBAL (1 M, tol.), temperature controlled addition over 1.5 h; stirred at - 78 °C for 4.5 h	**89** : **92** 3 : 1

Consequently, the amount of DIBAL was reduced to 2.1 equivalents, which was added dropwise to the solution of the bis-lactone **89** in diethyl ether keeping the temperature at – 78 °C to avoid the formation of **93** (see Entry d). It was inferred from the NMR spectrum that the desired hemiacetal **92** was slowly being formed in this reaction, however, the major product was in fact the recovered lactone **89** resulting in a ratio of lactone **89** to hemiacetal **92** of 3 : 1.

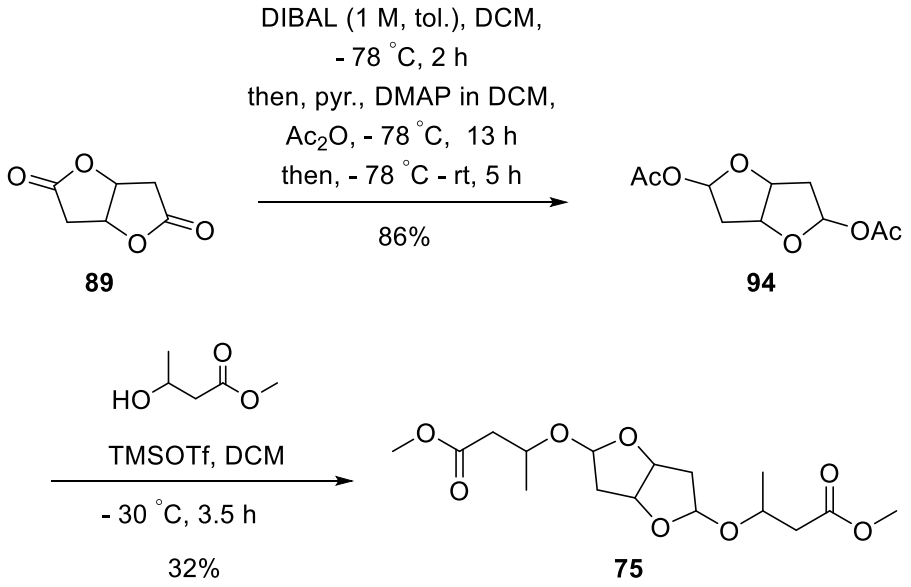

Scheme 3.3.17 An alternative route for the synthesis of the desired disubstituted acetal 75.

It became evident that the DIBAL reduction of the bis-lactone **89** to the hemiacetal **92** was a challenging step in the synthesis of the desired cross-linker as it was not efficient and reproducible upon scale-up. The major drawbacks of the reaction were the instability of the bis-lactone **89** resulting in the opening of the ring structure and the formation of the tetrahydroxy compound **93**. In addition, the high polarity of the hemiacetal **92** and the instability of the bis-lactone **89** made the separation of these compounds impractical. Consequently, an alternative synthetic route was developed to obtain the desired disubstituted acetal **75**, which is displayed in Scheme 3.3.17. The bis-lactone **89** was firstly treated with DIBAL at – 78 ̊C for 2 h resulting in the formation of the aluminium hemiacetal intermediates, which were subsequently acetylated using acetic anhydride, pyridine and DMAP to give the anomeric acetals **94** as a mixture of 3 diastereomers (combined yield: 86%).[351,352] One of the diastereomers could be separated due to a difference in polarity compared to the other two. Consequently, the synthesis was continued with one of the acetal diastereomers, which was exposed to methyl 3-hydroxybutanoate in the presence of TMSOTf at – 30 ̊C for 3.5 h to give the desired disubstituted acetal **75** in moderate yield (32%).[353] Comparing the NMR spectra of the disubstituted acetals obtained from both synthetic routes confirmed that both resulted in formation of the desired product.

3.3.5 The carbonate cross-linker – a backup design

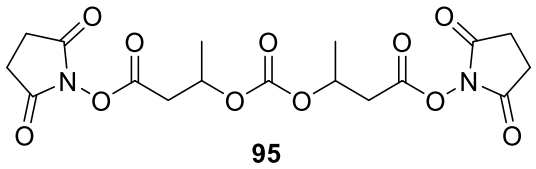

Figure 3.3.3 The carbonate cross-linker.

During our synthetic efforts towards the novel furo[3,2-*b*]furan and pyrano[3,2-*b*]pyran cross-linkers, a backup design of an acid-labile cross-linker was developed given the challenging synthesis encountered. The carbonate functional group was chosen (see Figure 3.3.3) as an additional acid-labile group. Carbonates are known to be more stable than silyl or acetal groups, however, they are also prone to both acidic and basic hydrolysis.[338,354,355]

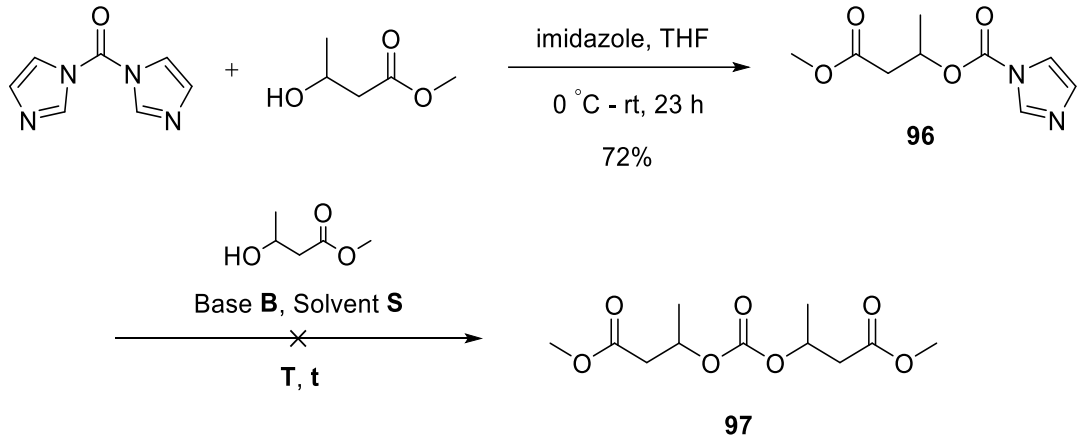

Entry	Base **B**	Solvent **S**	Temperature **T**	Reaction time **t**
a	Et_3N	DCM	rt	15 h
b	Et_3N	MeCN	reflux	18 h
c	NaH	DMF	90 °C	21.5 h

Scheme 3.3.18 Attempted synthesis of the disubstituted carbonate 97 using CDI.

As shown in Scheme 3.3.18, the synthesis of the carbonate cross-linker was started with the nucleophilic substitution of 1,1′-carbonyldiimidazole (CDI) with methyl 3-hydroxybutanoate resulting in the formation of the mono-substituted carbamate **96** in good yield (73%). In order

to achieve the second nucleophilic substitution to obtain the disubstituted carbonate **97**, the carbamate **96** was treated with methyl 3-hydroxybutanoate in the presence of triethylamine in tetrahydrofuran at room temperature, however, only starting material was recovered after the reaction (Entry a). Consequently, the reaction was repeated firstly with triethylamine at reflux in acetonitrile (Entry b) and secondly with sodium hydride in *N,N*-dimethylformamide at 90 ˚C (Entry c). Unfortunately, both reactions did not result in formation of the desired disubstituted carbonate **97**, but starting material was detection after the reactions.

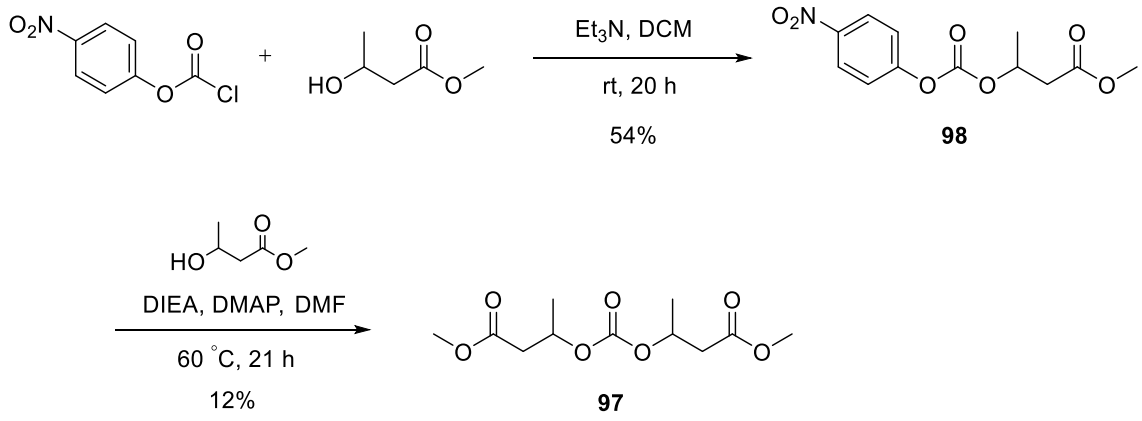

Scheme 3.3.19 Synthesis of the disubstituted carbonate 97 using 4-nitrophenyl chloroformate.

An alternative approach was taken for the synthesis of the disubstituted carbonate **97** as displayed in Scheme 3.3.19. Nucleophilic substitution of 4-nitrophenyl chloroformate with methyl 3-hydroxybutanoate resulted in the mono-substituted carbonate **98** in good yield (54%). Next, the mono-substituted carbonate **98** was treated with methyl 3-hydroxybutanoate and DIEA in the presence of DMAP at 60 ˚C for 21 h leading to the generation of the desired carbonate **97** in low yield (12%). It is noteworthy that several purification attempts (column chromatography and preparative TLC) were made to separate the carbonate product **97** from residual methyl 3-hydroxybutanoate, however, the compounds could not be separated with these methods due to similar polarities. Since the boiling point of methyl 3-hydroxybutanoate was reported to be 80 - 82 ˚C at 22.5 mmHg[356] and the predicted boiling point for the carbonate **97** was found to be 195.57 ± 44.3 ˚C at 22.5 mmHg (calculated using ACD/Labs Software V12.1.0.50374), the mixture was heated *in vacuo* to remove the residual methyl 3-hydroxybutanoate. These purifications attempts might be a reason for the low yield obtained in this reaction, which can now be optimised if this reaction is repeated in the future.

3.4 Conclusion and Future Work

Novel acid-cleavable cross-linkers were designed to overcome the challenges observed in cross-linking mass spectroscopy methods using common non-cleavable or MS-cleavable cross-linkers. Incorporating these acid-labile cross-linkers, a new workflow for XL-MS to analyse PPIs of histone proteins was proposed, which was based on the simultaneously occurring acid-catalysed cleavage of the cross-linked proteins and the resulting derivatisation of lysine residues during acid histone extraction. Two novel linker groups were designed, the pyrano[3,2-*b*]pyran acetal and the furo[3,2-*b*]furan acetal, and their synthetic routes were developed and optimised resulting in the synthesis of the disubstituted furo[3,2-*b*]furan acetal **75** in overall 4 steps (22% over 4 steps), which is the key precursor for the final acetal cross-linker. Similarly, the disubstituted carbonate **97** was also synthesised in overall 2 steps.

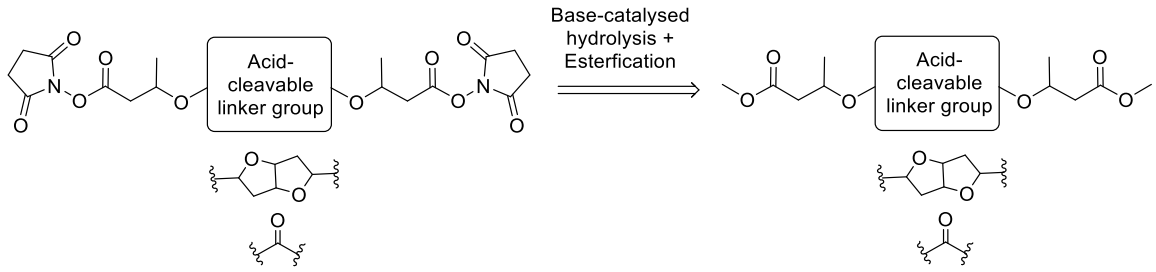

Scheme 3.4.1 Two remaining steps for the synthesis of the acid-cleavable cross-linker. Base-catalysed hydrolysis followed by esterification of the disubstituted precursors leads to the formation of the desired cross-linker functionalised with *N*-hydroxysuccinimide esters.

With the disubstituted acetal and carbonate in hand, the desired acid-cleavable cross-linkers can be synthesised in further 2 steps via base-catalysed hydrolysis and the subsequent esterification with *N*-hydroxysuccinimide in the future (see Scheme 3.4.1). The synthetic route established for the furo[3,2-*b*]furan cross-linker can then be adopted for the synthesis of the pyrano[3,2-*b*]pyran cross-linker. A degradation study to monitor the acid-catalysed decay of the novel cross-linkers in various pH environments can also be beneficial prior their use in the *in vitro* XL-MS experiments. In addition, the acid-cleavable cross-linkers can be tested on model peptide systems to optimise both the cross-linking and the acid-catalysed cleavage procedures.

4 FINAL REMARKS

Two novel approaches, CLICK-seq and XL-MS using acid-cleavable cross-linkers, to study and understand epigenetic events around histone proteins have been proposed in this work and the initial steps towards developing these techniques were taken. Although many challenges were experienced hindering the development of both methods, several new strategies were developed to overcome these obstacles and ensure the continuity of these projects. Numerous novel concepts were developed in this work, which will provide a valuable foundation for future studies.

5 EXPERIMENTAL

5.1 General methods

All reagents were purchased from commercial sources and utilised as supplied from the manufacturers. The palladium precatalysts were obtained from Sigma-Aldrich. The anhydrous solvents used in this project were either purchased from commercial sources (mainly Sigma-Aldrich or Fluorochem) or were freshly distilled under N_2 from calcium hydride (dichloromethane, toluene, triethylamine), magnesium (methanol) and sodium benzophenone (tetrahydrofuran, diethyl ether). The use of water refers to distilled water. Reactions requiring anhydrous conditions were conducted under an atmosphere of dry N_2. The glassware used for the palladium reactions were oven-dried, then directly attached to the Schlenk line and degassed using vacuum and N_2 (3 cycles). The liquid reagents used for the palladium reactions were degassed either via N_2 flow (1 h) or the freeze-pump-thaw method (3 cycles). Room temperature (rt) refers to ambient temperature. Water/ice bath was used to achieve temperatures of 0 ˚C and acetone/dry ice bath was used for temperature below 0 ˚C. Bulk solutions were concentrated using Büchi rotary evaporator and the compounds were dried using high vacuum pumps or a speedvac concentrator (Thermo Scientific Savant). Thin-layer chromatography (TLC) using aluminium plates coated with Merck Kiesegel 60 F254 (230 – 400 mesh) was carried out to monitor the reactions, which were visualised under UV (254 nm) or by staining with potassium permanganate solution, ninhydrin solution, phoshomolybdic acid solution, bromocresol green solution or iodine, as appropiate. Flash column chromatography was carried out using either Merck Kiesegel or Fluorochem 60 silica gel (230–400 mesh, 40 – 63 μm). Preparative TLC plates were purchased from Merck Group.

Hydrogenation reaction were conducted in a 3911 Parr shaker hydrogenator (increased pressure: ~ 3.5 atm). Microwave irradiation was carried out using a Discoverer SP system (CEM Technology). All ^{1}H and ^{13}C NMR spectra were recorded on a Bruker Advance 400 spectrometer at 400 MHz and 101 MHz, respectively. Chemical shifts (δ) in proton spectra are quoted in ppm (parts per million) downfield from Me_4Si and are referenced to a residual solvent signal. The ^{1}H NMR data is reported as follows: chemical shift, multiplicity (s: singlet, d: doublet, t: triplet, m: multiplet, br.: broad signal or a combination of these), coupling constant (in Hz), integration, assignment. DOSY and TOSCY experiments were conducted by Imperial College London, Department of Chemistry, NMR service. High and low resolution mass spectra (HRMS, EI, ESI) were recorded by the Imperial College London, Department of

Chemistry, Mass Spectroscopy Service using Micromass Platform II and Micromass AutoSpeq-Q spectrometers. The LC-MS/MS data was acquired using an LTQ Velos Pro linear ion trap (Thermo Scientific) at the Department of Chemical Engineering, Imperial College London (DiMaggio group). The LC conditions consisted of a linear gradient starting at 100% solvent A (99.4% water, 0.5% acetonitrile and 0.1% formic acid) and 100% B (99.5% acetonitrile and 0.5% water). The tandem mass spectra were collected using electrospray ionisation (ESI) as the primary ionisation method over a mass range of 200 – 2000 m/z and collision ionisation detection (CID) fragmentation with a collision energy of 35%. The software Xcalibur (Thermo Scientific) was used to analyse and visualised the obtained LC-MS/MS data. All solvents used were LC-MS grade and purchased from either Sigma-Aldrich or Fisher Scientific. The Pierce C18 spin columns were supplied from Thermo Fisher Scientific. The synthetic peptide sequence GEAKSQVFK[me3]TNHFQKSTVR was purchased from GenScript and the human native nucleosomes (HeLa derived, product code: 52039) were obtained from AMS Biotechnology (Europe) Limited.

5.2 Experimental for R&D I

5.2.1 General Procedures

General procedure A: Solvent and base studies for the Pd-catalysed Hofmann-type elimination.

N,N,N-Trimethyl-4-phenylbutan-1-aminium iodide [**31**] (1 equiv.), palladium(II) acetate (0.22 equiv., 22 mol%) and tris(2,4,6-trimethoxyphenyl)phosphine (0.58 equiv., 58 mol%) were flushed with N_2 for 1 h in a sealed tube. Solvent **S** (0.05 mM, degassed with N_2 flow for 1 h) and base **B** (4 equiv., degassed with N_2 flow for 1 h, if liquid) were added and the reaction mixture was heated at 80 °C for 24 h in a sealed tube. After cooling down to room temperature, water was added to the mixture and the aqueous layer was extracted with ethyl acetate (5 x). The combined organic layers were concentrated with N_2 flow and analysed via quantitative ^{1}H NMR (400 MHz, CD_3CN) using trimethyl benzene-1,3,5-tricarboxylate (30 µL, 0.1 M in DMSO) as internal standard.

General procedure B: Activation of NHC-Pd precatalyst by base for the Pd-catalysed Hofmann-type elimination.

Trimethylammonium substrate **E** (1 equiv.), NHC-Pd precatalyst **PC** and base **B** were combined, degassed using the Schlenk technique (vacuum + N_2 cycle (3x)) and dissolved in acetonitrile (0.06 mM, degassed via the freeze, pump, thaw method (3 rounds)). The reaction mixture was heated at 80 °C for 22 h. After cooling down to room temperature, the mixture was diluted with dichloromethane (5 mL), filtered through celite and washed with dichloromethane (10 mL). The combined organic layers were concentrated with N_2 flow and analysed via quantitative ^{1}H NMR (400 MHz, CD_3CN) using trimethyl benzene-1,3,5-tricarboxylate (30 µL, 0.1 M in DMSO) as internal standard.

General procedure C: Formation of NHC-palladium precatalysts.

Palladium chloride (1 eqiuv.), NHC ligand (1.1 equiv.), potassium carbonate (5 equiv.) and pyridine (0.20 mmol/mL, 61 equiv.) were mixed and the suspension was heated at 80 °C overnight. After cooling down to room temperature, the reaction mixture was diluted with dichloromethane and filtered through a plug of celite. The filtrate was concentrated *in vacuo*

and triturated with dichloromethane and diethyl ether. The precipitate was collected and washed with diethyl ether to give the desired NHC-palladium precatalysts.

General procedure D: Pierce C18 Spin column purification.

The Pierce C18 Spin Column was activated by adding the prepared activation solution (200 µL, 50% MeOH in H_2O) and centrifuging the column at 1500 x g for 1 min. The activation step was repeated. Next, equilibration solution (200 µL, 0.5% TFA and 5% MeCN in H_2O) was added and the column was centrifuged at 1500 x g for 1 min. This step was repeated again. Sample buffer (25 µL, 2% TFA and 20% MeCN in H_2O) was added to the reacted peptide solution to get a total concentration of 0.5% TFA and 5% MeCN in H_2O (total volume: 1 : 3 sample buffer : peptide solution) and the sample was loaded to the wetted spin column by centrifugation (1500 x g, 1 min). The loading of the sample was repeated to ensure complete binding. The spin column loaded with the peptide sample was washed thrice by adding washing solution (200 µL, 0.5% TFA and 5% MeCN in H_2O) and centrifuging the column at 1500 x g for 1 min. The spin column was placed into a new LoBind Eppendorf tube (1.5 mL) and elution solution (100 µL, 70% MeCN in H_2O) was added and the column centrifuged 1500 x g for 1 min to collect the purified peptide sample. The purified peptides were dried by speedvac evaporation.

5.2.2 Synthesis of trimethyllysine

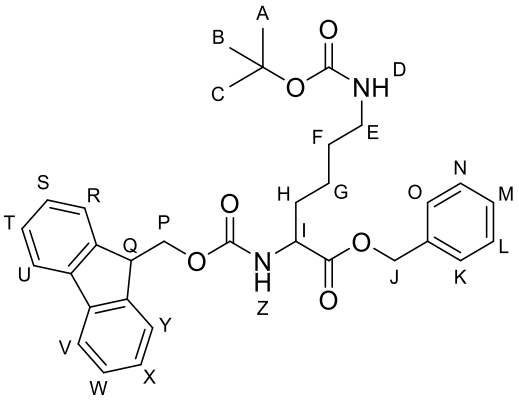

Fmoc-Lys(Boc)-OBn [**10**]: Fmoc-Lys(Boc)-OH (499.7 mg, 1.07 mmol) was dissolved in *N*, *N*-dimethylformamide (5 mL) and potassium carbonate (221.2 mg, 1.60 mmol) was added. The reaction was cooled to 0 ˚C and benzyl bromide (0.14 mL, 1.17 mmol) was slowly added. The mixture was warmed to rt and stirred for 45 h. Ethyl acetate (50 mL) was added and the mixture was washed with aqueous lithium chloride solution (3 x 75 mL, 5%). The organic layer was dried with $MgSO_4$, filtered, concentrated *in vacuo* and purified via column chromatography (pentane : ethyl acetate, 7 : 3) to give **10** as a white solid (500.8 mg, 85%): R_f 0.5 (pentane : ethyl acetate, 8 : 2); ^{1}H NMR (400 MHz, $CDCl_3$) δ 7.76 (d, *J = 7.5 Hz*, 2H, U + V), 7.60 (d, *J = 7.4 Hz*, 2H, R + Y), 7.29 – 7.42 (m, 9H, K – L, S, T, W, X), 5.44 (d, *J = 7.8 Hz*, 1H, Z), 5.10 – 5.23 (m, 2H, J), 4.53 (br. s, 1H, D), 4.34 – 4.46 (m, 3H, P + I), 4.21 (t, *J = 7.0 Hz*, 1H, Q), 2.95 – 3.13 (m, 2H, E), 1.66 – 1.91 (m, 2H, H), 1.43 (s, 9H, A – C), 1.31 – 1.48 (m, 4H, F + G); ^{13}C NMR (100 MHz, $CDCl_3$) δ 172.3, 156.0, 156.0, 143.9, 143.8, 141.3, 135.3, 128.7, 128.5, 128.4, 128.2, 127.7, 127.1, 125.1, 79.2, 67.2, 67.0, 53.8, 47.2, 40.1, 32.2, 29.6, 28.4, 22.3; HRMS (ESI) *m/z* calc for $C_{33}H_{39}N_2O_6$ 559.2808, found: 559.2820.

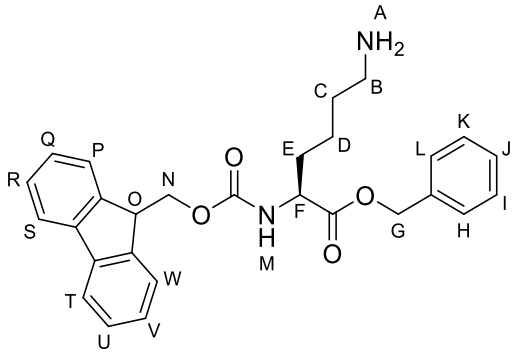

Fmoc-Lys-OBn [**11**]: Fmoc-Lys(Boc)-OBn (200.7 mg, 0.36 mmol) was dissolved in dichloromethane (2.75 mL) and trifluoroacetic acid (2.75 mL) was slowly added and the reaction mixture was stirred at room temperature for 21 h. The mixture was concentrated *in vacuo*, diluted with water (10 mL) and neutralised with aqueous sodium bicarbonate solution (sat.). The aqueous solution was extracted with chloroform (3 x 30 mL) and the combined organic layers were dried with $MgSO_4$, filtered and concentrated *in vacuo* to give **11** as a clear oil (74.1 mg, 45%) (The product was taken on without further purification): ^{1}H NMR (400 MHz, $CDCl_3$) δ 7.76 (d, *J = 7.3 Hz*, 2H, S + T), 7.58 (d, *J = 7.4 Hz*, 2H, P + W), 7.43 – 7.27 (m, 9H, H – L + Q – R + U – V), 5.65 – 5.38 (m, 1H, M), 5.25 – 5.06 (m, 2H, G), 4.47 – 4.31 (m, 3H, F + N), 4.20 (t, *J = 7.0 Hz*, 1H, O), 3.28 (br. s, 3H, A), 2.64 (t, *J = 6.9 Hz*, 2H, B), 1.91 – 1.77 (m, 1H, E^a), 1.74 – 1.59 (m, 1H, E^b), 1.52 – 1.31 (m, 4H, C + D); ^{13}C NMR (100 MHz, $CDCl_3$) δ 172.5, 156.1, 144.0, 143.9, 141.4, 135.4, 128.8, 128.7, 128.5, 127.8, 127.2, 125.1, 120.1, 67.3, 67.2, 54.0, 47.3, 41.4, 32.4, 31.9, 22.5; HRMS (ESI) *m/z* calc for $C_{28}H_{31}N_2O_4$ 459.2284, found: 459.2290.

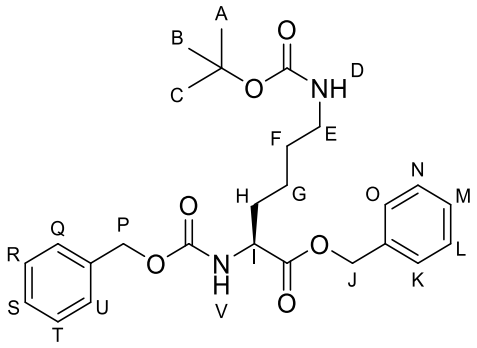

Cbz-Lys(Boc)-OBn [**15**]: Cbz-Lys(Boc)-OH (511.4 mg, 1.35 mmol) was dissolved in dry *N,N*-dimethylformamide (5 mL) and potassium carbonate (273.6 mg, 1.98 mmol) and benzyl bromide (0.18 mL, 1.45 mmol) were added. The reaction mixture was stirred at room temperature for 45 h. Next, the mixture was diluted with ethyl acetate (50 mL) and washed with aqueous lithium chloride solution (3 x 75 mL, 5%). The organic phase was dried with $MgSO_4$, filtered, concentrated *in vacuo* and purified via column chromatography (pentane : ethyl acetate, 7 : 3) to give **15** as a white solid (598.2 mg, 97%): R_f 0.6 (pentane : ethyl acetate, 7 : 3); ^{1}H NMR (400 MHz, $CDCl_3$) δ 7.39 – 7.29 (m, 10H, K – O, Q – U), 5.41 (d, *J = 8.1 Hz*, 1H, V), 5.21 – 5.13 (m, 2H, J), 5.10 (s, 2H, P), 4.52 (br. s, 1H, D), 4.40 (td, *J = 8.0, 4.8 Hz*, 1H, I), 3.07 – 3.00 (m, 2H, E), 1.89 – 1.64 (m, 2H, H), 1.42 (s, 9H, A - C), 1.52 – 1.21 (m, 4H, F + G); ^{13}C NMR (100 MHz, $CDCl_3$) δ 172.2, 156.0, 156.0, 136.2, 135.3, 128.6, 128.5, 128.4, 128.2, 128.1,79.2, 67.2, 67.0, 53.8, 40.0, 32.2, 29.6, 28.4, 22.3; HRMS (ESI) *m/z* calc for $C_{26}H_{35}N_2O_6$ 471.2495, found: 471.2500.

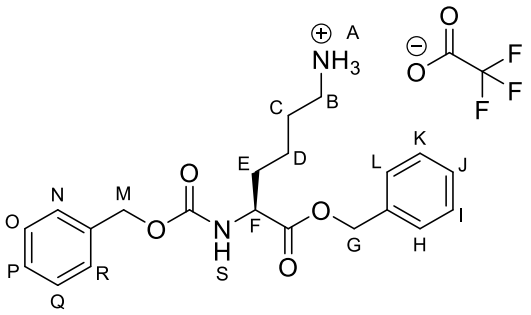

Cbz-Lys-OBn · TFA [**18**]: Cbz-Lys(Boc)-OBn [**15**] (427.4 mg, 0.91 mmol) was dissolved in dichloromethane (8 mL) and cooled to 0 ˚C. Trifluoroacetic acid (2 mL, 26.12 mmol) was added to the solution and the reaction was stirred at 0 ˚C for 5 h. Next, the solution was concentrated *in vacuo*, washed with dichloromethane (4 x 20 mL) and concentrated *in vacuo* to give **18** as a clear oil (518.9 mg, quant.) (The product was taken on without further purification): ^{1}H NMR (400 MHz, $CDCl_3$) δ 7.53 (br. s, 3H, A), 7.33 – 7.22 (m, 10H, H -L, N -R), 5.61 (d*, J = 8.2 Hz*, 1H, S), 5.30 (s, 1H, G^a), 5.18 – 5.11 (m, 1H, G^b), 5.10 – 5.01 (m, 2H, M), 4.36 – 4.31 (m, 1H, F), 2.92 – 2.82 (m, 2H, B), 1.85 – 1.54 (m, 4H, E + C), 1.40 – 1.29 (m, 2H, D); ^{13}C NMR (100 MHz, $CDCl_3$) δ 172.0, 161.08, 156.5, 135.9, 135.0, 128.7, 128.6, 128.4, 128.0, 117.0, 114.1, 67.5, 67.4, 53.4, 39.7, 31.9, 26.5, 21.7; HRMS (ESI) *m/z* calc for $C_{21}H_{27}N_2O_4$ 371.1971, found: 371.1980.

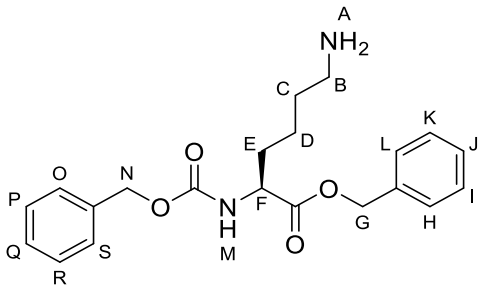

Cbz-Lys-OBn [**16**]: Cbz-Lys(Boc)-OBn [**15**] (507.4 mg, 1.08 mmol) was dissolved in dichloromethane (5.4 mL) and cooled to 0 ˚C. Trifluoroacetic acid (3.6 mL, 47.01 mmol) was added to the solution and the reaction was stirred at 0 ˚C for 1 h 30 min. Next, the mixture was concentrated *in vacuo*, then diluted in water (10 mL) and neutralised with aqueous sodium bicarbonate (sat.). The aqueous layer was extracted with dichloromethane (3 x 30 mL) and the organic layers were combined, dried with $MgSO_4$, filtered and concentrated *in vacuo* to give **16** as a clear oil (259.9 mg, 65%) (The product was taken on without further purification): ^{1}H NMR (400 MHz, $CDCl_3$) δ 7.40 – 7.27 (m, 10H, H – L + O – S), 5.46 (d, *J = 8.3 Hz*, 1H, M), 5.22 – 5.09 (m, 4H, G + N), 4.46 – 4.36 (m, 1H, F), 2.61 (t, *J = 6.7 Hz*, 2H, B), 1.98 (br. s, 2H, A), 1.90 – 1.78 (m, 1H, E^a), 1.74 – 1.61 (m, 1H, E^b), 1.48 – 1.23 (m, 4H, C + D); ^{13}C NMR (100 MHz, $CDCl_3$) δ 172.5, 156.0, 136.4, 135.4, 128.7, 128.7, 128.6, 128.5, 128.3, 128.2, 67.2, 67.1, 54.0, 41.8, 33.0, 32.5, 22.5; HRMS (ESI) *m/z* calc for $C_{21}H_{27}N_2O_4$ 331.1971, found: 331.1981.

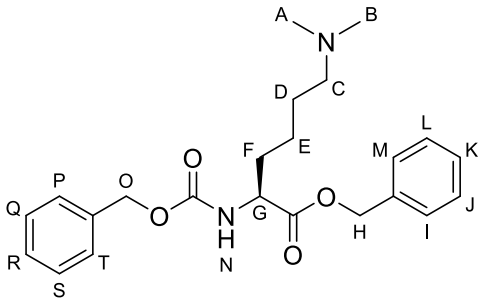

Cbz-Lys(NMe$_2$)-OBn [**17**]: *Method A*: Formaldehyde solution (0.4 mL, 14.1 mmol, 37 wt.% in water) was added to a solution of Cbz-Lys-OBn [**16**] (250.0 mg, 0.70 mmol) in acetonitrile (25 mL) and the mixture was stirred at room temperature for 15 min. Then, sodium cyanoborohydride (88.3 mg, 1.41 mmol) was added and the reaction mixture was stirred for 15 min. Next, acetic acid (5.0 mL, 87.3 mmol) was added and the mixture was stirred for 47 h. After acetonitrile was removed *in vacuo*, the residue was diluted in water (10 mL) and neutralised with aqueous sodium bicarbonate solution (sat.). The aqueous layer was extracted with chloroform (4 x 50 mL). The combined organic layers were dried with $MgSO_4$, filtered, concentrated *in vacuo* and purified via column chromatography (chloroform : methanol, 85 : 15) to give **17** as a clear oil (75.8 mg, 28%).

Method B: Formaldehyde solution (0.04 mL, 1.56 mmol, 37 wt.% in water) was added to a solution of Cbz-Lys-OBn · TFA [**18**] (208.6 mg, 0.43 mmol) in methanol (8.6 mL). After stirring the reaction mixture at room temperature for 30 min, sodium cyanoborohydride (135.3 mg, 2.15 mmol) was added and the mixture was stirred for 19 h. Next, methanol was removed *in vacuo* and the residue was diluted in brine (20 mL). The aqueous layer was extracted with chloroform (3 x 50 mL). The organic layers were combined, dried with $MgSO_4$, filtered, concentrated *in vacuo* and purified via column chromatography (chloroform : methanol, 85 : 15) to give **17** as a clear oil (92.3 mg, 54%): R_f 0.4 (chloroform : methanol, 8.5 : 1.5); ^{1}H NMR (400 MHz, $CDCl_3$) δ 7.41 – 7.28 (m, 10H, I – M + P – T), 5.49 (d, *J = 8.2 Hz*, 1H, N), 5.23 – 5.07 (m, 4H, H + O), 4.44 – 4.37 (m, 1H, G), 2.33 – 2.25 (m, 8H, A – C), 1.91 – 1.80 (m, 1H, F^a), 1.75 – 1.63 (m, 1H, F^b), 1.56 – 1.43 (m, 2H, D), 1.41 – 1.22 (m, 2H, E); ^{13}C NMR (100 MHz, $CDCl_3$) δ 172.4, 156.1, 136.4, 135.5, 128.8, 128.7, 128.6, 128.5, 128.3, 128.2, 67.3, 67.1, 58.8, 54.0, 44.8, 32.2, 26.4, 22.9; HRMS (ESI) *m/z* calc for $C_{23}H_{31}N_2O_4$ 399.2287, found: 399.2284.

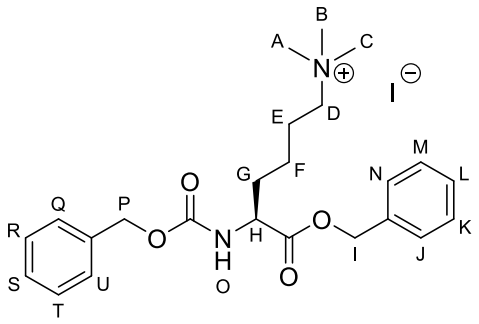

Cbz-Lys($^{+}$NMe$_3$)-OBn · I^{-} [**19**]: Methyl iodide (0.04 mL, 0.68 mmol) was added to a solution of Cbz-Lys(NMe$_2$)-OBn [**17**] (245.8 mg, 0.62 mmol) in tetrahydrofuran (10 mL) and the mixture was stirred at room temperature for 24 h. The reaction mixture was concentrated *in vacuo*, redissolved in dichloromethane (10 mL) and concentrated *in vacuo* (repeated 5 x) to give **19** as a white solid (332.1 mg, quant.): ^{1}H NMR (400 MHz, CD$_3$CN) δ 7.42 – 7.30 (m, 10H, J – N + Q – U), 6.17 (d, *J = 8.2 Hz*, 1H, O), 5.19 – 5.06 (m, 4H, I + P), 4.28 – 4.18 (m, 1H, H), 3.27 – 3.20 (m, 2H, D), 3.03 (s, 9H, A – C), 1.91 – 1.81 (m, 2H, G), 1.79 – 1.65 (m, 4H, E + F); ^{13}C NMR (100 MHz, CD$_3$CN) δ 173.0, 157.2, 138.0, 137.0, 129.5, 129.4, 129.2, 129.0, 128.9, 128.6, 67.5, 67.1, 66.2, 54.8, 53.9, 53.8, 53.8, 31.5, 23.0, 22.9; MS (ES) *m/z* 413.06 (M^{+}, 100%).

5.2.3 First generation Hofmann elimination screening

Hofmann elimination using common inorganic and organic bases (Table 2.1.3)

Cbz-Lys($^{+}$NMe$_3$)-OBn • I$^-$ [**19**] (1 equiv.) was dissolved in solvent **S** and base **B** was added. The reaction mixture was heated at temperature **T** in a sealed tube. After the reaction time **t** was completed, the reaction mixture was filtered through cotton wool, concentrated *in vacuo*, dissolved in the MS eluent, filtered through a PTFE syringe filter and analysed via LC-MS (see table below for details).

Entry	B	S	T	t	Reaction outcome
a	5 equiv. Ag_2O*	MeOH : H_2O, (2 : 1) 0.01 mM	100 °C	2 d	Major P: Cbz-Lys($^{+}$NMe$_3$)-OBn • I$^-$ Traces: Cbz-Lys(NMe_2)-OBn
b	1.5 equiv. NaOH	MeOH : H_2O ,(2 : 1) 0.004 mM	150 °C (MW)	18 h	Major P: Cbz-Lys(OH)-OH Minor P: Cbz-Lys(NMe_2)-OBn
c	10 equiv. NaOH	DMF 0.01 mM	145 °C	1 d	Detected compounds summarised in the total ion chromatograms below: Cbz-Lys(alkene)-OH (product, green) Cbz-Lys(NMe_2)-OH (side prod., red) Cbz-Lys($^{+}$NMe$_3$)-OBn • I$^-$ (SM, grey) Cbz-Lys(OH)-OBn (side prod., blue) Cbz-Lys(NH_2)-OBn (side prod., light red, right side)
d	10 equiv. K_2CO_3	DMF 0.01 mM	145 °C	3 d	
e	10 equiv. piperidine	DMF 0.01 mM	145 °C	2 d	
f	10 equiv. DIPA	DMF 0.01 mM	145 °C	1 d	

*freshly synthesised from silver(I) nitrate (1 equiv.) and potassium hydroxide (1.1 equiv.) in water.

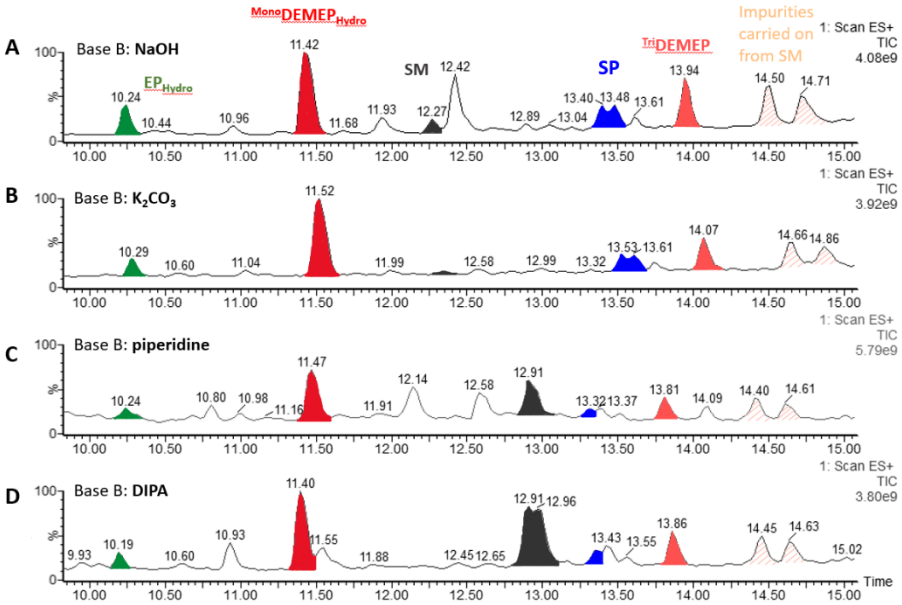

Hofmann elimination using non-nucleophilic bases (Table 2.1.4)

Base **B** (10 equiv.) was added to a solution of Cbz-Lys($^{+}$NMe$_3$)-OBn • I^{-} [**19**] (1 equiv.) in *N,N*-dimethylformamide (0.01 mM) and the reaction was heated at 70 ˚C for 2 d in a sealed tube. Next, the reaction mixture was concentrated *in vacuo*, dissolved in the MS eluent, filtered through a PTFE syringe filter and analysed via LC-MS (see table below for details).

Entry	**B**	**Reaction outcome**
a*	DBU	Complex mixture: Previous side products were prevented, but harsh conditions led to the decomposition of the SM. Traces of Cbz-Lys(alkene)-OBn (product) were detected.
b	DBU	Complex mixture, but desired alkene product was not detected.
c	BTMG**	Complex mixture, but desired alkene product was not detected.
d	proton sponge	Complex mixture, but desired alkene product was not detected.
f	KHMDS***	Complex mixture, but desired alkene product was not detected.

*Reaction was heated at 145 ˚C; **2-*tert*-butyl-1,1,3,3-tetramethylguanidine; ***potassium bis(trimethylsilyl)amide.

5.2.4 Second generation Hofmann elimination screening

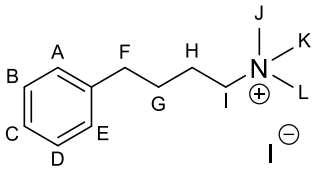

***N,N,N*-trimethyl-4-phenylbutan-1-aminium iodide** [**31**]: Methyl iodide (0.75 mL, 12 mmol) was added to a solution of 4-phenylbutylamine (0.32 mL, 2 mmol) in tetrahydrofuran (2 mL). The reaction was stirred at room temperature for 3 h. The precipitate was collected, washed with tetrahydrofuran (2 mL) and dried to give **31** as a white solid (0.23 g, 36%): ^{1}H NMR (400 MHz, CD_3CN) δ 7.32 – 7.18 (m, 5H, A – E), 3.30 – 3.25 (m, 2H, I), 3.02 (s, 9H, J – L), 2.67 (t, *J = 8.0 Hz*, 2H, F), 1.79 – 1.71 (m, 2H, H), 1.67 – 1.59 (m, 2H, G); ^{13}C NMR (100 MHz, CD_3CN) δ ; 141.7, 128.4, 128.4, 126.0, 66.3, 52.9, 52.9, 52.9, 34.6, 27.7, 22.1; HRMS (ESI) *m/z* calc for $C_{13}H_{22}N$ 192.1752, found: 192.1750.

A small selection of non-nucleophilic bases in combination with various solvents for the Hofmann elimination (Table 2.1.5)

N,N,N-trimethyl-4-phenylbutan-1-aminium iodide [**31**] (10 mg, 0.031 mmol) was dissolved in solvent **S** (1 mL) and base **B** (0.313 mmol, 10 equiv.) was added. The reaction was heated in a sealed tube to 75 ˚C for 48 h. Water (2 mL) was added to the mixture at room temperature and the reaction solution was extracted with ethyl acetate (2 x 1 mL). The combined organic layers were washed with water (2 mL) and the aqueous phase was extracted with ethyl acetate (2 mL). The organic layers were combined, concentrated via N_2 flow and the reaction outcome was analysed via quantitative ^{1}H NMR (400 MHz, CD_3CN) using trimethyl benzene-1,3,5-tricarboxylate (30 μL, 0.1 M in DMSO) as internal standard (see Table below for details).

*No product was detected, only SM		**B**				
		DBU	DBN	TBD***	Proton sponge	BTMG
S	DMF**	*	*	*	*	*
	DMSO	*	*	*	*	*
	MeCN	*	*	*	*	*

**Aqueous lithium hydroxide solution (5%) was used instead of water. ***1,5,7-triazabicyclo(4.4.0)dec-5-en.

Effect of temperature on the Hofmann elimination using DBU (Table 2.1.6)

N,N,N-trimethyl-4-phenylbutan-1-aminium iodide [**31**] (15 mg, 0.047 mmol) was dissolved in *N,N*-dimethylformamide (1 mL) and DBU (0.14 mL, 0.94 mmol, 20 equiv.) was added. The reaction was heated in a sealed tube at temperature **T**. After the completion of the reaction time **t**, the mixture was cooled to room temperature and aqueous lithium hydroxide solution (2 mL, 5%) was added. Next, the aqueous layer was extracted with ethyl acetate (5 x 5 mL). The organic layers were combined, concentrated with N_2 flow and analysed via quantitative ^{1}H NMR (400 MHz, CD_3CN) using trimethyl benzene-1,3,5-tricarboxylate (30 µL, 0.1 M in DMSO) as internal standard (see table below for details).

Entry	**T**	**t**	Reaction outcome
a	75 °C	3 d	Mainly SM, no alkene product detected.
b	100 °C	3 d	Mainly SM, no alkene product detected.
c	125 °C	3 d	Mainly SM, no alkene product detected.
d	150 °C	3 d	Traces of alkene product detected (< 0.5%).
e*	200 °C	2 d	Traces of alkene product detected (< 0.5%).

*neat, no solvent used.

Expanding the library of bases investigated for the Hofmann elimination (Table 2.1.7)

Hofmann elimination with potassium bases and 18-crown-6:

N,N,N-trimethyl-4-phenylbutan-1-aminium iodide [**31**] (1 equiv.) was dissolved in *N,N*-dimethylformamide (0.04 mM) and base **B** (20 equiv.) and 18-crown-6 (1 equiv., dried excessively) was added. The reaction was heated in a sealed tube at temperature **T** for 5 d. Next, the mixture was cooled down to room temperature and aqueous lithium hydroxide solution (2 mL, 5%) was added. Next, the aqueous layer was extracted with ethyl acetate (5 x 5 mL). The organic layers were combined, concentrated with N_2 flow and analysed via quantitative ^{1}H NMR (400 MHz, CD_3CN) using trimethyl benzene-1,3,5-tricarboxylate (30 µL, 0.1 M in DMSO) as internal standard (see table below for details).

Entry	**B**	**T**	Reaction outcome
a	KO^{t}Bu	150 °C	Traces of alkene product detected (< 0.1%).
b	KF	150 °C	Mainly SM, no alkene product detected.
c*	KOPh	125 °C	Mainly SM, no alkene product detected.

*KOPh was synthesised with phenol (1 equiv.) and potassium hydroxide (1 equiv.) in water.

Hofmann elimination with aqueous ammonium bicarbonate solution:

N,N,N-trimethyl-4-phenylbutan-1-aminium iodide [**31**] (15 mg, 0.05 mmol) was dissolved in aqueous ammonium bicarbonate solution (2 mL, 100 mM) and the reaction mixture was heated at 125 °C for 3 d in a sealed tube. After cooling the mixture down to room temperature, the aqueous solution was extracted with ethyl acetate (3 x 5 mL). The organic layers were combined, concentrated with N_2 flow and analysed via quantitative ^{1}H NMR (400 MHz, CD_3CN) using trimethyl benzene-1,3,5-tricarboxylate (30 µL, 0.1 M in DMSO) as internal standard. The NMR spectrum revealed that the desired alkene product was not formed, but mainly starting material was present.

5.2.5 Micelle-catalyzed elimination of phenylbutyl trimethylamine

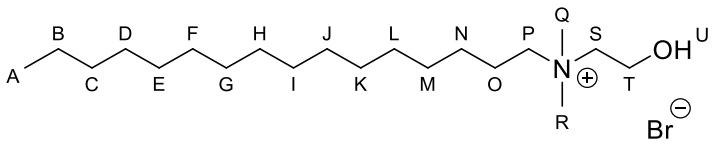

***N*-(2-hydroxyethyl)-*N*,*N*-dimethylhexadecan-1-aminium bromide (CDHAB)** [**35**]: 1-Bromohexadecane (342.5 mg, 1.12 mmol) and 2-(dimethylamino)ethan-1-ol (0.11 mL, 1.12 mmol) was dissolved in methanol : dichloromethane (3 : 1, 1.6 mL) and the reaction mixture was stirred under reflux for 24 h. The reaction was concentrated *in vacuo* to give **35** as a white solid (515.6 mg, quant.) (The product was taken on without further purification): ^{1}H NMR (400 MHz, CD_3OD) δ 4.00 – 3.97 (m, 2H, T), 3.50 – 3.45 (m, 2H, S), 3.44 – 3.37 (m, 2H, P), 3.16 (s, 6H, Q + R), 1.87 – 1.72 (m, 2H, O), 1.47 – 1.20 (m, 27H, B – N, U), 0.93 – 0.87 (m, 3H, A); ^{13}C NMR (100 MHz, CD_3OD) δ 66.8, 66.5, 56.9, 52.2, 33.1, 30.8, 30.7, 30.6, 30.6, 30.5, 30.2, 27.4, 23.7, 23.7, 14.4; HRMS (ESI) *m/z* calc for $C_{20}H_{44}NO$ 314.3423, found: 314.3430.

Micelle-catalysed Hofmann elimination screening

N,N,N-trimethyl-4-phenylbutan-1-aminium iodide [**31**] (15 mg, 0.047 mmol), base **B** and cationic surfactant **CS** was dissolved in solvent **S** and the solution was mixed for 5 min via vortex agitation (up to 1400 rpm) and then heated at temperature **T** in a sealed tube. After the completion of the reaction time **t**, the aqueous solution was extracted with ethyl acetate (5 x 5 mL). The organic layers were combined, concentrated with N_2 flow and analysed via quantitative ^{1}H NMR (400 MHz, CD_3CN) using trimethyl benzene-1,3,5-tricarboxylate (30 µL, 0.1 M in DMSO) as internal standard. The NMR analysis revealed that minimal formation of the desired alkene product occurred in some reactions (see table below for details) but mainly starting material was present.

Entry	**CS**	**B**	**S**	**T**	**t**	Conversion to **Product**
a	CDHAB [**35**] (0.099 M)	NaOH (0.186 M)	water	39 °C	13 d	2%
b	CDHAB [**35**] (0.099 M)	NaOH (2 M)	water	39 °C	7 d	< 1%
c	CDHAB [**35**] (0.5 M)	NaOH (0.94 M)	water	39 °C	7 d	3%
d	CDHAB [**35**] (0.2 M)	NaOH (1 M)	water	60 °C	7 d	-
e	CTAB (0.2 M)	NaOH (1 M)	water	60 °C	7 d	-
f	CDHAB [**35**] (0.099 M)	NaOH (0.186 M)	acetonitrile	39 °C	7 d	2%

5.2.6 Pd-catalyzed Hofmann-type elimination on model small molecules

5.2.6.1 Synthetic procedures

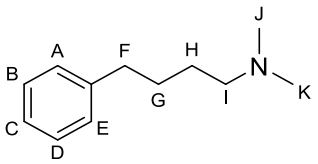

***N,N*-Dimethyl-4-phenylbutan-1-amine** [**39**]: 4-Phenylbutan-1-amine (3.0 mL, 20.0 mmol) was cooled to 0 ˚C and formic acid (3.6 mL, 94.9 mmol) was slowly added. Next, formaldehyde solution (3.8 mL, 41.8 mmol, 36 wt.% in water) was added at 0 ˚C and the mixture was warmed up to room temperature and subsequently heated under reflux for 42 h. After cooling down to room temperature, aqueous hydrogen chloride solution (11 mL, 3.5 M) was added and the mixture was stirred for 5 min. The reaction mixture was concentrated to dryness, dissolved in water (15 mL) and aqueous sodium hydroxide solution (~ 25 mL, 5 M) was added until pH 12 was reached. The aqueous solution was extracted with diethyl ether (4 x 75 mL). The organic layers were combined, dried with $MgSO_4$, filtered and concentrated *in vacuo* to give **39** as a clear oil (2.73 g, 81%) (The product was taken on without further purification): ^{1}H NMR (400 MHz, $CDCl_3$) δ 7.30 – 7.15 (m, 5H, A – E), 2.63 (t, *J = 8.0 Hz*, 2H, I), 2.28 – 2.25 (m, 2H, F), 2.20 (s, 6H, J + K), 1.68 – 1.59 (m, 2H, H), 1.54 – 1.46 (m, 2H, G); ^{13}C NMR (100 MHz, $CDCl_3$) δ 142.5, 128.4, 128.2, 125.7, 59.8, 45.6, 35.9, 29.3, 27.5; HRMS (ESI) *m/z* calc for $C_{12}H_{20}N$ 178.1596, found: 178.1596.

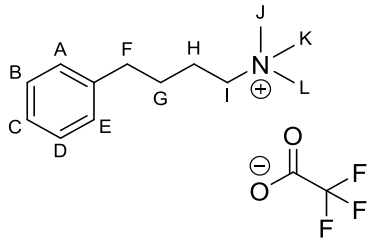

***N,N,N*-trimethyl-4-phenylbutan-1-aminium trifluoromethanesulfonate** [**41**]: *N,N*-Dimethyl-4-phenylbutan-1-amine [**39**] (414.1 mg, 2.34 mmol) was dissolved in anhydrous diethyl ether (10 mL) and methyl triflate (0.32 mL, 2.80 mmol) was slowly added to the solution at 0 ˚C. Then, the reaction was warmed up to room temperature and stirred for 1 h. The resulting white precipitate was collected, washed with diethyl ether (20 mL) and dried *in vacuo* to give **41** as a white solid (796.3 mg, quant.): ^{1}H NMR (400 MHz, CD_3CN) δ 7.31 – 7.19 (m, 5H, A – E), 3.25 – 3.21 (m, 2H, I), 2.99 (s, 9H, J – L), 2.67 (t, *J = 8.0 Hz*, 2H, F), 1.79 – 1.71 (m, 2H, H), 1.67 – 1.59 (m, 2H, G); ^{13}C NMR (100 MHz, CD_3CN) δ 142.7, 129.4, 129.3, 127.0, 67.4, 67.3, 53.9, 53.8, 53.8, 35.6, 28.7, 23.1; HRMS (ESI) *m/z* calc for $C_{13}H_{22}N$ 192.1752, found: 192.1745.

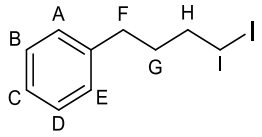

(4-Iodobutyl)benzene [**43**]: Triphenyl phosphine (2.58 g, 9.83 mmol) was dissolved in dichloromethane (20 mL) and iodine (2.49 g, 9.83 mmol) was added. After stirring at room temperature for 15 min, the red solution was turned yellow and imidazole (1.11 g, 16.38 mmol) was added. The reaction mixture was stirred for 10 min and 4-phenylbutan-1-ol (1 mL, 6.55 mmol) and dichloromethane (10 mL) was added. The mixture was stirred at room temperature for 3 h. Aqueous sodium bisulfite solution (60 mL, sat.) was added and the aqueous layer was extracted with dichloromethane (3 x 100 mL). The combined organic layers were dried with $MgSO_4$, concentrated *in vacuo* and purified via column chromatography (pentane, 100%) to give **43** as a clear oil (1.55 g, 91%): ^{1}H NMR (400 MHz, $CDCl_3$) δ 7.31 – 7.17 (m, 5H, A – E), 3.20 (t, *J = 6.9 Hz*, 2H, I), 2.64 (t, *J = 7.5 Hz*, 2H, F), 1.90 – 1.83 (m, 2H, H), 1.78 – 1.70 (m, 2H, G); ^{13}C NMR (100 MHz, $CDCl_3$) δ 141.9, 128.5, 126.0, 34.9, 33.1, 32.3, 6.8; HRMS (ESI) *m/z* calc for $C_{10}H_{13}I$ 260.0062, found: 260.0057.

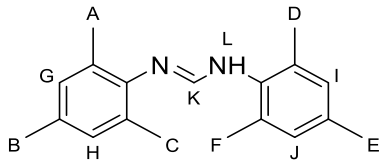

***N,N*-Dimesitylformimidamide** [**52**]: 2,4,6-Trimethylaniline (10.1 mL, 72.15 mmol), acetic acid (0.1 mL, 1.80 mmol) and methyl chloroformate (6.0 mL, 36.07 mmol) were mixed and the solution was heated up to 160 ˚C for 2 h 30 min. After cooling down to room temperature, the reaction was triturated with cold pentane (50 mL) and the resulting white solid was isolated via vacuum filtration and washed with cold pentane (50 mL) to give **52** as a white solid (10.01 g, 99%): ^{1}H NMR (400 MHz, $CDCl_3$) δ 7.19 (d, *J = 10.6 Hz*, 1H, K), 6.92 – 6.87 (m, 4H, G - J), 5.50 (d, *J = 9.9 Hz*, 1H, L), 2.28 – 2.20 (m, 18H, A – F); ^{13}C NMR (100 MHz, $CDCl_3$) δ 147.3, 142.7, 136.2, 134.0, 132.3, 129.4, 129.1, 129.0, 128.5, 20.9, 20.9, 18.8, 18.0; HRMS (ESI) *m/z* calc for $C_{19}H_{25}N_2$ 281.2018, found: 281.2020.

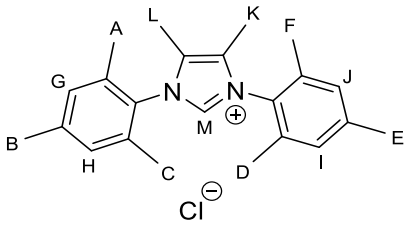

1,3-Dimesityl-4,5-dimethyl-1*H*-imidazol-3-ium chloride [**53**]: *N,N*-Dimesityl-formimidamide [**52**] (1.38 g, 4.92 mmol) was dissolved in acetonitrile (10 mL) and both *N,N*-diisopropylethylamine (1.03 mL, 5.91 mmol) and 2-chloro-3-butanone (1.0 mL, 9.84 mmol) were added to the solution. The reaction mixture was heated at 110 ˚C for 14 h. The solution was concentrated *in vacuo* and dissolved in toluene (12 mL). Aqueous hydrogen chloride solution (0.6 mL, 37%) and acetic anhydride (1.4 mL, 14.76 mmol) were added to the solution and the mixture was heated at 90 ˚C for 24 h. Next, the reaction mixture was diluted with water (100 mL) and extracted with dichloromethane (3 x 150 mL). The organic layers were collected, dried with $MgSO_4$, concentrated *in vacuo* and triturated with dichloromethane and diethyl ether to obtain **53** as an off-white solid (594.7 mg, 33%): ^{1}H NMR (400 MHz, $CDCl_3$) δ 10.50 (s, 1H, M), 7.01 (s, 4H, G -J), 2.32 (s, 6H, B + E), 2.08 (s, 12H, A, C, F, D), 2.04 (s, 6H, L + K); ^{13}C NMR (100 MHz, $CDCl_3$) δ 141.3, 137.7, 134.7, 130.0, 128.9, 127.5, 21.3, 17.7, 8.7; HRMS (ESI) *m/z* calc for $C_{23}H_{29}N_2$ 333.2331, found: 333.2329.

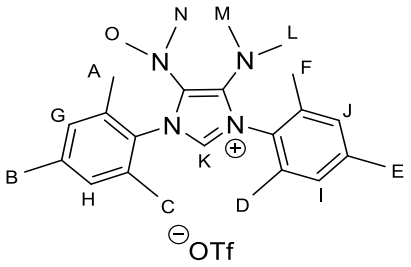

4,5-Bis(dimethylamino)-1,3-dimesityl-1H-imidazol-3-ium trifluoromethanesulfonate [**55**]: *n*-Butyllithium solution (1.8 mL, 4.39 mmol, 2.5 M in hexane) was added dropwise to a solution of *N*,*N*-dimesitylformimidamide [**52**] (1.12 g, 3.99 mmol) in diethyl ether (30 mL) at 0 °C and the reaction mixture was stirred for 1 h at 0 °C to obtain lithium dimesitylformamidinate. In a separate experiment, oxalyl chloride (1.2 mL, 13.98 mmol) was added slowly to a solution of *N,N*-dimethylformamide (1.1 mL, 13.98 mmol) in toluene (30 mL) at 0 °C. The mixture was stirred at room temperature for 2 h and it was again cooled to 0 °C to add diisopropylethylamine (2.1 mL, 11.98 mmol) dropwise. After stirring the solution at 0 °C for 1 h and at room temperature for 2 h, the mixture was filtered through a plug of celite. The filtrate was then added to the previously prepared lithium dimesitylformamidinate solution and the mixture was stirred at room temperature for 16 h 30 min. After filtering the mixture through celite, the filtrate was diluted with dichloromethane (40 mL) and cooled down to – 30 °C and trimethylsilyl trifluoromethanesulfonate (0.7 mL, 3.99 mmol) was added dropwise. The reaction solution was stirred at – 30 °C for 4 h, slowly warmed up to room temperature and stirred at this temperature for 6 h. Next, the reaction mixture was concentrated *in vacuo*, dissolved in aqueous sodium bicarbonate solution (100 mL, sat.) and extracted with dichloromethane (4 x 150 mL). The organic layers were combined, dried with $MgSO_4$, filtered, concentrated *in vacuo* and triturated with dichloromethane and pentane to give **55** as a red solid (258.5 mg, 13%): ^{1}H NMR (400 MHz, $CDCl_3$) δ 8.80 (s, 1H, K, 7.04 (4H, G – J), 2.68 (s, 12H, L – O), 2.36 (s, 6H, B + E), 2.16 (s, 12H, A, C, D, F); ^{13}C NMR (100 MHz, CD_3CN) δ 141.9, 135.8, 129.4, 128.8, 125.8, 124.6, 123.7, 37.5, 15.9, 12.4; HRMS (ESI) *m/z* calc for $C_{25}H_{35}N_4$ 391.2874, found: 391.2862.

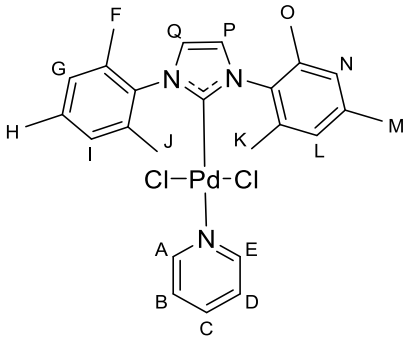

Pyr-Pd-PEPPSI-IMes [**48**]: Prepared by general procedure **C** with palladium chloride (74.1 mg, 0.42 mmol), IMes • HCl (156.6 mg, 0.46 mmol), potassium carbonate (288.8 mg, 2.09 mmol) and pyridine (2.1 mL, 25.58 mmol) to give **48** as light yellow solid (201.6 mg, 86%): ^{1}H NMR (400 MHz, $CDCl_3$) δ 8.53 – 8.51 (m, 2H, A + E), 7.57 – 7.53 (m, 1H, C), 7.12 – 7.08 (m, 2H, B + D), 7.07 (s, 2H, P + Q), 7.05 (br. s, 4H, G, I, L, N), 2.38 (s, 6H, H + M), 2.36 (s, 12H, F, J, K, O); ^{13}C NMR (100 MHz, $CDCl_3$) δ 151.7, 139.3, 137.5, 136.5, 135.2, 129.4, 124.3, 124.0, 21.4, 19.3; HRMS (ESI) *m/z* calc for $C_{26}H_{29}N_3Cl_2{}^{106}Pd$ 561.0777, found: 561.0774.

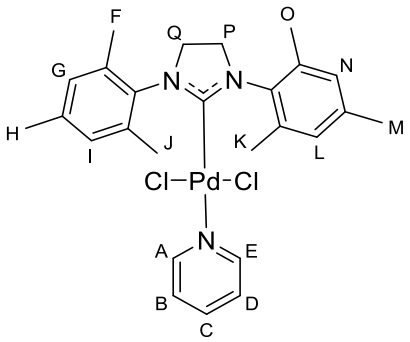

Pyr-Pd-PEPPSI-SIMes [**49**]: Prepared by general procedure **C** with palladium chloride (65.8 mg, 0.37 mmol), SIMes • HCl (139.9 mg, 0.41 mmol), potassium carbonate (256.3 mg, 1.85 mmol) and pyridine (1.8 mL, 22.75 mmol) to give **49** as off-white solid (108.9 mg, 52%): ^{1}H NMR (400 MHz, $CDCl_3$) δ 8.46 – 8.39 (m, 2H, A + E), 7.56 – 7.49 (m, 1H, C), 7.11 – 7.04 (m, 2H, B + D), 7.01 (br. s, 4H, G, I, L, N), 4.02 (s, 4H, Q + P), 2.58 (s, 12H, F, J, K, O), 2.33 (s, 6H, H + M); ^{13}C NMR (100 MHz, $CDCl_3$) δ 184.5, 151.4, 138.4, 137.3, 137.2, 134.9, 129.5, 123.9. 51.1, 21.2, 19.4; *The mass could not be obtained with various MS techniques.*

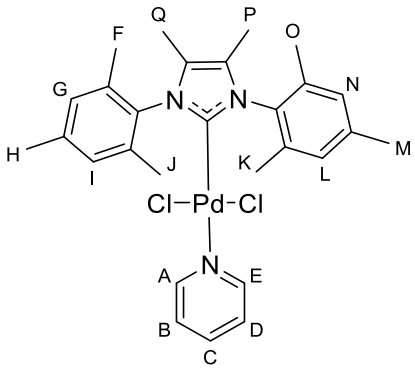

Pyr-Pd-PEPPSI-^{Me}IMes [**50**]: Prepared by general procedure **C** with palladium chloride (70.9 mg, 0.40 mmol), ^{Me}Mes • HCl [**53**] (162.2 mg, 0.44 mmol), potassium carbonate (276.2 mg, 2.00 mmol) and pyridine (2.0 mL, 24.48 mmol) to give **50** as off-white solid (134.1 mg, 57%): ^{1}H NMR (400 MHz, $CDCl_3$) δ 8.51 – 8.45 (m, 2H, A + E), 7.57 – 7.48 (m, 1H, C), 7.11 – 7.06 (m, 2H, B + D), 7.05 (br. s, 4H, G, I, L, N), 2.37 (s, 6H, H + M), 2.29 (s, 12H, F, J, K, O), 1.88 (s, 6H, P + Q); ^{13}C NMR (100 MHz, $CDCl_3$) δ 151.7, 148.4, 139.0, 137.4, 137.0, 133.5, 129.4, 127.5, 123.9, 21.4, 19.3, 9.4; *The mass could not be obtained with various MS techniques.*

5.2.6.2 Screening of the Pd-catalysed Hofmann-type elimination

Ligand screening for the Pd-catalysed Hofmann-type elimination (Subchapter 2.2.3)

N,N,N-Trimethyl-4-phenylbutan-1-aminium iodide [**31**] (1 equiv.), palladium(II) acetate (10 mol%) and ligand **L** (50 mol%) were flushed with N_2 for 1 h in a sealed tube. Acetonitrile (0.05 mM, degassed with N_2 flow for 1 h) and triethylamine (4 equiv., degassed with N_2 flow for 1 h) were added and the reaction mixture was heated at 80 °C for 24 h in a sealed tube. After cooling down to room temperature, water was added to the mixture and the aqueous layer was extracted with ethyl acetate (5 x). The combined organic layers were concentrated with N_2 flow and analysed via quantitative ^{1}H NMR (400 MHz, CD_3CN) using trimethyl benzene-1,3,5-tricarboxylate (30 µL, 0.1 M in DMSO) as internal standard. The results are summarised in the table below.

Entry	**Ligand L**	Conversion to **Product [32]**
a*	(*o*-tol)$_3$P	1%
b	(*o*-tol)$_3$P	2%
c	CyPh$_2$P	1%
d**	^{t}Bu$_3$PH BF$_4$	< 1%
e	(*p*-OMePh)$_3$P	5%
f	*rac*-BINAP	1%
g	dppf	< 1%
h	BrettPhos	1%
i	SPhos	2%
j	^{t}BuDavePhos	1%

*The reaction was heated at 60 °C; **4.5 equiv. of base was used.

Solvent screening for the Pd-catalysed Hofmann-type elimination (Table 2.2.2)

The solvent screening was performed according to general procedure **A** with triethylamine as base. In case of co-solvents, these were degassed individually and added to the reaction mixture. The results are summarised in the table below.

Entry	**Solvent S**	Conversion to **Product**
a	DMSO	< 1%
b	NMP	1%
c	H_2O : MeCN, (1 : 1)	2%
d	Toluene	1%
e	Dioxane	1%
f	THF	1%

Investigation of reaction time t (Table 2.2.3)

The experiments for the investigation of the reaction time **t** were performed according to general procedure **A** with acetonitrile as solvent and triethylamine as base. The experiments, however, were conducted with varying reaction time **t**, which are summarised in the table below alongside with the results of these reactions.

Entry	**t**	Conversion to **Product**
a	24 h	2%
b	18 h	1%
c	12 h	1%
d	9 h	1%
e	6 h	2%

Base screening for the Pd-catalysed Hofmann-type elimination (Table 2.2.4 & Table 2.2.5)

The base screening was performed according to general procedure **A**. In case of solid bases, these were added to the sealed tube alongside with the starting material, the catalyst and ligand were flushed with N_2 for 1 h. The liquid bases were degassed individually with N_2 for 1 h and then added to the reaction mixture. In case of co-solvents, these were degassed individually with N_2 for 1 h and added to the reaction mixture. The results are summarised in the table below.

Entry	**Base B**	**Solvent S**	Conversion to **Product [32]**
a	K_2CO_3	MeCN	2%
b	KO^{t}Bu	MeCN	< 1%
c	NaOAc	MeCN	-
d*	KOPh	MeCN	-
e	DBU	MeCN	2%
f	Proton Sponge	MeCN	2%
g	Cy_2NMe	MeCN	1%
h	Et_3N	H_2O : MeCN (1 : 4)	< 1%
i	K_2CO_3	H_2O : MeCN (1 : 4)	< 1%
j	Cs_2CO_3	MeCN	< 1%
k	Cs_2CO_3	*n*-butanol	< 1%
l**	Cs_2CO_3	H_2O : MeCN (1 : 4)	< 1%
m***	K_2CO_3	H_2O : MeCN (1 : 4)	< 1%

*KOPh was synthesised with phenol (1 equiv.) and potassium hydroxide (1 equiv.) in water; **1 equiv. ^{n}Bu$_4$NBr was added to the reaction; ***1 equiv. Ag_2CO_3 was added to the reaction.

Base screening for the Pd-catalysed Hofmann-type elimination using BrettPhos (Table 2.2.6)

The base screening was performed according to general procedure **A**, but BrettPhos was used as ligand. In case of solid bases, these were added to the sealed tube alongside with the starting material, the catalyst and ligand were flushed with N_2 for 1 h. The liquid bases were degassed individually with N_2 for 1 h and then added to the reaction mixture. In case of co-solvents, these were degassed individually with N_2 for 1 h and added to the reaction mixture. The results are summarised in the table below.

Entry	**Base B**	**Solvent S**	Conversion to **Product [32]**
a	Et_3N	MeCN	1%
b	K_2CO_3	H_2O : MeCN (1 : 4)	< 1%
c	Cs_2CO_3	MeCN	< 1%
d	Cs_2CO_3	*n*-butanol	< 1%

Room-temperature Pd-catalysed Hofmann-type elimination (Table 2.2.7)

Palladium(II) acetate (0.22 equiv., 22 mol%) and Ligand **L** were dissolved in Solvent **S** (0.05 mM, not degassed) and stirred at room temperature for 10 min. Then, *N,N,N*-trimethyl-4-phenylbutan-1-aminium iodide [**31**] (1 equiv.) and caesium carbonate (4 equiv.) were added to the 'pre-activated' palladium complex and the reaction mixture was stirred at room temperature for the reaction time **t**. Next, water was added to the mixture and the aqueous layer was extracted with ethyl acetate (5 x). The combined organic layers were concentrated with N_2 flow and analysed via quantitative ^{1}H NMR (400 MHz, CD_3CN) using trimethyl benzene-1,3,5-tricarboxylate (30 µL, 0.1 M in DMSO) as internal standard. The results are summarised in the table below.

Entry	**Ligand L**		**Solvent S**	**t**	Conversion to **Product[32]**
a	58 mol%	(*p*-OMePh)$_3$P	MeCN	30 min	1%
b	58 mol%	(*p*-OMePh)$_3$P	*n*-butanol	30 min	1%
c	77 mol%	(*p*-OMePh)$_3$P	MeCN	30 min	< 1%
d	77 mol%	(*p*-OMePh)$_3$P	H_2O : MeCN (1 : 10)	30 min	1%
e	77 mol%	(*p*-OMePh)$_3$P	MeCN	24 h	< 1%
f*	77 mol%	(*p*-OMePh)$_3$P	MeCN	15 h	< 1%
g*	55 mol%	BrettPhos	MeCN	15 h	1%

*The reaction was performed under inert conditions and the solvent was degassed with N_2 for 1 h prior to its addition to the catalyst and ligand.

Investigation of the metal-to-ligand ratio and catalyst loading (Table 2.2.8)

These experiments were performed according to general procedure **A** with acetonitrile as solvent and triethylamine as base. However, the amount of palladium(II) acetate (**x** mol%) and tris(2,4,6-trimethoxyphenyl)phosphine (**y** mol%) were varied. The results are summarised in the table below.

Entry	**x** mol%	**y** mol%	Conversion to **Product [32]**
a	10	10	1%
b	10	20	< 1%
c	10	50	1%
d	20	20	< 1%
e	20	40	< 1%

Homeopathic Pd-catalysed Hofmann-type elimination reaction (Subchapter 2.2.7)

Scheme 2.2.6: Palladium(II) acetate (0.4 mg, 3.3 mol%) and tris(2,4,6-trimethoxyphenyl) phosphine (2.2 mg, 13.2 mol%) were combined and degassed using the Schlenk technique (vacuum + N_2 cycle (3x)). Acetonitrile was degassed via the freeze, pump, thaw method (3 rounds) and added (1 mL) to the catalyst and ligand. The reaction mixture was stirred at room temperature for 30 min. Next, *N,N,N*-trimethyl-4-phenylbutan-1-aminium iodide [**31**] (15.0 mg, 0.047 mmol) and caesium carbonate (61.3 mg, 0.19 mmol) were added and the mixture was stirred at room temperature for 18 h. Water (2 mL) was added to the mixture and the aqueous layer was extracted with ethyl acetate (5 x 5 mL). The combined organic layers were concentrated with N_2 flow and analysed via quantitative ^{1}H NMR (400 MHz, CD_3CN) using trimethyl benzene-1,3,5-tricarboxylate (30 µL, 0.1 M in DMSO) as internal standard to confirm the formation of 4-phenylbutene **[32]** (< 0.1%).

Scheme 2.2.7: This reaction was performed according to the protocol by De Vries[195] by heating the reaction mixture at 135 ˚C for 22 h. The reaction was processed (as described above) and analysed via quantitative ^{1}H NMR (400 MHz, CD_3CN) using trimethyl benzene-1,3,5-tricarboxylate (30 µL, 0.1 M in DMSO) as internal standard, which confirmed that the desired 4-phenylbutene **[32]** was not formed.

Stoichiometric Pd-catalysed Hofmann-type elimination (Subchapter 2.2.8)

Scheme 2.2.8: Palladium(II) acetate (3.5 mg, 33 mol%) and tris(2,4,6-trimethoxyphenyl) phosphine (21.9 mg, 132 mol%) were combined, degassed using the Schlenk technique (vacuum + N_2 cycle (3x)) and dissolved in acetonitrile (1 mL, degassed via the freeze, pump, thaw method (3 rounds)). The mixture was stirred at room temperature for 30 min prior to the addition of *N,N,N*-trimethyl-4-phenylbutan-1-aminium iodide [**31**] (15.9 mg, 0.05 mmol) and caesium carbonate (61.3 mg, 0.19 mmol). The mixture was first stirred at room temperature for 1 h and then palladium(II)acetate (3.5 mg) and tris(2,4,6-trimethoxyphenyl)phosphine (21.9 mg) were added again. This step was repeated so that ~ 1 equiv. of catalyst was used in total. After the last addition, the reaction mixture was stirred at room temperature for 18 h. Water (2 mL) was added to the mixture and the aqueous layer was extracted with ethyl acetate (5 x 5 mL). The combined organic layers were concentrated with N_2 flow and analysed via quantitative ^{1}H NMR (400 MHz, CD_3CN) using trimethyl benzene-1,3,5-tricarboxylate (30 µL, 0.1 M in DMSO) as internal standard to confirm the formation of 4-phenylbutene **[32]** (2%).

Scheme 2.2.9 & Scheme 2.2.10: These experiments were performed according to general procedure **A**. However, stoichiometric amount of palladium(II) acetate (1 equiv.) was used and the amount of tris(2,4,6-trimethoxyphenyl)phosphine (**x** equiv.) was adjusted accordingly. The results are summarised in the table below.

Entry	**x** equiv. (Ligand)	**Base B**	**Solvent S**	Conversion to **Product [32]**
a	2	Et_3N	MeCN	< 1%
b	2.2	Cs_2CO_3	*n*-butanol	< 1%

Scheme 2.2.11: Palladium(II) acetate (11.3 mg, 0.05 mmol), tris(2,4,6-trimethoxyphenyl) phosphine (71.1 mg, 0.20 mmol) and silver carbonate (55.7 mg, 0.20 mmol) were combined, degassed using the Schlenk technique (vacuum + N_2 cycle (3x)) and dissolved in tetrahydrofuran (2 mL, degassed via the freeze, pump, thaw method (3 rounds)). The reaction mixture was stirred at room temperature for 10 min. Next, *N,N,N*-trimethyl-4-phenylbutan-1-aminium iodide [**31**] (16.1 mg, 0.05 mmol) was added and the mixture was stirred at room temperature for 24 h. Water (2 mL) was added to the mixture and the aqueous layer was extracted with ethyl acetate (5 x 5 mL). The combined organic layers were concentrated with N_2 flow and analysed via quantitative ^{1}H NMR (400 MHz, CD_3CN) using trimethyl benzene-1,3,5-tricarboxylate (30 µL, 0.1 M in DMSO) as internal standard to confirm the formation of 4-phenylbutene **[32]** (< 1%).

Control reactions (Subchapter 2.2.9)

Base-free Pd-catalysed Hofmann-type elimination (Table 2.2.9): Palladium(II) acetate (**x** mol%) and tris(2,4,6-trimethoxyphenyl) phosphine (**y** mol%) were combined, degassed using the Schlenk technique (vacuum + N_2 cycle (3x)) and dissolved in solvent **S** (0.05 mM, degassed via the freeze, pump, thaw method (3 rounds)). The reaction mixture was stirred at room temperature for 30 min. Next, *N,N,N*-trimethyl-4-phenylbutan-1-aminium iodide [**31**] (1 equiv.) was added and the mixture was stirred at room temperature for 24 h. Water (2 mL) was added to the mixture and the aqueous layer was extracted with ethyl acetate (5 x 5 mL). The combined organic layers were concentrated with N_2 flow and analysed via quantitative ^{1}H NMR (400 MHz, CD_3CN) using trimethyl benzene-1,3,5-tricarboxylate (30 µL, 0.1 M in DMSO) as internal standard. The results are summarised in the table below.

Entry	**x** mol%	**y** mol%	**Solvent S**	Conversion to **Product [32]**
a	100	400	THF	2%
b	0.33	132	MeCN	1%
c*	0.33	132	MeCN	1%
d**	0.33	132	MeCN	2%

*1 equiv. silver(I) bromide was added to the reaction; **1 equiv. silver(I) triflate was added to the reaction.

In the absence of a palladium catalyst (Table 2.2.10): *N,N,N*-trimethyl-4-phenylbutan-1-aminium iodide [**31**] (1 equiv.) and ligand **L** (68 mol%) were combined, degassed using the Schlenk technique (vacuum + N_2 cycle (3x)) and dissolved in acetonitrile (0.05 mM, degassed via the freeze, pump, thaw method (3 rounds)).Next, triethylamine (4 equiv., degassed via the freeze, pump, thaw method (3 rounds)) was added and the reaction mixture was heated at 80 ˚C for 21 h. After cooling the mixture down to room temperature, water (2 mL) was added and the aqueous layer was extracted with ethyl acetate (5 x 5 mL). The combined organic layers were concentrated with N_2 flow and analysed via quantitative ^{1}H NMR (400 MHz, CD_3CN) using trimethyl benzene-1,3,5-tricarboxylate (30 µL, 0.1 M in DMSO) as internal standard, which confirmed that both reactions using either ligands (**L** = tris(2,4,6-trimethoxyphenyl) phosphine or BrettPhos) did not give 4-phenylbutene **[32]**, but only starting material.

Possible side reactions of the product (Subchapter 2.2.10)

Heck cross coupling reaction (Scheme 2.2.12): Palladium(II) acetate (3.3 mg, 33 mol%) and tris(2,4,6-trimethoxyphenyl)phosphine (20.7 mg, 132 mol%) were combined, degassed using the Schlenk technique (vacuum + N_2 cycle (3x)) and dissolved in acetonitrile (1 mL, degassed via the freeze, pump, thaw method (3 rounds)). After stirring at room temperature for 30 min, *N,N,N*-trimethyl-4-phenylbutan-1-aminium iodide [**31**] (14.2 mg, 0.044 mmol) was added and the mixture was stirred at room temperature for 1 h 30 min. Next, 4-phenylbutene (0.01 mL, 0.067 mmol) and caesium carbonate (57.9 mg, 0.18 mmol) were added and the mixture was heated at 80 ˚C for 24 h. After cooling the mixture down to room temperature, water (2 mL) was added and the aqueous layer was extracted with ethyl acetate (5 x 5 mL). The combined organic layers were concentrated with N_2 flow and analysed via quantitative ^{1}H NMR (400 MHz, CD_3CN) using trimethyl benzene-1,3,5-tricarboxylate (30 µL, 0.1 M in DMSO) as internal standard, which confirmed that only starting material was recovered.

Hydroamination and hydroalkylamination control reaction (Scheme 2.2.14): Palladium (II) acetate (20.7 mg, 22 mol%) and ligand **L** (68 mol%) were combined, degassed using the Schlenk technique (vacuum + N_2 cycle (3x)), dissolved in acetonitrile (1 mL, degassed via the freeze, pump, thaw method (3 rounds)) and stirred at room temperature for 10 min. In a separate experiment, trimethylamine hydrochloride (40.0 mg, 0.42 mmol) was dissolved in acetonitrile (0.7 mL) and triethylamine (0.2 mL, 1.67 mmol) and 4-phenylbutene (0.06 mL, 0.42 mmol) were added to the solution. The pre-activated catalytic solution was added to the mixture and the reaction was heated at 80 ˚C for 20 h. After cooling the mixture down to room temperature, water (2 mL) was added and the aqueous layer was extracted with ethyl acetate (5 x 5 mL). The combined organic layers were concentrated with N_2 flow and analysed via quantitative ^{1}H NMR (400 MHz, CD_3CN) using trimethyl benzene-1,3,5-tricarboxylate (30 µL, 0.1 M in DMSO) as internal standard, which confirmed that only starting material was recovered. Both ligands (**L**) tris(2,4,6-trimethoxyphenyl)phosphine and BrettPhos were investigated in this experiment.

The investigation of the electrophile (Subchapter 2.2.11)

The effect of counterion (Table 2.2.11): Palladium(II) acetate (**x** mol%) and ligand **L** (**y** mol%) were combined, degassed using the Schlenk technique (vacuum + N_2 cycle (3x)) and dissolved in acetonitrile (1 mL, degassed via the freeze, pump, thaw method (3 rounds)). After stirring at room temperature for 30 min, *N,N,N*-trimethyl-4-phenylbutan-1-aminium trifluoromethane-sulfonate [**41**] (1 equiv.) and base **B** (4 equiv.) were added and the mixture was heated at 80 ℃ for 22 h. After cooling the mixture down to room temperature, water (2 mL) was added and the aqueous layer was extracted with ethyl acetate (5 x 5 mL). The combined organic layers were concentrated with N_2 flow and analysed via quantitative ^{1}H NMR (400 MHz, CD_3CN) using trimethyl benzene-1,3,5-tricarboxylate (30 µL, 0.1 M in DMSO) as internal standard. The results are summarised in the table below.

Entry	**x** mol%	**y** mol%	**Ligand L**	**Base B**	Conversion to **Product [32]**
a	22	68	(*p*-OMePh)$_3$P	Et_3N	< 1%
b	22	68	(*p*-OMePh)$_3$P	Cs_2CO_3	1%
c	100	310	(*p*-OMePh)$_3$P	Et_3N	< 1%
d	100	310	(*p*-OMePh)$_3$P	Cs_2CO_3	-
e	22	68	BrettPhos	Et_3N	-
f	22	68	BrettPhos	Cs_2CO_3	< 1%
g	100	310	BrettPhos	Et_3N	-
h	100	310	BrettPhos	Cs_2CO_3	< 1%

Pd-catalysed elimination of (4-iodobutyl)benzene (Scheme 2.2.17): (4-Iodobutyl)benzene [**43**] (16.8 mg, 0.065 mmol), palladium(II) acetate (4.8 mg, 33 mol%) and tris(2,4,6-trimethoxyphenyl)phosphine (30.1 mg, 132 mol%) were flushed with N_2 for 30 min in a sealed tube. Acetonitrile (1 mL, degassed via the freeze, pump, thaw method (3 rounds)) and triethylamine (0.04 mL, 0.26 mmol, degassed via the freeze, pump, thaw method (3 rounds)) were added and the reaction mixture was stirred at room temperature for 24 h. Next, water (2 mL) was added to the mixture and the aqueous layer was extracted with ethyl acetate (5 x 5 mL). The combined organic layers were concentrated with N_2 flow and analysed via quantitative ^{1}H NMR (400 MHz, CD_3CN) using trimethyl benzene-1,3,5-tricarboxylate (30 µL, 0.1 M in DMSO) as internal standard to confirm the formation of 4-phenylbutene [**32**] (1%).

Pd-catalysed Hofmann-type elimination in deuterated acetonitrile (Scheme 2.2.18)

Palladium(II) acetate (1.6 mg, 22 mol%) and tris(2,4,6-trimethoxyphenyl)phosphine (6.5 mg, 58 mol%) were dissolved in CD_3CN (1 mL) and the mixture was stirred at room temperature for 10 min. After the addition of *N,N,N*-trimethyl-4-phenylbutan-1-aminium iodide [**31**] (10.1 mg, 0.032 mmol) and base **B** were added, the mixture was degassed via the freeze, pump, thaw method (3 rounds). Next, the reaction mixture was transferred into a J-Young NMR tube and trimethyl benzene-1,3,5-tricarboxylate (30 µL, 0.1 M in DMSO) was added as internal standard. The reaction was heated at 80 °C for 15 h 30 min. The reaction progress was monitored via ^{1}H NMR after 2 h 30 min and after 15 h 30 min, which confirmed that only starting material was detected after the reaction with either triethylamine or caesium carbonate as base **B**.

Ligandless Pd-catalysed Hofmann-type elimination (Table 2.2.12)

Palladium(II) acetate (22 mol%), *N,N,N*-trimethyl-4-phenylbutan-1-aminium iodide [**31**] (1 equiv.) and additive **A** (1 equiv.) were dissolved in solvent **S** (0.05 mM, degassed with N_2 flow for 1 h) under inert conditions. After the addition of base **B** (4 equiv., liquid bases were degassed with N_2 flow for 1 h), the reaction mixture was heated at 80 °C for 24 h. After cooling the mixture down to room temperature, water (2 mL) was added and the aqueous layer was extracted with ethyl acetate (5 x 5 mL). The combined organic layers were concentrated with N_2 flow and analysed via quantitative ^{1}H NMR (400 MHz, CD_3CN) using trimethyl benzene-1,3,5-tricarboxylate (30 µL, 0.1 M in DMSO) as internal standard. The results are summarised in the table below.

Entry	**Additive A**	**Base B**	**Solvent S**	Conversion to **Product [32]**
a*	^{n}Bu$_4$NBr	Et_3N	MeCN	1%
b	^{n}Bu$_4$NBr	Et_3N	MeCN	< 1%
c	^{n}Bu$_4$NBr	Et_3N	H_2O : MeCN, (1 : 1)	< 1%
d	^{n}Bu$_4$NBr	K_2CO_3	H_2O : MeCN, (1 : 1)	< 1%
e	Ph_4PCl	Et_3N	H_2O : MeCN, (1 : 1)	< 1%

* Tris(2,4,6-trimethoxyphenyl)phosphine (58 mol%) was added.

$Pd_2(dba)_3$ – an alternative palladium source (Subchapter 2.2.14)

Scheme 2.2.20: This reaction was conducted according to general procedure **A** with acetonitrile as solvent and triethylamine as base, however, $Pd_2(dba)_3$ was used instead of $Pd(OAc)_2$. Quantitative ^1H NMR analysis confirmed the formation of 4-phenylbutene [**32**] (1%).

Pd-catalysed Hofmann-type elimination using Fu conditions (Table 2.2.13 & Scheme 2.2.22): Tris(dibenzylideneacetone)-dipalladium(0) (3.5 mol%), di-tert-butyl(methyl)phosphonium tetrafluoroborate (14 mol%) and potassium-*tert*-butoxide (0.25 equiv.) were combined, degassed using the Schlenk technique (vacuum + N_2 cycle (3x)) and dissolved in solvent **S** (0.05 mM, degassed via the freeze, pump, thaw method (3 rounds)). After the addition of dicyclohexylamine (1.2 equiv.), the reaction mixture was stirred at room temperature for 1 h 30 min. Next, *N,N,N*-trimethyl-4-phenylbutan-1-aminium iodide [**31**] (1 equiv.) was added and the mixture was stirred at room temperature for 21 h 30 min. After adding water (2 mL), the aqueous layer was extracted with ethyl acetate (5 x 5 mL). The combined organic layers were concentrated with N_2 flow and analysed via quantitative ^1H NMR (400 MHz, CD_3CN) using trimethyl benzene-1,3,5-tricarboxylate (30 µL, 0.1 M in DMSO) as internal standard. The results are summarised in the table below.

Entry	**Solvent S**	Conversion to **Product [32]**
a	dioxane	1%
b	MeCN	1%
c*	dioxane	< 1%
d**	dioxane	1%
e***	dioxane	< 1%
f****	dioxane	-

*The reaction was heated at 100 °C; **1 equiv. silver(I) bromide was added; ***1 equiv. silver(I) triflate was added; ****Increased amount of $Pd_2(dba)_3$ (33 mol%) and $HP(^tBu)MeBF_4$ (132 mol%) were used.

Suzuki reaction of quaternary ammonium substrates (Subchapter 2.2.15)

Scheme 2.2.24 & Scheme 2.2.25: Electrophile **E** (1 equiv.), palladium(II) acetate (2.5 mol%), XPhos (5 mol%), boronic acid **BA** (3 equiv.) and caesium carbonate (3 equiv.) were combined, degassed using the Schlenk technique (vacuum + N_2 cycle (3x)) and dissolved in tetrahydrofuran (0.5 mM, degassed via the freeze, pump, thaw method (3 rounds)). The reaction mixture was heated at 60 °C for 20 h. After cooling the mixture down to room temperature, water (2 mL) was added and the aqueous layer was extracted with ethyl acetate (5 x 5 mL). The combined organic layers were concentrated with N_2 flow and analysed via quantitative ^{1}H NMR (400 MHz, CD_3CN) using trimethyl benzene-1,3,5-tricarboxylate (30 µL, 0.1 M in DMSO) as internal standard. The results are summarised in the table below.

Entry	**Electrophile E**	**Boronic acid BA**	Reaction outcome
a	Trimethyl-4-phenylbutan-1-aminium iodide [**31**]	4-Methoxyphenylboronic acid	Only SM
b	Trimethyl-4-phenylbutan-1-aminium iodide [**31**]	2-Methoxyphenylboronic acid	Only SM
c	(4-Iodobutyl)benzene [**43**]	4-Methoxyphenylboronic acid	SM + 4-phenylbutene [**32**] (5%)

Expanding the library of ligands (Table 2.2.14): Palladium(II) acetate (22 mol%) and Ligand **L** (44 mol%) were combined, flushed with N_2 flow for 30 min and dissolved in acetonitrile (0.05 mM, degassed via the freeze, pump, thaw method (3 rounds)). After stirring at room temperature for 15 min, *N,N,N*-trimethyl-4-phenylbutan-1-aminium iodide [**31**] (1 equiv.) and caesium carbonate (4 equiv.) were added and the reaction mixture was heated at 80 ̊C for 10 h. After cooling the mixture down to room temperature, water (2 mL) was added and the aqueous layer was extracted with ethyl acetate (5 x 5 mL). The combined organic layers were concentrated with N_2 flow and analysed via quantitative ^{1}H NMR (400 MHz, CD_3CN) using trimethyl benzene-1,3,5-tricarboxylate (30 μL, 0.1 M in DMSO) as internal standard. The results are summarised in the table below.

Entry	**Ligand L**	Reaction outcome
a	XPhos	Only SM, no P
b	XantPhos	Only SM, no P
c	DPEPhos	Only SM, no P
d	dppe	Only SM, no P
e	dppp	Only SM, no P
f	dppf	Only SM, no P

Investigation of IPr-Pd precatalysts (Scheme 2.2.27 & Scheme 2.2.28): *N,N,N*-trimethyl-4-phenylbutan-1-aminium iodide [**31**] (1 equiv.), IPr-Pd precatalyst **PC** (**x** mol%), *p*-tolylboronic acid (2 equiv.) and potassium carbonate (3 equiv.) were combined, degassed using the Schlenk technique (vacuum + N_2 cycle (3x)) and dissolved in tetrahydrofuran (0.25 mM, degassed via the freeze, pump, thaw method (3 rounds)). The reaction mixture was heated at 60 °C for 22 h 30 min. After cooling down to room temperature, the mixture was diluted with dichloromethane (5 mL), filtered through celite and washed with dichloromethane (15 mL). The combined organic layers were concentrated with N_2 flow and analysed via quantitative ^{1}H NMR (400 MHz, CD_3CN) using trimethyl benzene-1,3,5-tricarboxylate (30 µL, 0.1 M in DMSO) as internal standard. The results are shown in the table below.

Entry	**x mol% Precatalyst PC**		Reaction outcome
a	3 mol%	Pd-PEPPSI-IPr	Mainly SM, traces of 4-phenylbutene [**32**]
b	3 mol%	(IPr)Pd(cinnamyl)Cl	Mainly SM, traces of 4-phenylbutene [**32**]
c	100 mol%	Pd-PEPPSI-IPr	Mainly SM, traces of 4-phenylbutene [**32**]
d	100 mol%	(IPr)Pd(cinnamyl)Cl	Mainly SM, traces of 4-phenylbutene [**32**]

In situ generated NHC-Pd complexes (Table 2.2.15): Tris(dibenzylideneacetone)-dipalladium(0) (**x** mol%) and Ligand **L** (**y** mol%) were combined, degassed using the Schlenk technique (vacuum + N_2 cycle (3x)) and dissolved in tetrahydrofuran : *N*-methylpyrrolidone (2 : 1, 0.21 mM, individually degassed via the freeze, pump, thaw method (3 rounds)). After stirring at room temperature for 15 min, *N,N,N*-trimethyl-4-phenylbutan-1-aminium iodide [**31**] (1 equiv.) was added and the mixture was heated at 75 °C for 24 h. After cooling down to room temperature, the mixture was diluted with dichloromethane (5 mL), filtered through celite and washed with dichloromethane (15 mL). The combined organic layers were concentrated with N_2 flow and analysed via quantitative ^{1}H NMR (400 MHz, CD_3CN) using trimethyl benzene-1,3,5-tricarboxylate (30 µL, 0.1 M in DMSO) as internal standard. The results are shown in the table below.

Entry	**x mol%**	**y mol%**	**Ligand L**	Reaction outcome
a	2	8	IPr • HCl	only SM, no P
b	50	200	IPr • HCl	only SM, no P
c	2	8	IMes • HCl	only SM, no P
d	50	200	IMes • HCl	only SM, no P

Investigation of pyr-Pd-PEPPSI-IMes (Table 2.2.16): These experiments were conducted according to general procedure **B** with pyr-Pd-PEPPSI-IMes (**x** mol%) as precatalyst and caesium carbonate (**y** equiv.) as base. The results are given in the table below.

Entry	**Electrophile E**	**x mol%**	**y equiv.**	Conversion to **Product [32]**
a	Trimethylammonium iodide [**31**]	3	3	< 1%
b	Trimethylammonium triflate [**41**]	3	3	1%
c	Trimethylammonium iodide [**31**]	100	4	< 1%
d	Trimethylammonium triflate [**41**]	100	4	< 1%

Investigation of modified pyr-Pd-PEPPSI-IMes precatalysts with Cs_2CO_3 (Table 2.2.17): These experiments were conducted according to general procedure **B** with modified Pd-PEPPSI-IMes precatalyst **PC** (1 equiv.) and caesium carbonate (4 equiv.) as base. The results are given in the table below.

Entry	**Electrophile E**	**Precatalyst PC**	Conversion to **Product [32]**
a	Trimethylammonium iodide [**31**]	pyr-Pd-PEPPSI-IMes	< 1%
b	Trimethylammonium triflate [**41**]	pyr-Pd-PEPPSI-IMes	< 1%
c	Trimethylammonium iodide [**31**]	pyr-Pd-PEPPSI-SIMes	< 1%
d	Trimethylammonium triflate [**41**]	pyr-Pd-PEPPSI-SIMes	< 1%
e	Trimethylammonium iodide [**31**]	pyr-Pd-PEPPSI-^{Me}IMes	1%
f	Trimethylammonium triflate [**41**]	pyr-Pd-PEPPSI-^{Me}IMes	1%

Investigation of modified pyr-Pd-PEPPSI-IMes precatalysts with KO^{t}Bu (Table 2.2.18): These experiments were conducted according to general procedure **B** with modified Pd-PEPPSI-IMes precatalyst **PC** (1 equiv.) and potassium-*tert*-butoxide (4 equiv., 12% in THF, degassed with freeze, pump, thaw method (3 cycles)) as base. The results are given in the table below.

Entry	**Electrophile E**	**Precatalyst PC**	Conversion to **Product [32]**
a	Trimethylammonium iodide [**31**]	pyr-Pd-PEPPSI-IMes	< 1%
b	Trimethylammonium triflate [**41**]	pyr-Pd-PEPPSI-IMes	< 1%
c	Trimethylammonium iodide [**31**]	pyr-Pd-PEPPSI-SIMes	< 1%
d	Trimethylammonium triflate [**41**]	pyr-Pd-PEPPSI-SIMes	< 1%
e	Trimethylammonium iodide [**31**]	pyr-Pd-PEPPSI-^{Me}IMes	< 1%
f	Trimethylammonium triflate [**41**]	pyr-Pd-PEPPSI-^{Me}IMes	< 1%

Investigation of modified pyr-Pd-PEPPSI-IMes precatalysts in TBAB (Table 2.2.19): Trimethylammonium substrate **E** (1 equiv.), NHC-Pd precatalyst **PC** (1 equiv.), caesium carbonate (1 equiv.) and tetrabutylammonium bromide (12.4 equiv.) were combined, degassed using the Schlenk technique (vacuum + N_2 cycle (3x)) and heated at 140 °C for 22 h. After cooling down to room temperature, the mixture was diluted with dichloromethane (5 mL), filtered through celite and washed with dichloromethane (10 mL). The combined organic layers were concentrated with N_2 flow and analysed via quantitative ^{1}H NMR (400 MHz, CD_3CN) using trimethyl benzene-1,3,5-tricarboxylate (30 µL, 0.1 M in DMSO) as internal standard. The results are given in the table below.

Entry	**Electrophile E**	**Precatalyst PC**	Conversion to **Product [32]**
a	Trimethylammonium iodide [**31**]	pyr-Pd-PEPPSI-IMes	< 1%
b	Trimethylammonium triflate [**41**]	pyr-Pd-PEPPSI-IMes	< 1%
c	Trimethylammonium iodide [**31**]	pyr-Pd-PEPPSI-SIMes	< 1%
d	Trimethylammonium triflate [**41**]	pyr-Pd-PEPPSI-SIMes	< 1%
e	Trimethylammonium iodide [**31**]	pyr-Pd-PEPPSI-^{Me}IMes	< 1%
f	Trimethylammonium triflate [**41**]	pyr-Pd-PEPPSI-^{Me}IMes	< 1%

5.2.7 Investigation of Pd-catalysed Hofmann-type elimination on model peptide

5.2.7.1 Pd-catalysed Hofmann-type elimination using amine ligands

Preparation of palladium catalyst complexes:

Catalyst complex **58**:

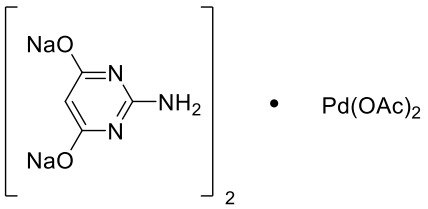

2-Amino-4,6-dihydroxypyrimidine (13.4 mg, 0.11 mmol) was dissolved in aqueous sodium hydroxide solution (2 mL, 0.1 M) at 65 ˚C in a volumetric flask (V = 5 mL) prior to the addition of palladium(II) acetate (11.2 mg, 0.05 mmol). The mixture was stirred at 65 ˚C for 30 min at open air to give a yellow-orange solution. After cooling to room temperature, water was added to dilute the solution to 5.00 mL leading to a 0.1 M pyrimidine catalyst **58** stock solution.

Catalyst complex **59**:

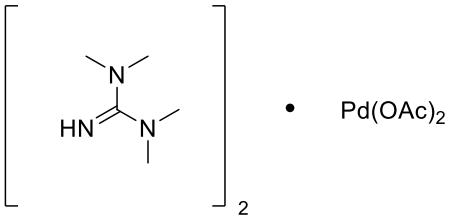

1,1,3,3-Tetramethylguanidine (11.5 mg, 0.1 mmol) was dissolved in aqueous sodium hydroxide solution (1 mL, 0.1 M) and water (2 mL) in a volumetric flask (V = 5 mL). After the addition of palladium(II) acetate (11.2 mg, 0.05 mmol), the mixture was stirred at 65 ˚C for 45 min to give a brown solution. Next, the solution was cooled to room temperature and further diluted with water (total volume 5 mL) to give a 0.1 M guanidine catalyst **59** stock solution.

Palladium-catalysed elimination trials in aqueous buffer (no scavenger, *Scheme 2.3.1*)

The peptide GEAKSQVFK[me$_3$]TNHFQKSTVR [**56**] (0.8 µL, 1.5 nmol, water (c = 4.2 mg/mL)) was diluted with sodium phosphate buffer (49.2 µL, Na_2HPO_4/NaH_2PO_4 in water, 50 mM, pH = 8.00) in a LoBind Eppendorf tube (1.5 mL). Catalyst stock solution **58** or **59**

(7.5 µL, 75 nmol, 50 equiv.) was added to the mixture and the reaction was vortexed, briefly centrifuged and heated to 37 ℃ for 18 h. After cooling to room temperature, the mixture was centrifuged at 17000 x g for 10 min. The reacted peptide was desalted using Pierce C18 spin columns (see general procedure **D**) prior to dissolving the dried peptide in the MS eluent (20 µL, 0.1% TFA and 0.5% MeCN in H_2O) to analyse it via LC-MS/MS (12 µL injection).

Palladium-catalysed elimination trials in aqueous buffer (with scavenger, *Scheme 2.3.2 & Scheme 2.3.4*)

Scheme 2.3.2: The peptide GEAKSQVFK[me_3]TNHFQKSTVR [**56**] (2.7 µL, 5 nmol, water (c = 4.2 mg/mL)) was diluted with sodium phosphate buffer (47.3 µL, Na_2HPO_4/NaH_2PO_4 in water, 50 mM, pH = 8.00) in a LoBind Eppendorf tube (1.5 mL). Catalyst stock solution **58** or **59** (25 µL, 250 nmol, 50 equiv.) was added to the mixture and the reaction was vortexed, briefly centrifuged and heated to 37 ℃ for 18 h. The mixture was briefly centrifuged and aqueous scavenger **S** solution (28.5 µL, 285 nmol, 50 mM) was added to the solution to scavenge the Pd-catalyst. The reaction was heated at 37 ℃ for an additional 1 h 30 min. After cooling to room temperature, the mixture was centrifuged at 17000 x g for 10 min. The reacted peptide was desalted using Pierce C18 spin column (see general procedure **D**) prior to dissolving the dried peptide in the MS eluent (20 µL, 0.1% TFA and 0.5% MeCN in H_2O) to analyse it via LC-MS/MS (2 µL injection).

Scavenger **S**	**Equiv. to Pd**
DTT	5.7
MPA	5.7

This procedure was repeated for the investigation of high temperature on the Pd-catalysed elimination on the model peptide (*Scheme 2.3.4*). The peptide was treated with the Pd-complex **58** or **59** at 100 ℃ for 18 h and DTT was used as scavenger.

Control reaction without Palladium catalyst (with scavenger, *Scheme 2.3.3*)

The peptide GEAKSQVFK[me_3]TNHFQKSTVR [**56**] (2.7 µL, 5 nmol, water (c = 4.2 mg/mL)) was diluted with sodium phosphate buffer (47.3 µL, Na_2HPO_4/NaH_2PO_4 in water, 50 mM, pH = 8.00) in a LoBind Eppendorf tube (1.5 mL). The mixture was vortexed, briefly

centrifuged and heated to 37 °C for 18 h. The reaction was briefly centrifuged and aqueous DTT solution (28.5 µL, 285 nmol, 50 mM) was added to the solution. The reaction was heated at 37 °C for an additional 1 h 30 min. After cooling to room temperature, the mixture was centrifuged at 17000 x g for 10 min. The reacted peptide was purified using Pierce C18 spin column (see general procedure **D**) prior to dissolving the dried peptide in the MS eluent (20 µL, 0.1% TFA and 0.5% MeCN in H_2O) to analyse it via LC-MS/MS (2 µL injection).

5.2.7.2 Pd-catalysed Hofmann-type elimination using phosphine ligands (Subchapter 2.3.4)

Palladium(II) acetate (0.05 mmol) and Ligand **L** (0.10 mmol) were dissolved in acetonitrile (5 mL, 0.1 M, degassed for 1 h with N_2 flow) and the reaction mixture was stirred at room temperature for 1 h under inert atmosphere. In a separate experiment, the peptide GEAKSQVFK[me$_3$]TNHFQKSTVR (2.7 µL, 5 nmol, water (c = 4.2 mg/mL)) was diluted with solvent **S** (47.3 µL, degassed for 1 h with N_2 flow) in a LoBind Eppendorf tube (1.5 mL) under N_2 atmosphere. The pre-activated catalyst solution (25 µL, 250 nmol, 50 equiv.) was added to the mixture and the reaction was vortexed, briefly centrifuged and heated to 37 °C for 20 h in a sealed Eppendorf tube. The mixture was briefly centrifuged and aqueous DTT solution (28.5 µL, 285 nmol, 50 mM) was added to the solution to scavenge the Pd-catalyst. The reaction was heated at 37 °C for an additional 1 h 30 min. After cooling to room temperature, the mixture was dried using a speedvac concentrator. After dissolving the mixture in H_2O including 0.5% TFA and 5% MeCN (100 µL), the mixture was centrifuged at 17000 x g for 10 min. The reacted peptide was desalted using the Pierce C18 spin column (see general procedure **D**) prior to dissolving the dried peptide in the MS eluent (20 µL, 0.1% TFA and 0.5% MeCN in H_2O) to analyse it via LC-MS/MS (2 µL injection).

Entry	Ligand **L**	Solvent **S**
a	(*p*-OMePh)$_3$P	Na_2HPO_4/NaH_2PO_4 in water, 50 mM, pH = 8.00
b	BrettPhos	Na_2HPO_4/NaH_2PO_4 in water, 50 mM, pH = 8.00
c	BrettPhos	Acetonitrile

5.2.7.3 Pd-catalysed Hofmann-type elimination using NHC ligands (Subchapter 2.3.5)

Palladium-catalysed Suzuki coupling using Pd-NHC precatalysts

The peptide GEAKSQVFK^{9}[**mod**]TNHFQKSTVR (2.7 µL, 5 nmol, water (c = 4.2 mg/mL)) was transferred to a LoBind Eppendorf tube (1.5 mL) and flushed with N_2. The aqueous basic buffer **BB** was degassed by bubbling N_2 through the solution for 30 min. The peptide was diluted in basic buffer **BB** (47.3 µL) and flushed with N_2. The catalyst stock solution was prepared by adding **Pd-NHC** precatalyst (0.01 mmol) and boronic acid **BA** (0.0104 mmol) into a vial, flushing it with N_2, dissolving it in tetrahydrofuran (1 mL, degassed with N_2 for 1 h) and stirring it at room temperature for 10 min. The catalyst solution (25 µL, 250 nmol, 0.01 M, 50 equiv.) was added to the diluted peptide and the mixture was flushed with N_2. After sealing the Eppendorf tube with parafilm, the reaction was vortexed and heated to 60 °C for 20 h. The mixture was then vortexed and aqueous DTT solution (28.5 µL, 285 nmol, 50mM) was added to the solution to scavenge the Pd-catalyst. The reaction was heated at 60 °C for an additional 1 h 30 min. After cooling to room temperature, the mixture was concentrated to dryness using a speedvac evaporator. The reacted peptide was dissolved in equilibration solution (100 µL, 0.5% TFA and 5% MeCN in H_2O) and purified using the Pierce C18 spin column (see general procedure **D**). After concentrating the purified peptide to dryness, it was dissolved in the MS eluent (20 µL, 0.1% TFA and 0.5% MeCN in H_2O) to analyse it via LC-MS/MS (2 µL injection).

Scheme	K^{9}[**mod**]	Basic buffer **BB**	**Pd-NHC**	Boronic acid **BA**
Scheme 2.3.7	K^{9}[me$_3$]	Na_2HPO_4/NaH_2PO_4 in water, 50 mM, pH = 8.00	Pd-PEPPSI-IPr or (IPr)Pd(cinnamyl)Cl	*p*-tolylboronic acid
Scheme 2.3.8	K^{9}[me$_3$]	Na_2HPO_4/NaH_2PO_4 in water, 50 mM, pH = 8.00	No Pd-NHC	*p*-tolylboronic acid
Scheme 2.3.9	K^{9}[me$_3$]	NH_4HCO_3 in water, 50 mM, pH ~ 8.00	Pd-PEPPSI-IPr or (IPr)Pd(cinnamyl)Cl	*p*-tolylboronic acid
Scheme 2.3.10	K^{9}[me$_3$]	Na_2HPO_4/NaH_2PO_4 in water, 50 mM, pH = 8.00	Pd-PEPPSI-IPr or (IPr)Pd(cinnamyl)Cl	(Pentylphenyl) boronic acid

Scheme 3.3.11	$K^9[me_2]$	Na_2HPO_4/NaH_2PO_4 in water, 50 mM, pH = 8.00	Pd-PEPPSI-IPr or (IPr)Pd(cinnamyl)Cl	*p*-tolylboronic acid
Scheme 2.3.14	Propionylated peptide with $K^9[me_3]$	Na_2HPO_4/NaH_2PO_4 in water, 50 mM, pH = 8.00	Pd-PEPPSI-IPr	*p*-tolylboronic acid (0.02 mmol)

Trypsin digestion of peptide products after reacting with Pd-IPr precatalysts

After the reaction described above for *Scheme 2.3.7*, the peptide sample was dried using a speedvac evaoporator and redissolved in aqueous triethylammonium bicarbonate solution (50 µL, 50 mM). Trypsin (0.5 µL) was added and the mixture was heated at 37 °C for 21 h. After drying the sample using a speedvac concentrator, the peptide mixture was dissolved in the MS eluent (20 µL, 0.1% TFA and 0.5% MeCN in H_2O) and analysed via LC-MS/MS (2 µL injection).

*Propionylation of starting peptide **56***

The peptide GEAKSQVFK[me_3]TNHFQKSTVR [**56**] (2.7 µL, 5 nmol, water (c = 4.2 mg/mL)) was exposed to propionic anhydride in isopropanol (5 µL, 25% solution). Ammonium hydroxide solution (5 µL, 28-30% NH_3) was added straight after to keep the pH between 7 and 9 and the sample was vortexed, centrifuged and heated at 37 °C for 15 min. Next, the volume of the sample was decreased to about 10-15 µL using a speedvac concentrator and a second round of propionylation was performed repeating the steps described above. The mixture was then dried and purified using Pierce C18 spin column (see general procedure **D**) before it was exposed to the Suzuki conditions displayed in *Scheme 2.3.14*.

Palladium-catalysed Hofmann-type elimination using pyr-Pd-PEPPSI-IMes

The peptide GEAKSQVFK[me_3]TNHFQKSTVR [**56**] (2.7 µL, 5 nmol, water (c = 4.2 mg/mL)) was transferred to a LoBind Eppendorf tube (1.5 mL) and diluted with aqueous sodium phosphate buffer (47.3 µL, Na_2HPO_4/NaH_2PO_4 in water, 50 mM, pH = 8.00, degassed for 1 h with N_2 flow) and flushed with N_2. The catalyst stock solution was prepared by dissolving pyr-Pd-PEPPSI-IMes (0.01 mmol) and potassium-*tert*-butoxide (0.04 mmol, 12% in THF) in

tetrahydrofuran (0.1 M, degassed for 1 h with N_2 flow) and stirring it at room temperature for 10 min. The catalyst solution (25 µL, 250 nmol, 0.01 M, 50 equiv.) was added to the diluted peptide and the mixture was flushed with N_2. After sealing the Eppendorf tube with parafilm, the reaction was vortexed and heated to 60 °C for 20 h. The mixture was then vortexed and aqueous DTT solution (28.5 µL, 285 nmol, 50 mM) was added to the solution to scavenge the Pd-catalyst. The reaction was heated at 60 °C for an additional 1 h 30 min. After cooling to room temperature, the mixture was concentrated to dryness using a speedvac evaporator. The reacted peptide was redissolved in equilibration solution (100 µL, 0.5% TFA and 5% MeCN in H_2O) and desalted using the Pierce C18 spin column (see general procedure **D**). After concentrating the purified peptide to dryness, it was dissolved in the MS eluent (20 µL, 0.1% TFA and 0.5% MeCN in H_2O) and analysed via LC-MS/MS (2 µL injection).

Identification of lysine methylation levels in histones (Subchapter 2.4)

Histone acid extraction

An aliquot of the commercially available native nucleosome (HeLa-derived) (11.8 µL, c = 0.85 mg/mL) was thawed to room temperature and ammonium bicarbonate (188.2 µL, 100 mM) was added. Next, aqueous H_2SO_4 solution (400 µL, 0.6 N) was slowly added. The sample was vortexed and rotated at 4 °C in the cold room for 16 h 30 min. After centrifugation at 18000 x g for 10 min at 4 °C, the supernatant was transferred into a new LoBind Eppendorf tube (2 mL), TCA (150 µL) was added to precipitate the histones and the sample was rotated at 4 °C for 1 h. The histones were pelleted by centrifugation (18000 x g, 4 °C, 10 min) and washed firstly with acidified acetone (1 mL, 0.1% HCl) and centrifugated (18000 x g, 4 °C, 10 min) and secondly with acetone (1 mL, 100%) and centrifugated (18000 x g, 4 °C, 10 min) again. After removal of the supernatant, the histone pellet was air dried and stored at – 80 °C.

Propionylation and Trypin digestion

The histone pellet collected after histone acid extraction was thawed to room temperature and resuspended in ammonium bicarbonate (10 µL, 100mM). The sample was vortexed and centrifugated for 10 s and propionic anhydride in isopropanol (5 µL, 25% solution) was added. Ammonium hydroxide solution (5 µL, 28-30% NH_3) was added straight after to keep the pH between 7 and 9 and the sample was vortexed, centrifuged and heated to 37 °C for 15 min. Next,

the volume of the sample was decreased to about 10-15 µL using a speedvac concentrator and a second round of propionylation was performed repeating the steps described above.

To digest the propionylated histones into peptides, ammonium bicarbonate (50 µL, 100 mM) and trypsin (1 µL) were added and the sample was vortexed, centrifuged and heated to 37 ˚C for 16 h. The volume of the sample was decreased to about 10-15 µL using a speedvac concentrator and two rounds of propionylation were performed. After drying the sample after the second round of propionylation, the peptides were desalted and purified using Pierce C18 Spin Columns.

Pierce C18 Spin Column purification

The Pierce C18 Spin Column was activated by adding the prepared activation solution (200 µL, 50% MeOH in H_2O) and centrifuging the column at 1500 x g for 1 min. The activation step was repeated. Next, equilibration solution (200 µL, 0.5% TFA and 5% MeCN in H_2O) was added and the column was centrifuged at 1500 x g for 1 min. This step was repeated again. The propionylated histone peptides were dissolved in equilibration solution (100 µL, 0.5% TFA and 5% MeCN in H_2O) and the sample was loaded to the wetted spin column by centrifugation (1500 x g, 1 min). The loading of the sample was repeated to ensure complete binding. The spin column leaded with the peptide sample was washed thrice by adding washing solution (200 µL, 0.5% TFA and 5% MeCN in H_2O) and centrifuging the column at 1500 x g for 1 min. The spin column was placed into a new LoBind Eppendorf tube (1.5 mL) and elution solution (100 µL, 70% MeCN in H_2O) was added and the column centrifuged 1500 x g for 1 min to collect the purified peptide sample. The purified histone peptides were dried by speedvac evaporation.

MS/MS analysis

MS eluent (20 µL, 0.1% TFA and 0.5% MeCN in H_2O) was added to the dried histone peptides and the sample was sonicated for 10 min. The peptide sample was then transferred to the MS vial to run a MS/MS measurement (10 µL injection).

5.3 Experimental for R&D II

5.3.1 Synthetic efforts towards the diaryldialkoxysilyl cross-linker

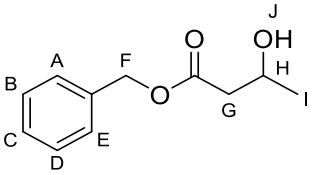

Benzyl 3-hydroxybutyrate [**67**]: Benzyl 3-oxobutanoate (1.0 mL, 5.79 mmol) was dissolved in tetrahydrofuran (60 mL) and water (12 mL) and cooled to 0 ˚C. Sodium borohydride (66.4 mg, 1.76 mmol) was slowly added and the reaction mixture was stirred for 30 min at 0 ˚C. An additional amount of sodium borohydride (21.5 mg, 0.57 mmol) was then added and the mixture was stirred for 30 min before a final portion of sodium borohydride (23.4 mg, 0.62 mmol) was added. After stirring at room temperature for 1 h 30 min, the reaction mixture was diluted with water (50 mL) and then extracted with diethyl ether (3 x 100 mL). The combined organic layers were dried with $MgSO_4$, filtered, concentrated *in vacuo* and purified via column chromatography (pentane : ethyl acetate, 4 : 1) to give **67** as a clear oil (1.056 g, 94%): R_f 0.71 (ethyl acetate : pentane, 2 : 8); ^{1}H NMR (400 MHz, CD_3CN) δ 7.41 – 7.31 (m, 5H, A – E), 5.11 (s, 2H, F), 4.17 – 4.08 (m, 1H, H), 2.94 (br. s, 1H, J), 2.48 – 2.39 (m, 2H, G), 1.15 (d, *J = 6.3 Hz*, 3H, I); ^{13}C NMR (100 MHz, $CDCl_3$) δ 172.9, 135.7, 128.8, 128.6, 128.4, 66.6, 64.4, 42.9, 22.6; HRMS (ESI) *m/z* calc for $C_{11}H_{15}O_3$ 195.1017, found: 195.1021.

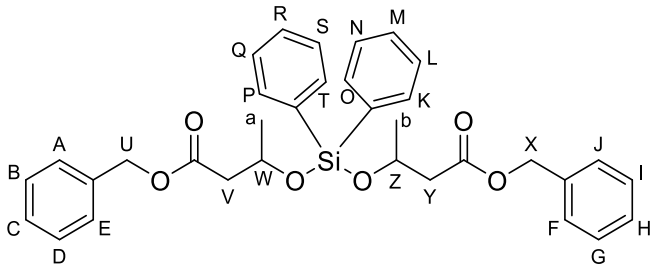

Dibenzyl 3,3'-((diphenylsilanediyl)bis(oxy))dibutyrate [**68**]: Benzyl 3-hydroxybutyrate [**67**] (508.5 mg, 2.62 mmol) was dissolved in dichloromethane (10 mL) and the solution was cooled to 0 ˚C. After the addition of imidazole (446.0 mg, 6.55 mmol), dichlorodiphenylsilane (0.25 mL, 1.19 mmol) was added and the reaction mixture was slowly warmed to room temperature and stirred for 15 h. Next, water (40 mL) was added and the mixture was extracted with dichloromethane (4 x 100 mL). The organic layers were combined, dried with $MgSO_4$,

filtered, concentrated *in vacuo* to give **68** as a clear oil (662.6 mg, 99%) (The product was taken on without further purification): ^{1}H NMR (400 MHz, CD_3CN) δ 7.65 – 7.23 (m, 20H, A – T), 5.14 – 4.93 (m, 4H, U + X), 4.48 -4.40 (m, 2H, W + Z), 2.63 – 2.41 (m, 4H, V + Y), 1.22 – 1.16 (m, 6H, a + b); ^{13}C NMR (100 MHz, CD_3CN) δ 171.8, 135.8, 135.1, 134.9, 131.3, 129.4, 129.0, 128.8, 128.7, 67.8, 66.8, 44.9, 24.0, 23.9; HRMS (ESI) *m/z* calc for $C_{34}H_{36}O_6NaSi$ 591.2179, found: 591.2184.

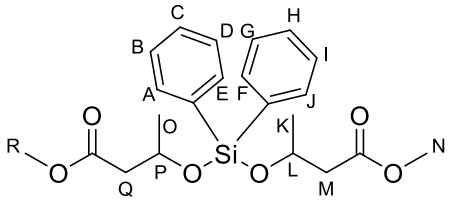

Dimethyl 3,3'-((diphenylsilanediyl)bis(oxy))dibutyrate [**71**]: Methyl 3-hydroxybutyrate (0.30 mL, 2.65 mmol) was dissolved in dichloromethane (10 mL) and the solution was cooled to 0 ℃. After the addition of imidazole (451.6 mg, 6.63 mmol), dichlorodiphenylsilane (0.25 mL, 1.19 mmol) was added and the reaction mixture was slowly warmed to room temperature and stirred for 18 h. Next, water (30 mL) was added and the mixture was extracted with dichloromethane (4 x 70 mL). The organic layers were combined, dried with $MgSO_4$, filtered and concentrated *in vacuo* to give **71** as a clear oil (493.4 mg, quant.) (The product was taken on without further purification): ^{1}H NMR (400 MHz, $CDCl_3$) δ 7.67 – 7.57 (m, 4H, A, E, F, J), 7.44 – 7.29 (m, 6H, B – D, G - I), 4.50 – 4.42 (m, 2H, L + P), 3.62 (s, 3H, R or N), 3.61 (s, 3H, R or N), 2.66 – 2.37 (m, 4H, M + Q), 1.25 – 1.22 (m, 6H, K + O); ^{13}C NMR (100 MHz, $CDCl_3$) δ 171.8, 171.8, 135.2, 135.1, 135.1, 130.4, 130.4, 130.3, 127.9, 127.8, 66.7, 51.6, 44.4, 44.4, 23.8, 23.8; HRMS (ESI) *m/z* calc for $C_{22}H_{28}O_6SiNa$ 439.1553, found: 439.1566.

5.3.2 Synthetic efforts towards the pyrano[2,3-*b*]pyran cross-linker

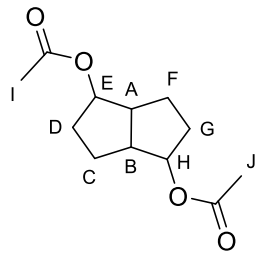

***rac*-2,6-Diacetoxybicyclo[3.3.0]octane** [**79**]: 1,5-Cyclooctadiene (2.7 mL, 22.1 mmol) was added to palladium(II) acetate (100.9 mg, 0.45 mmol) and lead(IV) tetraacetate (10.78 g, 24.3 mmol) in acetic acid (15 mL). The reaction mixture was stirred at room temperature for 6 d and then poured into ice-cooled water (30 mL). The aqueous layer was extracted with diethyl ether (3 x 50 mL). Next, the combined organic layers were washed with water (2 x 50 mL) and brine (2 x 50 mL), dried with Na_2SO_4, filtered, concentrated *in vacuo* and purified via column chromatography (pentane: ethyl acetate, 9 : 1) to give **79** as a clear oil (3.19 g, 64%): ^{1}H NMR (400 MHz, $CDCl_3$) δ 5.14 - 5.10 (m, 2H, E + H), 2.78 – 2.70 (m, 2H, A + B), 2.08 (s, 6H, I + J), 1.86 – 1.69 (m, 4H, C + F), 1.67 – 1.47 (m, 4H, D + G); ^{13}C NMR (100 MHz, $CDCl_3$) δ 170.8, 77.2, 44.7, 32.3, 22.8, 21.1; HRMS (ESI) *m/z* calc for $C_{12}H_{19}O_4$ 227.1283, found: 227.1279.

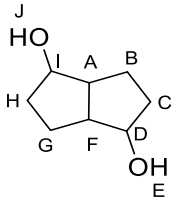

cis-Bicyclo[3.3.0]octan-2,6-diol [**80**]: Potassium hydroxide (140.7 mg, 2.51 mmol) was added to a solution of rac-2,6-diacetoxybicyclo[3.3.0]octane [**79**] (189.0 mg, 0.84 mmol) in methanol (2 mL) at 0 ˚C. The reaction mixture was stirred at 0 ˚C for 45 min, warmed up to room temperature and stirred for another 5 h 30 min. Next, the solution was poured into ice-cooled water (20 mL) and extracted with ethyl acetate (3 x 50 mL). The combined organic layers were washed with water (2 x 50 mL) and brine (2 x 50 mL), dried with $MgSO_4$, filtered, concentrated *in vacuo* and purified via column chromatography (pentane: ethyl acetate, 7 : 3) to give **80** as

a clear oil (46.6 mg, 39%): ^{1}H NMR (400 MHz, $CDCl_3$) δ 3.98 (s, 2H, D + I), 2.80 (br. S, 2H, E + J), 2.62 – 2.53 (m, 2H, A + F), 1.96 – 1.63 (m, 8H, B + C, G + H); ^{13}C NMR (100 MHz, $CDCl_3$) δ 72.9, 48.9, 39.1, 20.3; HRMS (ESI) *m/z* calc for $C_8H_{15}O_2$ 143.1072, found: 143.1068.

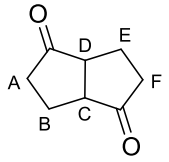

***rac*-2,6-diacetoxybicyclo[3.3.0]octane** [**77**]: *Method A*: DMSO (0.09 mL, 1.29 mmol) was slowly added to a solution of oxalyl chloride (0.05 mL, 0.58 mmol) in dichloromethane (1.5 mL) at – 60 ˚C. Next, a solution of the diol **80** (38.1 mg, 0.27 mmol) in dichloromethane (1 mL) and 20 min later triethylamine (0.45 mL, 3.14 mmol) were dropwise added to the reaction mixture keeping the temperature at – 60 ˚C. After an additional 20 min of stirring at – 60 ˚C, the solution was slowly warmed up to room temperature and stirred for an additional 15 min. The reaction was carefully quenched with water (15 mL) and the aqueous layer was extracted with dichloromethane (3 x 50 mL). The combined organic fractions were washed with water (200 mL), then brine (2 x 200 mL, sat.), dried with $MgSO_4$ and filtered. After concentrating the organic solution *in vacuo*, the mixture was purified via column chromatography (pentane : ethyl acetate, 7 : 3) to give **77** as a clear oil (20.4 mg, 55%).
Method B: The diol **80** (0.27 g, 1.93 mmol) was dissolved in dichloromethane (30 mL) and Dess-Martin periodinane (1.72 g, 4.05 mmol) was added to the solution. The reaction mixture was stirred at room temperature for 3 h. Next, it was diluted with diethyl ether (50 mL) and washed with aqueous sodium thiosulfate solution (50 mL, 1 M) and aqueous sodium bicarbonate solution (50 mL, sat.). The aqueous layers were combined and extracted with diethyl ether (3 x 150 mL). The collected organic layers were washed with brine (3 x 500 mL, sat.), dried with $MgSO_4$, filtered, concentrated *in vacuo* and purified via column chromatography (pentane : ethyl acetate, 7 : 3) to give **77** as a clear oil (0.24 g, 90%): ^{1}H NMR (400 MHz, $CDCl_3$) δ 2.99 – 2.93 (m, 2H, C + D), 2.46 – 2.38 (m, 2H, H_{ax} or H_{eq} of A/F), 2.27 – 2.21 (m, 4H, B + E), 2.18 – 2.09 (m, 2H, H_{ax} or H_{eq} of A/F); ^{13}C NMR (100 MHz, $CDCl_3$) δ 220.3, 49.5, 37.6, 23.1; HRMS (ESI) *m/z* calc for $C_8H_{11}O_2$ 139.0754, found: 139.0754.

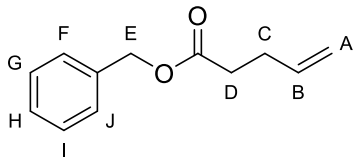

Benzyl pent-4-enoate [**83**] - Pent-4-enoic acid (1.0 mL, 0.010 mol) was dissolved in *N,N*-dimethylformamide (20 mL) and potassium carbonate (4.06 g, 0.029 mol) was added. After stirring the reaction mixture at rt for 5 min, benzyl bromide (1.4 mL, 0.012 mol) was added and the mixture was stirred at rt for 17 h. Next, aqueous LiCl solution (50 mL, 5%) was added and the aqueous layer was extracted with ethyl acetate (3 x 75 mL). The organic layers were combined, dried with $MgSO_4$, filtered, concentrated *in vacuo* and purified via column chromatography (pentane : ethyl acetate, 9 : 1) to give **83** as a clear oil (1.64 g, 88%): ^{1}H NMR (400 MHz, $CDCl_3$) δ 7.51 – 7.28 (m, 5H, F – J), 5.90 – 5.75 (m, 1H, B), 5.12 (s, 2H, E), 5.11 – 4.95 (m, 2H, A), 5.11 – 4.95 (m, 4H, C + D); ^{13}C NMR (100 MHz, $CDCl_3$) δ 173.0, 136.7, 136.1, 129.4, 128.7, 128.4, 115.7, 66.4, 33.7, 29.0; HRMS (CI) *m/z* calc for $C_{12}H_{14}O_2$ 190.0994, found: 190.1003.

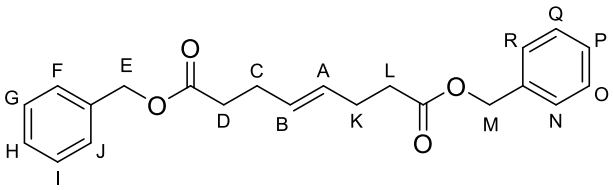

Dibenzyl (*E*)-oct-4-enedioate [**84**] - Benzyl pent-4-enoate [**83**] (3.78 g, 0.020 mol) was dissolved in dichloroethane (10 mL) and the 2nd generation Grubbs catalyst (0.34 g, 0.0004 mol) was added to the solution. The reaction mixture was heated under reflux for 2 h 30 min. After the reaction was cooled down to room temperature, it was filtered through a plug of celite and washed with dichloromethane (30 mL). The organic solution was concentrated *in vacuo* and the resulting mixture was purified twice via column chromatography (1st: pentane : ethyl acetate, 9 : 1; 2nd: a gradient from 100% pentane to pentane : ethyl acetate, 9 : 1) to yield **84** as a clear oil (0.75 g, 11%): ^{1}H NMR (400 MHz, $CDCl_3$) δ 7.38 – 7.30 (m, 10H, F – J, N – R), 5.42 – 5.38 (m, 2H, A + B), 5.11 (s, 4H, E + M), 2.37 – 2.30 (m, 4H, H_{ax} or H_{eq} of C/K, H_{ax} or H_{eq} of D/L), 2.10 – 1.93 (m, 2H, H_{ax} or H_{eq} of C/K), 1.73 – 1.65 (m, 2H, H_{ax} or H_{eq} of D/L); HRMS (ESI) *m/z* calc for $C_{22}H_{25}O_4$ 353.1753, found: 353.1764.

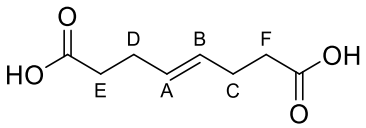

(*E*)-Oct-4-enedioic acid [**85**]: Lithium hydroxide (402.4 mg, 16. 80 mmol) was added to a solution of dibenzyl (*E*)-oct-4-enedioate [**84**] (592.2 mg, 1.68 mmol) in tetrahydrofuran, methanol and water (3 : 2 : 2, total V = 14 mL) and the reaction mixture was heated at 90 ˚C for 7 d. After cooling to room temperature, the mixture was diluted with water (5 mL), acidified with aqueous hydrogen chloride solution (6 N) and extracted with dichloromethane (3 x 20 mL). The combined organic layers were concentrated *in vacuo* and the mixture was triturated with ethyl acetate and pentane to give **85** as a white solid (71.2 mg, 25%): ^{1}H NMR (400 MHz, $CDCl_3$) δ 5.52 – 5.49 (m, 2H, A + B), 2.45 – 2.40 (m, 4H, E + F), 2.33 – 2.29 (m, 4H, D + C); HRMS (ESI) *m/z* calc for $C_8H_{11}O_4$ 171.0657, found: 171.0652.

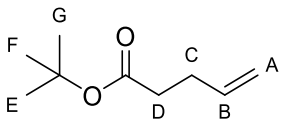

***Tert*-butyl pent-4-enoate** [**88**]: *N,N*-Dimethylpyridin-4-amine (0.019 g, 0.0002 mol) and *tert*-butanol (2.8 mL, 0.029 mol) were added to a solution of pent-4-enoic acid (1.0 mL, 0.010 mol) in dichloromethane (15 mL). The reaction mixture was cooled to 0 ˚C and *N,N'*-dicyclohexyl-methanediimine (2.22 g, 0.011 mol) was added. After stirring for 18 h at room temperature, the formed urea was filtered off and washed with dichloromethane (40 mL). The filtrate was washed with aqueous hydrogen chloride (2 x 50 mL, 0.1 M), aqueous sodium bicarbonate (2 x 50 mL, sat.) and brine (1 x 50 mL, sat.), dried with $MgSO_4$, filtered, concentrated *in vacuo* and purified via column chromatography (pentane : ethyl acetate, 8 : 2) to give **88** as a white solid (0.59 g, 39%): ^{1}H NMR (400 MHz, $CDCl_3$) δ 5.90 – 5.80 (m, 1H, B), 5.11 – 5.00 (m, 2H, A), 2.40 – 2.31 (m, 4H, C + D), 1.47 (s, 9H, E – G); ^{13}C NMR (100 MHz, $CDCl_3$) δ 172.5, 137.0, 115.2, 80.2, 34.8, 29.1, 28.1; *The mass could not be obtained with various MS techniques.*

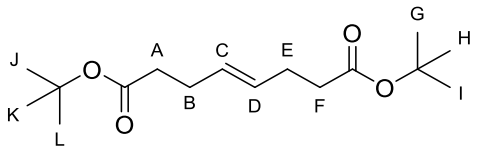

Di-*tert*-butyl (*E*)-oct-4-enedioate [**87**]: *Tert*-butyl pent-4-enoate [**88**] (74.2 mg, 0.47 mmol) was dissolved in dichloromethane (5 mL) and the solution was degassed with N_2 for 10 min. Next, Hoveyda-Grubbs catalyst 2nd generation (1.5 mg, 0.002 mmol) and *p*-benzoquinone (0.5 mg, 0.0005 mmol) were added and the reaction was stirred under reflux for 4 h. The reaction mixture was filtered through a plug of celite and washed with diethyl ether (30 mL). Brine (50 mL, sat.) was added to the filtrate and the organic layer was separated. The aqueous layer was extracted with diethyl ether (2 x 75 mL) and the organic layers were combined, dried with $MgSO_4$, filtered, concentrated *in vacuo* and purified via column chromatography (pentane : ethyl acetate, 8 : 2) to give **87** as white solid (32.8 mg, 24%): ^{1}H NMR (400 MHz, $CDCl_3$) δ 5.48 (br. S, 2H, C + D), 2.28 (s, 8H, A, B, E,F), 1.46 (s, 18H, G – L); ^{13}C NMR (100 MHz, $CDCl_3$) δ 172.5, 129.4, 80.2, 35.4, 28.1, 28.1; HRMS (CI) *m/z* calc for $C_{16}H_{28}O_4Na$ 307.1885, found: 307.1880.

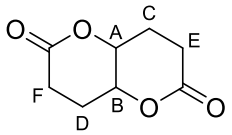

Hexahydropyrano[3, 2-*b*]pyran-2,6-dione [**76**]: (*E*)-Oct-4-enedioic acid [**85**] (33.8 mg, 0.20 mmol) was dissolved in water (1 mL) and sodium hydrogen carbonate (32.9 mg, 0.39 mmol) was added. Next, silver (I) nitrate (67.6 mg, 0.40 mmol) in water (2 mL) was added to the reaction mixture dropwise and the reaction was stirred at room temperature for 5 min. The precipitate was filtered off, washed with water (15 mL) and dried *in vacuo* (caution: light-sensitive) to give (*E*)-oct-4-enedioic acid, silver(I) salt [**81**] as a grey-white solid (72.8 mg, 95%).

Iodine (14.9 mg, 0.06 mmol) in dichloromethane (5 mL) was added to (*E*)-oct-4-enedioic acid, silver(I) salt [**81**] (20.6 mg, 0.05 mmol) in dichloromethane (3 mL) slowly and the reaction mixture was stirred at room temperature for 27 h. Aqueous sodium thiosulfate solution (5 mL, 1 M) and water (10 mL) was added to the reaction mixture and the aqueous layer was extracted with ethyl acetate (3 x 30 mL). The organic layers were combined, dried with $MgSO_4$, filtered and concentrated *in vacuo*. **76** could not be isolated via recrystallisation, but NMR (^{1}H, ^{13}C, COSY, HSQC) and MS analysis of the crude mixture suggested that the bis-lactone **76** was present in the mixture: ^{1}H NMR (400 MHz, CD_3CN) δ 4.39 – 4.16 (m, 2H, A + B), 1.83 – 1.70 (m, 4H, C + D), 1.68 – 1.51 (m, 4H, E + F); ^{13}C NMR (100 MHz, CD_3CN) δ 176.5, 81.7, 34.7, 23.8; GC-MS (EI) (rt: 10.66 – 10.70 min, 10.77 – 10.80 min) *m/z* 170.1 $(M+H)^+$.

5.3.3 Synthetic efforts towards the furo[2,3-*b*]furan cross-linker

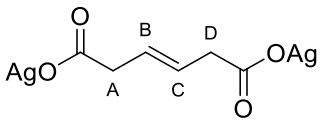

(*E*)-Hex-3-enedioic acid, silver(I) salt [**90**] – (*E*)-Hex-3-enedioic acid (0.39 g, 2.71 mmol) was dissolved in water (13 mL) and sodium hydrogen carbonate (0.46 g, 5.43 mmol) was added. Next, silver (I) nitrate (0.94 g, 5.51 mmol) in water (8 mL) was added to the reaction mixture dropwise and the reaction was stirred at room temperature for 5 min. The precipitate was filtered off, washed with water (70 mL) and dried *in vacuo* (caution: light-sensitive) to give **90** as a white solid (0.96 g, 99%): ^{1}H NMR (400 MHz, D_2O) δ 5.59 – 5.56 (m, 2H, B + C), 2.85 – 2.83 (m, 4H, A + D); HRMS (ESI) *m/z* calc for $C_6H_7O_4^-$ 143.0339, found: 143.0339.

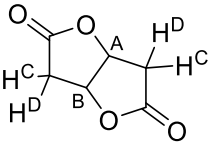

Tetrahydrofuro[3,2-*b*]furan-2,5-dione [**89**] – Iodine (2.10 g, 5.86 mmol) in dichloromethane (30 mL) was added to (*E*)-hex-3-enedioic acid, silver(I) salt [**90**] (1.64 g, 6.45 mmol) in dichloromethane (15 mL) slowly and the reaction mixture was stirred at room temperature for 40 h. Aqueous sodium thiosulfate solution (20 mL, 1 M) and water (40 mL) was added to the reaction mixture and the aqueous layer was extracted with ethyl acetate (3 x 100 mL). The organic layers were combined, dried with $MgSO_4$, filtered and concentrated *in vacuo*. The crude mixture was recrystallized with ethyl acetate and pentane. The precipitate was filtered off, washed with pentane and dried to give **89** as a white solid (0.67 g, 81%): ^{1}H NMR (400 MHz, CD_3CN) δ 5.23 – 5.19 (m, 2H, A + B), 3.03 – 2.90 (m, 2H, H^C or H^D), 2.76 (d, *J* = *18.8 Hz*, 2H, H^C or H^D); ^{13}C NMR (100 MHz, CD_3CN) δ 175.1, 80.0, 35.8; HRMS (ESI) *m/z* calc for $C_6H_7O_4$ 143.0339, found: 143.0339.

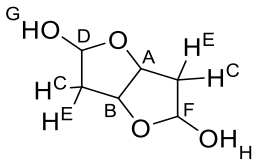

Hexahydrofuro[3,2-*b*]furan-2,5-diol [**92**]: DIBAL solution (0.9 mL, 0.92 mmol, 1 M in toluene) was added slowly to the bis-lactone **89** (43.7 mg, 0.31 mmol) at – 78 ˚C and the reaction mixture was stirred at – 78 ˚C for 6 h. After the addition of methanol (10 mL), the mixture was warmed up to 0 ˚C and water (3 mL) was added to the solution. Next, $MgSO_4$ and celite were added and the mixture was stirred at room temperature for 30 min, filtered, washed with diethyl ether (20 mL) and concentrated *in vacuo* to obtain **92** as a white solid (28.5 mg, 63%) (The product was taken on without further purification): ^{1}H NMR (400 MHz, CD_3CN) δ 5.46 (td, *J = 5.2, 3.2 Hz*, 2H, D + F), 4.73 – 4.70 (m, 2H, A + B), 3.99 (d, *J = 4.9 Hz*, 2H, H^C or H^E), 2.17 – 2.11 (m, 2H, G + H), 1.91 – 1.89 (m, 2H, H^C or H^E); ^{13}C NMR (100 MHz, CD_3CN) δ 99.3, 81.3, 41.0; HRMS (ESI) *m/z* calc for $C_6H_9O_4$ 145.0495, found: 145.0497.

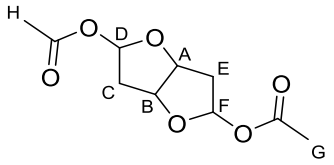

Hexahydrofuro[3,2-*b*]furan-2,5-diyl diacetate [**94**]: The furo[3,2-*b*]furan lactone **89** (46.4 mg, 0.33 mmol) was dissolved in dichloromethane (1.6 mL) and cooled to – 78 ˚C. DIBAL solution (0.75 mL, 0.75 mmol, 1 M in toluene) was added dropwise to the mixture keeping the temperature at about – 78 ˚C and the reaction mixture was stirred at that temperature for 2 h. First, pyridine (0.16 mL, 1.96 mmol), then a solution of DMAP (159.6 mg, 1.31 mmol) in dichloromethane (1.1 mL) and then acetic anhydride (0.37 mL, 3.91 mmol) were successively added dropwise keeping the temperature at about – 78 ˚C. The mixture was stirred at - 78 ˚C for 13 h and then gradually warmed up to – 20 ˚C over 5 h. Aqueous sodium chloride solution (12 mL, sat.) was added to the mixture at – 20 ˚C and the mixture was warmed up to room temperature. After stirring at room temperature for 30 min, the aqueous layer was extracted with dichloromethane (3 x 50 mL). The combined organic layers were washed with aqueous sodium bicarbonate solution (3 x 150 mL, sat.) and aqueous copper sulfate solution (150 mL, sat.), dried with Na_2SO_4, filtered, concentrated *in vacuo* and purified via preparative TLC (ethyl acetate : pentane, 7 : 3) to give **94** as an anomeric mixture of 3 diastereomers (65.6 mg, 86%), of which one diastereomer was isolated (25.0 mg, 33%): R_f 0.2 (pentane :

ethyl acetate, 1 : 1); ^{1}H NMR (400 MHz, CD_2Cl_2) δ 6.28 - 6.21 (m, 2H, D + F), 4.77 – 4.74 (m, 2H, A + B), 2.47 – 2.39 (m, 2H, H_{ax} or H_{eq} of C + E), 2.38 – 2.31 (m, 2H, H_{ax} or H_{eq} of C + E), 2.05 (s, 6H, G + H); ^{13}C NMR (100 MHz, CD_2Cl_2) δ 170.7, 100.2, 85.1, 40.4, 21.8; *The mass could not be obtained with various MS techniques.*

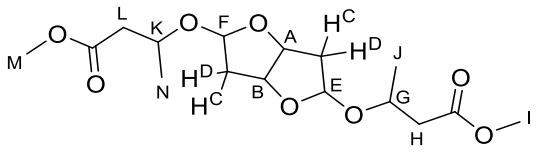

Dimethyl 3,3'-((hexahydrofuro[3,2-*b*]furan-2,5-diyl)bis(oxy))dibutyrate [**75**]: *Method A*: Methyl 3-hydroxybutyrate (0.05 mL, 0.002 mmol) and catalytic amount of rhenium(VII) oxide (~10 mg, caution: hygroscopic!), were added to a solution of the hemiacetal **92** (17.5 mg, 0.12 mmol) in dichloromethane (1 mL) and the reaction mixture was stirred at room temperature for 27 h. Next, the mixture was filtered through a plug of celite and washed with dichloromethane (20 mL). The organic solution was concentrated *in vacuo* and purified via preparative TLC (pentane : ethyl acetate, 1 : 1) to give **75** (18.7 mg, 45%).

Method B: First trimethylsilyl trifluoromethanesulfonate (0.02 mL, 0.09 mmol) and then methyl 3-hydroxybutyrate (0.01 mL, 0.08 mmol) were added dropwise to a solution of the acetal **94** (9.1 mg, 0.04 mmol) in dichloromethane (2 mL) while keeping the temperature at – 30 ˚C. The reaction mixture was stirred at – 30 ˚C for 3 h 30 min and subsequently quenched with aqueous sodium bicarbonate solution (3 mL, sat.) at – 20 ˚C. After slowly warming up to room temperature, the mixture was further diluted with dichloromethane (10 mL) and the organic layer was separated. The aqueous layer was extracted with dichloromethane (2 x 20 mL). The combined organic layers were washed with aqueous sodium bicarbonate solution (50 mL, sat.) and brine (50 mL, sat.), dried with $MgSO_4$, filtered, concentrated *in vacuo* and purified via preparative TLC (pentane : ethyl acetate, 1 : 1) to yield **75** as a clear oil (4.5 mg, 32%): ^{1}H NMR (400 MHz, CD_3CN) δ 5.32 (ddd, *J = 5.7, 3.8, 2.1 Hz*, 2H, E + F), 4.69 – 4.53 (m, 2H, A + B), 4.13 – 3.99 (m, 2H, G + K), 3.61 (s, 6H, I + M), 2.49 – 2.34 (m, 4H, H + L), 2.13 – 2.05 (m, 2H, H^C or H^D), 2.00 – 1.92 (m, 2H, H^C or H^D), 1.15 (dd, *J = 21.8, 6.3 Hz*, 6H, J + N); ^{13}C NMR (100 MHz, CD_3CN) δ 171.6, 171.5, 105.6, 105.5, 103.2, 103.1, 81.3, 81.3, 70.8, 69.0, 51.0, 42.1, 41.4, 39.9, 39.7, 21.1, 18.7; HRMS (ESI) *m/z* calc for $C_{16}H_{26}O_8Na$ 369.1525, found: 369.1531.

5.3.4 Synthetic efforts towards the carbonate cross-linker

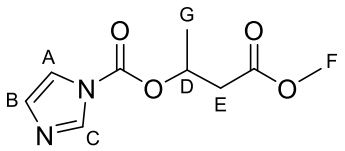

4-Methoxy-4-oxobutan-2-yl 1H-imidazole-1-carboxylate [**96**]: Imidazole (27.2 mg, 0.40 mmol) was added to the solution of methyl 3-hydroxybutyrate (0.7 mL, 6.0 mmol) in tetrahydrofuran (10 mL) at 0 ˚C prior to the addition of 1,1'-carbonyldiimidazole (810.8 mg, 5 mmol). The reaction mixture was stirred at 0 ˚C for 15 min and at room temperature for 23 h. After the addition of water (40 mL), the organic layer was separated. The aqueous layer was washed with dichloromethane (4 x 75 mL), dried with $MgSO_4$, filtered, concentrated *in vacuo* and purified via column chromatography (pentane : ethyl acetate, 6 : 4) to give **96** as a clear oil (764.3 mg, 72%): ^{1}H NMR (400 MHz, $CDCl_3$) δ 8.09 (s, 1H, C), 7.39 (t, *J = 1.5 Hz*, 1H, A or B), 7.05 – 7.04 (m, 1H, A or B), 5.53 – 5.45 (m, 1H, D), 3.69 (s, 3H, F), 2.84 – 2.64 (m, 2H, E), 1.48 (d, *J = 6.4 Hz*, 3H, G); ^{13}C NMR (100 MHz, $CDCl_3$) δ 170.1, 148.0, 137.2, 130.8, 117.2, 72.3, 52.2, 40.4, 19.9; HRMS (ESI) *m/z* calc for $C_9H_{13}N_2O_4$ 213.0870, found: 213.0870.

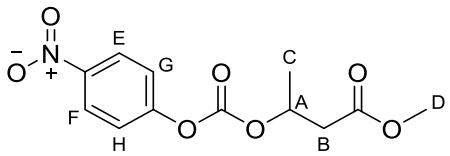

Methyl 3-(((4-nitrophenoxy)carbonyl)oxy)butanoate [**98**]: Triethylamine (2.5 mL, 17.78 mmol) was added to a solution of methyl 3-hydroxybutyrate (1.0 mL, 8.89 mmol) in dichloromethane (3 mL). A solution of 4-nitrophenyl chloroformate (1.97 g, 9.78 mmol) in dichloromethane (5 mL) was added dropwise to the reaction mixture over 30 min. The mixture was stirred at room temperature for 20 h and subsequently quenched with aqueous ammonium chloride solution (10 mL, sat.). The organic layer was separated, and the aqueous layer was extracted with dichloromethane (2 x 30 mL). The combined organic layers were washed with brine (3 x 50 mL), dried with $MgSO_4$, filtered, concentrated *in vacuo* and purified via column chromatography (pentane : ethyl acetate, 8 : 2) to yield **98** as an oil (1.36 g, 54%): ^{1}H NMR (400 MHz, CD_3CN) δ 8.31 – 8.25 (m, 2H, E + F), 7.46 – 7.40 (m, 2H, G + H), 5.24 – 5.16 (m, 1H, A), 3.67 (s, 3H, D), 2.80 – 2.61 (m, 2H, B), 1.40 (d, *J = 6.4 Hz*, 3H, C); ^{13}C NMR (100

MHz, CD_3CN) δ 171.4, 156.6, 152.9, 146.6, 126.3, 123.2, 74.3, 52.4, 40.7, 19.8; *The mass could not be obtained with various MS techniques.*

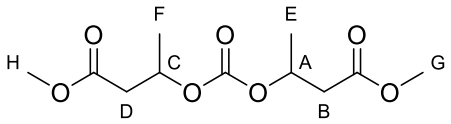

Dimethyl 3,3'-(carbonylbis(oxy))dibutyrate [**97**]: Methyl 3-(((4-nitrophenoxy) carbonyl)-oxy)butanoate [**98**] (321.7 mg, 1.14 mmol) was added dropwise to the solution of methyl 3-hydroxybutyrate (0.13 mL, 1.14 mmol), *N,N*-diisopropylethylamine (0.40 mL, 2.27 mmol) and DMAP (16.7 mg, 0.14 mmol) in *N,N*-dimethylformamide (9 mL) at room temperature and the mixture was stirred at 60 ˚C for 21 h. Next, aqueous lithium chloride solution (20 mL, 5%) was added to the mixture and the aqueous layer was extracted with dichloromethane (3 x 50 mL). The combined organic layers were washed with aqueous lithium chloride solution (3 x 150 mL, 5%), dried with $MgSO_4$, filtered and concentrated *in vacuo*. The mixture was first purified via column chromatography (dichloromethane : methanol, 99 : 1), however, **97** and residual methyl 3-hydroxybutyrate could not be separated. Next, the mixture was heated under vacuum removing residual methyl 3-hydroxybutyrate to give **97** as a clear oil (34.6 mg, 12%): ^{1}H NMR (400 MHz, CD_3CN) δ 5.10 – 4.98 (m, 2H, A + C), 3.63 (d, *J = 1.1 Hz*, 6H, G + H), 2.68 – 2.51 (m, 4H, B + D), 1.28 (dd, *J = 6.3, 1.6 Hz*, 6H, E + F); ^{13}C NMR (100 MHz, CD_3CN) δ 171.5, 154.6, 72.3, 52.3, 40.9, 19.9; HRMS (ESI) *m/z* calc for $C_{11}H_{18}O_7Na$ 285.0950, found: 285.0952.

6 REFERENCES

1 A. D. Goldberg, C. D. Allis and E. Bernstein, *Cell*, 2007, **128**, 635–638.

2 F. L. Cherblanc, R. W. M. Davidson, P. Di Fruscia, N. Srimongkolpithak and M. J. Fuchter, *Nat. Prod. Rep.*, 2013, **30**, 605–624.

3 C. D. Allis and T. Jenuwein, *Nat. Rev. Genet.*, 2016, **17**, 487–500.

4 N. A. Villota-Salazar, A. Mendoza-Mendoza and J. M. González-Prieto, *Front. Life Sci.*, 2016, **9**, 347–370.

5 H. J. Muller and E. Altenburg, *Genetics*, 1930, **15**, 283–311.

6 B. McCLINTOCK, *Cold Spring Harb. Symp. Quant. Biol.*, 1951, **16**, 13–47.

7 M. F. Lyon, *Nature*, 1961, **190**, 372–373.

8 M. A. H. Surani, S. C. Barton and M. L. Norris, *Nature*, 1984, **308**, 548–550.

9 J. McGrath and D. Solter, *Cell*, 1984, **37**, 179–183.

10 W. Reik, W. Dean and J. Walter, *Science (80-.).*, 2012, **293**, 1089–1093.

11 F. Santos and W. Dean, *Reproduction*, 2004, **127**, 643–651.

12 I. H. Park, R. Zhao, J. A. West, A. Yabuuchi, H. Huo, T. A. Ince, P. H. Lerou, M. W. Lensch and G. Q. Daley, *Nature*, 2008, **451**, 141–146.

13 P. Perry, S. Sauer, N. Billon, W. D. Richardson, M. Spivakov, G. Warnes, F. J. Livesey, M. Merkenschlager, A. G. Fisher and V. Azuara, *Cell Cycle*, 2004, **3**, 1645–1650.

14 B. E. Bernstein, T. S. Mikkelsen, X. Xie, M. Kamal, D. J. Huebert, J. Cuff, B. Fry, A. Meissner, M. Wernig, K. Plath, R. Jaenisch, A. Wagschal, R. Feil, S. L. Schreiber and E. S. Lander, *Cell*, 2006, **125**, 315–326.

15 A. P. Feinberg, *Nature*, 2007, **447**, 433–440.

16 A. Portela and M. Esteller, *Nat. Biotechnol.*, 2010, **28**, 1057–68.

17 C. H. Arrowsmith, C. Bountra, P. V Fish, K. Lee and M. Schapira, *Nat. Rev. Drug Discov.*, 2012, **11**, 384–400.

18 F. L. Cherblanc, R. W. M. Davidson, P. Di Fruscia, N. Srimongkolpithak and M. J.

Fuchter, *Nat. Prod. Rep.*, 2013, **30**, 605–624.

19 C. B. Yoo and P. Jones, *Nat. Rev. Drug Discov.*, 2006, **5**, 37–50.

20 A. Sparmann and M. van Lohuizen, *Nat. Rev. Cancer*, 2006, **6**, 846–856.

21 R. K. McGinty and S. Tan, *Chem. Rev.*, 2015, **115**, 2255–2273.

22 T. Kouzarides, *Cell*, 2007, **128**, 693–705.

23 A. Bird, *Nature*, 1986, **321**, 209–213.

24 K. D. Robertson, *Nat. Rev. Genet.*, 2005, **6**, 597–610.

25 F. F. Costa, *Gene*, 2008, **410**, 9–17.

26 M. A. Valencia-Sanchez, J. Liu, G. J. Hannon and R. Parker, *Genes Dev.*, 2006, **20**, 515–524.

27 B. E. Bernstein, E. L. Humphrey, R. L. Erlich, R. Schneider, P. Bouman, J. S. Liu, T. Kouzarides and S. L. Schreiber, *Proc. Natl. Acad. Sci. U. S. A.*, 2002, **99**, 8695–8700.

28 H. Santos-Rosa, R. Schneider, A. J. Bannister, J. Sherriff, B. E. Bernstein, N. C. T. Emre, S. L. Schreiber, J. Mellor and T. Kouzarides, *Nature*, 2002, **419**, 407–411.

29 X. Shi, T. Hong, K. L. Walter, M. Ewalt, E. Michishita, T. Hung, D. Carney, P. Peña, F. Lan, M. R. Kaadige, N. Lacoste, C. Cayrou, F. Davrazou, A. Saha, B. R. Cairns, D. E. Ayer, T. G. Kutateladze, Y. Shi, J. Côté, K. F. Chua and O. Gozani, *Nature*, 2006, **442**, 96–99.

30 G. Schotta, M. Lachner, K. Sarma, A. Ebert, R. Sengupta, G. Reuter, D. Reinberg and T. Jenuwein, *Genes Dev.*, 2004, **18**, 1251–1262.

31 J. C. Rice, S. D. Briggs, B. Ueberheide, C. M. Barber, J. Shabanowitz, D. F. Hunt, Y. Shinkai and C. D. Allis, *Mol. Cell*, 2003, **12**, 1591–1598.

32 A. H. F. M. Peters, S. Kubicek, K. Mechtler, R. J. O'Sullivan, A. A. H. A. Derijck, L. Perez-Burgos, A. Kohlmaier, S. Opravil, M. Tachibana, Y. Shinkai, J. H. A. Martens and T. Jenuwein, *Mol. Cell*, 2003, **12**, 1577–1589.

33 T. Suganuma and J. L. Workman, *Cell*, 2008, **135**, 604–607.

34 J. S. Lee, E. Smith and A. Shilatifard, *Cell*, 2010, **142**, 682–685.

35 M. B. Chandrasekharan, F. Huang and Z. W. Sun, *Epigenetics*, 2010, **5**, 460–468.

36 T. Kouzarides, *Curr. Opin. Genet. Dev.*, 2002, **12**, 198–209.

37 C. Martin and Y. Zhang, *Nat. Rev. Mol. Cell Biol.*, 2005, **6**, 838–49.

38 J. C. Black, C. Van Rechem and J. R. Whetstine, *Mol. Cell*, 2012, **48**, 491–507.

39 K. Hyun, J. Jeon, K. Park and J. Kim, *Exp. Mol. Med.*, 2017, **49**, e324.

40 Q. Feng, H. Wang, H. H. Ng, H. Erdjument-Bromage, P. Tempst, K. Struhl, Y. Zhang, C. Hill and N. Carolina, *Curr. Opin. Cell Biol.*, 2002, **12**, 1052–1058.

41 J. Huang and S. L. Berger, *Curr. Opin. Genet. Dev.*, 2008, **18**, 152–158.

42 Y. Shi, F. Lan, C. Matson, P. Mulligan, J. R. Whetstine, P. A. Cole, R. A. Casero and Y. Shi, *Cell*, 2004, **119**, 941–953.

43 Y. I. Tsukada, J. Fang, H. Erdjument-Bromage, M. E. Warren, C. H. Borchers, P. Tempst and Y. Zhang, *Nature*, 2006, **439**, 811–816.

44 S. Tillib, S. Petruk, Y. Sedkov, A. Kuzin, M. Fujioka, T. Goto and A. Mazo, *Mol. Cell. Biol.*, 1999, **19**, 5189–5202.

45 C. J. Woo, P. V. Kharchenko, L. Daheron, P. J. Park and R. E. Kingston, *Cell*, 2010, **140**, 99–110.

46 M. Tsai, O. Manor, Y. Wan, N. Mosammaparast, J. K. Wang, F. Lan, Y. Shi, E. Segal and H. Y. Chang, *Science (80-.).*, 2010, **329**, 689–693.

47 A. Verdel, S. Jia, S. Gerber, T. Sugiyama, S. Gygi, S. I. S. Grewal and D. Moazed, *Science (80-.).*, 2013, **303**, 672–676.

48 T. Bartke, M. Vermeulen, B. Xhemalce, S. C. Robson, M. Mann and T. Kouzarides, *Cell*, 2010, **143**, 470–484.

49 J. R. Horton, A. K. Upadhyay, H. H. Qi, X. Zhang, Y. Shi and X. Cheng, *Nat. Struct. Mol. Biol.*, 2010, **17**, 38–44.

50 T. Jenuwein and C. D. Allis, *Science (80-.).*, 2001, **293**, 1074–1080.

51 B. D. Strahl and C. D. Allis, *Nature*, 2000, **403**, 41–45.

52 C. A. Musselman, M. E. Lalonde, J. Côté and T. G. Kutateladze, *Nat. Struct. Mol. Biol.*,

2012, **19**, 1218–1227.

53 C. A. Musselman, S. Khorasanizadeh and T. G. Kutateladze, *Biochim. Biophys. Acta - Gene Regul. Mech.*, 2014, **1839**, 686–693.

54 D. J. Patel and Z. Wang, *Annu. Rev. Biochem.*, 2013, **82**, 81–118.

55 W. Fischle, S. T. Boo, H. L. Dormann, B. M. Ueberheide, B. A. Garcia, J. Shabanowitz, D. F. Hunt, H. Funabiki and C. D. Allis, *Nature*, 2005, **438**, 1116–1122.

56 S. Akbarian and H. S. Huang, *Biol. Psychiatry*, 2009, **65**, 198–203.

57 Y. Shi, *Nat. Rev. Genet.*, 2007, **8**, 829–833.

58 E. L. Greer and Y. Shi, *Nat. Rev. Genet.*, 2012, **13**, 343–57.

59 J. C. Black and J. R. Whetstine, *Biopolymers*, 2013, **99**, 127–135.

60 R. A. Varier and H. T. M. Timmers, *Biochim. Biophys. Acta - Rev. Cancer*, 2011, **1815**, 75–89.

61 Z. Wu, J. Connolly and K. K. Biggar, *FEBS J.*, 2017, **284**, 2732–2744.

62 M. Luo, *Chem. Rev.*, 2018, **118**, 6656–6705.

63 A. Barski, S. Cuddapah, K. Cui, T.-Y. Roh, D. E. Schones, Z. Wang, G. Wei, I. Chepelev and K. Zhao, *Cell*, 2007, **129**, 823–37.

64 P. Collas, *Mol. Biotechnol.*, 2010, **45**, 87–100.

65 M. Kuo and C. D. Allis, *Methods*, 1999, **433**, 425–433.

66 M. J. Buck and J. D. Lieb, *Genomics*, 2004, **83**, 349–360.

67 P. J. Park, *Nat. Rev. Genet.*, 2009, **10**, 669–80.

68 T. S. Furey, *Nat. Rev. Genet.*, 2012, **13**, 840–52.

69 D. E. Schones and K. Zhao, *Nat. Rev. Genet.*, 2008, **9**, 179–91.

70 B. E. Bernstein, E. Birney, I. Dunham, E. D. Green, C. Gunter and M. Snyder, *Nature*, 2012, **489**, 57–74.

71 E. A. Feingold *et al.*, *Science (80-.).*, 2004, **306**, 636–640.

72 B. E. Bernstein, J. a Stamatoyannopoulos, J. F. Costello, B. Ren, A. Milosavljevic, A.

Meissner, M. Kellis, M. a Marra, A. L. Beaudet, J. R. Ecker, P. J. Farnham, M. Hirst, E. S. Lander, T. S. Mikkelsen and J. a Thomson, *Nat. Biotechnol.*, 2010, **28**, 1045–8.

73 S. E. Peach, E. L. Rudomin, N. D. Udeshi, S. a Carr and J. D. Jaffe, *Mol. Cell. Proteomics*, 2012, **11**, 128–37.

74 T. A. Egelhofer *et al.*, *Nat. Struct. Mol. Biol.*, 2011, **18**, 91–94.

75 A. L. Clayton, S. Rose, M. J. Barratt and L. C. Mahadevan, *EMBO J.*, 2000, **19**, 3714–3726.

76 C. M. Rivera and B. Ren, *Cell*, 2013, **155**, 39–55.

77 C. Crane-Robinson, T. R. Hebbes, A. L. Clayton and A. W. Thorne, *Methods A Companion to Methods Enzymol.*, 1997, **12**, 48–56.

78 J. Chaumeil, I. Okamoto and E. Heard, *Methods Enzymol.*, 2003, **376**, 405–419.

79 L. M. P. Britton, M. Gonzales-Cope, B. M. Zee and B. A. Garcia, *Expert Rev. Proteomics*, 2011, **8**, 631–643.

80 R. Noberini, G. Sigismondo and T. Bonaldi, *Epigenomics*, 2016, **8**, 429–445.

81 Y. Zheng, X. Huang and N. L. Kelleher, *Curr. Opin. Chem. Biol.*, 2016, **33**, 142–150.

82 C. E. Thomas, N. L. Kelleher and C. A. Mizzen, *J. Proteome Res.*, 2006, **5**, 240–247.

83 J. J. Pesavento, Y. Bin Kim, G. K. Taylor and N. L. Kelleher, *J. Am. Chem. Soc.*, 2004, **126**, 3386–3387.

84 B. Meyer, D. G. Papasotiriou and M. Karas, *Amino Acids*, 2011, **41**, 291–310.

85 N. Siuti and N. L. Kelleher, *Anal. Biochem.*, 2010, **396**, 180–187.

86 H. Huang, S. Lin, B. A. Garcia and Y. Zhao, *Chem. Rev.*, 2015, **115**, 2376–2418.

87 S. E. Ong, G. Mittler and M. Mann, *Nat. Methods*, 2004, **1**, 119–126.

88 M. Bremang, A. Cuomo, A. M. Agresta, M. Stugiewicz, V. Spadotto and T. Bonaldi, *Mol. Biosyst.*, 2013, **9**, 2231–2247.

89 X. Cao, A. M. Arnaudo and B. A. Garcia, *Epigenetics*, 2013, **8**, 477–485.

90 N. Nady, L. Krichevsky, N. Zhong, S. Duan, W. Tempel, M. F. Amaya, M. Ravichandran and C. H. Arrowsmith, *J. Mol. Biol.*, 2012, **423**, 702–718.

91 K. E. Moore, S. M. Carlson, N. D. Camp, P. Cheung, R. G. James, K. F. Chua, A. Wolf-Yadlin and O. Gozani, *Mol. Cell*, 2013, **50**, 444–456.

92 S. M. Carlson, K. E. Moore, E. M. Green, G. M. Martín and O. Gozani, *Nat. Protoc.*, 2014, **9**, 37–50.

93 S. M. Carlson and O. Gozani, *J. Mol. Biol.*, 2014, **426**, 3350–3362.

94 S. A. Jacobs and S. Khorasanizadeh, *Science (80-.).*, 2002, **295**, 2080–2083.

95 H. Liu, M. Galka, E. Mori, X. Liu, Y. fen Lin, R. Wei, P. Pittock, C. Voss, G. Dhami, X. Li, M. Miyaji, G. Lajoie, B. Chen and S. S. C. Li, *Mol. Cell*, 2013, **50**, 723–735.

96 R. Wang and M. Luo, *Curr. Opin. Chem. Biol.*, 2013, **17**, 729–737.

97 R. Wang, W. Zheng and M. Luo, *Anal. Biochem.*, 2014, **450**, 11–19.

98 S. E. Ong and M. Mann, *Nat. Protoc.*, 2007, **1**, 2650–2660.

99 A. R. Knapp, C. Ren, X. Su, D. M. Lucas, J. C. Byrd, M. A. Freitas and M. R. Parthun, *Methods*, 2007, **41**, 312–319.

100 B. M. Zee, R. S. Levin, B. Xu, G. LeRoy, N. S. Wingreen and B. A. Garcia, *J. Biol. Chem.*, 2010, **285**, 3341–3350.

101 A. N. D. Scharf, T. K. Barth and A. Imhof, *Nucleic Acids Res.*, 2009, **37**, 5032–5040.

102 D. Bonenfant, H. Towbin, M. Coulot, P. Schindler, D. R. Mueller and J. van Oostrum, *Mol. Cell. Proteomics*, 2007, **6**, 1917–1932.

103 J. J. Pesavento, H. Yang, N. L. Kelleher and C. A. Mizzen, *Mol. Cell. Biol.*, 2008, **28**, 468–486.

104 B. D. Fodor, S. Kubicek, M. Yonezawa, R. J. O'Sullivan, R. Sengupta, L. Perez-Burgos, S. Opravil, K. Mechtler, G. Schotta and T. Jenuwein, *Genes Dev.*, 2006, **20**, 1557–1562.

105 B. A. Garcia, S. Mollah, B. M. Ueberheide, S. A. Busby, T. L. Muratore, J. Shabanowitz and D. F. Hunt, *Nat. Protoc.*, 2007, **2**, 933–938.

106 P. Drogaris, H. Wurtele, H. Masumoto, A. Verreault and P. Thibault, *Anal. Chem.*, 2008, **80**, 6698–6707.

107 M. D. Plazas-Mayorca, B. M. Zee, N. L. Young, I. M. Fingerman, G. LeRoy, S. D.

Briggs and B. A. Garcia, *J. Proteome Res.*, 2009, **8**, 5367–5374.

108 Q. Zhang, K. Zhang, Y. Zou, A. Perna and Y. Wang, *J. Am. Soc. Mass Spectrom.*, 2007, **18**, 1569–1578.

109 M. M. MacKeen, H. B. Kramer, K. H. Chang, M. L. Coleman, R. J. Hopkinson, C. J. Schofield and B. M. Kessler, *J. Proteome Res.*, 2010, **9**, 4082–4092.

110 L. P. Blair, N. L. Avaritt, R. Huang, P. A. Cole, S. D. Taverna and A. J. Tackett, *Epigenetics*, 2011, **6**, 491–500.

111 T. Bonaldi, A. Imhof and J. T. Regula, *Proteomics*, 2004, **4**, 1382–1396.

112 M. D. Plazas-Mayorca, J. S. Bloom, U. Zeissler, G. Leroy, N. L. Young, P. A. Dimaggio, L. Krugylak, R. Schneider and B. A. Garcia, *Mol. Biosyst.*, 2010, **6**, 1719–1729.

113 R. Liao, H. Wu, H. Deng, Y. Yu, M. Hu, H. Zhai, P. Yang, S. Zhou and W. Yi, *Anal. Chem.*, 2013, **85**, 2253–2259.

114 W. Peters, S. Willnow, M. Duisken, H. Kleine, T. Macherey, K. E. Duncan, D. W. Litchfield, B. Lüscher and E. Weinhold, *Angew. Chemie - Int. Ed.*, 2010, **49**, 5170–5173.

115 R. Wang, G. Ibáñez, K. Islam, W. Zheng, G. Blum, C. Sengelaub and M. Luo, *Mol. Biosyst.*, 2011, **7**, 2970–2981.

116 I. R. Bothwell, K. Islam, Y. Chen, W. Zheng, G. Blum, H. Deng and M. Luo, *J. Am. Chem. Soc.*, 2012, **134**, 14905–14912.

117 S. Willnow, M. Martin, B. Lüscher and E. Weinhold, *ChemBioChem*, 2012, **13**, 1167–1173.

118 K. Islam, W. Zheng, H. Yu, H. Deng and M. Luo, *ACS Chem. Biol.*, 2011, **6**, 679–684.

119 K. Islam, I. Bothwell, Y. Chen, C. Sengelaub, R. Wang, H. Deng and M. Luo, *J. Am. Chem. Soc.*, 2012, **134**, 5909–5915.

120 K. Islam, Y. Chen, H. Wu, I. R. Bothwell, G. J. Blum, H. Zeng, A. Dong, W. Zheng, J. Min, H. Deng and M. Luo, *Proc. Natl. Acad. Sci. U. S. A.*, 2013, **110**, 16778–16783.

121 R. Wang, K. Islam, Y. Liu, W. Zheng, H. Tang, N. Lailler, G. Blum, H. Deng and M. Luo, *J. Am. Chem. Soc.*, 2013, **135**, 1048–1056.

122 A. W. Hofmann, *Justus Liebigs Ann. Chem.*, 1851, **78**, 253–286.

123 A. W. Hofmann, *Justus Liebigs Ann. Chem.*, 1851, **79**, 11–39.

124 A. W. Hofmann, *Berichte der Dtsch. Chem. Gesellschaft*, 1881, **14**, 659–669.

125 A. W. Hofmann, *Berichte der Dtsch. Chem. Gesellschaft*, 1881, **14**, 494–496.

126 A. C. Cope and E. R. Trumbull, in *Organic Reactions*, 1960, pp. 317–493.

127 D. H. Froemsdorf and M. D. Robbins, *J. Am. Chem. Soc.*, 1967, **89**, 1737–1739.

128 R. A. Bartsch, R. A. Read, D. T. Larsen, D. K. Roberts, K. J. Scott and B. R. Cho, *J. Am. Chem. Soc.*, 1979, **101**, 1176–1181.

129 D. T. LEWIS, *Advanced Organic Chemistry*, 2006, vol. 192.

130 V. J. Shiner and M. L. Smith, *J. Am. Chem. Soc.*, 1958, **80**, 4095–4098.

131 E. D. Hughes, C. K. Ingold and C. S. Patel, *J. Chem. Soc.*, 1933, 526–530.

132 R. A. Bartsch and J. ZÁvada, *Chem. Rev.*, 1980, **80**, 453–494.

133 J. R. I. Eubanks, L. B. Sims and A. Fry, *J. Am. Chem. Soc.*, 1991, **113**, 8821–8829.

134 A. Sekine, T. Ohshima and M. Shibasaki, *Tetrahedron*, 2002, **58**, 75–82.

135 R. B. Gupta and R. W. Franck, *J. Am. Chem. Soc.*, 1989, **111**, 7668–7670.

136 A. C. Cope and D. L. Ross, *J. Am. Chem. Soc.*, 1961, **83**, 3854–3858.

137 J. L. Coke, G. D. Smith and G. H. Britton, *J. Am. Chem. Soc.*, 1975, **97**, 4323–4327.

138 P. Seuron and G. Solladie, *J. Org. Chem.*, 1980, **45**, 715–719.

139 W. Eschweiler, *Berichte der Dtsch. Chem. Gesellschaft*, 1905, **38**, 880–882.

140 H. T. Clarke, H. B. Gillespie and S. Z. Weisshaus, *J. Am. Chem. Soc.*, 1933, **55**, 4471–4587.

141 D. R. Lide, in *CRC Handbook of Chemistry and Physics*, 2016, pp. 94–103.

142 N. Jentoft and D. G. Dearborn, *J. Biol. Chem.*, 1979, **254**, 4359–4365.

143 Z. Z. Brown, M. M. Müller, S. U. Jain, C. D. Allis, P. W. Lewis and T. W. Muir, *J. Am. Chem. Soc.*, 2014, **136**, 13498–13501.

144 S. L. Wu, Y. T. Tao and W. H. Saunders, *J. Am. Chem. Soc.*, 1984, **106**, 7583–7588.

145 V. J. Traynelis and J. G. Dadura, *J. Org. Chem.*, 1961, **26**, 686–691.

146 T. Ishikawa, *Superbases for Organic Synthesis: Guanidines, Amidines, Phosphazenes and Related Organocatalysts*, 2009.

147 M. J. Minch, S. S. Chen and R. Peters, *J. Org. Chem.*, 1978, **43**, 31–33.

148 C. A. Bunton, A. A. Kamego and P. Ng, *J. Org. Chem.*, 1974, **39**, 3469–3471.

149 B. Y. Yano, Y. Yoshida, A. Kurashima, Y. Tamura and W. Tagaki, *J. Chem. Soc. Perkin Trans. 2*, 1979, **8**, 1128–1132.

150 K. A. Wilk and B. Burczyk, *J. Phys. Chem.*, 1989, **93**, 8219–8223.

151 L. Brinchi, P. Di Profio, R. Germani, G. Savelli and C. A. Bunton, *Langmuir*, 1997, **13**, 4583–4587.

152 E. J. Fendler and J. H. Fendler, *Adv. Phys. Org. Chem.*, 1970, **8**, 271–406.

153 C. A. Bunton, *Prog. Solid State Chem.*, 1973, **8**, 239–281.

154 S. Tascioglu, *Tetrahedron*, 1996, **52**, 11113–11152.

155 T. Dwars, E. Paetzold and G. Oehme, *Angew. Chemie - Int. Ed.*, 2005, **44**, 7174–7199.

156 M. N. Khan, *Micellar Catal.*, 2006, **1**, 1–483.

157 F. Mancin, P. Scrimin, P. Tecilla and U. Tonellato, *Coord. Chem. Rev.*, 2009, **253**, 2150–2165.

158 N. J. Buurma, *Annu. Reports Prog. Chem. - Sect. B*, 2012, **108**, 316–333.

159 G. La Sorella, G. Strukul and A. Scarso, *Green Chem.*, 2015, **17**, 644–683.

160 C. Dai, X. Wu, W. Li, Q. You, M. Zhao, M. Du, Y. Liu and Y. Li, *Soft Matter*, 2015, **11**, 7817–7826.

161 E. Des, M. Cationiques, S. U. R. Les, V. Relatives and C. Lapinte, *Tetrahedron Lett.*, 1973, **14**, 1113–1116.

162 C. A. Bunton and G. Savelli, *Adv. Phys. Org. Chem.*, 1986, **22**, 213–309.

163 S. S. Lukashenko and A. I. Konovalov, *Russ. J. Gen. Chem.*, 2008, **78**, 163–170.

164 A. Chatterjee, S. Maiti, S. K. Sanyal and S. P. Moulik, *Langmuir*, 2002, **18**, 2998–3004.

165 M. J. Guttieri and W. F. Maier, *J. Org. Chem.*, 1984, **49**, 2875–2880.

166 E. Wenkert, A. L. Han and C. J. Jenny, *J. Chem. Soc. Chem. Commun.*, 1988, 975–976.

167 J. T. Reeves, D. R. Fandrick, Z. Tan, J. J. Song, H. Lee, N. K. Yee and C. H. Senanayake, *Org. Lett.*, 2010, **12**, 4388–4391.

168 L. G. Xie and Z. X. Wang, *Angew. Chemie - Int. Ed.*, 2011, **50**, 4901–4904.

169 X. Q. Zhang and Z. X. Wang, *J. Org. Chem.*, 2012, **77**, 3658–3663.

170 X. Q. Zhang and Z. X. Wang, *Org. Biomol. Chem.*, 2014, **12**, 1448–1453.

171 P. Maity, D. M. Shacklady-Mcatee, G. P. A. Yap, E. R. Sirianni and M. P. Watson, *J. Am. Chem. Soc.*, 2013, **135**, 280–285.

172 A. Ojida, H. Tsutsumi, N. Kasagi and I. Hamachi, *Tetrahedron Lett.*, 2005, **46**, 3301–3305.

173 S. V. Chankeshwara, E. Indrigo and M. Bradley, *Curr. Opin. Chem. Biol.*, 2014, **21**, 128–135.

174 C. Reactions, A. C. Frisch and M. Beller, *Angew. Chemie - Int. Ed.*, 2005, **44**, 674–688.

175 S. L. Wiskur, A. Korte and G. C. Fu, *J. Am. Chem. Soc.*, 2004, **126**, 82–83.

176 C. M. McMahon and E. J. Alexanian, *Angew. Chemie - Int. Ed.*, 2014, **53**, 5974–5977.

177 R. F. Heck and J. P. Nolley, *J. Org. Chem.*, 1972, **37**, 2320–2322.

178 T. Mizoroki, K. Mori and A. Ozaki, *Bull. Chem. Soc. Japan*, 1971, **44**, 581–581.

179 K. Mori, T. Mizoroki and A. Ozaki, *Bull. Chem. Soc. Jpn.*, 1973, **46**, 1505–1508.

180 R. F. Heck, *Org. React.*, 1982, **27**, 345–390.

181 J. Tsuji, *Palladium Reagents and Catalysts: Innovations in Organic Chemistry*, 1995.

182 I. P. Beletskaya and A. V. Cheprakov, *Chem. Rev.*, 2000, **100**, 3009–3066.

183 A. Hallberg and G. D. Daves, *Chem. Rev.*, 1989, **89**, 1433–1445.

184 A. De Meijere and F. E. Meyer, *Angew Chem Int Ed Engl*, 1994, **33**, 2379–2411.

185 W. Cabri and I. Candiani, *Acc. Chem. Res.*, 1995, **28**, 2–7.

186 G. T. Crisp, *Chem. Soc. Rev.*, 1998, **27**, 427–436.

187 M. Shibasaki, C. D. J. Boden and A. Kojima, *Tetrahedron*, 1997, **53**, 7371–7395.

188 A. Biffis, M. Zecca and M. Basato, *J. Mol. Catal.*, 2001, **173**, 249–274.

189 M. W. Hooper, M. Utsunomiya and J. F. Hartwig, *J. Org. Chem.*, 2003, **68**, 2861–2873.

190 A. F. Littke and G. C. Fu, *Angew Chem Int Ed Engl*, 2002, **41**, 4176–4211.

191 W. A. Herrmann, K. Öfele, D. V. Preysing and S. K. Schneider, *J. Organomet. Chem.*, 2003, **687**, 229–248.

192 T. Jeffery, *J. Chem. Soc., Chem. Commun.*, 1984, 1287–1289.

193 T. Jeffery, *Tetrahedron Lett.*, 1985, **26**, 2667–2670.

194 T. Jeffery, *Synthesis (Stuttg).*, 1987, **1**, 70–71.

195 A. H. M. de Vries, J. M. C. A. Mulders, J. H. M. Mommers, H. J. W. Henderickx and J. G. de Vries, *Org. Lett.*, 2003, **5**, 3285–3288.

196 W. A. Herrmann, C. Brossmer, K. Öfele, C. -P Reisinger, T. Priermeier, M. Beller and H. Fischer, *Angew. Chemie Int. Ed. English*, 1995, **34**, 1844–1848.

197 A. B. Dounay and L. E. Overman, *Chem. Rev.*, 2009, **103**, 533–568.

198 A. Spencer, *J. Organomet. Chem.*, 1983, **258**, 101–108.

199 W. A. Herrmann, C. Brossmer, C. P. Reisinger, T. H. Riermeier, K. Öfele and M. Beller, *Chem. - A Eur. J.*, 1997, **3**, 1357–1364.

200 M. Qadir, T. Möchel and K. K. Hii, *Tetrahedron*, 2000, **56**, 7975–7979.

201 J. P. Wolfe, S. Wagaw and S. L. Buchwald, *J. Am. Chem. Soc.*, 1996, **118**, 7215–7216.

202 M. S. Driver and J. F. Hartwig, *J. Am. Chem. Soc.*, 1996, **118**, 7217–7218.

203 D. W. Old, J. P. Wolfe and S. L. Buchwald, *J. Am. Chem. Soc.*, 1998, **120**, 9722–9723.

204 J. P. Ebran, A. L. Hansen, T. M. Gøgsig and T. Skrydstrup, *J. Am. Chem. Soc.*, 2007, **129**, 6931–6942.

205 J. Sherwood, J. H. Clark, I. J. S. Fairlamb and J. M. Slattery, *Green Chem.*, 2019, **21**, 2164–2213.

206 H. L. Parker, J. Sherwood, A. J. Hunt and J. H. Clark, *ACS Sustain. Chem. Eng.*, 2014, **2**, 1739–1742.

207 E. Burello and G. Rothenberg, *Adv. Synth. Catal.*, 2003, **345**, 1334–1340.

208 F. Zhao, B. M. Bhanage, M. Shirai and M. Arai, *J. Mol. Catal. A Chem.*, 1999, **142**, 383–388.

209 F. Ozawa, A. Kubo and T. Hayashi, *Chem. Lett.*, 1992, 2177–2180.

210 C. Amatore, E. Carre and A. Jutand, *Organometallics*, 1995, **14**, 1818–1826.

211 C. Amatore and A. Jutand, *J. Organomet. Chem.*, 1999, **576**, 254–278.

212 B. P. Fors, P. Krattiger, E. Strieter and S. L. Buchwald, *Org. Lett.*, 2008, **10**, 3505–3508.

213 V. V. Grushin, *Chem. Rev.*, 1996, **96**, 2011–2033.

214 D. Gauthier, A. T. Lindhardt, E. P. K. Olsen, J. Overgaard and T. Skrydstrup, *J. Am. Chem. Soc.*, 2010, **132**, 7998–8009.

215 C. Amatore and A. Jutand, *Acc. Chem. Res.*, 2000, **33**, 314–321.

216 J. A. Cella and S. W. Bacon, *J. Org. Chem.*, 1984, **49**, 1122–1125.

217 I. D. Hills and G. C. Fu, *J. Am. Chem. Soc.*, 2004, **126**, 13178–13179.

218 P. W. N. M. Van Leeuwen, *Appl. Catal. A Gen.*, 2001, **212**, 61–81.

219 M. Tromp, J. R. A. Sietsma, J. A. Van Bokhoven, G. P. F. Van Strijdonck, R. J. Van Haaren, A. M. J. Van der Eerden, P. W. N. M. Van Leeuwen and D. C. Koningsberger, *Chem. Commun.*, 2003, **9**, 128–129.

220 M. Larhed and A. Hallberg, *J. Org. Chem.*, 1996, **61**, 9582–9584.

221 C. Amatore, E. Carré, A. Jutand, M. A. M'Barki and G. Meyer, *Organometallics*, 1995, **14**, 5605–5614.

222 J. F. Hartwig, M. Kawatsura, S. I. Hauck, K. H. Shaughnessy and L. M. Alcazar-Roman, *J. Org. Chem.*, 1999, **64**, 5575–5580.

223 A. F. Littke, C. Dai and G. C. Fu, *J. Am. Chem. Soc.*, 2000, **122**, 4020–4028.

224 H. J. W. Henderickx, J. G. De Vries, D. S. M. Pharma, C. V Synthesis, V. De and P. O. Box, *Org. Lett.*, 2003, **5**, 3285–3288.

225 M. T. Reetz, J. G. De Vries, M. T. Reetz and J. H. G, *Chem. Commun.*, 2004, 1559–1563.

226 J. G. De Vries, *Dalt. Trans.*, 2006, 421–429.

227 L. J. Gooßen, L. Huang, M. Arndt, K. Gooßen and H. Heydt, *Chem. Rev.*, 2015, **115**, 2596–2697.

228 P. W. Roesky, *Angew. Chemie - Int. Ed.*, 2009, **48**, 4892–4894.

229 T. E. Müller and M. Beller, *Chem. Rev.*, 1998, **98**, 675–703.

230 T. E. Müller, K. C. Hultzsch, M. Yus, F. Foubelo and M. Tada, *Chem. Rev.*, 2008, **108**, 3795–3892.

231 Z. Dong, Z. Ren, S. J. Thompson, Y. Xu and G. Dong, *Chem. Rev.*, 2017, **117**, 9333–9403.

232 J. Hannedouche and E. Schulz, *Organometallics*, 2018, **37**, 4313–4326.

233 E. Chong, P. Garcia and L. L. Schafer, *Synthesis (Stuttg).*, 2014, **46**, 2884–2896.

234 M. Kawatsura and J. F. Hartwig, *J. Am. Chem. Soc.*, 2000, **122**, 9546–9547.

235 M. Nobis and B. Driessen-Hölscher, *Angew. Chemie Int. Ed.*, 2001, **40**, 3983–3985.

236 F. E. Michael and B. M. Cochran, *J. Am. Chem. Soc.*, 2006, **128**, 4246–4247.

237 A. E. Nako, J. Oyamada, M. Nishiura and Z. Hou, *Chem. Sci.*, 2016, **7**, 6429–6434.

238 B. Zou, H. F. Jiang and Z. Y. Wang, *European J. Org. Chem.*, 2007, 4600–4604.

239 T. Mizoroki, H. Reaction and M. Oestreich, *The Mizoroki – Heck reaction*, 2009.

240 M. T. Reetz and E. Westermann, *Angew. Chemie - Int. Ed.*, 2000, **39**, 165–168.

241 A. H. M. De Vries, F. J. Parlevliet, L. Schmieder-van De Vondervoort, J. H. M. Mommers, H. J. W. Henderickx, M. A. M. Walet and J. G. De Vries, *Adv. Synth. Catal.*, 2002, **344**, 996–1002.

242 T. Jeffery, *Tetrahedron*, 1996, **52**, 10113–10130.

243 C. Amatore, A. Jutand and G. Le Duc, *Chem. - A Eur. J.*, 2011, **17**, 2492–2503.

244 M. T. Reetz and G. Lohmer, 1998, **1**, 481–483.

245 A. F. Littke and G. C. Fu, *Angew. Chemie Int. Ed.*, 1998, **37**, 3387–3388.

246 J. H. Kirchhoff, C. Dai and G. C. Fu, *Angew. Chemie Int. Ed.*, 2002, **41**, 1945.

247 C. Amatore, A. Jutand, F. Khalil, M. A. M'Barki and L. Mottier, *Organometallics*, 1993, **12**, 3168–3178.

248 C. Amatore, A. Jutand and A. Thuilliez, *J. Organometalic Chem.*, 2002, **643**, 416–423.

249 E. Janusson, H. S. Zijlstra, P. P. T. Nguyen, L. Macgillivray, J. Martelino and J. S. McIndoe, *Chem. Commun.*, 2017, **53**, 854–856.

250 C. Amatore and A. Jutand, *Coord. Chem. Rev.*, 1998, **178**–**180**, 511–528.

251 Y. Macé, A. R. Kapdi, I. J. S. Fairlamb and A. Jutand, *Organometallics*, 2006, **25**, 1795–1800.

252 A. C. Bissember, A. Levina and G. C. Fu, *J. Am. Chem. Soc.*, 2012, **134**, 14232–14237.

253 M. R. Netherton, C. Dai, K. Neuschutz and G. C. Fu, *J. Am. Chem. Soc.*, 2001, **123**, 10099–10100.

254 T. Wang, S. Yang, S. Xu, C. Han, G. Guo and J. Zhao, *RSC Adv.*, 2017, **7**, 15805–15808.

255 P. L. Tuertscher, H. J. Davis and R. J. Phipps, *Synthesis (Stuttg).*, 2018, **50**, 793–802.

256 L. Hie, N. F. Fine Nathel, T. K. Shah, E. L. Baker, X. Hong, Y. F. Yang, P. Liu, K. N. Houk and N. K. Garg, *Nature*, 2015, **524**, 79–83.

257 P. Lei, G. Meng, Y. Ling, J. An and M. Szostak, *J. Org. Chem.*, 2017, **82**, 6638–6646.

258 P. Lei, G. Meng and M. Szostak, *ACS Catal.*, 2017, **7**, 1960–1965.

259 R. Dorta, N. M. Scott, C. Costabile, L. Cavallo, C. D. Hoff and S. P. Nolan, *J. Am. Chem. Soc.*, 2005, **127**, 2485–2495.

260 A. R. Chianese, X. Li, M. C. Janzen, J. W. Faller and R. H. Crabtree, *Organometallics*, 2003, **22**, 1663–1667.

261 H. Jacobsen, A. Correa, A. Poater, C. Costabile and L. Cavallo, *Coord. Chem. Rev.*, 2009, **253**, 687–703.

262 L. Cavallo, A. Correa, C. Costabile and H. Jacobsen, *J. Organomet. Chem.*, 2005, **690**, 5407–5413.

263 C. M. Crudden and D. P. Allen, *Coord. Chem. Rev.*, 2004, **248**, 2247–2273.

264 D. J. Nelson and S. P. Nolan, *Chem. Soc. Rev.*, 2013, **42**, 6723–6753.

265 S. Díez-González and S. P. Nolan, *Coord. Chem. Rev.*, 2007, **251**, 874–883.

266 T. Droege and F. Glorius, *Angew. Chemie - Int. Ed.*, 2010, **49**, 6940–6952.

267 N. Hadei, E. A. B. Kantchev, C. J. O'Brien and M. G. Organ, *Org. Lett.*, 2005, **7**, 3805–3807.

268 A. Hopkinson, M. Organ, G. Chass, C. Valente and D.-C. Fang, *Synthesis (Stuttg).*, 2008, **2008**, 2776–2797.

269 G. Achonduh, M. G. Organ, N. Hadei, A. Lough, J. Nasielski, C. J. O'Brien and E. A. B. Kantchev, *Chem. - A Eur. J.*, 2010, **16**, 10844–10853.

270 C. J. O'Brien, E. A. B. Kantchev, C. Valente, N. Hadei, G. A. Chass, A. Lough, A. C. Hopkinson and M. G. Organ, *Chem. - A Eur. J.*, 2006, **12**, 4743–4748.

271 S. Shi and M. Szostak, *Chem. Commun.*, 2017, **53**, 10584–10587.

272 G. Altenhoff, R. Goddard, C. W. Lehmann and F. Glorius, *J. Am. Chem. Soc.*, 2004, **126**, 15195–15201.

273 M. G. Organ, S. Çalimsiz, M. Sayah, K. H. Hoi and A. J. Lough, *Angew. Chemie - Int. Ed.*, 2009, **48**, 2383–2387.

274 C. Valente, S. Çalimsiz, K. H. Hoi, D. Mallik, M. Sayah and M. G. Organ, *Angew. Chemie - Int. Ed.*, 2012, **51**, 3314–3332.

275 C. Valente, M. Pompeo, M. Sayah and M. G. Organ, *Org. Process Res. Dev.*, 2014, **18**, 180–190.

276 M. G. Organ, M. Abdel-Hadi, S. Avola, I. Dubovyk, N. Hadei, E. A. B. Kantchev, C. J. O'Brien, M. Sayah and C. Valente, *Chem. - A Eur. J.*, 2008, **14**, 2443–2452.

277 C. J. O'Brien, E. A. B. Kantchev, G. A. Chass, N. Hadei, A. C. Hopkinson, M. G. Organ, D. H. Setiadi, T. H. Tang and D. C. Fang, *Tetrahedron*, 2005, **61**, 9723–9735.

278 K. Hirano, S. Urban, C. Wang and F. Glorius, *Org. Lett.*, 2009, **11**, 1019–1022.

279 A. V. Astakhov, O. V. Khazipov, A. Y. Chernenko, D. V. Pasyukov, A. S. Kashin, E.

G. Gordeev, V. N. Khrustalev, V. M. Chernyshev and V. P. Ananikov, *Organometallics*, 2017, **36**, 1981–1992.

280 V. Calò, A. Nacci, A. Monopoli and P. Cotugno, *Angew. Chemie - Int. Ed.*, 2009, **48**, 6101–6103.

281 T. T. Gao, A. P. Jin and L. X. Shao, *Beilstein J. Org. Chem.*, 2012, **8**, 1916–1919.

282 T. Wang, J. Guo, X. Wang, H. Guo, D. Jia, H. Wang and L. Liu, *RSC Adv.*, 2019, **9**, 5738–5741.

283 O. Boutureira and G. J. L. Bernardes, *Chem. Rev.*, 2015, **115**, 2174–2195.

284 J. M. Antos and M. B. Francis, *Curr. Opin. Chem. Biol.*, 2006, **10**, 253–262.

285 M. Yang, J. Li and P. R. Chen, *Chem. Soc. Rev.*, 2014, **43**, 6511–6526.

286 M. Jbara, S. K. Maity and A. Brik, *Angew. Chemie - Int. Ed.*, 2017, **56**, 10644–10655.

287 C. D. Spicer, T. Triemer and B. G. Davis, *J. Am. Chem. Soc.*, 2012, **134**, 800–803.

288 M. Martínez-Calvo and J. L. Mascareñas, *Coord. Chem. Rev.*, 2018, **359**, 57–79.

289 K. Kim, D. A. Fancy, D. Carney and T. Kodadek, *J. Am. Chem. Soc.*, 1999, **121**, 11896–11897.

290 S. D. Tilley and M. B. Francis, *J. Am. Chem. Soc.*, 2006, **128**, 1080–1081.

291 H. G. Lee, G. Lautrette, B. L. Pentelute and S. L. Buchwald, *Angew. Chemie - Int. Ed.*, 2017, **56**, 3177–3181.

292 E. V. Vinogradova, C. Zhang, A. M. Spokoyny, B. L. Pentelute and S. L. Buchwald, *Nature*, 2015, **526**, 687–691.

293 R. A. A. Al-Shuaeeb, S. Kolodych, O. Koniev, S. Delacroix, S. Erb, S. Nicolaÿ, J. C. Cintrat, J. D. Brion, S. Cianférani, M. Alami, A. Wagner and S. Messaoudi, *Chem. - A Eur. J.*, 2016, **22**, 11365–11370.

294 J. Willwacher, R. Raj, S. Mohammed and B. G. Davis, *J. Am. Chem. Soc.*, 2016, **138**, 8678–8681.

295 T. S. Young and P. G. Schultz, *J. Biol. Chem.*, 2010, **285**, 11039–11044.

296 K. Wals and H. Ovaa, *Front. Chem.*, 2014, **2**, 1–12.

297 C. H. Kim, J. Y. Axup and P. G. Schultz, *Curr. Opin. Chem. Biol.*, 2013, **17**, 412–419.

298 K. Lang and J. W. Chin, *Chem. Rev.*, 2014, **114**, 4764–4806.

299 K. Kodama, S. Fukuzawa, H. Nakayama, K. Sakamoto, T. Kigawa, T. Yabuki, N. Matsuda, M. Shirouzu, K. Takio, S. Yokoyama and K. Tachibana, *ChemBioChem*, 2007, **8**, 232–238.

300 J. M. Chalker, C. S. C. Wood and B. G. Davis, *J. Am. Chem. Soc.*, 2009, **131**, 16346–16347.

301 C. D. Spicer and B. G. Davis, *Chem. Commun.*, 2011, **47**, 1698–1700.

302 Z. Gao, V. Gouverneur and B. G. Davis, *J. Am. Chem. Soc.*, 2013, **135**, 13612–13615.

303 A. Dumas, C. D. Spicer, Z. Gao, T. Takehana, Y. A. Lin, T. Yasukohchi and B. G. Davis, *Angew. Chemie - Int. Ed.*, 2013, **52**, 3916–3921.

304 P. Meert, S. Dierickx, E. Govaert, L. De Clerck, S. Willems, M. Dhaenens and D. Deforce, *Proteomics*, 2016, **16**, 1970–1974.

305 Y. R. Luo, *Handbook of bond dissociation energies in organic compounds*, CRC Press LLC, 2002.

306 S. B. Blakey and D. W. C. MacMillan, *J. Am. Chem. Soc.*, 2003, **125**, 6046–6047.

307 F. Lu, Z. Chen, Z. Li, X. Wang, X. Peng, C. Li, R. Li, H. Pei, H. Wang and M. Gao, *Asian J. Org. Chem.*, 2018, **7**, 141–144.

308 M. Guisán-Ceinos, V. Martín-Heras and M. Tortosa, *J. Am. Chem. Soc.*, 2017, **139**, 8448–8451.

309 W. J. Guo and Z. X. Wang, *Tetrahedron*, 2013, **69**, 9580–9585.

310 S. Yu, S. Liu, Y. Lan, B. Wan and X. Li, *J. Am. Chem. Soc.*, 2015, **137**, 1623–1631.

311 G. De La Herrán, A. Segura and A. G. Csákÿ, *Org. Lett.*, 2007, **9**, 961–964.

312 S. Ueno, N. Chatani and F. Kakiuchi, *J. Am. Chem. Soc.*, 2007, **129**, 6098–6099.

313 G. Li, Y. Chen and J. Xia, *Chinese J. Org. Chem.*, 2018, **38**, 1949–1962.

314 E. A. Standley and T. F. Jamison, *J. Am. Chem. Soc.*, 2013, **135**, 1585–1592.

315 S. S. Wang and G. Y. Yang, *Catal. Sci. Technol.*, 2016, **6**, 2862–2876.

316 B. L. Lin, L. Liu, Y. Fu, S. W. Luo, Q. Chen and Q. X. Guo, *Organometallics*, 2004, **23**, 2114–2123.

317 L. L. Liao, G. M. Cao, J. H. Ye, G. Q. Sun, W. J. Zhou, Y. Y. Gui, S. S. Yan, G. Shen and D. G. Yu, *J. Am. Chem. Soc.*, 2018, **140**, 17338–17342.

318 F. Schwizer, Y. Okamoto, T. Heinisch, Y. Gu, M. M. Pellizzoni, V. Lebrun, R. Reuter, V. Köhler, J. C. Lewis and T. R. Ward, *Chem. Rev.*, 2018, **118**, 142–231.

319 C. S. Beshara, C. E. Jones, K. D. Daze, B. J. Lilgert and F. Hof, *ChemBioChem*, 2010, **11**, 63–66.

320 D. M. Homden and C. Redshaw, *Chem. Rev.*, 2008, **108**, 5086–5130.

321 J. Rappsilber, *J. Struct. Biol.*, 2011, **173**, 530–540.

322 E. V. Petrotchenko and C. H. Borchers, *Mass Spectrom. Rev.*, 2010, **29**, 862–876.

323 A. Leitner, T. Walzthoeni, A. Kahraman, F. Herzog, O. Rinner, M. Beck and R. Aebersold, *Mol. Cell. Proteomics*, 2010, **9**, 1634–1649.

324 B. Yang, Y. J. Wu, M. Zhu, S. B. Fan, J. Lin, K. Zhang, S. Li, H. Chi, Y. X. Li, H. F. Chen, S. K. Luo, Y. H. Ding, L. H. Wang, Z. Hao, L. Y. Xiu, S. Chen, K. Ye, S. M. He and M. Q. Dong, *Nat. Methods*, 2012, **9**, 904–906.

325 F. Liu, D. T. S. Rijkers, H. Post and A. J. R. Heck, *Nat. Methods*, 2015, **12**, 1179–1184.

326 H. Buncherd, W. Roseboom, L. J. de Koning, C. G. de Koster and L. De Jong, *J. Proteomics*, 2014, **108**, 65–77.

327 D. Fasci, H. Van Ingen, R. A. Scheltema and A. J. R. Heck, *Mol. Cell. Proteomics*, 2018, **17**, 2018–2033.

328 J. D. Chavez, C. R. Weisbrod, C. Zheng, J. K. Eng and J. E. Bruce, *Mol. Cell. Proteomics*, 2013, **12**, 1451–1467.

329 X. Zhong, A. T. Navare, J. D. Chavez, J. K. Eng, D. K. Schweppe and J. E. Bruce, *J. Proteome Res.*, 2017, **16**, 720–727.

330 C. E. Stieger, P. Doppler and K. Mechtler, *J. Proteome Res.*, 2019, **18**, 1363–1370.

331 A. Leitner, R. Reischl, T. Walzthoeni, F. Herzog, S. Bohn, F. Förster and R. Aebersold, *Mol. Cell. Proteomics*, 2012, **11**, 1–12.

332 M. L. Mendes, L. Fischer, Z. A. Chen, M. Barbon, F. J. O'Reilly, S. Giese, M. Bohlke-Schneider, A. Belsom, T. Dau, C. W. Combe, M. Graham, M. R. Eisele, W. Baumeister, C. Speck and J. Rappsilber, *Mol. Syst. Biol.*, 2019, **15**, e8994.

333 D. Shechter, H. L. Dormann, C. D. Allis and S. B. Hake, *Nat. Protoc.*, 2007, **2**, 1445–1457.

334 M. C. Parrott, J. C. Luft, J. D. Byrne, J. H. Fain, M. E. Napier and J. M. Desimone, *J. Am. Chem. Soc.*, 2010, **132**, 17928–17932.

335 M. C. Parrott, M. Finniss, J. C. Luft, A. Pandya, A. Gullapalli, M. E. Napier and J. M. Desimone, *J. Am. Chem. Soc.*, 2012, **134**, 7978–7982.

336 G. Leriche, L. Chisholm and A. Wagner, *Bioorganic Med. Chem.*, 2012, **20**, 571–582.

337 S. A. Jacques, G. Leriche, M. Mosser, M. Nothisen, C. D. Muller, J. S. Remy and A. Wagner, *Org. Biomol. Chem.*, 2016, **14**, 4794–4803.

338 P. G. M. Wuts and T. W. Greene, *Greene's Protective Groups in Organic Synthesis*, 2006.

339 R. Schwalm, H. Binder and D. Funhoff, *J. Appl. Polym. Sci.*, 2000, **78**, 208–216.

340 F. Zhu, Q. Yang, Y. Zhuang, Y. Zhang, Z. Shao, B. Gong and Y. M. Shen, *Polymer (Guildf).*, 2014, **55**, 2977–2985.

341 E. R. Gillies, A. P. Goodwin and J. M. J. Fréchet, *Bioconjug. Chem.*, 2004, **15**, 1254–1263.

342 M. Renz and B. Meunier, *Eur. Hournal Org. Chem.*, 1999, **1999**, 737–750.

343 P. M. Henry, M. Davies, G. Ferguson, S. Phillips and R. Restivo, *J.C.S. Chem. Comm.*, 1974, 112–113.

344 M. M. Alam, R. Varala and S. R. Adapa, *Synth. Commun.*, 2003, **33**, 3035–3040.

345 H. Michiyo, H. Noriyuki, T. Kamashita, H. Suemune and K. Sakai, *Chem. Pharm. Bull.*, 1988, **36**, 1550–1553.

346 B. R. Kusuma, L. B. Peterson, H. Zhao, G. Vielhauer, J. Holzbeierlein and B. S. J. Blagg, *J. Med. Chem.*, 2011, **54**, 6234–6253.

347 T. J. Donohoe and R. M. Lipiński, *Angew. Chemie - Int. Ed.*, 2013, **52**, 2491–2494.

348 Z. L. Li, A. Lv, F. S. Du and Z. C. Li, *Macromolecules*, 2014, **47**, 5942–5951.

349 W. Sittiwong, M. W. Richardson, C. E. Schiaffo, T. J. Fisher and P. H. Dussault, *Beilstein J. Org. Chem.*, 2013, **9**, 1526–1532.

350 C. Gonzalez, S. Kavoosi, A. Sanchez and S. F. Wnuk, *Carbohydr. Res.*, 2016, **432**, 17–22.

351 D. J. Kopecky and S. D. Rychnovsky, *J. Org. Chem.*, 2000, **65**, 191–198.

352 H. M. Sheldrake, C. Jamieson and J. W. Burton, *Angew. Chemie - Int. Ed.*, 2006, **45**, 7199–7202.

353 N. Inada, K. Nakamoto, T. Yokogawa and Y. Ueno, *Eur. J. Med. Chem.*, 2015, **103**, 460–472.

354 J. Østergaard and C. Larsen, *Molecules*, 2007, **12**, 2396–2412.

355 T. Banno, K. Toshima, K. Kawada and S. Matsumura, *J. Surfactants Deterg.*, 2009, **12**, 249–259.

356 H. Burghart-Stoll and R. Brückner, *European J. Org. Chem.*, 2012, 3978–4017.